UNIVERSITÀ DEGLI STUDI DI PADOVA

DEPARTMENT OF PHARMACEUTICAL AND PHARMACOLOGICAL SCIENCES

Doctoral School In Molecular Sciences

Pharmaceutical Sciences Curriculum - XXXV Cycle

Overcoming biological barriers by lipid-based nanocarriers

Ph.D. Programme Coordinator: Prof. Leonard Prins

Supervisor: Prof. Stefano Salmaso

Ph.D Student: Büşra Arpaç

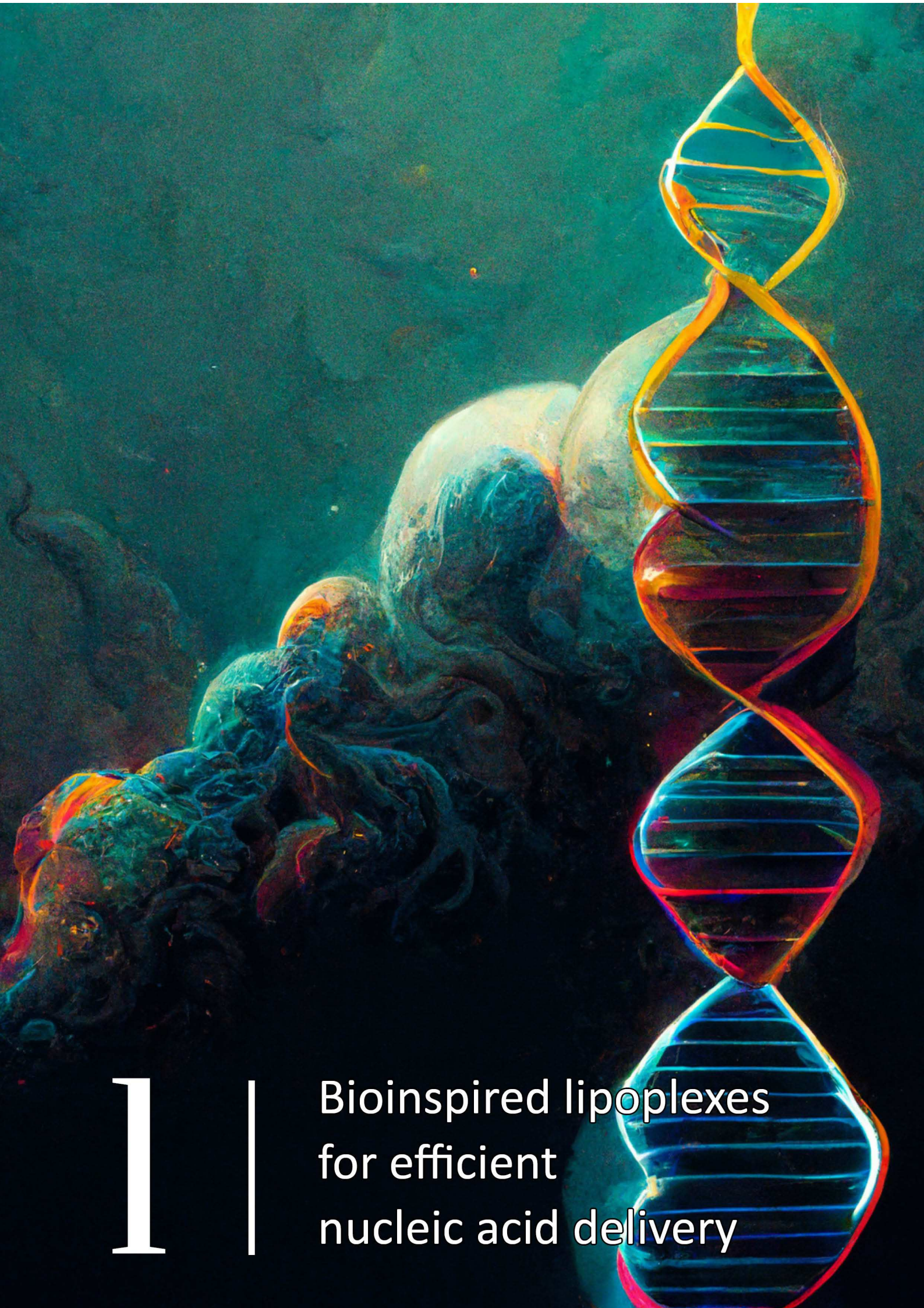

1 | Bioinspired lipoplexes for efficient nucleic acid delivery

CONTENTS

1. ABBREVIATIONS **6**
2. ABSTRACT **8**
3. RIASSUNTO **10**
4. INTRODUCTION **12**
4.1. GENE THERAPY: ON OVERVIEW 12
4.1.1. Routes of gene delivery 14
4.1.2. Challenges in gene delivery 17
4.1.2.1. Extracellular barriers 17
4.1.2.2. Intracellular barriers 18
4.2. RNA INTERFERENCE AND SIRNAS 22
4.2.1. Application of RNAi 24
4.3. GENE DELIVERY STRATEGIES 25
4.3.1. Physical methods for gene delivery 26
4.3.2. Viral vectors 26
4.3.3. Non-viral vectors 27
4.4. LIPOPLEXES AS GENE DELIVERY SYSTEMS 30
4.4.1. Preparation methods of the lipoplexes 32
4.4.2. Composition of lipoplexes 34
4.5. CELL PENETRATION ENHANCERS 37
4.5.1. Cellular internalization mechanisms of CPEs 38
4.5.2. Non-peptidic CPEs 40
5. AIM OF THE PROJECT **43**
6. MATERIALS AND METHODS **44**
6.1. MATERIALS 44
6.1.1. Reagents 44
6.1.2. Scientific equipment 45
6.2. METHODS 46
6.2.1. Analytical methods 46
6.2.1.1. Determination of Cy3-dsDNA concentration by Spectrofluorometric analysis 46
6.2.1.2. siRNA concentration assessment by RiboGreen Assay 47
6.2.1.3. Determination of the arginine groups by Sakaguchi Assay 47
6.2.1.4. Phospholipid assessment by Stewart Assay 48
6.2.1.5. Validation of non-loaded dsDNA removal from the lipoplexes 50
6.2.2. Synthesis of the oligocationic enhancer 50
6.2.2.1. Synthesis of the lipid anchor 51
6.2.2.2. Synthesis of the arginine decorated dendron 52
6.2.2.3. Huisgen cycloaddition of the lipid anchor to arginine decorated dendron 53
6.2.3. Lipoplexes preparation 55
6.2.3.1. Selection of the OCE ratio within lipoplexes 56
6.2.3.2. Investigation of the lipid composition of lipoplexes 57
6.2.3.3. Selection of the N/P ratio for lipoplexes loading 59
6.2.3.4. Preparation of the siRNA-loaded lipoplexes 59
6.2.4. Characterization of the lipoplexes 60
6.2.4.1. Particle size and zeta potential measurement 60
6.2.4.2. Loading efficiency and capacity assessment 60
6.2.4.3. Release studies 61

6.2.4.4. Complexation efficiency and displacement assay 61
6.2.4.5. Stability studies 62
6.2.5. Hemolysis assay 62
6.2.6. In vitro cellular studies 63
6.2.6.1. Cytotoxicity assessment by MTT assay 63
6.2.6.2. Membrane toxicity assessment by LDH assay 63
6.2.6.3. Cellular uptake 64
6.2.6.4. Gene silencing 64
6.2.6.5. Intracellular trafficking studies 67
7. RESULTS AND DISCUSSION 68
7.1. SYNTHESIS OF THE OLIGOCATIONIC ENHANCER 68
7.1.1. Synthesis of the lipid anchor 70
7.1.2. Synthesis of the arginine decorated dendron 72
7.1.3. Huisgen cycloaddition of the lipid anchor to arginine decorated dendron and removal of the protecting groups 73
7.2. LIPOPLEXES PREPARATION 75
7.2.1. Selection of the OCE ratio 75
7.2.2. Selection of the lipid composition 77
7.2.3. N/P ratio effect on lipoplexes colloidal and biopharmaceutical features 83
7.2.4. siRNA-loaded lipoplexes: formulation and characterization 90
7.3. HEMOLYSIS ASSAY 92
7.4. IN VITRO CELLULAR STUDIES 93
7.4.1. Cytotoxicity assessment by MTT assay 93
7.4.2. Membrane toxicity assessment by LDH assay 94
7.5.3. Cellular uptake 95
7.5.4. Gene silencing by flow cytometric analysis 98
7.5.5. Visualization of the gene silencing by confocal microscopy 100
7.5.6. Intracellular trafficking 101
8. CONCLUSIONS 104

1. ABBREVIATIONS

APS	Ammonium persulfate
Arg_4-DAG	Tetraarginyl-decorated diacyl-gliceroyl-Dendron
bp	Base pair
CE	Complexation efficiency
$CHCl_3$	Chloroform
Chol	Cholesterol
CPP	Cell penetrating peptides
CPE	Cell penetrating enhancer
Cy-3dsDNA	Cyanine 3 - deoxyribunucleic acid double strand
COVID-19	Coronavirus disease 2019
Da	Dalton
DAPI	4',6-Diamidino-2-phenylindoledihydrochloride
DLS	Dinamic Light Scattering
DMEM	Dubecco's modified eagle's medium
DMSO	Dimethyl sulfoxide
DOPE	1,2-Dioleoyl-sn-glycero-3-phosphoethanolamine
dsDNA	Deoxyribonucleic acid double strand
dsRNA	Ribonucleic acid double strand
EDTA	Ethylenediaminetetraacetic acid
FACS	Fluorescence-activated cell sorting
FDA	Food and drug administration
FBS	Fetal bovine serum
HBS	HEPES saline buffer
HEPES	4-(2-hydroxyethyl)-1-piperazineethanesulfonic acid
HSPC	Hydrogenated soy phosphatidylcholine
ITC	Isothermal titration calorimetry
LC	Loading capacity
LE	Loading efficiency
MeOH	Methanol
miRNA	micro RNA

$mPEG_{2KDa}$-DSPE	1,2-distearoyl-sn-glycero-3phosphoethanolamine-N-[methoxy(polyethyleneglycol)-2000]
$mPEG_{5KDa}$-DSPE	1,2-distearoyl-sn-glycero-3phosphoethanolamine-N-[methoxy(polyethyleneglycol)-5000]
mRNA	Messenger RNA
MTT	Methylthiazolyldiphenyl-tetrazolium bromide
MW	Molecular weight
NP	Nanoparticles
ON	Oligonucleotide
PBS	Phosphate buffer saline
PEG	Polyethylene glycol
PFA	Paraformaldehyde
RNAi	RNA interference
RNase	Ribonucleases
rpm	Revolutions per minute
RPMI	Roswell park memorial institute
SD	Standart deviation
SDS	Sodium dodecyl sulfate
siCTRL	siRNA duplex non-targeting negative control
sieGFP	eGFP targeting siRNA duplex
shRNA	Short hairpin RNA
siRNA	Small interference RNA
TBE	Tris-borate-EDTA
TFH	Thin film hydration
TEM	Transmission electron microscope
TEMED	N,N,N',N'-Tetramethylethylenediamine
Tris	2-Amino-2-hydroxymethyl-propane-1,3-diol
ZP	Zeta potential

2. ABSTRACT

Oligonucleotides have recently been studied as therapeutic agents for various pathologies such as genetic disorders, viral infections and cancer. Among the different types of oligonucleotides used for therapeutic purposes siRNA is raising greater interest, because its action applies the natural mechanism of RNAi, which can lower the expression of pathologically overexpressed or mutated proteins. To exploit the therapeutic action of the oligonucleotides is necessary to develop a dedicated delivery system that allows them to reach intact and at high concentration the action site minimizing the exposure of other tissues. For this reason, the delivery system must be designed to protect the drug from enzymatic degradation and rapid excretion, allowing it to have a long duration of action. A possible delivery system for oligonucleotides can be the formulation of lipoplexes, which consists of complexes between cationic liposomes and oligonucleotides. Liposomes composed of cationic lipids allow a great loading of nucleic acid via electrostatic interactions and generate complexes in which the genetic materials are protected and targeted to the desired site.

Within this thesis project, lipoplexes were formulated for the delivery of oligonucleotides and were prepared using an innovative oligocationic enhancer (OCE) synthesized by our group. This lipid consisted of a dendrimeric portion functionalized by four arginines, which provide cationic charges, and a lipid anchor, which favors the insertion into the liposome bilayer. OCE, in addition to the advantage to condense the genetic material, allows a high loading degree, it also has the property of being a cell penetration enhancer.

Lipoplexes were formulated using HSPC/Cholesterol at a molar ratio of 2:1 and employing OCE in a range of 0-10% (mol/mol) for the determination of the optimum ratio. 4% of OCE was selected for providing high surface charge (> +40 mV) and high membrane association efficiency (~ 90%). Using a 4% (mol/mol) OCE ratio, the effect of the lipid saturation on the lipoplexes was investigated using saturated phospholipid HSPC or unsaturated phospholipid EPC. Independently from the lipid saturation lipoplexes were characterized by sizes around 200 nm, low polydispersity index (< 0.2) and high positive surface charge (~ +40 mV). Other than the formulations generated with the excess of DOPE, namely HSPC/DOPE (1:3 mol/mol), HSPC/DOPE (1:2 mol/mol) and their EPC counterparts, lipoplexes were characterized with high loading efficiency (> 80%) independently from the lipid composition. Even though EPC-based lipoplexes have shown a similar particle size, polydispersity index, zeta potential and loading efficiency, they were excluded from the study for their very fast release profile.

For the determination of the optimum N/P ratio, the lipoplexes with 1:1 HSPC/DOPE, 2:1 HSPC/DOPE, 2:1:1 HSPC/Cholesterol/DOPE and 2:1 HSPC/Cholesterol composition were generated with 4 mol% of

OCE at decreasing N/P ratios from 10:1 to 1:1. Control lipoplexes without OCE were also generated to derive information about the contribution of the OCE in the loading of lipoplexes at each N/P ratio tested. The lipoplexes assembled using a 10:1 N/P ratio were selected for further studies since these lipoplexes have the lowest loss of fed dsDNA and, almost complete loading of the fed dsDNA (~80 %) and also providing a size around 200 nm, and low polydisperse systems. These screening studies allowed the identification of suitable formulations namely 1:1 HSPC/DOPE, 2:1 HSPC/DOPE, 2:1:1 HSPC/Cholesterol/DOPE and 2:1 HSPC/Cholesterol lipoplexes with 4% OCE and generated at N/P ratio of 10:1. These formulations have shown great stability up to 4 IU/mL heparin concentration and hemocompatible when tested on rat blood, up to lipid concentration of 0.3 mg/mL.

The formulation parameters were then transferred for the assembly of lipoplexes loaded with biologically active siRNA. In-vitro cytotoxicity studies conducted by MTT and LDH assays showed that siRNA-loaded lipoplexes induced negligible toxicity within the siRNA concentration range used in the studies. Cellular association studies revealed that the inclusion of the OCE significantly increases the association of the lipoplexes. Silencing efficiency as a proxy for the therapeutic activity of the siRNA-loaded lipoplex library was measured by the flow cytometric analysis and showed the inclusion of the fusogenic lipid DOPE significantly increases the eGFP silencing. Furthermore, the silencing efficiency of the 1:1 HSPC:DOPE lipoplexes was also shown by imaging with confocal microscopy. Finally, the intracellular fate of the lipoplexes generated in 1:1 HSPC/DOPE composition was investigated by measuring its colocalization with acidic compartments such as late endosomes and lysosomes by confocal microscopy. Our results showed a limited colocalization of the lipoplexes with the acidic compartments within 8 hours, suggesting that DOPE is triggering the endosomal escape of the lipoplexes resulting in high silencing efficiency.

3. RIASSUNTO

Gli oligonucleotidi sono stati recentemente studiati come agenti terapeutici per varie patologie come malattie genetiche, infezioni virali e cancro. Tra i diversi tipi di oligonucleotidi utilizzati a fini terapeutici sta suscitando maggiore interesse il siRNA, perché alla sua azione applica il meccanismo naturale dell'RNAi, che è in grado di silenziare l'espressione di proteine patologicamente sovraespresse o mutate. Per sfruttare l'azione terapeutica degli oligonucleotidi è necessario sviluppare un sistema di rilascio dedicato che consenta loro di raggiungere intatto e ad alta concentrazione il sito d'azione minimizzando l'esposizione di altri tessuti. Per questo motivo, il sistema di somministrazione deve essere progettato in modo da proteggere il farmaco dalla degradazione enzimatica e dalla rapida escrezione, consentendogli di avere una lunga durata d'azione. Un possibile sistema di rilascio per oligonucleotidi può essere la formulazione di lipoplessi, che consiste in complessi tra liposomi cationici e oligonucleotidi. I liposomi composti da lipidi cationici consentono un grande carico di acido nucleico tramite interazioni elettrostatiche e generano complessi in cui i materiali genetici sono protetti e mirati al sito desiderato.

Nell'ambito di questo progetto di tesi, i lipoplessi sono stati formulati per il rilascio di oligonucleotidi e sono stati preparati utilizzando un innovativo potenziatore oligocationico sintetizzato dal nostro gruppo. Questo lipide era costituito da una porzione dendrimerica funzionalizzata da quattro arginine, che forniscono cariche cationiche, e da un'ancora lipidica, che favorisce l'inserimento nel doppio strato liposomiale. OCE, oltre al vantaggio di condensare il materiale genetico, consente un elevato grado di carico, ha anche la proprietà di essere un potenziatore della penetrazione cellulare.

I lipoplessi sono stati formulati utilizzando HSPC/colesterolo a un rapporto molare di 2:1 e impiegando OCE in un intervallo di 0-10% (mol/mol) per la determinazione del rapporto OCE ottimale. Il 4% di OCE è stato selezionato per fornire un'elevata carica superficiale (> +40 mV) e un'elevata efficienza di associazione della membrana (~ 90%). Utilizzando un rapporto OCE del 4% (mol/mol), l'effetto della saturazione lipidica sui lipoplessi è stato studiato utilizzando HSPC fosfolipidico saturo o EPC fosfolipidico insaturo. Indipendentemente dalla saturazione lipidica, i lipoplessi erano caratterizzati da dimensioni intorno a 200 nm, basso indice di polidispersione (< 0,2) e carica superficiale positiva elevata (~ +40 mV). Oltre alle formulazioni generate con l'eccesso di DOPE, ovvero HSPC/DOPE (1:3 mol/mol), HSPC/DOPE (1:2 mol/mol) e le loro controparti EPC, i lipoplessi sono stati caratterizzati con un'elevata efficienza di caricamento (> 80 %) indipendentemente dalla composizione lipidica. Anche se i lipoplessi basati su EPC hanno mostrato una dimensione delle particelle, un indice di polidispersità, un potenziale zeta e un'efficienza di carico simili, sono stati esclusi dallo studio per il loro profilo di rilascio molto rapido.

Per la determinazione del rapporto N/P ottimale, i lipoplessi con composizione 1:1 HSPC/DOPE, 2:1 HSPC/DOPE, 2:1:1 HSPC/colesterolo/DOPE e 2:1 HSPC/colesterolo sono stati generati con 4 mol% di OCE a rapporti N/P decrescenti da 10:1 a 1:1. Sono stati generati anche lipoplessi di controllo senza OCE per ricavare informazioni sul contributo dell'OCE nel carico dei lipoplessi a ciascun rapporto N/P testato. I lipoplessi assemblati utilizzando un rapporto N/P di 10:1 sono stati selezionati per ulteriori studi poiché questi lipoplessi hanno la più bassa perdita di dsDNA alimentato e, il caricamento quasi completo del dsDNA alimentato (~ 80 %) e fornendo anche una dimensione di circa 200 nm, e sistemi a bassa polidispersione. Questi studi di screening hanno consentito l'identificazione di formulazioni idonee e precisamente 1:1 HSPC/DOPE, 2:1 HSPC/DOPE, 2:1:1 HSPC/colesterolo/DOPE e 2:1 HSPC/colesterolo lipoplessi con 4% OCE e generati a N /P rapporto di 10:1. Queste formulazioni hanno mostrato grande stabilità fino a una concentrazione di eparina di 4 IU/mL ed emocompatibili quando testate su sangue di ratto, fino a una concentrazione di lipidi di 0,3 mg/mL.

I parametri di formulazione sono stati quindi trasferiti per l'assemblaggio di lipoplessi caricati con siRNA biologicamente attivo. Studi di citotossicità in vitro condotti da saggi MTT e LDH hanno mostrato che i lipoplessi caricati con siRNA inducevano una tossicità trascurabile all'interno dell'intervallo di concentrazione di siRNA utilizzato negli studi. Studi di associazione cellulare hanno rivelato che l'inclusione dell'OCE aumenta significativamente l'associazione dei lipoplessi. L'efficienza del silenziamento come proxy per l'attività terapeutica della libreria lipoplex caricata con siRNA è stata misurata dall'analisi citometrica a flusso e ha mostrato che l'inclusione del lipide fusogeno DOPE aumenta significativamente il silenziamento dell'eGFP. Inoltre, l'efficienza di silenziamento dei lipoplessi 1:1 HSPC:DOPE è stata dimostrata anche dall'imaging con microscopia confocale. Infine, il destino intracellulare dei lipoplessi generati nella composizione 1:1 HSPC/DOPE è stato studiato misurando la sua colocalizzazione con compartimenti acidi come endosomi tardivi e lisosomi mediante microscopia confocale. I nostri risultati hanno mostrato una colocalizzazione limitata dei lipoplessi con i compartimenti acidi entro 8 ore, suggerendo che il DOPE sta innescando la fuga endosomiale dei lipoplessi con conseguente elevata efficienza di silenziamento.

4. INTRODUCTION

4.1. Gene therapy: on overview

Gene therapy is a medical treatment approach with the potential to have a huge impact on human health in the twenty-first century. The US Food and Drug Administration (FDA) defines gene therapy as a technique that alters a person's genes to treat or cure diseases, and suggests several working mechanisms[1]:

- Using a healthy copy of the gene to replace a disease-causing gene
- Knocking down a disease-causing gene that is not functioning properly
- Delivering a new or modified gene into the body for the treatment of a disease.

In general, there are two types of gene therapy: germline gene therapy and somatic gene therapy. The distinction between these two procedures is that in somatic gene therapy, genetic material is delivered into some target cells, but the alteration is not transmitted to future generations. In germline gene therapy instead, the therapeutic or changed gene is carried down to future generations. This distinction is significant since the present ethical and medical regulations only permit gene therapy on somatic cells[2]. There are 3 types of somatic gene delivery systems: in vivo, in situ and ex vivo delivery. In vivo and situ delivery is applied by directly transferring the genetic material to the patients. In the in vivo delivery, the vectors are administered systemically in the blood circulation or the cerebrospinal fluid of the patient, while in the in situ delivery the vectors are injected directly into a specific organ through direct injection, e.g., into the tumor in case of melanoma[3]. The ex vivo delivery approach includes the transfer of the genetic materials into the explanted target (e.g. bone marrow) which occurs ex vivo and then the genetically modified tissue is transferred to the patient[4].

Gene therapy can be used in the treatment of a variety of conditions in addition to genetic disorders[5]. To date, cancer has been the most commonly treated condition with gene therapy. It accounts for more than 60% of all ongoing clinical gene therapy trials worldwide, with monogenetic and cardiovascular disorders following closely after[2].

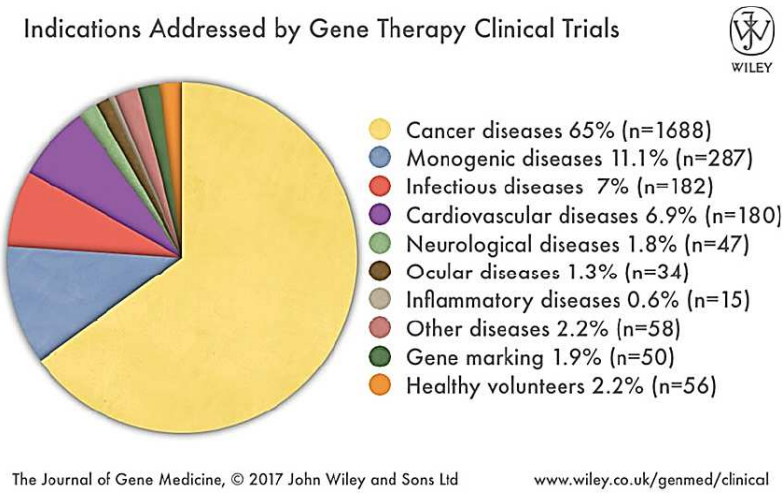

***Figure 4.1**. Graphical presentation of different indications that have been addressed by gene therapy in clinical trials[6].*

Gene delivery refers to the process of introducing genetic materials such as DNA or RNA into the host cells to yield a therapeutic benefit[7]. DNA is found in the nucleus of cells and is responsible for genetic information storage, while mRNA is a type of RNA that is transcribed from a DNA template that works as an intermediate between DNA and protein. In the 1990s, protein expression was achieved by directly injecting DNA or messenger RNA into the target organ, resulting in the blooming of the NA-based vaccine investigation. In 2003, the first commercialized gene therapy, Gendicine (human recombinant p53adenovirus), was approved by China Food and Drug Administration (CFDA) for head and neck squamous cell carcinoma[8]. Being an adenoviral-mediated gene therapy system, Gendicide encouraged the investigation and exploitation of viral vectors for gene delivery. Indeed, in 2017, Luxturna, an adeno-associated virus-based DNA therapy was approved by FDA for individuals with vision loss[9].

Plasmid DNA and viral DNA have been commonly investigated in the following decades, while messenger RNA was underutilized due to its poor stability and high manufacturing costs. Those limiting factors have been over the year overcome with different approaches and mRNA-based therapy has attracted attention and has been intensively explored in the fields of protein therapy, cancer immunotherapy, and vaccination[10]. Today, mRNA-loaded lipid nanoparticles (LNPs) for intracellular delivery of nucleic acids have revolutionized vaccine research and development. They enable the quick development of potential antigens for preclinical testing, elicit significant humoral and cellular immune responses, and provide a uniform platform for vaccine production[11]. Very recent examples of these systems are the Pfizer/BioNTech and Moderna mRNA vaccines that were approved for immediate use less than a year after COVID-19 arose, highlighting the mRNA platform technology's development speed and efficiency[12].

Gene therapy also includes the strategies of nucleic acid delivery for the modulation of mRNA biosynthesis and translation steps. Antisense oligonucleotides (ODN), ribozymes, and RNA interference (RNAi) are currently used to silence the expression of a target gene. Antisense oligonucleotides (ASO) are commonly investigated after their discovery by Stephenson and Zamecnik in 1978[13]. ASOs were first used in the treatment of tumors, but the antitumoral effect was not well understood and activity differed depending on their size and structure[13]. ASOs are short sequences of DNA or RNA that are complementary to messenger RNA (mRNA) sequences and function by forming a double-stranded stretch when they hybridize with the mRNA. An RNA-DNA duplex is formed in the case of DNA ODNs, which is recognized by an RNAse and degraded. Although this process has been successful in vitro, in vivo applications are limited due to a lack of an appropriate delivery mechanism.

Ribozymes are catalytically active RNA molecules with three helices that trans-esterify or hydrolyze single-stranded regions of their own or other RNAs. Ribozymes have not been extensively studied for therapeutic applications due to their short serum stability of seconds to minutes[14].

Eventually, the exploitation of small interfering RNA (siRNA) for RNAi and gene silencing is quickly becoming the new paradigm for gene downregulation, with reports claiming that siRNA is 1000 times more effective than antisense ODNs at silencing target genes[15]. The use of siRNA and RNA interference will be further discussed in *section 4.2.*

4.1.1. Routes of gene delivery

Different administration routes to control the in vivo fate of viral and non-viral vectors have been exploited. The selection of the carrier of course has to be carefully associated with the administration route. The accessibility of vectors to target organs/sites/cells varies significantly depending on the administration route. As a result, choosing the correct administration route is crucial[16].

- *Parenteral delivery:* Intravenous administration of nonviral gene delivery systems is a well-studied route of administration. This approach has been largely investigated to treat many cancer types and especially disseminated cancer diseases. As a result, current cancer gene delivery systems that are administered intravenously should be able to deliver the genetic cargo to target cells and thus targeting is a required feature of this family of therapeutic systems[17].

- *Oral delivery:* while the parenteral administration route of nucleic acid-loaded carriers has shown the efficiency of delivery to target tissues, this approach can only be pursued in a clinical setting. Furthermore, being invasive, the parenteral administration reduces patient compliance, and it can induce unwanted off-target effects due to systemic administration. Oral delivery, on the other

hand, can improve patient compliance while also making administration easier. However, it can only be considered for a local treatment at the intestinal epithelium since systemic absorption is negligible. Indeed, oral administration of nucleic acid-loaded carriers allows for transfection of cells in a large surface area (i.e. the intestinal epithelium) and holds an advantage for the treatment of intestinal diseases[18]. For example, siRNA-loaded nanoparticle-in-microsphere oral systems (NIMOS) have shown successful gene silencing in inflammatory bowel disease that leads to a reduction of colonic levels of TNF-α, suppression of expression of other pro-inflammatory cytokines (e.g., interleukin (IL)-1β, interferon (IFN)-γ) and chemokines (MCP-1), an increase in body weight, and reduced tissue myeloperoxidase activity, suggesting a potential treatment for this disease[19]. The gastrointestinal tract, specifically the intestine, is rich in a diversity of immune cells, including antigen-presenting dendritic cells (DCs) and macrophages, and also a variety of T cells and B cells, making the oral delivery an appealing target for DNA vaccine delivery[20]. One strategy to improve the efficiency of oral vaccines is to functionalize nanocarriers to improve their transcytosis from the intestinal lumen to immune cells that is present in sub-epithelia. Indeed, in mice and pigs, functionalizing plasmid DNA-containing PLGA microparticles with Ulex europaceous agglutinin (UEA-1) to preferentially target M cells resulted in increased systemic IgG and mucosal IgA responses when compared to non-targeted particles[21].

- *Pulmonary delivery:* Pulmonary delivery offers a non-invasive method of delivering biomacromolecules such as therapeutic genes. Several pulmonary genetic diseases, such as cystic fibrosis and alpha-1 antitrypsin deficiency, and inflammatory diseases such as asthma, emphysema, transplant, radiation-associated damage, and pulmonary alveolitis and fibrosis may benefit from gene therapy. Moreover, cancer gene therapy is a hot topic, and genetic immunization for cancer and infectious diseases in the lungs is also being studied[22]. Reduced systemic side effects, absence of interaction with serum proteins, and the ability to reduce the dose of topically administered formulations are all advantages of local pulmonary gene delivery. Efficient gene delivery systems, on the other hand, must first overcome anatomical, physical, immunologic, and metabolic barriers in the lungs[23]. Polymeric nonviral vectors for pulmonary gene transfection have been commonly investigated. Especially for the treatment of pulmonary diseases, lung in situ administration via inhalation is preferred due to reduced administration dosages, side effects, and enhanced therapeutic effects [24]. PEI-nucleic acid polyplexes were also used to generate nano-embedded microparticle (NEM) powder to achieve a suitable aerodynamic diameter for deep lung deposition. NEMs were produced by spray drying using trehalose as a stabilizer and resulted in an average size of 1-5 μm. Redispersed particles performed similarly to or better than polyplexes that were not spray-dried when tested for cellular uptake and transfection in vitro with lung adenocarcinoma cells field[25]. Aerosolized lipid nanoparticles (LNPs) with different phospholipid compositions were also suggested for the pulmonary

delivery of mRNA. LNPs showed encapsulation efficiency higher than 80% by virtue of the presence of ionizable lipid DLin-MC3-DMA and at least 14 days of storage stability at 4 °C. Optimized LNPs were characterized by high intracellular protein expression in vitro and even after aerosolization. In vivo studies were carried out by the administration of luciferase encoding mRNA loaded in LNPs and showed that luciferase protein was predominately expressed in the mouse lung before and after nebulization, suggesting that LNPs have the potential to be used for pulmonary mRNA delivery via aerosolization[26].

- *Intranasal delivery:* Intranasal administration allows therapeutic biomolecules to be delivered to the brain without having to cross the blood-brain barrier. Although the mechanisms by which intranasally administered substances enter the CNS are not completely understood, mounting evidence suggests that substances can enter the brain via a combination of perineuronal, perivascular, and lymphatic transport pathways. Furthermore, the predominant nose-to-brain pathway will be largely affected by the region of the nasal cavity where the formulation distributes upon administration, as well as the physicochemical properties of the drug and the carrier being administered[27]. Gene therapy by nasal administration route has been investigated to modulate various genetic factors correlated to neuronal and brain disorders. Huntington's Disease (HD) is a hereditary neurodegenerative disease caused by the production and accumulation of misfolded protein (huntingtin, HTT) in neuronal cells caused by a mutated HTT gene (mHTT), resulting in progressive neuronal damage and degeneration. In a recent study by Sava et al, anti-HTT siRNA-loaded chitosan-based nanoparticles were prepared by the polyelectrolyte complexation method and their efficiency was evaluated on the YAC128 transgenic mouse model of Huntington's Disease. Their results showed that chitosan nanoparticles successfully protected anti-HTT siRNA from degradation and upon intranasal administration siRNA loaded nanoparticles provided about a 50% decrease in HTT mRNA expression, suggesting a promising approach for HD[28].

- *Ocular delivery:* Over the last few decades ocular gene therapy has been investigated for a wide range of inherited retinal disorders (IRDs), nonhereditary retinal degenerations, and acquired, multifactorial retinal diseases that necessitate frequent, repeated intravitreal injections (IVIs). The eye is an appealing organ for gene therapy research. To begin with, since local administration is applied intravitreally, the eye only requires a small dose of therapeutic material. Second, the blood-ocular barrier, which is made up of retinal pigment epithelium (RPE) and retinal vascular endothelial cells, creates an immune-privileged environment that may limit the host immune response and systemic exposure upon intraocular administration. Finally, a variety of high-resolution, non-invasive imaging modalities can be used to quantify therapeutic responses in the retina and choroid[29]. Today, many siRNA-based drugs are in clinical investigation mainly for the treatment of age-related macular

degeneration (AMD)[30,31], glaucoma[32,33], ocular pain and dry eye disease (DED)[34,35]. Ocular disease treatment requires local administration since the retina and vitreous limit the biodistribution of nanocarriers upon systemic administration due to the blood-retinal barrier (BRB)[35].

4.1.2. Challenges in gene delivery

Gene delivery is a multistep process that starts with the administration of the nucleic acid cargo, locally or systemically, followed by cellular uptake, and ends with arrival to the target site; cytosol, or nucleus, depending on the aimed treatment[36]. Considering this, the gene therapy process is a multi-step process, that can be separately investigated and improved. In general, limiting factors in gene therapy is investigated under 2 general class: extracellular and intracellular barriers.

4.1.2.1. Extracellular barriers

Extracellular barriers refer to any factor that prevents nucleic acid from reaching target cells following its administration. The access through extracellular barriers depends on the cells to be targeted and the delivery route of the system. For example, the effect of extracellular barriers was found to be significantly lower after local DNA administration by direct tissue injection compared to the systemic DNA delivery after intravenous injection[37].

- *Degradation by nucleases:* Upon systemic administration, therapeutic NAs are easily degraded by nucleases, leading to fast renal clearance and short half-life[38]. Almost 70% of the administered ASOs can degrade in 1 minute, resulting in low gene silencing[39]. Several chemical modification techniques, such as the conjugation of bases, sugar, and chemical modifications of the backbone, phosphodiester linkage modifications, or the use of synthetic nucleotides, have been used to enhance the stability of therapeutic NAs, resulting in an enhancement in therapeutic efficiency[40]. Furthermore, the employment of the carrier systems such as lipoplexes or polyplexes can also provide protection against nucleases.

- *Opsonization:* Mature macrophages residing in the reticuloendothelial system (RES), such as the liver, spleen, and lungs, phagocytose oligonucleotides after they are administered into the systemic circulation[41]. PEGylated colloidal systems can be employed to minimize RES clearance by adjusting surface coatings and using different PEG molecular weights, chain densities, and conformations to produce a vehicle with opsonin-avoidance properties. The use of the PEG has also received regulatory approval due to its lack of toxicity and immunogenicity, making it a very appealing component in the design of gene delivery systems[42]. Indeed, in a study conducted by

Eliyahu et al, PEGylation was shown to reduce the hemolytic activity and erythrocytes aggregation caused by lipoplexes (i.e. NA loaded liposomes with the cationic surface)[43].

- *Glomerular filtration:* Rapid kidney excretion of 'free' oligonucleotides or small conjugates is a significant limitation in ON delivery. Molecules with a molecular weight of less than 5000 Da are rapidly filtered by the glomerulus and accumulate in the urine in the absence of re-uptake. This limitation can be overcome by the size manipulation of the ONs, for example, the macro molecularization by PEG conjugation, or by using a suitable nanocarrier to load the ONs[44]

- *Endothelial barrier:* Upon systemic administration, oligonucleotides must cross the vessel endothelium before reaching the tissue parenchymal cells; the endothelial cells that line the vascular lumen act as a barrier for their passage. Endothelial cells form tight intercellular junctions with very small intercellular spaces by tightly adhering to the underlying extracellular matrix via integrins and to each other via several adhesion molecules. To facilitate ONs passage across the endothelial layer, cell-penetrating peptides, targeting ligands, or molecular conjugates can be used[45].

Finally, to be effective, NAs must be delivered to the cytosol or nuclei within the target cells. To deliver the ONs into the target cells, passive and active targeting methods can be employed[46]. Passive targeting, which is based on the enhanced permeability and retention (EPR) effect, was first outlined by Matsumara and Maeda in 1986[47]. Passive targeting occurs in virtue of the leaky vascular and defective lymphatic drainage that is typically found in tumors and allows biodistribution and accumulation in the tumoral tissues. Today several products on market such as Doxil™, Abraxane™, Marqibo™, and DaunoXome™ are passively targeted to the tumor according to this mechanism[48].

The strategy based on active cellular targeting requires that the drug delivery systems are decorated with ligands to increase the affinity to target cells, which promote cell uptake, and importantly, reduce the migration of the carriers back to the systemic circulation. Selection of the ligands is made based on the overexpressed receptors on the target cells[49]. Even after a successful target ONs face cellular internalization limits since cell membranes are impermeable to ONs due to their large size, negative charge, and hydrophilic features which prohibit the simple diffusion across the biological membranes. Attempts have been made to promote intracellular delivery of the NAs, such as using physical techniques and viral/non-viral vectors[50]. These approaches will be further discussed in *section 4.3.*

4.1.2.2. Intracellular barriers

- *Endo/lysosomal degradation*: After internalization by endocytosis, nucleic acid cargo traffic into the early endosomes. The luminal pH of endosomes is gradually lowered to 5.5 by vacuolar ATPase proton pumps that actively transport protons into the early endosome (which has a slightly

acidic pH of 6.3) that matures into the late endosome. Finally, the late endosome fuses with the lysosome (pH 4-5), and lysosomal enzymes degrade the intraluminal contents (Figure 4.2)[51]. NA cargo/carrier system must escape these intracellular vesicular compartments to avoid degradation in the lysosomes and reach the cytosol to provide for the desired biological activity. Endosomal escape into cytosol represents one of the major intracellular barriers to efficient NA delivery.

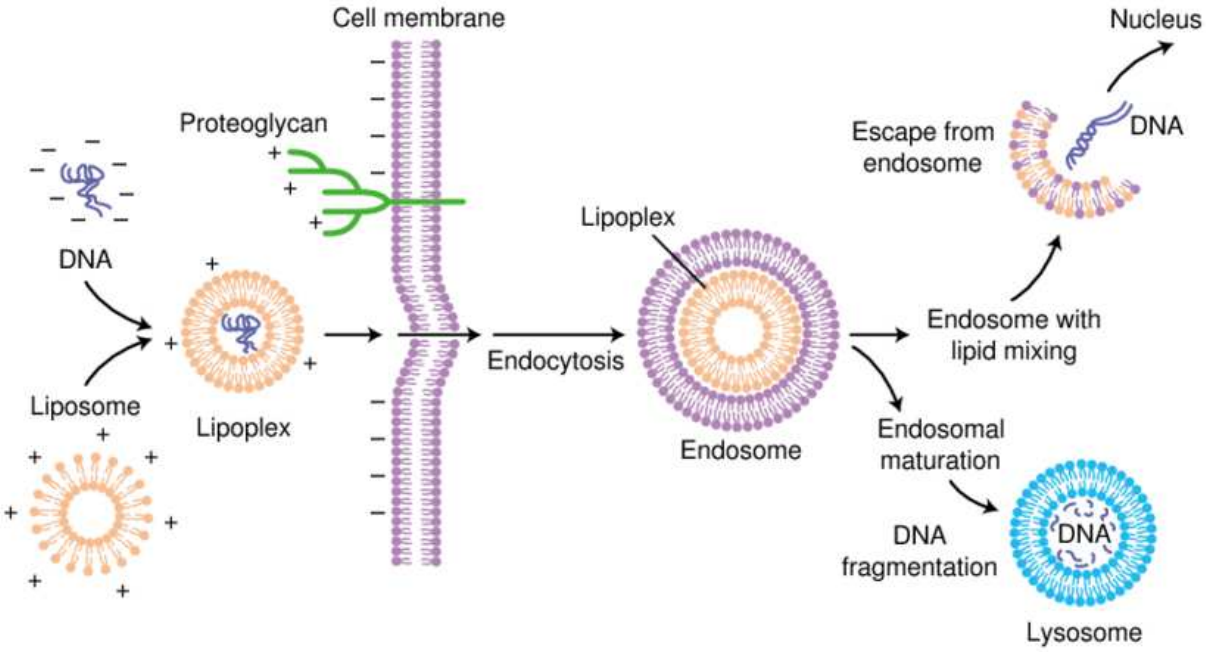

Figure 4.2. *Summary of the steps involved in lipoplex-mediated transfection at the cellular level.*

Different mechanisms have been suggested for NA's escape into the cytosol:

i) Endosomal membrane fusion: Indeed, viruses have been identified in early times as natural carriers possessing intrinsic mechanisms for endosomal escape and intracellular release of their cargo. The virus can fuse with the cell membrane or the endosomal membrane. Conformational changes in the viral proteins cause fusion between the viral capsid and the cellular membranes. Interaction with specific cellular receptors or the exposure to a change of the pH occurring in endosomes can trigger this conformational change[52]. Depending on the protein of the capsid the mechanism can vary but the basic principle for the fusion is the conformational change of the capsid protein into a rodlike structure upon exposure to the triggering condition, such as pH change. Following this change, the fusion protein folds back on itself, thus leading fusion protein and its transmembrane domain into close contact. Further interaction of the viral capsid protein and the host cell membrane causes the pore formation and cytosolic release[53].

The mechanisms for endosomal escape have been largely studied to transfer the mechanism onto synthetic carriers. One approach to promote endosomal fusion is the employment of synthetic fusogenic peptides. Until today, many synthetic fusogenic peptides were synthesized to mimic the fusogenic part of viruses and have been used for the decoration of lipoplexes or polyplexes to promote their endosomal escape[15]. One successful example is influenza hemagglutinin-derived fusogenic peptide decoration of the commercially available Lipofectamine. Cationic lipids decorated with peptides have shown up to 3.5 higher silencing efficiency compared to the not decorated formulation[54]. The hydrophobicity of fusion peptides is a shared characteristic that is provided by specific amino acids such as tryptophan (Trp), alanine (Ala), and also glycine (Gly). Their mechanism of action is based on the interaction between the aromatic residues' side chains of the amino acids with the lipids of the target cells, promoting pore formation and endosomal escape[55].

Lipid-based carriers for NA delivery can also be engineered by including functional components that contribute to endosomal escape. Fusogenic lipids in lipid-based nanocarriers interact with the endosomal membrane-like viruses, releasing nucleic acid in the cytosol. Anionic, and zwitterionic lipids with a cylindrical molecular shape self-organize in a bilayer lamellar structure when dispersed in water. The inverted non-bilayer hexagonal phase is formed when cationic and anionic lipids combine to form ion pairs and adopt a cone shape. Cone shape assemblies thus induce the conversion of the bilayer into a non-bilayer phase such as the hexagonal phase. This process primes the membrane fusion of the liposomes with the endosomal membrane resulting in the cytosolic NA payload release[56]. In lipid-based nanocarriers, one of the commonly used helper lipids is 1,2-dioleyl-sn-glycerol-3-phosphoethanolamine (DOPE, Figure 4.3. Indeed by transitioning from the bilayer structures to inverted hexagonal structures in the low endosomal pH, DOPE controls the fusion process[57].

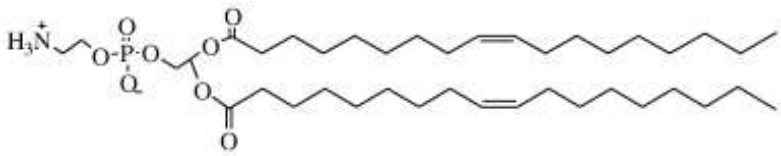

Figure 4.3. *Chemical structure of DOPE*

Biophysical characteristics underlying the process of fusogenicity are that phosphatidylethanolamine (PE), that is the head group of DOPE, unlike the majority of phospholipids, has a minimally hydrated and small headgroup that takes up less space than the respective hydrocarbon chains and possess a cone shape, which makes it meta-stable in a lamellar phase. Once the amino group of PE is protonated, the cationic charge promotes electrostatic intramolecular interactions between the cationic amine group and phosphate groups of the polar headgroups of adjacent zwitterionic or anionic phospholipids, maximizing the formation of cone assemblies which explains why these molecules have

a strong tendency to acquire the inverted hexagonal phase above the phase transition temperature (T_H) (for DOPE the T_H is 10 °C). And also, the Intercalation of amphiphilic molecules with a protonatable acidic group (negatively charged at physiological pH) between PE molecules facilitates electrostatic repulsion and enables the formation of bilayer structures, which leads to liposome formation at physiological pH and temperature. While stable liposomes are formed at physiological pH, acidification (endosomal environment) causes protonation of the carboxylic groups of the amphiphiles, lowering their stabilizing effect and therefore leading to liposomal destabilization, because PE molecules revert to their inverted hexagonal phase under these conditions[58].

ii) The proton sponge effect (pH buffering effect): Certain cationic polymers with a high pH buffering capability over a wide pH range have been observed to exhibit the 'proton sponge' phenomenon. Secondary and/or tertiary amine groups with pKa close to endosomal/lysosomal pH are commonly found in these polymers. The membrane-bound ATPase proton pumps actively transfer protons from the cytosol into the endosomes during endosome maturation, resulting in acidification of endosomal compartments and activation of proteolytic enzymes. Polymers with the 'proton sponge' property will become protonated at this point, preventing endosome acidification. As a result, in an attempt to lower the pH, the ATPase proton pumps will pump more protons into the endosomes to decrease the endosomal pH. ATPase proton pump, transfers protons and chloride ions which increases the osmotic pressure of endosomes and causes water influx. The osmotic pressure increase eventually causes endosomes to swell and rupture, releasing their contents into the cytosol[59].

iii) Membrane destabilization/disruption: The membrane destabilization or disruption model relies on a complex mechanism where either the NA-vector complex or only the vector directly interacts with the internal surface of the endosomal membrane through electrostatic and/or hydrophobic interactions, thus providing local membrane destabilization and permeability increase field[51]. However, since the unspecific destabilization of the plasma membrane decreases the viability of the cells, to minimize the cytotoxicity, the destabilizing effect needs to be activated during the endo/lysosomal pathway[60]. One strategy is to engineer carrier systems that undergo a pH-depended alteration when exposed to the endosomes microenvironment which selectively triggers interaction between the carrier system and the internal surface of the endosomal membrane resulting in the endosomal escape while avoiding cytotoxicity[61,62].

- *Nuclear translocation:* The transport of macromolecules through the nuclear membrane is a crucial step in eukaryotic cell metabolism. The nuclear pore complexes (NPCs), which form an aqueous channel through the nuclear membrane, regulate protein and ribonucleoprotein trafficking. The membrane allows the diffusion of molecules smaller than 40 kDa and 10 nm, while bigger molecules

require specific nuclear localization signals (NLS), thus creating an important bio-barrier to plasmid DNA delivery into the nucleus[63]. More than 40 years ago, the inefficient nuclear uptake of plasmid DNA from the cytoplasm was shown by Capecchi et al. In their study, the transfection efficiency of plasmid DNA encoding the thymidine kinase, injected into the cytosol, was determined to be less than 0.1-0.001 % of the cytosolically injected plasmid DNA[64]. Dividing cells present a significant increase in the nuclear permeability and thus it is considerably more efficient for NA nanocarriers to deliver their cargo including naked DNAs, into the nucleus during cell mitosis. Because most cells in vivo are non-dividing (quiescent), nuclear access for nanoparticles remains a challenge for carrier-based DNA delivery systems[65].

4.2. RNA interference and siRNAs

RNA interference (RNAi) is the regulatory system of many eukaryotic cells, in which small double-stranded RNA (dsRNA) molecules (21-28 nucleotides) are employed to prompt the silencing of specific genes[66]. Soon after the identification of the dsDNA by Andrew Fire and Craig Mello in 1998, these small interfering RNAs (siRNAs) became a widely-used tool in biomedical research due to their potential use in the treatment of many genetic disorders as therapeutic agent[67, 68].

Non-coding RNAs (ncRNAs) are non-protein-coding RNAs that regulate gene silencing, DNA imprinting, and demethylation among other roles and they can be divided into 2 sub-families: Small ncRNAs and long ncRNAs. Small ncRNAs include a broad range of recently discovered non-coding RNAs, including microRNAs (miRNAs) and small interfering RNAs (siRNAs).

Synthetic siRNA has been proposed to silence the translation of RNA into target proteins while leaving endogenous mRNA pathways unaffected. Also, MicroRNAs (miRNAs) have been proposed as therapeutic agents; miRNAs are a sub-type of natural RNA that plays a role in cell differentiation, proliferation, and survival by inhibiting or degrading mRNA translation.

The first step of the RNA interference mechanism of action is the cleavage of longer dsRNAs (> 21 bp) by the RNase III into siRNAs which typically have 2 nucleotide overhang on the 3’ end of both, passenger (sense) and guide (antisense) strands for the recognition by the enzymatic machinery of RNAi[69]. At this step Dicer, an RNAi pathway enzyme is responsible for this transformation and channeling the siRNAs to the RNA-induced silencing complex (RISC)[68]. Upon binding to the RISC, the Argouate (Ago) family of nucleases interacts with the siRNA leading to RNA double-strand unwinding. Eventually, the passenger strand is degraded and the guide strand governs the mRNA degradation, thus inhibiting the mRNA translation process (Figure 4.4)[10, 70].

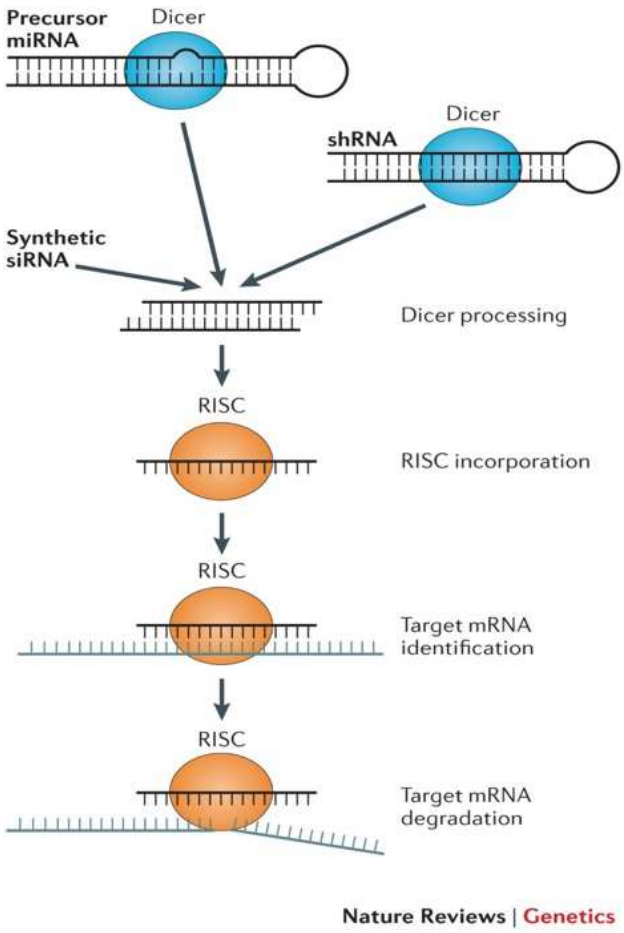

***Figure 4.4**. Gene knockdown mechanism by siRNAs* [71]

Primary studies on the RNAi mechanism of action were performed on nematode C*aenorhabditis Elegans* by Guo and Kempheus that showed the silencing effect of antisense RNA on the PAR-1 gene. Later on, *C. Elegans* was used by Fire and Mello, to show a specific reduction in gene expression with dsRNA introduction[72]. In 2001, Tuschl et al, have shown that siRNA-mediated gene silencing can provide suppression of endogenous and heterologous genes in mammalian cells[73].

Concerning their activity, antisense strands of the siRNAs can remain stably associated n RISC for several weeks and suppress the mRNA translation for several weeks in both dividing and non-dividing cells. Although the siRNA intracellular concentration decreases as cells replicate, in virtue of its catalytic activity that participates in sequential cleavages, only a small amount of cytosolic siRNA is needed for gene knockdown which makes the delivery challenge feasable[71].

4.2.1. Application of RNAi

RNAi is a powerful biological molecular tool for the inhibition of gene expression. It can be used for the regulation of abnormal protein expression in a variety of biological targets, including those that are difficult to control by using classical small molecules or proteins. Indeed, the expression of specific genes is dysregulated in several diseases such as hepatitis, cardiovascular diseases, and cancer, therefore, the employment of the RNAi holds great potential within modern medicine[74].

The first RNAi-based therapeutic molecule, Patisiran (Onpattro®), is a siRNA-based drug that was approved by the FDA in 2018 for the treatment of hereditary transthyretin amyloidosis (hATTR) with stage 1 or 2 polyneuropathy[67, 75]. Patisiran targets the mutated transthyretin (TTR) gene, that encodes the dysfunctional transthyretin protein. By targeting the mutant mRNA in the liver, siRNA prevents the production of dysfunctional transthyretin protein, its misfold and degradation products, and finally its deposition in the nervous system, heart, and other organs. Patisiran is delivered upon formulation in lipid-based nanocarriers that protect the RNA against degradation and facilitate its delivery to hepatocytes[76].

Following FDA approval in November 2019, Givosiran (Givlaari®) became the second approved siRNA product. Givosiran is used to treat acute hepatic porphyria, a genetic disease in which a genetically mutated replicate of aminolevulinic acid synthase (ALAS1) is involved in an early step of heme production and induces a buildup of porphyrin molecules. Givosiran decreases blood levels of aminolevulinic acid, porphobilinogen, and neurotoxic intermediates responsible for the disease symptoms in patients. Givosiran lowers the translation of the mRNA encoding ALAS1. Unlike Patisiran formulation, Givosiran was not formulated in lipid-based nanocarrier, rather the siRNA was conjugated to N-acetylgalactosamine (GalNac) which was selected as a targeting agent to bind the asialoglycoprotein receptor (ASGPR) on the hepatocytes and receptor binding of GaINAc moiety[77].

In 2020, Lumasiran (Oxlumo®) was approved by the FDA for the treatment of primary hyperoxaluria type 1 (PH1). PH1 is caused by a mutation in the serine-pyruvate aminotransferase gene, which results in inadequate glyoxylate removal from the liver, thus renal and bladder stones formation, as well as kidney damage. Lumisiran shows its effect by inhibiting oxalate synthesis in the liver by targeting the mRNA for glycolate oxidase, which reduces the amount of glyoxylate available for oxalate production. Similar to the Givosiran formulation, also the delivery of Lumisiran was pursued by the GAINac moiety conjugation to target the liber[78]. Some examples of the ongoing clinical trials for the siRNA drugs are shown in Table 4.1[79].

Table 4.1. *Examples of siRNA drugs in clinical trials*

siRNA drug	Formulation	Target	Disease
Atu027	siRNA with 2'-O-Me and cationic lipid	Protein Kinase N3	Advanced solid tumors (metastatic pancreatic cancer)
ALN-RSV	Lipid nanoparticles	VEGF gene and kinesin spindle protein gene	Solid tumors (liver metastasis from colon cancer)
DCR-MYC	Lipid nanoparticles	Myc	Hepatocellular carcinoma
siRNA EphA2-DOPC	DOPC liposomes	Ephrin type-A receptor2 gene	Advanced cancers

4.3. Gene delivery strategies

The main limitation of NA-based therapeutics is to deliver the active molecule to its site of action in the cytosol or nucleus of the cells. A variety of strategies are being investigated to overcome these limitations. Depending on the vector type, gene delivery systems can be classified under 3 major categories: viral, non-viral vectors, and physical methods (Figure 4.5). Regardless of the type, an ideal system is expected to protect genetic payload against degradation by nucleases in the extracellular environment, deliver the cargo into target cells by crossing cellular membranes, and should not have adverse effects; it is expected that the therapeutic treatment improves healthy functions, correct deficiencies, or inhibit disease-causing activities[80,81].

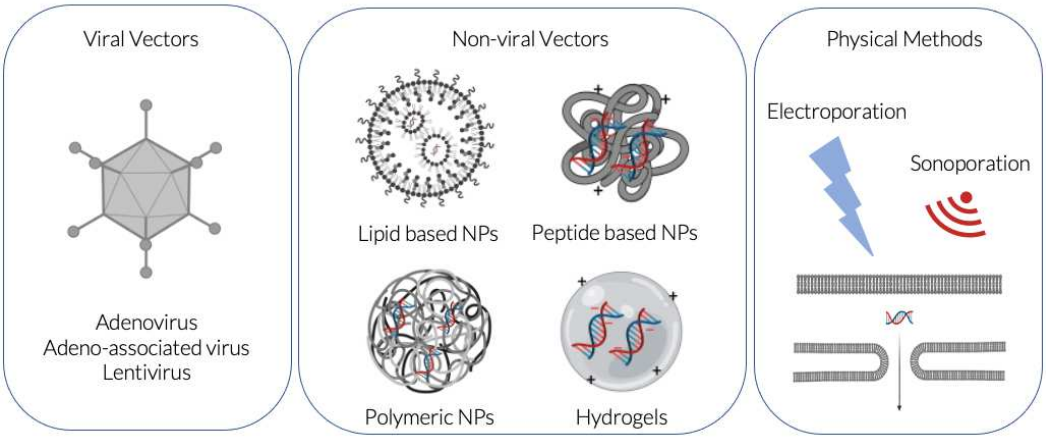

Figure 4.5*. Examples of commonly used gene delivery methods*

4.3.1. Physical methods for gene delivery

Although viral and nonviral chemical methods continue to dominate clinical and laboratory research, almost all physical approaches to intracellular delivery have advanced significantly in the last decade[82]. Physical methods allow small and large nucleic acid molecules, as well as any other non-permeable molecule in the plasma membrane, to penetrate directly into the cytosol, which would otherwise be unable to reach the cell cytosol due to the inability to diffuse through the plasma membrane or inability to be actively transported across the plasma membrane. Some of the physical methods include gene gun, jet, and hydrodynamic injections, sonoporation, magnetoporation, electroporation[83].

Electroporation is one of the most extensively investigated physical techniques which is based on pore formation on the cell membrane as a result of the potential difference applied across the membrane[84]. In a recent study, electrophoration has been found to promote the expression of minicircle DNA carrying HIV-a gag gene[85]. Although electroporation provides site-specific delivery of the ONs, it suffers from high cellular mortality[45]. Sonoporation is another promising method for the successful delivery of genetic material. Although the exact mechanism is not fully understood, previous experimental and theoretical analysis refers to pore formation due to the generation and collapse of nanobubbles upon local irradiation with ultrasounds[86]. In the study by Kida et al, lipid-based nanobubbles were found to successfully induce gene transfection both in vitro and in vivo upon the ultrasound-mediated sonoporation[87]. Sonoporation provides a non-invasive and site-specific delivery but it results in low transfection[45].

Physical methods can also be used in combination with non-viral vectors. A recent example is the employment of light activation of iron-oxide nanoparticles combined with PLGA nanoprojectiles for promoting intracellular macromolecule delivery in mammalian cells. In this study, using an intense laser pulse, iron-oxide nanoparticles are heated up which causes the evaporation of the surrounding water and the formation of vapor bubbles (VB). Upon the collapse of VBs, PLGA nanoprojectiles are scattered in the medium and those shot towards cells create pores in the cell membranes, thus allowing the delivery of mRNA and pDNA present in the medium. The transfection efficiency of the system was found to be 5.5-7.6 folds higher than the electroporation method[88].

4.3.2. Viral vectors

Viral vectors have found their application in gene therapy by efficiently delivering nucleic acids to specific cell types while evading detection by the host's immune system. Indeed, viral vectors are the

most selective and efficient delivery systems for large NA materials. Several types of viral vectors have been generated, including adenovirus, adeno-associated virus (AAV), retrovirus and herpes simplex virus, lentivirus, poxvirus, alphavirus, and baculovirus[89, 90]. Viral vectors are constituted by three components: (1) the protein capsid and/or envelope that encapsulates the genetic payload and dictate the vector's tissue or cell tropism and receptor recognition; (2) the transgene of interest, which provides the desired effect in the cells; and (3) the "regulatory cassette," which consists of a combination of enhancers, promoters, and auxiliary elements that control the stable or transient somatic expression of the transgene as a whole[91]. In general, viral vectors contain powerful promoters that are responsible for heterologous gene expression at high levels. The nucleic acid composition of each virus dictates the mode of gene expression to a great extent. In this regard, viruses with single-stranded RNA genomes, like alphaviruses, display a rapid initiation of transgene expression while also demonstrating their temporary nature. Retroviruses with a double-stranded RNA genome can also exploit chromosomal integration to establish long-term expression. Furthermore, herpes simplex virus-based viral vectors often cause a latent infection, in which the viral genome persists in host cells without causing any obvious harm[90].

In 2012, the European Medicines Agency has approved the use of the world's first AAV-based gene therapy, Glybera (alipogene tiparvovec) for the treatment of lipoprotein lipase deficiency in adults[92]. Later on, in 2017 the US Food and Drug Administration (FDA) approved the second AAV-based vector, Luxturna, a gene therapy used for the treatment of a rare form of inherited blindness.

Although the efficiency of viral vectors has been well established, they might be associated with several drawbacks such as immunogenicity, carcinogenicity, poor targeting specificity, incapacity to transfer large size genes, production cost and difficulty, and limited possibility of recurring administration caused by acute inflammatory response[93, 94].

4.3.3. Non-viral vectors

Potential risks with the viral vectors have led to the discovery and development of non-viral vectors. Indeed, non-viral vectors offer several advantages such as low immunogenic response, safety, high gene capacity, stability, and chemical design flexibility. Moreover, the production of the components and the assembly of non-viral vectors on a large scale is relatively simple. Non-viral vectors are in principle not limited by the molecular size of the genetic material to be loaded[95]. However, non-viral vectors suffer from low and transient transfection efficiency. Currently, many approaches including chemical modifications and surface decoration with targeting ligands and peptides are employed to increase the transfection efficiency of the non-viral systems[96].

Commonly investigated non-viral gene delivery systems are:

- *Polymeric nanoparticles:* one of the most commonly used non-viral gene delivery systems is the polymeric nanoparticles (PNP) or polyplexes. Polyplexes possess a spherical shape and sizes of about 50-1000 nm. Bearing a cationic polymer in their structure, PNPs can easily condensate the nucleic acids, resulting in the polyplexes that protect the NAs from degradation and deliver them into the cytosol[97]. Polymeric non-viral vectors have shown to be more effective, less cytotoxic, and immunogenic than viral systems. Polymeric vectors also allow for scale-up production while adhering to good manufacturing practices. Furthermore, in terms of loading efficiency, the gene-packaging capacity of synthetic polymeric nonviral vectors is much higher than viral vectors[23]. Some of the commonly used polycationic polymers to assemble polyplexes include polyamidoamine dendrimers (PAMAM), Poly(ethylene imine) (PEI), chitosan, albumin, and many others. These polymers were often combined with neutral or anionic polymers to modulate the physicochemical and biological features of the resulting carriers. First-generation cationic polymers such as polylysine and polyarginine have shown very limited transfection efficiency and endosomal escape, due to the lack of hydrophobic domain in their structure. Due to the residues of PEI and PAMAM polymers being unprotonated at physiological pH, these polymers are efficient "proton sponges" and have intrinsic endosomolytic activity. Following the endocytosis of PEI or PAMAM polyplexes, the exposure of the polyplexes to the endosomal pH leads to further protonation of the polymers and chloride influx in the endosomes. These events cause osmotic endosome swelling, the destabilization, and rupture of endosomal membranes, and thus endosomal escape to cytoplasm[98].

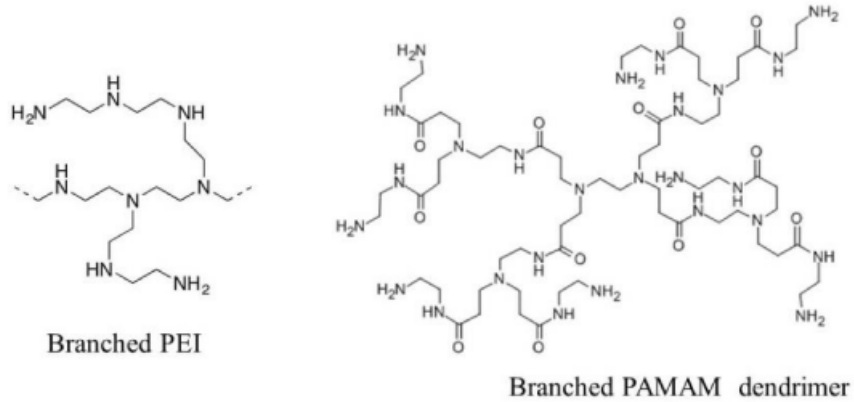

Figure 4.6*. Chemical structure of branched PEI and PAMAM polymers*

PAMAM is a dendrimer that can be linear or branched and consists of repeating amide/amine units. In several studies, PAMAM was used in combination with hyaluronic acid (HA) which can target the carrier to cancer cells overexpressing the CD44 receptor. Chen et al reported that siRNA/PAMAM/HA complexes successfully deliver siRNA into human breast tumor cells, that overexpress CD44[99]. In mice

bearing pulmonary tumors (mouse melanoma B16-F10), Gu et al. showed that incorporation of HA in pDNA/PAMAM polyplexes significantly improved tumor accumulation of pDNA[100]. Like PAMAM, PEI was also combined with HA. Han et al reported that PEI-HA conjugates can efficiently deliver siRNA and antisense ONs into tumor cells without causing toxicity[101].

- *Lipid-polymer hybrid systems:* To combine the advantages of both lipid and polymer-based systems in one carrier, lipid-polymer hybrid systems (LPHS) are generated and have had initial clinical success while overcoming drawbacks such as disassembly, limited blood circulation time, and NA payload leakage. Hybrid systems have the potential to be a reliable drug delivery platform[102] in virtue of their high encapsulation efficiency, well-defined release kinetics, well-tolerated serum stability, and well-triggered targeting properties. LPHS can be generated by different methods which significantly affects the loading efficiency of the systems; thereby, depending on the specific purpose and administration route of the system, the production method should be selected carefully. Some examples of lipid-polymer hybrid systems preparation methods are given in *Figure 4.6*[98]

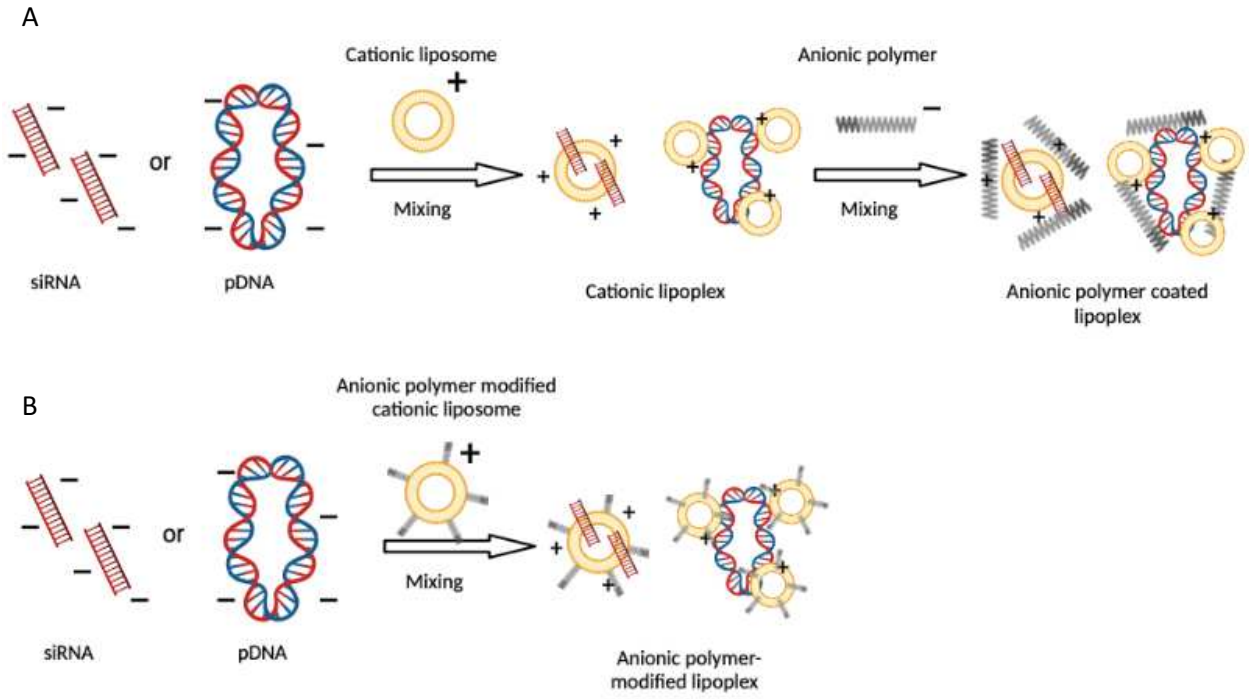

Figure 4.6. *Lipid-polymer hybrid systems are prepared according to multistep procedures: cationic liposomes are first complexed with negatively charged nucleic acids and subsequently coated with an anionic polymer (A), or cationic liposomes are precomplexed with anionic polymers before complexation with nucleic acids (B)* [98]

LPHS has been assembled using cationic lipid BHEM-Chol and PLGA polymers for systemic siRNA delivery using a modified nanoprecipitation method. NPs successfully delivered anti Plk1 siRNA

(targeted against the Plk1 oncogene) to BT474 cells in vitro and to the BT474 xenograft murine model in vivo[103] resulting in the inhibition of the tumor growth.

siRNA-loaded hybrid NPs made of DSPE-PEG, lecithin and newly synthesized cationic lipid G0-C14 and PLGA as polymer were developed for the delivery of siPHB1 to silence the prohibitin 1 expression. Long-term silencing of the prohibitin 1 gene and consequently efficient tumor growth inhibition in vivo (A549 xenograft BALB/C nude mice model) were achieved, which outperformed conventional lipofectamine complexes[104].

In another study, the combination of anionic cholesterol-grafted poly(amidoamine) (rPAA-Chol)/siRNA to DOTAP/DOPE/Cholesterol cationic liposomes provided higher tumor growth inhibition through transferrin receptor-mediated active-targeted delivery compared to the non targeted[105]. All these findings suggest that lipid-polymer hybrid systems can be promising for in-vivo tumor-targeted therapy.

4.4. Lipoplexes as gene delivery systems

Lipoplexes are defined as the complexes between nucleic acids and cationic lipids. Lipids have been used for gene delivery for a long time. Lipids with permanent or ionizable positively charged head groups can form lipoplexes through the electrostatic interaction with the anionic phosphate groups of the nucleic acids. Lipoplexes are commonly found as liposomes, solid lipid nanoparticles or lipid emulsions, due to the self-assembling lipid tail structures. Lipid-based carriers are more biocompatible, generally less toxic, and can load both hydrophilic and hydrophobic substances when compared to polymeric carriers[106].

Cationic SLNs have been proposed as a non-viral vector for gene delivery. The ability of cationic SLN to bind nucleic acids, protect them from DNAse or RNAse cleavage, and successfully deliver them into the cells has been previously demonstrated[107]. Cationic lipids are used in the preparation of SLN for gene therapy applications not only because they provide a positive charge for NA complexation, but also because their surfactant feature is required to set up the initial O/W emulsion, which is one of the conventional formulation techniques for SLN preparation. Cationic SLNs condense nucleic acids on their surfaces through electrostatic interactions; since complete condensation can be achieved at high N/P ratio, this implies an excess of positive charges in the nucleic acid-coated SLN complexes. This offer an advantage for transfection since, while the cationic charges reduce the mobility of nucleic acid associated with the SLN surface thus enhancing protection from environmental enzymes, they allow for interaction with the cell surfaces due to the cationic nature of the vectors[108].

Solid lipid nanoparticles have been employed extensively for the delivery of the siRNA[109, 110] and mRNA by different delivery routes[111]. mRNA-1273 and BNT162b21, two approved COVID-19 vaccines, use lipid nanoparticles to deliver mRNA encoding for COVID-19 capsular antigen. These systems were assembled using a microfluidics-based production method[112]. Many other mRNA-loaded lipid nanoparticle formulations for the prophylaxis and treatment of infecting agents, cancer, and genetic diseases have been developed and are being tested in clinical trials[113, 114]. Lipids, water phase, and surfactants make up the nanoemulsion, which has a droplet size distribution of about 200 nm. Nanoemulsions can be suitably made for gene delivery by including cationic lipids such as DOTAP, DOTMA, and DC-Cholesterol as lipidic components because these lipids will set strong electrostatic interactions with the anionic nucleic acid phosphate groups during the spontaneous assembly of the particles. A recent study employing siRNA-loaded cationic nanoemulsions showed increased in vitro cellular uptake of the siRNA and in vivo tumor reduction in glioma-bearing Wistar rats, suggesting a promising approach for glioblastoma treatment[115].

Cationic liposomes offer several advantages as gene delivery systems. Lipid-based vesicles and particles are a well-studied and clinically exploited drug delivery system that offers high bioavailability, high biocompatibility, extended circulation time, and a variety of targeting options. The physico-chemical features of these carriers allow the encapsulation of therapeutic molecules with diverse features which makes them such a versatile platform. In virtue of their aqueous core and the hydrophobic lipid bilayers. Liposomes can transport a wide range of therapeutic substances: hydrophilic compounds are entrapped inside the aqueous core, while lipophilic compounds are dissolved within the lipid bilayer[116].

The electrostatic interactions between the cationic liposomes and negatively charged nucleic acids can be controlled by changing the lipid composition thus modulating the surface charge density. Surface modification of the liposomes can be easily performed with PEGylation or with the inclusion of functional lipids. Furthermore, cationic liposomes with lipophilic chemical drugs in their lipid bilayers can deliver anticancer drugs and therapeutic nucleic acids simultaneously[117]. Cationic liposomes can be employed for the delivery of various nucleic acids such as plasmid DNA, antisense oligonucleotides, siRNA and mRNA.

In a study by Michel et al[118], cationic liposomes based on DC-Cholesterol and DOPE were generated by the thin-layer hydration method at DC-Cholesterol / DOPE molar ratios of 1:1 to 2:1, as a potential mRNA delivery system. Lipoplexes were characterized by the size of 180 nm, positive surface charge, low cytotoxicity and immunogenicity, and also high encapsulation efficiency, storage stability, and hemocompatibility. In-vitro cellular studies on A549 (adenocarcinoma human alveolar basal epithelial

cells) showed the successful transfection and long-acting transfection effect on cells which resulted in prolonged protein production, suggesting a safe and efficient delivery of the mRNA. In another study, liposomes were employed as a scaffold to generate lipoplexes loaded with siRNA; different cationic lipids, namely DOTAP and DC-Cholesterol and different ratios of helper lipids (DOPE and cholesterol) were used to investigate the effect of the lipid composition on physicochemical properties and endosomal escape efficiency of the formulations. Cationic liposomes with each lipid composition provided similar and high transfection efficiency by virtue of the high cationic charge provided by the cationic lipids. Differences in mRNA-mediated knock-down efficiency were observed, even though the transfection rate was similar for each formulation. Liposomes containing 50% DOPE resulted in an mRNA silencing rate of about 80%[119].

4.4.1. Preparation methods of the lipoplexes

Liposomes are classified based on their structure, size, preparation method, and composition; these features can be modulated depending on the liposome's therapeutic purpose, administration route and the type of molecule to be encapsulated. Different laboratory-scale liposome preparation techniques have been established and optimized in the past decades[120]. Production methods include the simple mixing of preformed cationic liposomes with NA aqueous solution (Figure 4.7, Panel A). Cationic liposomes prepared with different compositions by simple mixing with NA were found to efficiently provide gene silencing[121,122, 123]. Unfortunately, this technique cannot be employed for liposomes with high PEG density since PEG can reduce the NAs association to the outer surface and the electrostatic interaction can be weakened by PEG making them prone to instability and premature release[124]. Even though PEG sterically prevents the NAs from associating to the cationic liposomes, the PEGylation of lipoplexes is desired for RES evasion, prevention of protein corona formation, and aggregation in the bloodstream. Decoration of lipoplexes after the association of cationic liposomes with NAs can be a simple option to make PEGylated lipoplexes[125]. With this aim, PEG-DSPE micelles are incubated at temperatures varying between 25-55 °C with non-PEGylated NA/liposome complexes for the insertion of the lipid anchor of the DSPE into the liposomal bilayer (Figure 4.7, Panel B). The degree of the PEG insertion into the cationic liposomes then can be easily confirmed by looking at specific features including the zeta potential, which should decrease due to the PEG shielding of the surface charges[124, 126].

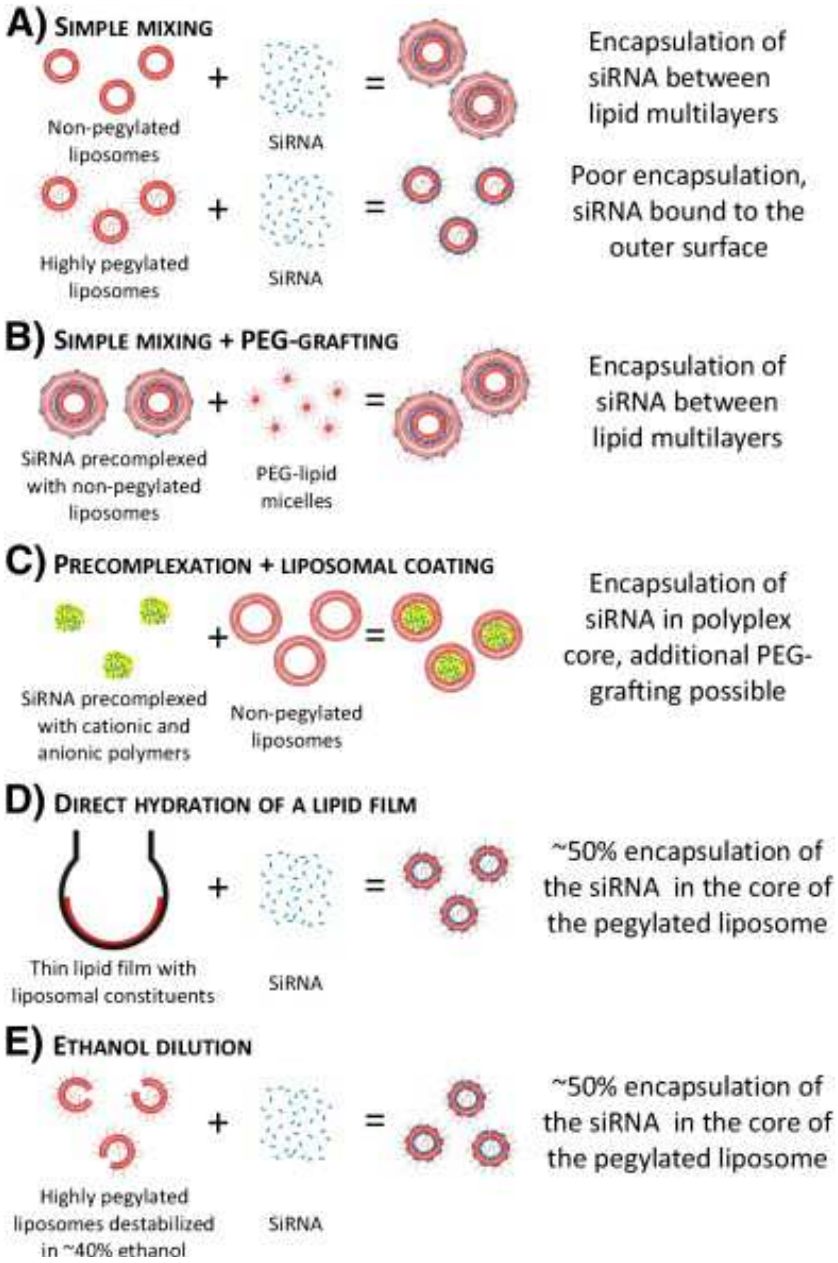

Figure 4.7. *Schematic representation of the NA-cationic liposome complex preparation methods*

Precomplexation of NA with cationic polymers and subsequent entrapment in liposomes before PEG-grafting is another method of generating lipoplexes, more precisely lipopolyplexes (Figure 4.7, Panel C). Nucleic acids can be complexes with cationic polymers such as protamine and mixed with higher molecular weight polyanions, such as hyaluronic acid, at different molar ratios resulting in negatively charged nanoparticles[127]. Then anionic polyplexes are incubated with cationic liposomes to provide the entrapment into liposomes. As a similar approach, NA can be condensed with protamine in the absence of high molecular weight anions, and the resulting cationic complexes formed can then be used to rehydrate lyophilized anionic liposomes[128].

The thin-film hydration (TFH) method followed by extrusion through suitable membranes is another simple approach to generate lipoplexes is very popular for small-scale production in a research laboratory (Figure 4.7, Panel D). This method involves removing the organic solvent where a lipid mixture is dissolved in a round-bottom flask to form a thin lipid film. Multilamellar vesicles (MLVs) are formed when the aqueous solution containing NAs is added and agitated. Finally, homogeneous small or large unilamellar vesicles (SUV and LUV) are obtained after extrusion through polycarbonate membranes with selected cut-off pore size[129, 130].

The TFH method to generate cationic liposomes implies that the cationic lipids present in the dried lipid film are evenly distributed both in the inner and outer surface of the lamellar vesicles, allowing for the incorporation of NA mostly into the aqueous core of liposomes while a fraction of NA may be surface associated[131]. In addition to this, the TFH method does not require any expensive or complicated equipment nor the use of high pressure and elevated temperature during the process. In a recent study, cationic siRNA-loaded cationic liposomes for the Herpes Simplex Virus-1 treatment were generated by the TFH method. Lipoplexes were characterized by nano-size, low PDI, high siRNA loading, and high stability[132].

Finally, the ethanol dilution method can be used as an alternative to the THF method to assemble lipoplexes. In this method, cationic and PEGylated liposomes are mixed with the NAs in the presence of ethanol in the buffer (Figure 4.7, Panel E). Ethanol is used to partially loose the liposome membrane to facilitate diffusion into the liposome and distribute evenly over the cationic charge. This method requires optimization of ethanol concentration in the medium since a low concentration of ethanol will not increase the permeability of the lipid membrane and prevent NA diffusion, while high ethanol concentration might induce dissociation of the liposomes[131].

4.4.2. Composition of lipoplexes

The physicochemical and biopharmaceutical properties of the lipoplexes such as fluidity, permeability, surface charge, and loading efficiency are greatly dependent on the choice of the components[116]. According to the shape concept, the morphology of the resulting self-assembled colloids is highly dependent on the packing parameter (p) of lipid molecules, which is defined as the polar head to hydrophobic tail ratio and defines the ability to fit into a specific lipid assembly morphology. For instance, if the packing parameter is lower than 1/3, above the CMC surfactants form micelles, while phospholipids that have a packing parameter of about 1 can assemble into a bilayer that can result in

liposomes. If the packing parameter is higher than 1, as in phosphatidyl-ethanolamine, these amphiphilic molecules form inverted hexagonal phase structures (H_{II})(Figure 4.8)[133].

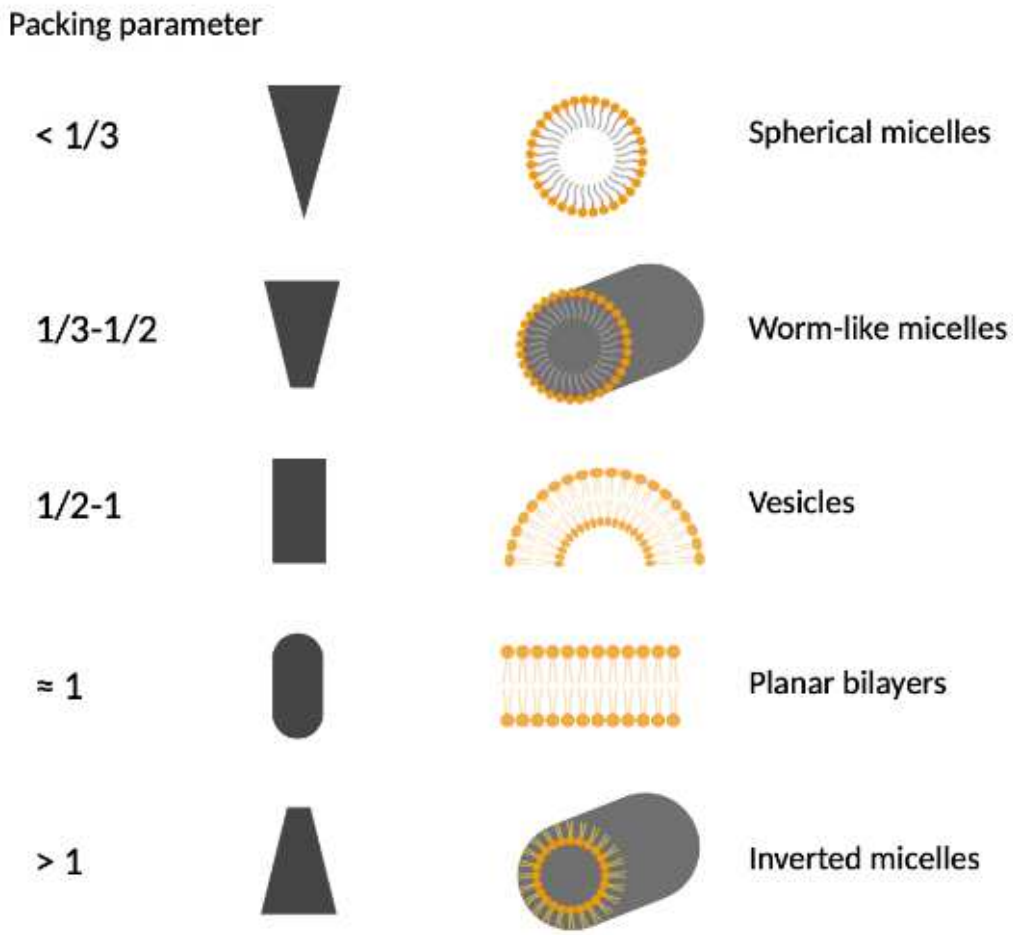

Figure 4.8. *Effect of the packing parameters of amphiphilic molecules on the assembled colloid morphology[133].*

The main components of the cationic liposomes are:

- Phospholipids: Phospholipids, which can be obtained from natural sources or be synthesized artificially, take up the majority of the lipid composition in liposomal formulations. Soybeans, egg yolks, and bovine tissues are the most common sources of natural lipids. Synthetic lipids are more chemically homogeneous, and the manufacturing process is repeatable, ensuring that each batch has the same phospholipid and fatty acid composition[134]. Phosphatidylcholines (PCs) are the most common lipids used in liposomal design because they are a major component of cellular membranes, indicating their high biocompatibility. PCs can be either saturated in the hydrocarbon alkyl acids, thus rigid and more impermeable to encapsulated molecule diffusion, or unsaturated and more flexible. The use of lipids with a high phase transition temperature (Tm), such as fully saturated DSPC or HSPC, makes the liposomal formulation more stable and reduces the risk of any encapsulated contents leaking out. On the contrary, unsaturated acyl chains occupy more steric space, disturbing the tight

packing of adjacent chains and allowing them to be more flexible, and resulting in the decrease of the Tm of the entire lipid bilayer[135].

- Cholesterol: The content of cholesterol is a critical variable in the liposomal structure that can affect the organization and stability of the bilayer. Numerous studies on the use of cholesterol as a stabilizer have been conducted, revealing that this steroid can enhance the packing of phospholipid molecules, decrease bilayer permeability to non-electrolyte and electrolyte substances, enhance vesicle colloidal stability over aggregation, alter the flexibility of intravesical interactions to make them more rigid and promote resistance to lipid bilayer shear stress, and prevent drug leakage[136-138]. Because of its peculiar characteristics to influence the lipid bilayer, most clinically approved liposomal nanoparticles (such as Doxil[139], Lipodox[140] and Myocet[141]) contain cholesterol. The most common ratio of phospholipids/cholesterol commonly used is 2:1 . However, the correlation between cholesterol-to-lipid ratio and stability and efficient formulation is not deeply understood[142].

The effect of the cholesterol on the transfection efficiency of the lipoplexes was studied in vitro. In this study cholesterol was stepwise (0, 0.125, 0.25, 0.375, and 0.5 to 1) included in the lipoplexes made of DC-cholesterol/DOPE/DNA and showed that 40 mol% cholesterol yielded about 10-fold improvement in terms of transfection. This result was explained by cholesterol-containing lipoplexes' entrance to cells partially by membrane fusion, and not being targeted to metabolic degradation[143]. Regardless of its advantages, research on liposomal formulations without cholesterol is ongoing. For instance, in a recent study, cationic liposomes for siRNA delivery were generated with two different cationic lipids (DOTAP and DC-Cholesterol) and with different ratios of helper lipids (Cholesterol and DOPE). Their results showed a composition-independent cellular association rate. In the gene knockdown studies, liposomes composed of DOTAP/DOPE (1:1 mol/mol) induced 80% of silencing, while this value was about 70% for the formulations generated with DOTAP/Cholesterol/DOPE (2:1:1 mol/mol) and 60% for the formulations generated with DOTAP/Cholesterol/DOPE (2/1.5/1 mol/mol)[119]. Overall, these studies show that the contribution of cholesterol to lipoplexes should be evaluated on a formulation basis.

- Cationic lipids: The main application of cationic lipids in the liposomal composition is for the delivery of nucleic acids. Commonly used cationic lipids are made up of three domains: a hydrophilic head group, a linker, and one or more hydrophobic acyl chains similar to the phospholipids. Cationic lipids are required to achieve different effects that include the efficient condensation of nucleic acids and their association with liposomes and also to facilitate the interaction of the lipoplexes with cell negatively charged surfaces, increasing transfection efficiency[144]. The majority of cationic lipids used in gene delivery have two alkyl chains, which allows them to form lamellar phases resulting in

increased transfection efficiency, meanwhile, single-tailed lipids can act as surfactants and form micelles, thus increasing their cytotoxicity[145]. Cationic lipids can be designed also taking inspiration from nature, which will be widely discussed in the following section.

4.5. Cell penetration enhancers

Successful delivery of drugs by colloidal carriers involves several challenges, such as long blood circulation, permeation through the biological barriers, biodistribution to target tissues, crossing the cell membrane of target cells, and endosomal escape to the cytosolic space upon endocytosis. Due to the negative charge and high molecular weight of macromolecules such as nucleic acids, cell membrane crossing and delivery to the target subcellular compartment have been considered a major barrier[146]. Efficient crossing of the biological membranes and cell uptake of the macromolecules and colloidal carriers was achieved by exploiting cell penetration enhancers (CPEs). Within the drug delivery science, the use of the CPEs has recently gained extensive attention[147]. Cell penetration enhancers can be classified into 2 groups: i) amphipathic helical peptides, which have lipophilic and hydrophilic tails that provide direct peptide translocation through the plasma membrane, and ii) cationic CPEs that consist of arginine-rich peptides, such as TAT or penetratin. Due to the presence of cationic charges, this group of peptides provides translocation across the cell membrane by electrostatic interactions mostly followed by active endocytosis[148,149].

The viral protein TAT (trans-activator of transcription), the first known peptidic CPE, was discovered in 1988. TAT is a small basic protein coded by two exons of the viral genome that range in length from 99 to 103 amino acids, with the 101-residue form being the most common. The sequence of TAT can be divided into 6 domains; a proline-rich acidic N-terminus (1-21), a cysteine-rich region (22-37), a hydrophobic core region (38-48), an arginine-rich basic domain (49-57), a glutamine-rich region (58-72) and a C-terminal domain (Figure 4.9)[150].

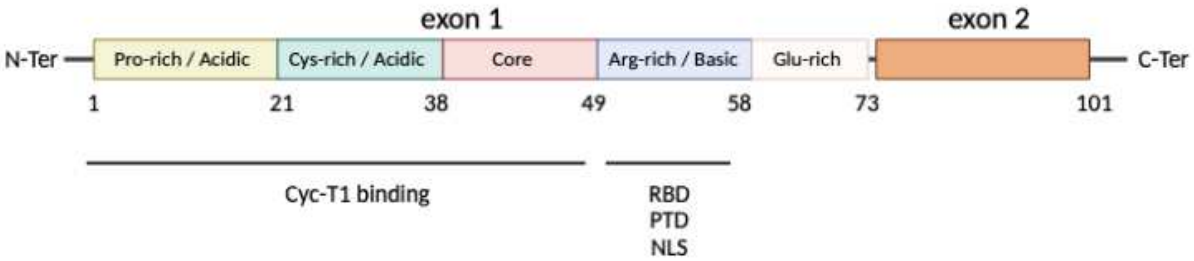

Figure 4.9. *Scheme of the functional domains of HIV-1 TAT[150].*

The protein transduction domain (PTD) of the TAT protein is composed of arginine and lysine residues and it is responsible for the efficient transduction of the protein through the cell membrane while the C-terminal domain is not required for TAT translocation functions in cell culture but it might help the viral pathogenesis in-vivo[150, 151].

Another breakthrough was made when natural (VP22 and AntP) and synthetic (transportation) polycationic peptides were employed to convey genes, proteins, small exogenous peptides, and even nanoparticles. Importantly, it was found that the full length of these peptides is not required and that small domain can also undergo efficient cellular entrance[149]. After these discoveries, many modifications of these sequences have been applied and these synthetic derivatives have shown successful intracellular cargo delivery. Their translocating features were associated with their polycationic domains, which are responsible for the crossing of biological membranes and achieving their transcriptional activator roles[152].

”Peptidic CPE” and ”protein transduction domain” terms are used to refer to short (5-30 amino acids), basic amino acid-rich, such as arginine or lysine, water-soluble, cationic, and/or amphipathic structured class of peptides. Their interest in the development of new drug delivery systems and more in general new therapies lies in their ability to cross the plasma membrane at low concentrations, transport large, biologically active molecules (such as proteins, oligonucleotides, plasmid DNA and RNA) in a receptor-independent manner, and not cause significant membrane damage[149].

4.5.1. Cellular internalization mechanisms of CPEs

Although extensive research on CPEs has been going on for over 30 years, the exact mechanism of CPE internalization into the cytoplasm remains uncertain. It is known that a variety of energy-dependent endocytic routes and direct membrane translocation, in a variety of forms, may play role in CPE internalization. The internalization behaviors of CPEs are critical for determining overall safety, and efficacy. Furthermore, understanding the pathway is important for developing cell-specific delivery systems[153].

Energy-dependent endocytic routes

Endocytosis is an active process in which macromolecules and colloids are transported into cells in vesicles or vacuoles and consists in active cellular internalization. The endocytosis mechanism is used by all types of cells in the body to either engulf nutrients or to communicate with their biological surroundings[154]. Internalization of ions and biomolecules dispersed in the surrounding medium can be done through different pathways which can be classified into two main categories: phagocytosis and

pinocytosis. Phagocytosis is a mechanism that allows the uptake and digestion of particles larger than 0.5 um. Although it is found in many cell types, only dedicated cells, such as macrophages, neutrophils, monocytes, dendritic cells, and osteoclasts are capable of highly efficient phagocytosis[155]. The treatment of diseases dominated by the hyperactivated activity of macrophages, such as rheumatoid arthritis, benefits greatly from understanding the mechanism of phagocytosis[156]. On the other hand, pinocytosis occurs in all cells and involves the uptake of solutes and fluids. Pinocytosis can occur at least according to four different mechanisms: macropinocytosis, clathrin-mediated endocytosis (CME), caveolae-mediated endocytosis, and clathrin- and caveolae-independent endocytosis (Figure 4.10)[153].

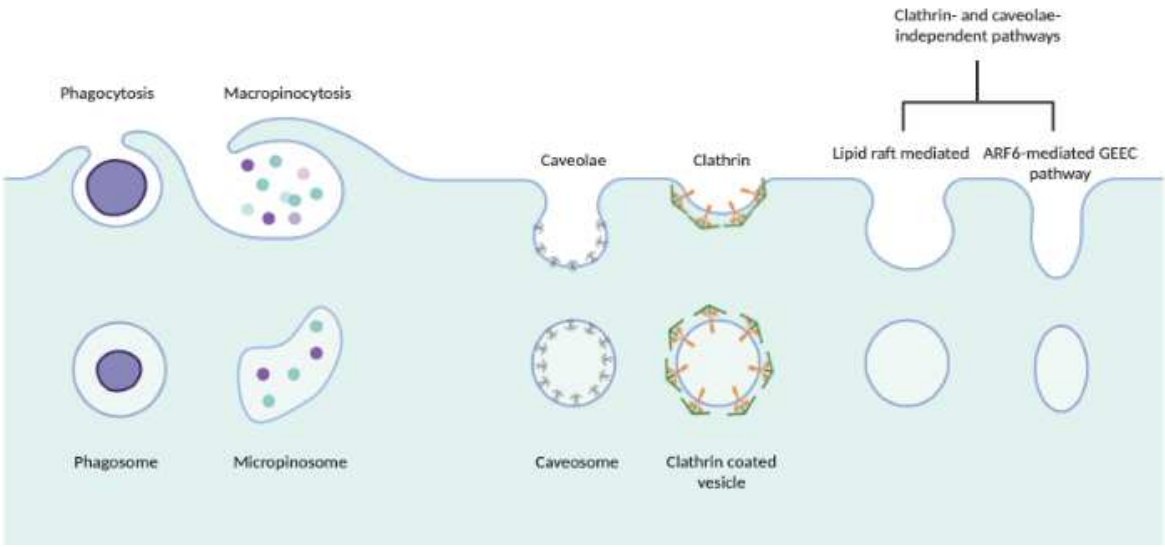

Figure 4.10. *Schematic representation of endocytic pathways: Phagocytosis, macropinocytosis, caveolar-mediated endocytosis, clathrin-mediated endocytosis, Clathrin- and caveolae- independent endocytosis[153].*

Earlier investigations on the internalization mechanism of the CPEs suggested a direct translocation through the cellular membrane, in consequence of the studies showing CPE's capability of membrane crossing at low temperature and in the presence of endocytosis inhibitors[157, 158]. Later on, in a study conducted by Richard et al, the involvement of endocytosis in the cellular internalization of CPE was proven and the fallacy of the previous studies was explained with the use of fixed cells, and the effect of the fixatives on the intracellular peptide disposition[159]. Recent studies showed that CPEs can be internalized by different energy-dependent pathways: macropinocytosis, upon membrane-associated proteoglycan-CPE interaction[160, 161], clathrin-[162, 163] and caveolar[164, 165] dependent and independent[166] endocytosis. Overall, the uptake pathway is mostly dictated by the physicochemical features of the CPE, the cargo to which the CPE is associated, the concentrations used, the cell membrane's structural

properties and CPE interactions with the cell membrane. Further investigations using combined analytical tooms are going to better understand the cell entry mechanisms of CPEs.

4.5.2. Non-peptidic CPEs

Despite the advantages offered by the peptidic CPEs, due to their cleavage by proteolytic enzymes in vivo and complex pharmacokinetic properties, efforts have been addressed to develop non-peptidic CPEs[167,168]. Many non-peptidic CPEs, then, have been designed to mimic the HIV TAT_{49-57} sequence by mainly focusing on the number and spatial display of guanidinium groups. Guanidine is found in a wide range of natural molecules, including the amino acid arginine. The Y-shaped guanidinium group has a highly symmetric planar structure that can form two strong parallel hydrogen bonds with biologically relevant anionic counterparts (Figure 4.11). In comparison to ammonium groups, which are also widely found in biomolecules, its geometry produces a more favorable hydrogen bond alignment. Furthermore, because the group maintains its protonated state over a wide pH range, electrostatic association with anionic molecules can occur via both charge pairing and hydrogen bonding[169,170].

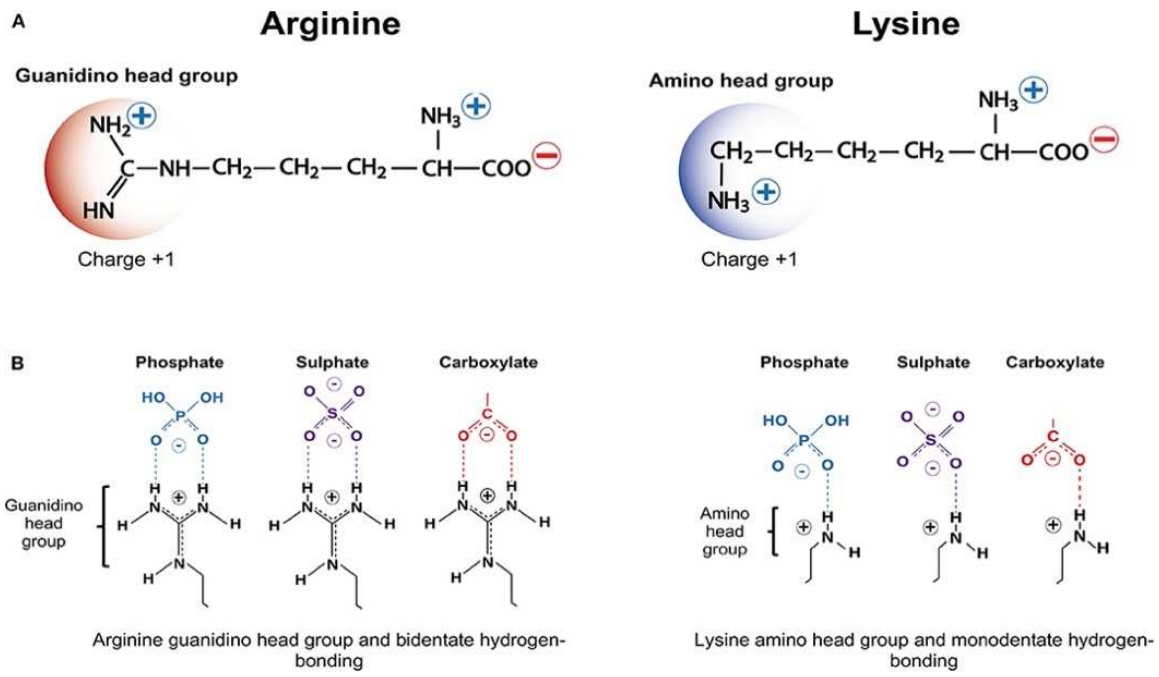

***Figure 4.11**. Schematic representation of arginine and lysine, with positively charged guanidino and amino head groups, respectively (A). Guanidino and amino head groups building bidentate and monodentate hydrogen bonding, respectively, with phosphate, sulfate, and carboxylate anionic moieties (B)[170].*

Recent research on linear TAT analogs has highlighted the relevance of multiple guanidine groups as well as the possibility to alter the backbone and spacing between guanidines without losing cellular association activity. When CPEs have to be employed to carry their cargo into cells, the simplicity of manufacture should be a key design factor. Many synthetic processes and purification steps are involved in the production of non-peptidic linear oligomers; for this reason, the development of CPEs that can be easily conjugated to their cargos and can be synthesized on large scale would be important requisites for extending their value in drug delivery applications[171].

One promising backbone for the synthesis of non-peptidic non-linear CPEs is dendrons. Dendrons are polymers with highly branched structures that, in combination with the presence of several peripheral groups, allow for the bioconjugation or complexation of their terminal ends with drugs and bioactive molecules[171,172]. These repeated branches create surfaces of different sizes around the focal point of the dendron as a consequence of the synthetic generation to which they refer (Figure 4.12)[173]. Besides the peripheral group conjugation or complexation, focal functionalization of dendrons opens the door to a variety of novel multivalent conjugate applications, including the generation of supramolecular assemblies such as films, liposomes, or membranes[174].

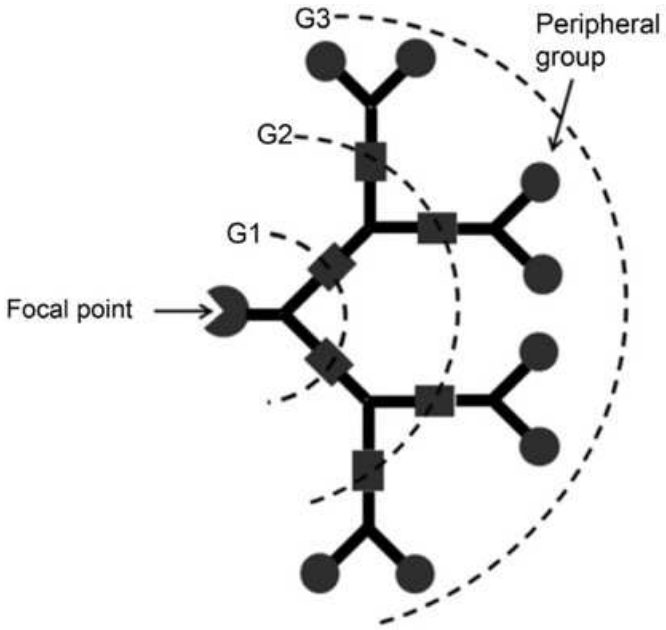

***Figure 4.12**. The schematic representation of a dendron shows the focal point, generations (G1, G2, and G3), and peripheral groups[173].*

Functionalized dendrimers can be employed for the delivery of different cargoes, such as small molecules, macromolecules and nanoparticles. These cargoes can be associated with the dendrimers by encapsulation into spaces between the dendron branches, surface/focal point conjugation, or a combination of both. Hydrogen bonding, van der Waals interactions, and electrostatic attractions

between opposite charges on the dendrimers and cargos are the driving forces behind these interactions[171].

To date, many guanidine functionalized dendron/dendrimers were investigated for oligonucleotide delivery as analogs of peptidic CPEs. One of the first studies performed using the dendrimeric product poly(propylene imine) (PPI) demonstrated that arginine derivatized PPI dendrimer conjugate caused minimal toxicity on the HeLa cell line. This conjugate also showed high transfection efficiency of HeLa and HEK 293 cells, compared to arginine-free dendrimer[175]. Similarly, Tziveleka et al showed that functionalization of the PPI with guanidinium groups results in a significant increase in transfection efficiency on HEK 293 and COS-7 cell lines. The increased transfection efficiency has been attributed to the improved penetrating capability of guanidinylated dendrimers due to the buildup of the guanidinium group on the dendrimeric surface[176]. In the study performed by Goodman et al, polyamide dendrimers with different numbers of guanidines (1, 3, 6, 9, and 12) were produced. Cell association studies showed that the dendron with the 9 guanidine group had similar penetrating efficiency as TAT_{49-57} on HeLa S3 cells. Moreover, deconvolution microscopy analysis showed the intracellular location of the dendrimer, indicating branched dendritic oligoguanidines' capability to cross the cell membrane[177].

5. AIM OF THE PROJECT

The aim of this thesis project was the development of a drug delivery system for therapeutic oligonucleotides. Cationic liposomes, formulated by using an oligocationic enhancer (OCE, Arg_4-DAG) were investigated to efficiently condense oligonucleotides. Arg_4-DAG was synthesized by our group and consisted of a dendrimeric structure functionalized with 4 arginine groups and a lipid anchor for liposome bilayer insertion. The synthesized OCE provides positive charges able to condense oligonucleotides allowing a **high loading efficiency** and improving oligonucleotide stability. Moreover, in virtue of the dendrimeric scaffold used for arginine conjugation, the oligo-arginine bearing dendrimer ensures a high density of cationic charge that allows the exploitation of this macromolecule as a cell-penetrating enhancer, which can favor cell interaction, **cellular uptake** and thus NA delivery.

Endosomal entrapment is one of the major pitfalls to successful intracellular oligonucleotide delivery. To overcome this issue, lipoplexes with different lipid compositions (including fusogenic helper lipids) were extensively investigated to select the one that ensures the **crossing of intracellular biobarriers**, namely endosomes upon lipoplexes uptake, and cytosolic release (Figure 5.1.)

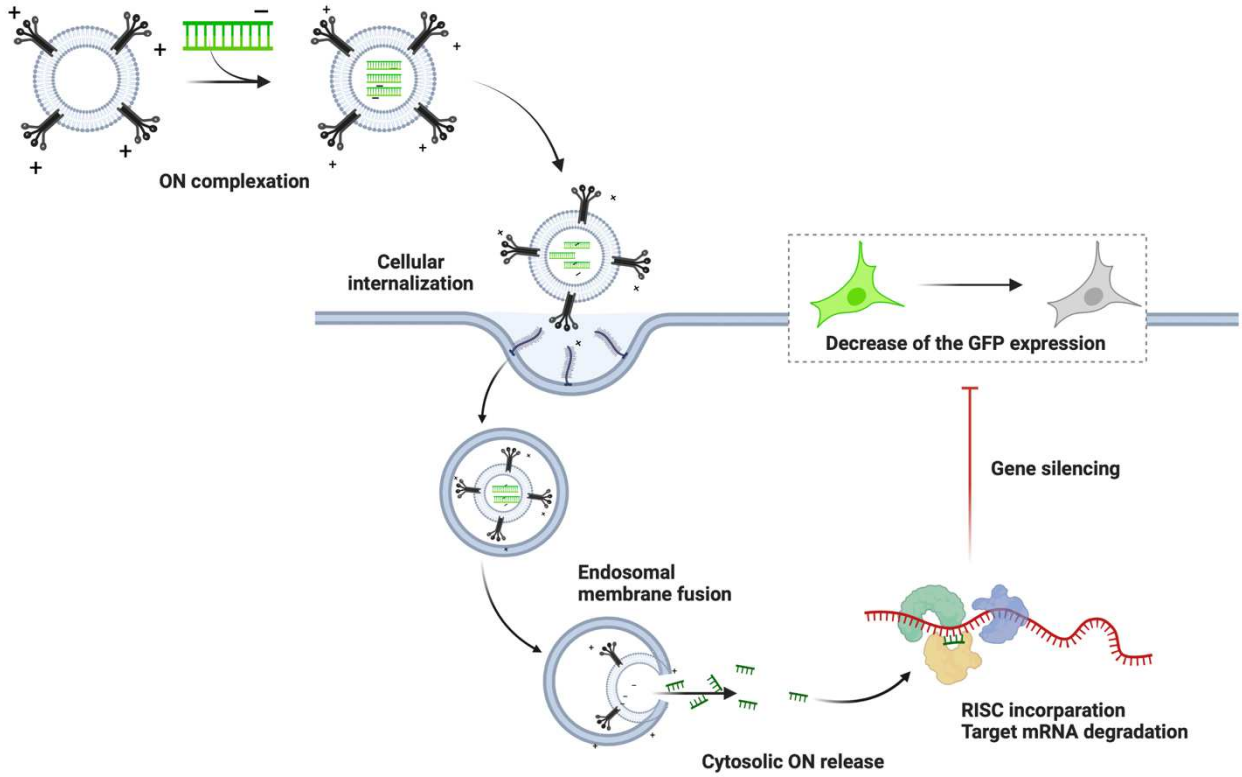

Figure 5.1. *Schematic representation of the lipoplexes assembly, intracellular access and cytosolic oligonucleotide release.*

6. MATERIALS and METHODS

6.1. Materials

6.1.1. Reagents

- Hydrogenated Soybean Phosphatidyl Choline (HSPC) was purchased from Lipoid (Ludwigshafen, Germany).
- 1,2-dioleoyl-sn-glycero-3-phosphoethanolamine (DOPE) was purchased from Avanti Polar Lipids (Alabama, USA).
- Cholesterol, ferric chloride hexahydrate ($FeCl_3 \cdot 6H_2O$), ammonium thiocyanate (NH_4SCN), D-(+)-Trehalose dihydrate, sodium citrate dihydrate ($Na_3C_6H_5O_7 \bullet 2H_2O$), sodium chloride (NaCl), potassium chloride (KCl), disodium hydrogen phosphate (Na_2HPO_4), were provided by Sigma-Aldrich (St. Louis, MO, USA).
- Acetonitrile (MeCN), chloroform ($CHCl_3$), ethanol (EtOH), and methanol (CH_3OH) were provided by Honeywell Riedel-de-Haën TM (Morris Plains, NJ, USA).
- 2-[4-(2-hydroxyethyl)piperazin-1-yl]ethanesulfonic acid (HEPES), 2,2'-bipyridine, Lysotracker Red DND-99 and Hoechst 33342 were purchased from Thermo Fischer SCIENTIFIC (Waltham, MA, USA).
- Water for reactions was "ultrapure" water (Milli-Q grade, 0.06 Siemens cm^{-1}) generated with the Millipore Milli-Q® purification system (Merck, MA, USA).
- Potassium dihydrogen phosphate (KH_2PO_4) was provided by Merck KGA, (Merk, MA, USA)
- Single-strand DNA oligonucleotides (19bp) were provided by Biomers Gmbh (Warsaw, USA).
- siRNA (sieGFP and siCTRL) and cyanine5-siCTRL were purchased from Eurogentec (Seraing, Belgium)
- Acrylamide for electrophoresis was provided by AppliChem (Darmstadt, Germany).
- GelRed for DNA electrophoresis staining was bought from Biotium (Fremont, CA, USA).
- Heparin 5000 UI/mL for stability test by electrophoresis analysis was provided from Teva (Petha Tiqwa, Israel)
- H1299 cells (lung epithelial cells derived from metastatic lymph nodes) were purchased from ATCC.
- All cell culture materials such as PBS, Dulbecco's Modified Eagle's Medium (DMEM), Foetal Bovine serum (FBS), penicillin, streptomycin, L-glutamine, trypsin and 3-(4,5-Dimethylthiazol-2-yl)-2,5-diphenyl tetrazolium bromide (MTT) were purchased from Sigma-Aldrich (St. Louis, USA).

6.1.2. Scientific equipment

- Dynamic Light Scattering (DLS) measurements were performed by Zetasizer UltraZS from Malvern Instrument LTD (Malvern, UK).
- Solvents were evaporated using Büchi Rotavapor R100 equipped with Büchi Vacuum pump V-100, Büchi Heatingbath B-100, Büchi interfaces I-100 and Recirculating
- Chiller F-305 from Büchi from BÜCHI Labortechnik AG (Postfach, Switzerland).
- Dialysis was performed using 500-1000 Da MWCO and 50-100 kDa MWCO Spectra/Por® Float-A- Lyzer® from Spectrum Labs, Inc (Rancho Dominguez, CA, USA).
- pH measurements were carried out with pH-meterSevenEasy S20-K Mettler Toledo with electrode Mettler Toledo Inlab Expert Pro-ISM (Schwarzenbach, Switzerland).
- UV-Vis Spectrophotometric analysis was performed using UV-Vis spectrophotometer Evolution 201 from Thermo Scientific (Madison, WI, USA)
- Ultrasound sonicator Powersonic 410 of Hwashin Technology (Seoul, Korea).
- Liposomes were extruded with a mini-extruder provided by Avanti Polar Lipid (Alabaster, AL, USA), using 200 nm membrane filters provided by Whatman (Clifton, NJ, USA).
- Samples were centrifuged with Z300 Hemle Labortechnik (Wehingen, Switzerland) and on a Sigma 1-14 Laborzentrifugen from Sigma Aldrich (Saint Louis, MO, USA).
- Samples were kept under stirring with Heating Rotating stirrers of VELP Scientifica (Usmate Velate, MB, Italy) and Vetrotecnica (Padua, Italy).
- A rotary stirrer was provided by ASAL s.r.l. Cernusco s/N (MI, Italy)
- Nanoparticles were lyophilized with a Hetossic HETO Lab Equipment freeze-dryer (Birkerod, Denmark)
- Flow cytometric analyses were performed with a CytoFLEX flow cytometer (Beckman Coulter, Krefeld, Germany).
- The agarose gels were imaged using a Perkin Elmer UV-Transilluminator Geliance 600 Imaging System.
- Confocal microscopy images were recorded on a Leica TCS SP5 confocal laser-scanning microscope (Leica microsystems, Mannheim, Germany), on spinning disc confocal 3I Marianas (Intelligent Imaging Innovation, Göttingen, Germany) or Zeiss LSM 800 (Jena, Germany).

6.2. Methods

6.2.1. Analytical methods

6.2.1.1. Determination of Cy3-dsDNA concentration by Spectrofluorometric analysis

In this project, a cyanine 3 labeled double-strand DNA (Cy3-dsDNA) was used as a model oligonucleotide during the formulative studies. The DNA strand with sequence 5'-cgg cct ggc aca tct c-3', with modification 'cy3' on the 5', was annealed to the DNA strand with sequence 5'-gag atg taa ggc g-3' to obtain a double-strand DNA (dsDNA). The first DNA strand (160.8 nmol) was dissolved in 1.608 mL of annealing buffer (solution 1), and the second DNA strand (282.6 nmol) was dissolved in 2.826 mL of annealing buffer (solution 2), both to reach a concentration of 100 µM. For the annealing, 200 µL of solution 1, and 200 µL of solution 2 were mixed creating solutions with a concentration of 50 µM. These solutions were then incubated at 95 °C for 5 minutes in a water bath. Then the heating was turned off and the solution was allowed to cool down to room temperature. Once the room temperature was reached, the Cy3-DNA double strands were stored at -20 °C.

A calibration line was generated for the quantification of the cy3-dsDNA by serial dilutions of a 50 µM Cy3-dsDNA to 4-32 nM concentration in 1% (v/v) Triton-X solution in HBS buffer at pH 7.4 using an LS 50 B Perkin-Elmer fluorimeter (Waltham, MA, USA) with an excitation wavelength of 554 nm and emission of 568 nm (Figure 6.1).

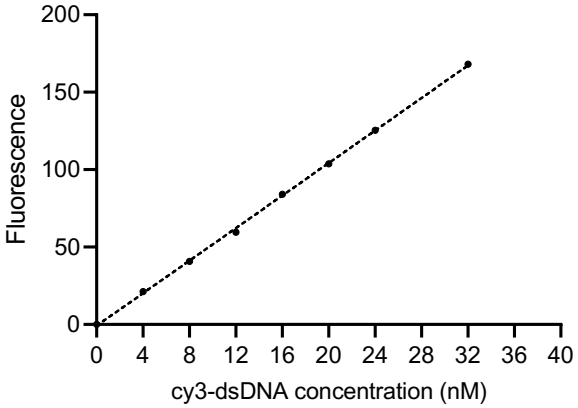

***Figure 6.1**. Calibration line of the* Cy3-dsDNA *obtained by spectrofluorometric analysis (y= 28,57x + 8,1482 and R^2 = 0,9992)*

6.2.1.2. siRNA concentration assessment by RiboGreen Assay

Ribogreen is an ultrasensitive fluorescent nucleic acid stain. Ribogreen assay is a simple and rapid procedure for measuring RNA concentration in solution for several molecular biology procedures. For the execution of the assay stock solutions were prepared as follows:

i. *Assay buffer (1x Tris-EDTA (TE) working solution):* it was prepared by diluting the concentrated TE buffer (20x) with DEPC-treated nuclease-free water (e.g. 2 mL TE-buffer 20x with 38 mL DEPC-treated nuclease-free water).

ii. *Stock solution of Triton 1% (w/w) solution* was prepared by adding 100 µL Triton x100 in 10 mL nuclease-free water. To avoid the creation of bubbles, the solution was pipetted slowly, mixed well, and gently heated to 40 °C. The stock solution of Triton 1% (w/w) was diluted to Triton 0.5% with 1x TE buffer.

iii. *Reagent:* On the day of the experiment, the Quant-iT^{TM} RiboGreen^{TM} RNA Reagent was allowed to warm to room temperature before opening the vial, then an aqueous working solution of the Quant-iT^{TM} RiboGreen^{TM} RNA Reagent was prepared by 200-fold dilution of the concentrated DMSO stock solution with TE resulting in the high-range assay.

For the execution of the Ribogreen assay, 2 different calibration lines were prepared. First, RNA standard curves in the 0-1 µg/mL range were generated by diluting a 4 µg/mL stock solution of RNA in TE buffer to a final 0.1 mL volume per sample. Second, RNA standard curves in the 0-1 µg/mL range were generated by diluting a 4 µg/mL stock solution in the TE buffer containing 0.5% (w/w) Triton to a final volume of 0.1 mL. These aliquots were subsequently added to 100 µL of Ribogreen reagent, reaching a final volume of 0.2 mL.

The fluorescence of the serial dilutions was measured using a fluorescence microplate reader (e.g. Victor plate reader) and the following fluorescence wavelengths: excitation ~480 nm, emission ~520 nm. The fluorescence value of the reagent blank was subtracted from each sample.

6.2.1.3. Determination of the arginine groups by Sakaguchi Assay

The colorimetric reaction resulting from the reaction of guanidine derivatives with alpha naphthol and sodium hypochlorite, which was observed by Sakaguchi (1925), has been extensively employed as a qualitative test for arginine. Within this study, the Sakaguchi assay was used for the quantitative assessment of the OCE association with the liposomal bilayer. For the execution of the assay 4 different solutions were prepared:

i. 10% (w/v) NaOH solution in Milli-Q water

ii. 0.1% (w/v) 8-Hydroxyquinoline in absolute EtOH

iii. 40% (w/v) urea solution in Milli-Q water

iv. 2% Sodium hypobromite (NaOBr) by mixing 10 mL of 10% (w/v) NaOH solution in Milli-Q water with 10 mL of 1.28 % (v/v) bromine solution in Milli-Q water.

The calibration line was prepared by mixing 10 µL of arginine solutions (0.5-10 µM) with 480 µL of HBS and 10 µL of 10% (w/w) NaOH solution (Figure 6.2). Then 20 µL of 0.1% (w/v) 8-Hydroxyquinoline in absolute EtOH were added to this mixture, briefly vortexed and the contents of the tube were cooled in the ice bath for 3 minutes. Twenty µL of 2% sodium hypobromite was added and upon vortexing for 5 seconds, 100 µL of 40% (w/v) urea solution in Milli-Q water was added and mixed thoroughly. After 10 min incubation at room temperature, 200 µL of each solution was placed in a 96-well plate, and the spectrophotometric absorbance was assessed at 490 nm using an Inno-M microplate spectrophotometer (LTEK, Korea).

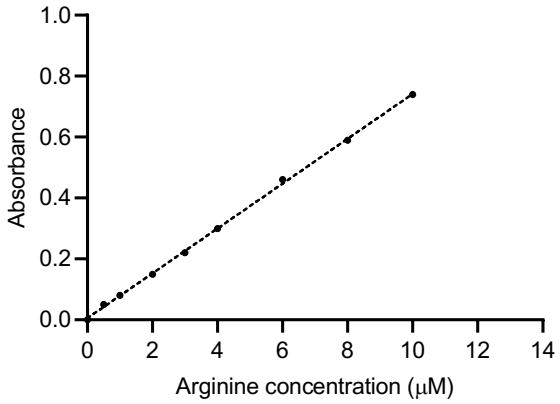

Figure 6.2. *Calibration line of arginine obtained with the sakaguchi assay (y= 0.0737x + 0.007 and R^2 = 0,9992).*

6.2.1.4. Phospholipid assessment by Stewart Assay

The Stewart assay was used for the quantification of phospholipids concentration (HSPC, EPC, and DOPE) in liposome formulations. Stewart reagent was prepared at 0.1 M (27 g/L) ferric chloride ($FeCl_3 \cdot 6H_2O$) and 0.4 M (30 g/L) ammonium thiocyanate (NH_4SCN) in water. This solution was stored in an amber bottle at room temperature and it was stable for several months.

1950 µL of chloroform ($CHCl_3$) were mixed with 50 µL of liposome samples in HBS buffer to induce dissociation of the vesicles and then 2 mL of the Stewart reagent were added to the mixture. Samples were vortexed for 20 seconds and centrifugated for 5 minutes at 1000 rpm. The complex between the

negative phosphate group of phospholipids with ammonium ferrothiocyanate migrated in $CHCl_3$ was detected by spectrophotometric analysis of the organic phase at 485 nm.

Dedicated calibration lines were generated for each of the lipid mixtures investigated in this project. 5 mg/mL lipid mixture stock solutions in chloroform were prepared. The calibration lines were constructed by preparing serial dilutions of each lipid mixture in chloroform from 0.25 mg/mL to 2 mg/mL. The concentration of liposome suspensions was derived using the specific calibration curve.

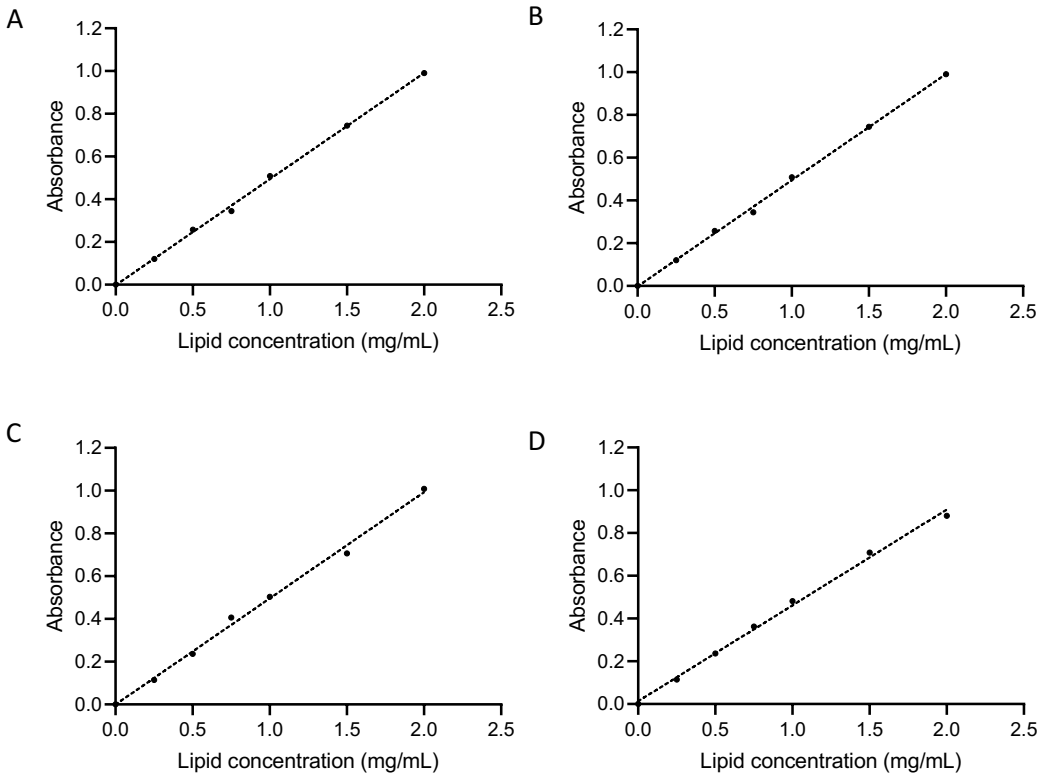

***Figure 6.3**. Calibration curve of 1:1 HSPC/DOPE (**A**), 2:1 HSPC/DOPE (**B**), 2:1:1 HSPC/Cholesterol/DOPE (**C**) and 2:1 HSPC/Cholesterol (**D**) in chloroform by UV-Vis Spectroscopy following the Stewart assay procedure. Equations of the calibration curve are: A) Y=0.496x-0.0003 R^2=0.9992, B) y=0.4863x+0.0177 R^2 = 0.9989, C) y=0.4964x-0.0014 R^2=0.9957 and D) y=0.4443x+0.0199 R^2 = 0.9955*

Lipid recovery of the lipoplexes was calculated using equation 6.1.

Equation 6.1:

$$Lipid\ recovery\% = \frac{Phospholipid\ in\ processed\ formulation\ (mg/mL)}{Phospholipid\ processed\ (mg/mL)} * 100$$

6.2.1.5. Validation of non-loaded dsDNA removal from the lipoplexes

The dialysis method to remove non-loaded dsDNA from the lipoplexes suspension was validated to assess the time required for the extensive removal of the non-loaded dsDNA. To this aim, firstly, Float-A-Lyzers were pre-conditioned in HBS (10 mM HEPES, 150 mM NaCl, pH 7.4). A stock cy3-dsDNA solution was diluted to a final volume of 1.5 mL at 250, 500, and 1000 nM concentrations with HBS buffer. These solutions were then transferred into 300 kDa Spectra/Por® Float-A-Lyzer each and dialyzed versus 2 L of HBS pH 7.4 at RT. At scheduled time points (2, 4, 6, 8, 10, 12, and 24 hours), 10 µL aliquots were withdrawn from the Float-A-Lyzers and underwent a 100-fold dilution with HBS, and then spectrofluorimetrically analyzed using LS 50 B Perkin-Elmer fluorimeter (Waltham, MA, USA) with an excitation wavelength of 554 nm and emission of 568 nm.

The kinetic profile of the dsDNA diffusions from 300 kDa Spectra/Por® Float-A-Lyzers is reported in Figure 6.4.

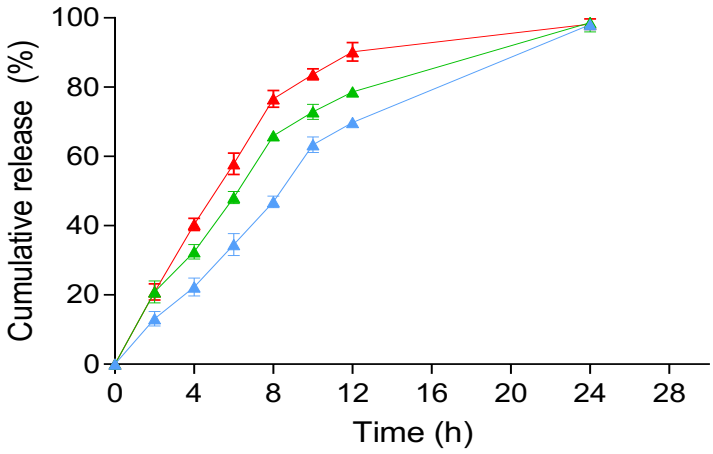

Figure 6.4. *Kinetic profile of cy3-dsDNA diffusion from 300 kDa Float-A-Lyzer to release buffer (10 mM HEPES, 150 mM NaCl, pH 7.4). Cy3-dsDNA concentrations in the solutions tested are 250 (▲), 500 (▲) and 1000 nM (▲) at time zero.*

6.2.2. Synthesis of the oligocationic enhancer

The OCE used to decorate liposomes, namely 3-(4-(12,17-diamino-4-(((3-(2-amino-5 guanidinopentanamido)-2-((2 amino-5-guanidinopentanamido)methyl)-2-methylpropanoyl)oxy)methyl)- 8-((2-amino-5-guanidinopentanamido)methyl)-17-imino-4,8-dimethyl-3,7,11-trioxo-2,6-dioxa-10,16 (diazaheptadecyl)-1H-1,2,3-triazol-1-yl)propane-1,2-diyl distearate (Arg_4-DAG) was synthesized in three main steps according to a modified procedure previously reported by our group in literature[178].

6.2.2.1. Synthesis of the lipid anchor

The lipid anchor (1-(2-propanoxy) glycerol-2,3-distearate ether) present in the OCE was synthesized in 2 steps.

i. Glycidyl propargyl ether (4.5 g, 40.13 mmol) was suspended in 100 mL of water and an acid-catalyzed epoxide ring-opening was provided by the addition of 4 mL of H_2SO_4 (7.36 g, 75 mmol) (Figure 6.5). Then the solution was neutralized with $NaHCO_3$ (12.6 g, 150 mmol). The resulting solution was freeze-dried and the solid residue was resuspended in 30 mL of methanol and centrifuged. The supernatant was collected and glycerol propargyl ether was isolated by flash chromatography (Silicagel 60 Å, 35-70 µm, gradient elution from 50:50 hexane, ethyl acetate to 30:70 hexane, ethyl acetate) and the organic solvent was removed under vacuum with a rotary evaporator to yield to 3.83 g of product as a colorless oil (24.4 mmol, 61% yield).
(^{1}H NMR (400 MHz, $CDCl_3$) δ 4.18 (d, *J* = 2.3 Hz, 2H), 3.89 (qd, *J* = 6.2, 4.1 Hz, 1H), 3.69 (dd, *J* = 11.5, 3.7 Hz, 1H), 3.65 – 3.53 (m, 3H), 3.20 (s, 3H), 2.48 (t, *J* = 2.4 Hz, 1H).

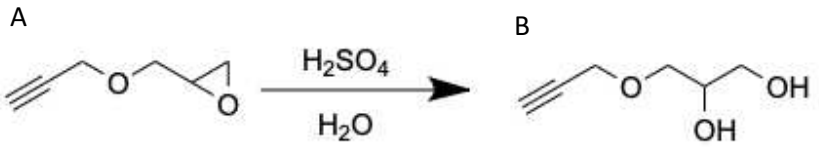

Figure 6.5. *Synthesis of the glycerol propargyl ether (B) from glycidyl propargyl ether (A)*

ii. 1-(2-propanoxy)glycerol-2,3-distearate ether was synthesized as reported in Figure 6.6. Glycerol propargyl ether (0.27 g, 2.06 mmol, 1 Eq.) was dissolved in 15 mL of $CHCl_3$, then the catalysts, 4-dimethyl aminopyridine (DMAP, 0.5 g, 4.13 mmol, 2 Eq.) and triethylamine (4.18 g, 41.27 mmol, 20 Eq.) were added under stirring. The solution was cooled down to 0 °C in an ice bath and stearoyl chloride (2.5 g, 8.25 mmol, 4 Eq.) solution in 5 mL of $CHCl_3$ was added dropwise. The reaction mixture was then brought to room temperature and 10 mL of $CHCl_3$ was added to obtain a clear solution under stirring for 15 minutes. The volume of the reaction mixture was reduced to 5 mL under vacuum and isolated by precipitation in 100 mL of cold diethyl ether. The precipitate was recovered by centrifugation (10000 rpm, 10 min). The precipitate was washed twice with diethyl ether (40 mL). Organic phases were collected and purified by flash chromatography (Silicagel 60 Å, 35-70 µm). The column was eluted in a gradient mode from 100% hexane to 50:50 hexane/diethyl ether. The fractions positive to UV light were collected, and the solvent was removed under vacuum yielding 1-(2-propanoxy) glycerol-2,3-distearate ether as a white powder (1.2 g, 1.81 mmol, 88% yield). ^{1}H NMR in $CDCl_3$ was performed to assess the identity of the products.

(^{1}H NMR (400 MHz, $CDCl_3$) δ 5.26 – 5.20 (m, 1H), 4.37 – 4.14 (m, 4H), 3.70 – 3.65 (m, 2H), 2.43 (t, *J* = 2.4 Hz, 1H), 2.32 (dt, *J* = 10.1, 7.6 Hz, 4H), 1.61 (dd, *J* = 12.9, 6.8 Hz, 4H), 1.25 (s, 61H), 0.88 (t, *J* = 6.8 Hz, 6H).

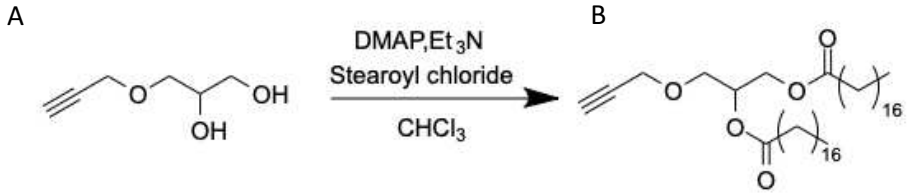

Figure 6.6. *Synthesis of 1-(2-propanoxy) glycerol-2,3-distearate ether (B) from glycerol propargyl ether (A)*

6.2.2.2. Synthesis of the arginine decorated dendron

(((2-(((5-azidopentyl)oxy)carbonyl)-2-methylpropane-1,3-diyl)bis(oxy))bis(carbonyl))bis(2-methylpropane-2,1,3-triyl) tetrakis(3-(2-((*tert*-butoxycarbonyl)amino)-5-(3- ((2,2,4,6,7-pentamethyl-2,3-dihydrobenzofuran-5-yl)sulfonyl)guanidino) pentanamido) propanoate) (Azide-Dendron-G2-BocArg_4(Pbf)) was synthesised by dissolving DMAP (79.33 mg, 0.649 mmol, 16.0 eq) in dry DMF (488 µL). The solution was added dropwise to a solution of Boc-Arg(Pbf)-OH (171 mg, 0.325 mmol, 8.0 eq), HOBt (43.87 mg, 0.325 mmol, 8.0 eq) and HBTU (123.13 mg, 0.325 mmol, 8.0 eq) in dry DMF (581 µL) under stirring at 0 °C. After 20 minutes of stirring, the commercial second-generation dendron (PFd-G2-Azide-Ammonium, 54 mg, 0.04 mmol, 1.0 eq) dissolved in DMF (457 µL) was added dropwise at 0 °C. Afterward, the ice bath was removed and the solution was stirred at room temperature for 16 h. The product was isolated by precipitation in 18 mL of Et_2O which was followed by centrifugation at 4,000 rpm for 5 minutes. The precipitate Azide-Dendron-G2-Boc-Arg_4(Pbf)OH, was dissolved in 12 mL of CH_2Cl_2 and washed three times with 10 mL of 0.5 M HCl/brine 50:50 v/v mixture and twice with 10 mL of deionized water. The aqueous phase was washed with fresh CH_2Cl_2 (8 mL). The organic phases were combined and dried over $MgSO_4$ and filtered. The product then was isolated by precipitation in Et_2O and collected by centrifugation and dried under nitrogen flux to obtain azide-dendron-G2-BocArg_4(Pbf)OH as a white solid (114.06 mg, 0.04 mmol, 100% yield). (^{1}H NMR in $CDCl_3$ was performed to assess the identity of the products.

^{1}H NMR (400 MHz, $CDCl_3$) δ 7.56 (s, 1H), 6.54 (s, 1H), 5.84 (s, 1H), 4.22 (dd, *J* = 47.4, 17.0 Hz, 2H), 3.41 (ddd, *J* = 44.9, 13.9, 7.2 Hz, 3H), 2.99 (s, 1H), 2.66 – 2.47 (m, 4H), 2.13 (d, *J* = 10.4 Hz, 2H), 1.83 (s, 1H), 1.67 (d, *J* = 13.8 Hz, 2H), 1.49 (s, 3H), 1.42 (s, 5H), 1.28 (t, *J* = 8.7 Hz, 1H)).

The reaction scheme of the synthesis is shown in *Figure 6.7.*

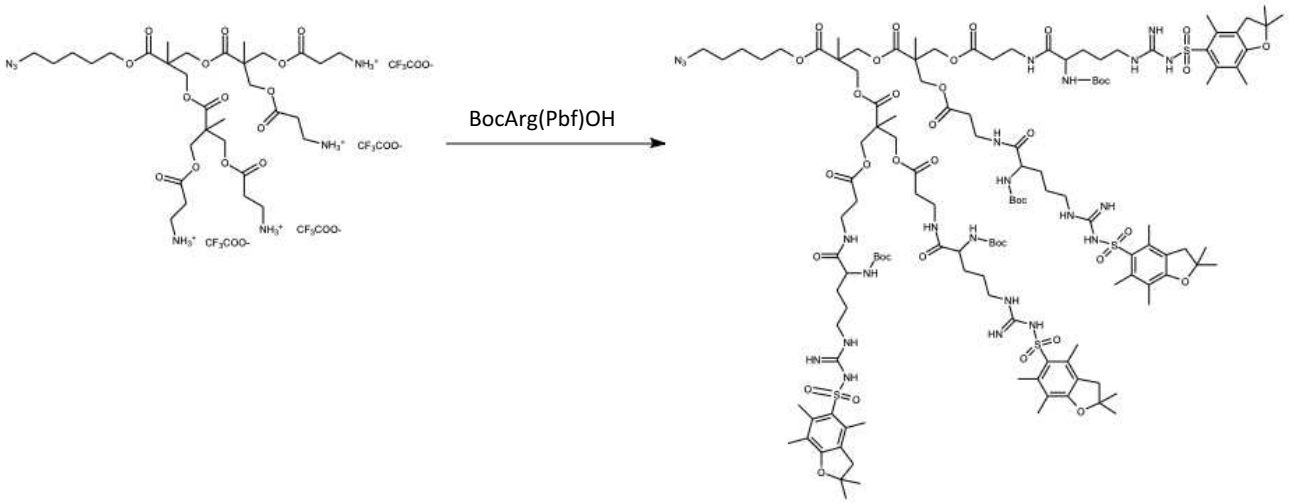

***Figure 6.7**. Synthesis of Azide-Dendron-G2-BocArg$_4$(Pbf)*

6.2.2.3. Huisgen cycloaddition of the lipid anchor to arginine decorated dendron

1-(2-propanoxy)glycerol-2,3-distearate ether and (((2-(((5-azidopentyl)oxy)carbonyl)-2-methylpropane-1,3-diyl)bis(oxy))bis(carbonyl))bis(2-methylpropane-2,1,3-triyl) tetrakis(3-(2-((*tert*-butoxycarbonyl)amino)-5-(3-((2,2,4,6,7-pentamethyl-2,3-dihydro benzofuran-5-yl)sulfonyl)guanidino) pentanamido) propanoate) was synthesised by reacting azide-dendron-G2-BocArg$_4$(Pbf)OH (50 mg, 0.0178 mmol, 1.0 eq.) in dry DCM (1800 µL) with propargyl-distearate (50 mg, 0.08545 mmol, 5.0 eq.) in the presence of 5.56 mg of 2,2-bipyridine (5.56 mg, 0.0356 mmol, 2.0 eq.) at 0 °C. 300 µL of CuI solution in dry MeCN (3.39 mg, 0.0178 mmol,1.0 eq.) was added to the degassed reaction vessel and the mixture was further degassed for 5 minutes at 0 °C. The reaction was left to react at RT 48 hours.

Afterward, 100 µL of an aqueous solution of sodium ascorbate at 3.5 mg/mL concentration was added to the reaction mixture and stirred for 48 h at RT (Figure 6.8.). The workup was performed by flash chromatographic purification using Silicagel 60 Å, 35-70 µm, eluted in a gradient mode from 100% Hexane to 100% Et_2O and from 100% Et_2O to 100% DCM and from 100% DCM to100% MeOH. The fractions positive to UV light were combined, solvent removed was under vacuum to obtain distearate-glyceride-Arg$_4$-Boc(Pbf)OH (24.7 mg, 0.0071 mmol, 40% yield) as a green waxy solid.

The final product (((2-(((6-(4-((2,3-bis(stearoyloxy)propoxy)methyl)-1*H*-1,2,3-triazol-1-yl)hexyl)oxy)carbonyl)-2-methylpropane-1,3-diyl)bis(oxy))bis(carbonyl))bis(2-methylpropane-2,1,3-triyl) tetrakis(3-(2-((*tert*-butoxycarbonyl)amino)-5-(3-((2,2,4,6,7-pentamethyl-2,3-

dihydrobenzofuran-5yl) sulfonyl)guanidino)pentanamido)propanoate) was identified by ^{1}HNMR analysis in $CDCl_3$.

^{1}H NMR (400 MHz, $CDCl_3$) δ 7.50 (s, 1H), 5.24 (s, 1H), 4.44 – 4.09 (m, 3H), 3.71 (s, 1H), 3.67 (d, *J* = 4.2 Hz, 1H), 3.55 (d, *J* = 27.9 Hz, 1H), 3.27 (d, *J* = 24.9 Hz, 1H), 2.97 (s, 1H), 2.69 – 2.53 (m, 3H), 2.51 (s, 2H), 2.38 – 2.26 (m, 1H), 2.10 (s, 2H), 1.95 (s, 1H), 1.76 (d, *J* = 31.8 Hz, 1H), 1.63 (s, 7H), 1.52 – 1.36 (m, 9H), 1.29 (d, *J* = 11.5 Hz, 9H), 0.90 (t, *J* = 6.8 Hz, 1H).

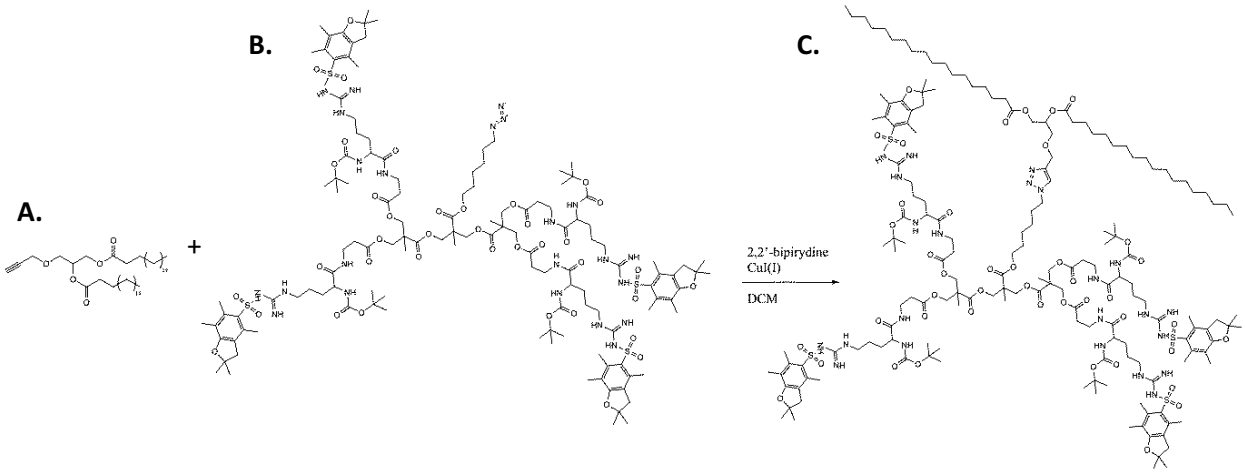

Figure 6.8. *Reaction scheme of (A) 1-(2-propanoxy)-glycerol-2,3-distearate ether and (B) Azide-Dendron-glyceride-BocArg$_4$(Pbf) to synthesize (C) distearate-glyceride-dendron-Arg$_4$-Boc(Pbf)OH.*

The deprotection of arginine groups of the distearate-glyceride-dendron-Arg$_4$-Boc(Pbf)OH was *performed by dissolving* 24.7 mg of (((2-(((6-(4-((2,3-bis(stearoyloxy)propoxy)methyl)-1*H*-1,2,3-triazol-1-yl)hexyl)oxy)carbonyl)-2-methylpropane-1,3-diyl)bis(oxy))bis(carbonyl))bis(2 methylpropane -2,1,3-triyl) tetrakis(3-(2-((*tert*-butoxycarbonyl)amino)-5-(3-((2,2,4,6,7-pentamethyl-2,3-dihydro benzofuran-5-yl)sulfonyl)guanidino)pentanamido)propanoate) in 200 µL of DCM and then 200 µL of TFA was added to the solution (Figure 6.9). The vessel was left under stirring at RT for 40 minutes and subsequently the product was isolated by precipitation in 5 mL of cold Et_2O. The precipitate was collected by centrifuge at 4000 rpm for 10 minutes in a swinging bucket and a further 3 minutes at 12000 rpm in a fixed rotor centrifuge. Diethyl ether was discharged, and the solid pellet was washed again with cold ether. The solid was dried under nitrogen flow. ESI-TOF mass spectroscopy was performed to assess the (((2-(((6-(4-((2,3-bis(stearoyloxy)propoxy)methyl)-1*H*-1,2,3-triazol-1-yl)hexyl)oxy)carzbonyl)-2-methylpropane-1,3-diyl)bis(oxy))bis(carbonyl))bis(2-methylpropane-2,1,3-triyl) tetrakis (3-(2-amino-5-guanidinopentanamido)propanoate) chemical identity. ESI-MS: 516 m/z $(M+4H)^{4+}$.

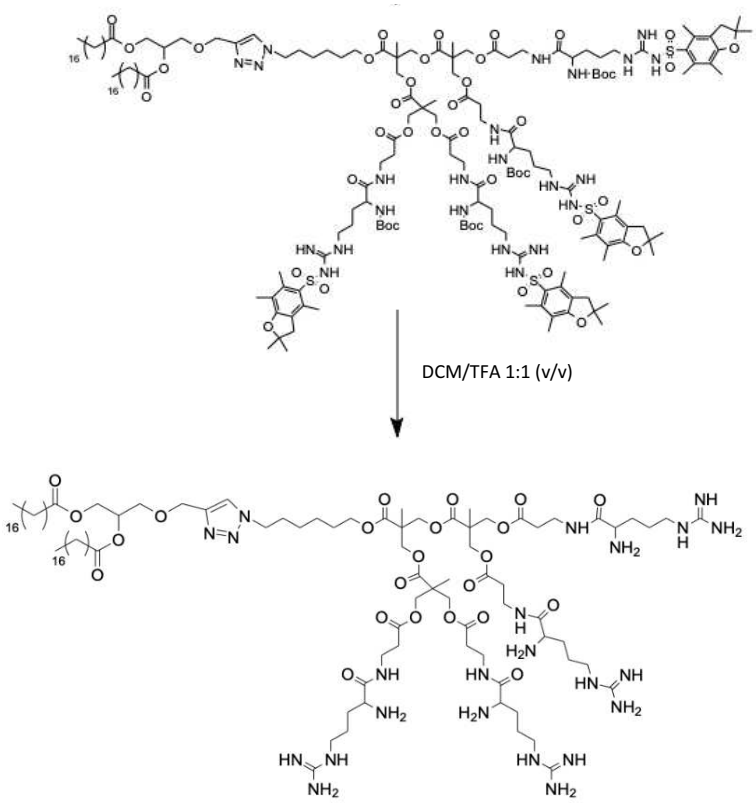

Figure 6.9. *Deprotection of the distearate-glyceride-dendron-Arg$_4$-Boc(Pbf)OH*

6.2.3. Lipoplexes preparation

NA-free liposomes and lipoplexes including the OCE component were generated by the thin layer hydration (TLH) method. Briefly, first, all lipids dissolved in organic solvents are added into a round bottom flask, and the solvent is removed by evaporation. OCE was also included in the lipid mixture prior to lipid film creation to promote the encapsulation of the NA into the aqueous core of the liposomes. The lipid film was then rehydrated with the HBS buffer or NA solution in HBS (10 mM HEPES, 150 mM NaCl, pH 7.4), and with the help of agitating forces e.g. vortexing, multilamellar vesicles (MLV) are formed. Finally, the MLV suspension was extruded through 200 nm MWCO polycarbonate membranes 11 times to reduce the vesicle size (Figure 6.10).

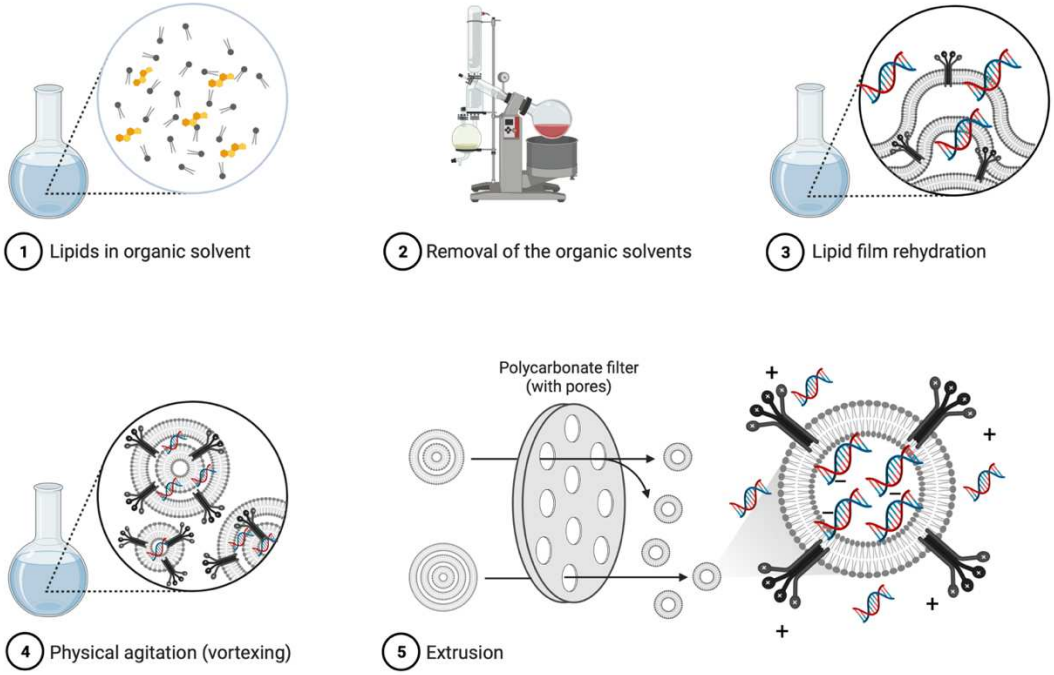

Figure 6.10. *Schematic representation of the lipoplexes production by thin lipid film hydration process.*

6.2.3.1. Selection of the OCE ratio within lipoplexes

Preliminary studies were conducted for the selection of the optimum OCE/lipid ratio within the liposomal composition. With this aim, liposomes were prepared with a 2:1 (mol/mol) HSPC/cholesterol composition including the OCE in the lipid mixture at increasing molar ratios, namely 0-10%.

Stock solutions of the HSPC and cholesterol were prepared at 6.67 mg/mL in $CHCl_3$. OCE was dissolved in MeOH at 0.1 mg/mL of concentration. 3.0 μmols of lipids (HSPC, Cholesterol, OCE) were mixed in a round bottom flask from the stock solutions at a 2:1 HSPC/Cholesterol molar ratio and 0, 2, 4, 6, 8, 10 mol% OCE. The solvent of the lipid mixture was subsequently evaporated under vacuum at 40 °C for 45 minutes resulting in lipid films.

Lipid films were then hydrated with 500 µl of HBS (10 mM HEPES, 150 mM NaCl, pH 7.4) and vortexed in the presence of glass beads (1 mm diameter) to enable the lipid detachment from the surface of the round bottom flask. After hydration, 500 µl of HBS was added to the suspension, briefly vortexed, and extruded 11 times through a 200 nm polycarbonate membrane with a manual extruder. Finally, cationic liposomes were incubated in a thermomixer at 37 °C and 300 rpm for 1 hour. The formulations were characterized in terms of particle size, PDI, and zeta potential by DLS.

OCE association to the liposome was quantified by the Sakaguchi assay as explained in *section 6.2.1.3.* Briefly, 500 µL of cationic liposomes generated at an increasing OCE ratio (0-10% mol/mol) were transferred into 50 kDa MWCO Amicon® Ultra-15 centrifugal filter units and centrifuged at 13000 rpm for 1 hour at RT. The cut-off of the devices was selected to allow the filtration and collection of the OCE non-associated with liposomes in the supernatant while retaining liposomal formulations. The concentrations of the OCE in the filtered medium were then derived from the calibration line generated with arginine solution in HBS (Figure 6.2). The results of this quantification were used to calculate the OCE insertion percentage according to equation 6.2 and then the insertion efficiency.

Equation 6.2:

$$OCE\ association\ (\%) = \frac{Fed\ OCE\ \left(\frac{ug}{mL}\right) - non - associated\ OCE\ \ (ug/mL)}{Fed\ OCE\ (ug/mL)}\ x\ 100$$

6.2.3.2. Investigation of the lipid composition of lipoplexes

A library of lipoplexes obtained with different lipid mixtures was investigated in this thesis project to assess their contribution to the colloidal and biopharmaceutical features of the lipids. The lipids and their ratios screened in the liposome formulation study are hydrogenated soybean phosphatidylcholine (HSPC), egg phosphatidylcholine (EPC), 1,2-dioleoyl-sn-glycero-3-phosphoethanolamine (DOPE), cholesterol and OCE (Figure 6.11). The lipids and their ratios were tested in the formulation to assess their effects on the lipoplexes in terms of colloidal stability, bilayer flexibility/rigidity, and release of payload; ii., fusion to the endosomal membrane and cytoplasmic NA release after internalization; iii. rigidity to the lipoplexes; iv. condensation of NA, respectively.

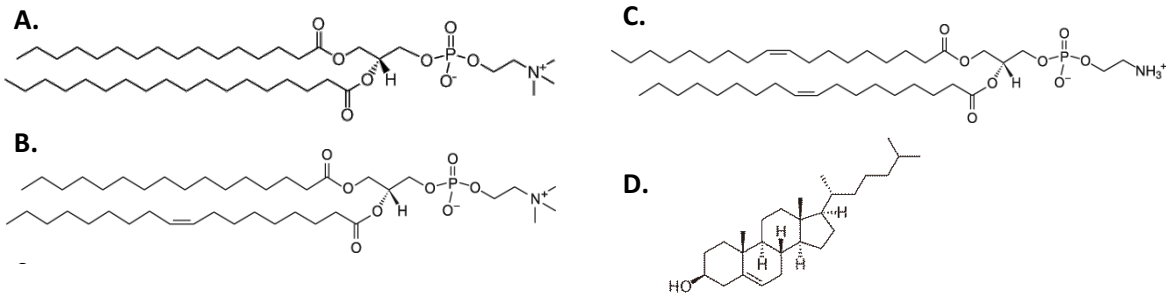

***Figure 6.11**. Chemical structure of HSPC (**A**), EPC (**B**), DOPE (**C**), and cholesterol (**D**).*

To investigate the effect of lipid saturation on the lipoplexes, saturated phospholipid HSPC or unsaturated phospholipid EPC were employed. HSPC/Cholesterol (2:1 mol/mol) and EPC/Cholesterol (2:1 mol/mol) formulations were initially generated without DOPE. DOPE inclusion was investigated since the literature reports its activity as fusogenic helper lipid[179,180]. Then cholesterol was gradually replaced with DOPE reaching 75% (mol/mol) with respect to total lipids.

The lipoplexes were prepared using stock solutions of HSPC, EPC, Cholesterol, and DOPE in $CHCl_3$ at 6.67 mg/mL of concentration, while the stock solution of the OCE was prepared in MeOH at 0.1 mg/mL of concentration. From the stock solutions, the following amount of lipids was withdrawn and mixed in the round bottom flask to generate the following formulations:

A) 1:3 (mol/mol) HSPC/DOPE or EPC:DOPE + 4% OCE (mol/mol) formulation: 1.16 mg (0.0014 mmol) of HSPC or EPC, 3.32 mg (0.0044 mmol) of DOPE and 0.511 mg (0.000248 mmol) of OCE;

B) 1:2 (mol/mol) HSPC:DOPE or EPC:DOPE + 4% OCE (mol/mol) formulation: 1.54 mg (0.0019 mmol) of HSPC or EPC, 2.94 mg (0.0039 mmol) of DOPE and 0.509 mg (0.000247 mmol) of OCE;

C) 1:1 (mol/mol) HSPC/DOPE or EPC:DOPE + 4% OCE (mol/mol) formulation: 2.3 mg (0.0029 mmol) of HSPC or EPC, 2.18 mg (0.0029 mmol) of DOPE and 0.505 mg (0.000245 mmol) of OCE;

D) 2:1 (mol/mol) HSPC/DOPE or EPC:DOPE + 4% OCE (mol/mol) formulation: 3 mg (0.0038 mmol) of HSPC/EPC, 1.44 mg (0.0019 mmol) of DOPE and 0.502 mg (0.000243 mmol) of OCE;

E) 2:1:1 (mol/mol) HSPC/Cholesterol/DOPE or EPC:Cholesterol:DOPE + 4% OCE (mol/mol) formulation: 2.57 mg (0.0032 mmol) of HSPC or EPC, 0.635 mg (0.0016 mmol) of cholesterol, 1.22 mg (0.0016 mmol) of DOPE and 0.565 mg (0.000273 mmol) of OCE;

F) 2:1 (mol/mol) HSPC/Cholesterol or EPC:Cholesterol + 4% OCE (mol/mol) formulation: 3.54 mg (0.0045 mmol) of HSPC or EPC, 0.873 mg (0.0022 mmol) of cholesterol and 0.583 mg (0.00028 mmol) of OCE.

The solvent was removed under vacuum. The lipid films were then hydrated with 500 µl of dsDNA solutions in HBS (10 mM HEPES, 150 mM NaCl, pH 7.4) of 10.2 to 12 µM to generate the lipoplexes at an N/P ratio of 10. N/P ratio is referred to the ratio of primary amino groups present in OCE and phosphate groups in dsDNA. The lipoplex suspensions were vortexed in the presence of glass beads (1 mm diameter) to enable lipid detachment from the surface of the round bottom flask. After hydration, 500 µL HBS was added into the suspension, briefly vortexed, and extruded 11 times through a 200 nm cut-off polycarbonate membrane with a manual extruder. Finally, lipoplexes were incubated in a thermomixer at 37 °C and 300 rpm for 1 hour. Lipoplexes were dialyzed for 24 hours in HBS (10 mM HEPES, 150 mM NaCl, pH 7.4) for the removal of the non-loaded cy3-dsDNA, and the loaded cy3-

dsDNA was assessed by the spectrofluorimetric analysis. The lipoplexes were characterized in terms of particle size, PDI, and zeta potential by DLS, colloidal stability, and release.

6.2.3.3. Selection of the N/P ratio for lipoplexes loading

The ratio between the cationic groups to negatively-charged nucleic acid phosphate (P) groups (N/P ratio) is the driving electrostatic interaction for the formulation of gene delivery vehicles. This ratio has to be carefully selected since it affects many formulation properties including such as surface charge, particle size, and stability[181]. Therefore, the optimization of this ratio for gene delivery systems is crucial.

Liposomes A-F with 4% (mol/mol) OCE were prepared as reported in section 6.2.3 and were then hydrated with 500 µL of dsDNA solutions in HBS at concentrations from 10.3 to 103.09 µM, to obtain lipoplexes at 10-1 N/P ratio range. Control lipoplexes without OCE were also generated with the same composition.

Lipoplexes then vortexed in the presence of glass beads (1 mm diameter) to enable lipid detachment from the surface of the round bottom flask. After rehydration, another 500 µl HBS was added into suspension, briefly vortexed, and extruded 11 times through a 200 nm cut-off polycarbonate membrane with a manual extruder. Finally, lipoplexes were incubated in a thermomixer at 37 °C and 300 rpm for 1 hour. Formulations were characterized in terms of particle size, PDI, and zeta potential by DLS. The loading efficiency of the formulations was quantified after the removal of the non-loaded dsDNA by spectrofluorimetric analysis. The complexation efficiency of each formulation was investigated by the agarose gel electrophoresis.

6.2.3.4. Preparation of the siRNA-loaded lipoplexes

Lipoplexes loaded with the siRNA were prepared following the method used to generate cy3-dsDNA loaded lipoplexes. Lipid films were obtained with the following lipid mixture: 1:1 and 2:1 mol/mol HSPC:DOPE, 2:1:1 mol/mol HSPC:Cholesterol:DOPE, and (2:1 mol/mol) HSPC:Cholesterol and 4% OCE as reported in section 6.2.3.2. The generated lipid films were hydrated with solutions of 21 nucleotide siRNA duplex targeting the green fluorescent protein (siEGFP) in HBS (10 mM HEPES and 150 mM NaCl) or 21 nucleotide siRNA duplex non-coding siRNA duplex (siCTRL) in HBS (10 mM HEPES and 150 mM NaCl) to obtain the lipoplexes at the N/P ratio of 10 and produced as explained in Section 6.2.3.

Generated formulations were characterized in terms of particle size, PDI, and zeta potential by DLS. The loading efficiency of the formulations was quantified after the removal of the non-loaded siRNA by Ribogreen Assay. The complexation efficiency of each formulation was qualitatively investigated by the agarose gel electrophoresis.

6.2.4. Characterization of the lipoplexes

6.2.4.1. Particle size and zeta potential measurement

The mean hydrodynamic diameter, polydispersity index, and zeta potential (ZP) of lipoplexes were assessed by Dynamic Light Scattering (DLS) using Zetasizer UltraZS from Malvern Instrument LTD (Malvern, UK). Before the analysis, lipoplexes were diluted to the concentration of 0.1 mg/mL in Milli-Q water. Measurements were carried out in triplicate. The size data (nm) were recorded in intensity.

6.2.4.2. Loading efficiency and capacity assessment

Freshly prepared lipoplexes loaded with Cy3-dsDNA or sieGFP were dialyzed as reported in *section 6.2.1*.5 to remove non-loaded Cy3-dsDNA or sieGFP. After the dialysis, 10 µL of the lipoplexes formulation was withdrawn from the Float-A-Lyzer, diluted fifty times with 0.1% (v/v) Triton X-100 solution in Milli-Q water, and incubated for 10 minutes to allow dissociation of the lipid bilayer and release of the loaded Cy3-dsDNA or sieGFP within aqueous phase of the lipoplexes.

The Cy3-dsDNA or sieGFP loading in the lipoplexes was quantified by spectrofluorimetric analysis using an LS 50 B Perkin-Elmer fluorimeter (Waltham, MA, USA) with an excitation wavelength of 554 nm and emission of 568 nm. The concentration of Cy3-dsDNA and sieGFP in the samples was calculated as reported in sections 6.2.1.1. and 6.2.1.2., respectively.

The loading efficiency of the liposomes was reported as the percentage of loaded Cy3-dsDNA/sieGFP after dialysis with respect to the initial Cy3-dsDNA/sieGFP used for the lipid film rehydration (Eq. 6.3). The loading capacity was reported as the amount of encapsulated Cy3-dsDNA/sieGFP determined after dialysis with respect to lipids (w/w %) (Eq. 6.4).

Equation 6.3

$$LE\% = \frac{cy3 - dsDNA\ after\ dialysis\ (mols)}{fed\ cy3 - dsDNA\ (mols)} x\ 100$$

Equation 6.4.

$$LC\% = \frac{cy3 - dsDNA\ \ after\ dialysis\ \ (\mu g)}{lipid\ recovered\ (\mu g)} x\ 100$$

6.2.4.3. Release studies

Lipoplexes composed of HSPC:DOPE (1:3, 1:2, 1:1 and 2:1 mol/mol), HSPC:Cholesterol:DOPE (2:1:1 mol/mol), HSPC:Cholesterol (2:1 mol/mol), EPC:DOPE (1:3, 1:2, 1:1 and 2:1 mol/mol), EPC:Cholesterol:DOPE (2:1:1 mol/mol) and EPC:Cholesterol (2:1 mol/mol) were loaded with Cy3-dsDNA at the N/P ratio of 10 as previously described in *section 6.2.3.3.* 1.5 mL of lipoplexes suspension with a Cy3-dsDNA concentration of 1 µM were transferred in a Float-A-Lyzer with a cut-off of 300 kDa and dialyzed against 2 L of HBS (20 mM HEPES, 150 mM NaCl), pH 7.4 and 0.1 M acetate buffer, pH 5.5 at 37 °C over 14 days. The release buffers were changed two times per day. Aliquots (20 µl) of each sample were withdrawn from the inside of the Float-A-Lyzer and diluted fifty times with 0.1% (v/v) Triton X-100 solution in Milli-Q water, and incubated for 10 minutes to disassociate the lipid bilayer and thus release the entrapped Cy3-dsDNA within aqueous phase of the lipoplexes.

The Cy3-dsDNA concentration was measured by spectrofluorimetric analysis using an LS 50 B Perkin-Elmer fluorimeter (Waltham, MA, USA) with an excitation wavelength of 554 nm and emission of 568 nm. The concentration of Cy3-dsDNA in the samples was derived from a titration curve as reported in section 6.2.1.1.

6.2.4.4. Complexation efficiency and displacement assay

Complexation efficiency

The ability of the lipoplexes to complex dsDNA and siRNA was assessed by agarose gel electrophoresis. To this aim, agarose gel solution (2% w/v) was prepared by dissolving 1 g of agarose with 50 mL of TAE buffer (40 mM Tris-acetate, 1 mM EDTA, pH 8). The agarose solution was completely dissolved by warming up the solution in a glycerin bath at 100 °C and subsequently allowed to cool down to 50°C. To enhance the visualization of the free dsDNA and siRNA within the gel, 2 µL of GelRed® nucleic acid gel stain solution was added into the agarose solution and mixed for 5 minutes. Afterward, the agarose solution was transferred into the gel casting box and allowed to be set at room temperature.
Lipoplexes containing an equivalent amount of dsDNA or siRNA (30 pmol) were loaded to the GelRed® nucleic acid gel stain containing agarose gel (2% w/v). The gel was run for 30 minutes at 100 V with TAE buffer and then gently shaken for 30 min in water containing GelRed® (1x) (Biotium, Fremont, CA). Finally, the gel was imaged using a Perkin Elmer UV-Transilluminator Geliance 600 Imaging System.

Heparin displacement

The displacement of dsDNA from lipoplexes was investigated by competition with heparin using agarose gel electrophoresis. To this aim, agarose gel solution (2% w/v) was prepared as reported in previous section.

Lipoplexes samples were prepared by mixing 10 µL of 3 mg/mL HSPC:DOPE (1:1 and 2:1 mol/mol), HSPC:Cholesterol:DOPE (2:1:1 mol/mol) and HSPC:Cholesterol (2:1 mol/mol) formulations at 10 N/P containing 30 pmol of dsDNA with 2 µL of aqueous heparin solutions at increasing concentrations (0.15-10 UI/mL). The samples were incubated for 15 min at room temperature and then loaded into the wells of the agarose gel. The equivalent of 30 pmol free dsDNA and lipoplexes without heparin were used as controls. The 2% agarose gel was run for 30 min at 100 V with TAE buffer, pH 8, and then gently shaken for 30 min in water containing GelRed® (1x) (Biotium, Fremont, CA). Finally, the gel was imaged using a Perkin Elmer UV-Transilluminator Geliance 600 Imaging System (Perkin Elmer, Shelton, CT, USA).

6.2.4.5. Stability studies

Lipoplexes composed of HSPC:DOPE (1:1 and 2:1 mol/mol), HSPC:Cholesterol:DOPE (2:1:1 mol/mol) and HSPC:Cholesterol (2:1 mol/mol) and loaded with cy3-dsDNA at the N/P ratio 10 were generated according to the procedure previously described in *section 6.2.3.3.* The colloidal stability was evaluated after dilution of lipoplexes at 0.1 mg/mL in buffer (10 mM HEPES, 0.15 M NaCl, pH 7.4) at 37 °C by measuring the size with DLS analysis Measurements were carried out in triplicate. The size data (nm) were recorded in intensity.

6.2.5. Hemolysis assay

Hemolytic activity of the lipoplexes was investigated by hemolysis assay. With this aim, 10 mL of rat blood was collected in heparinized tubes to prevent coagulation. Rat blood was centrifuged at 500g for 5 min at 4 °C, and levels of hematocrit and plasma were marked on the tube. Plasma was gently removed with a micropipette and replaced with a 150 mM NaCl solution resulting in 5% hematocrit[182]. Then, after three washing-centrifugation cycles of the red blood cells (RBCs), the supernatant was replaced with PBS, pH 7.4. 2 mg/mL of lipoplex formulations, namely, HSPC:DOPE (1:1 and 2:1 mol/mol), HSPC:Cholesterol:DOPE (2:1:1 mol/mol) and HSPC:Cholesterol (2:1 mol/mol) obtained at 10:1 N/P ratio were added to 40 µL of RCBs to yield lipid concentrations of 0.05, 0.1, 0.2, and 0.3 mg/mL. The test was also performed by using 1% v/v Triton X-100 as a positive control, and PBS solution as a negative control. All the samples were incubated for 1 h at 37 °C and then centrifuged

for 5 min at 500g. One hundred µL of supernatant was transferred on a 96-wells plate and the absorbance of released hemoglobin was measured spectrophotometrically at λ 570 nm by a microplate reader (Bio-Teck Instrument, Winooski, VT, USA).

6.2.6. In vitro cellular studies

6.2.6.1. Cytotoxicity assessment by MTT assay

H1299 cells stably expressing enhanced green fluorescence protein (eGFP) were cultured in RPMI-1640 medium supplemented with 10% FBS, 1% (v/v) L-Glutamine, 1% (v/v) penicillin/streptomycin at 37 °C in an atmosphere of 5 % CO2 (v/v). H1299-eGFP cells were seeded in 96-well plates at 7000 cells per well and incubated overnight. On the next day, cells were treated with HSPC:DOPE (1:1 and 2:1 mol/mol), HSPC:Cholesterol:DOPE (2:1:1 mol/mol) and HSPC:Cholesterol (2:1 mol/mol) liposomes without siRNA and lipoplexes loaded with siRNA (siCTRL) at increasing siRNA concentration in the 10-100 nM range for 4 h at 37 °C in opti-MEM. Afterward, treatments were removed and cells were incubated with 1% v/v Triton X-100 solution and with opti-MEM as positive and negative controls, respectively. Then, cells were washed with 200 µL of PBS three times and incubated for an additional 48 h in RPMI-1640 medium supplemented with 10% FBS.

After 48 hours of incubation, cell culture media were removed and replaced with a 180 mL complete medium (RPMI-1640, 10 %FBS) added of 20 µL of 5 mg/mL MTT solution in PBS. Cells were incubated for four hours at 37 °C to allow the formation of the formazan salts. Then the medium was discharged and replaced with 200 µL/well of DMSO. Finally, the plate was mildly shaken for 10 minutes to allow the dissolution of formazan crystals, and the spectrophotometric absorbance was read wavelength of 570 nm using a multimode plate reader (Victor NivoTM, PerkinElmer®). The absorbance was used to calculate the cell viability by referring to the absorbance of the untreated control.

6.2.6.2. Membrane toxicity assessment by LDH assay

Lactate dehydrogenase (LDH) is a cytosolic enzyme present in many different cell types and is a reliable indicator of cytotoxicity. Damage to the plasma membrane releases LDH into the surrounding cell culture media. Therefore, membrane toxicity of the lipoplexes was investigated by the LDH assay according to the manufacturer's protocol. To this aim, H1299-eGFP cells in RPMI 1640 with 10% FBS were seeded at a density of 7000 cells/well into 96 well plates and allowed to attach overnight. The following day, cells were treated with siRNA-loaded lipoplexes obtained with HSPC:DOPE (1:1 and 2:1 mol/mol), HSPC:Cholesterol:DOPE (2:1:1 mol/mol) and HSPC:Cholesterol (2:1 mol/mol), and 4 mol% OCE at 10:1 N/P ratio at increasing siRNA concentration (50, 75, and 100 nM) for 24 hours. Afterward,

50 µL of cell culture supernatant was transferred to a 96-well flat-bottom plate and 50 µL of the LDH titration mixture was added to each sample well and the plate was shaken at 100 rpm in a horizontal shaker at room temperature for 30 minutes. The reaction was stopped by adding 50 µL of stop solution (1 N HCl) and the absorbance was spectrophotometrically measured at 490 and 680 nm after 1 hour. To derive the LDH activity, the 680-nm absorbance value was subtracted (background signal from the instrument) from the 490-nm absorbance value. LDH release of treated cells was compared to nontreated cells (0%), and Triton-X lysed cells (100%, positive control). The LDH control treatment provided within the kit was also employed as a positive control.

6.2.6.3. Cellular uptake

H1299-eGFP cells in RPMI-1640 supplemented with 10% FBS were seeded in 96-well plates at 7000 cells per well and incubated overnight. On the next day, cells were treated with increasing concentrations of HSPC:DOPE (1:1 and 2:1 mol/mol), HSPC:Cholesterol:DOPE (2:1:1 mol/mol) and HSPC:Cholesterol (2:1 mol/mol) lipoplexes loaded with non coding cyanine-5 labeled-siRNA (cy5-siCTRL) at 10:1 N/P ratio (50, 75 and 100 nM siRNA concentration) for 4 h at 37 °C in opti-MEM. Afterward, treatments were removed and cells were washed with 200 µL/well of PBS and detached by incubation with 30 µL/well of trypsin for 5 min at 37°C. The activity of trypsin was quenched by adding 120 µL/well of RPMI 1640 containing 10% FBS. Cell suspensions were subsequently transferred into U-bottom 96 well plate and centrifuged for 5 minutes at 500g. The trypsin-containing medium was removed and cell pellets were resuspended in 80 µL of flow buffer (0.1% Sodium Azide, 1% Bovine Serum Albumin in PBS, pH 7.4) for flow cytometry analysis. Fluorescence of the cy5-siCTRL (excitation at 638 nm and detection with a 660 nm, 20 nm bandpass filter) was measured using a CytoFLEX flow cytometer. Finally, data analysis was performed using the FlowJo software for quantifying the percentage of positive cells as well as the mean fluorescence intensity (MFI).

6.2.6.4. Gene silencing

Quantification of the silencing efficiency by flow cytometric analysis

Gene silencing studies were performed to investigate the therapeutic efficiency of the lipoplexes as shown in Figure 6.12. H1299 cells stably expressing enhanced green fluorescence protein (eGFP-H1299 cells) were seeded in 96-well plates (7000 cells per well) and allowed to attach overnight. On the next day, cells were treated with HSPC:DOPE (1:1 and 2:1 mol/mol), HSPC:Cholesterol:DOPE (2:1:1 mol/mol) and HSPC:Cholesterol (2:1 mol/mol) lipoplexes loaded with eGFP-siRNA (sieGFP) at 10:1 N/P ratio or negative control-siRNA (siCTRL) in opti-MEM in the 10-100 nM range for 4 h at 37°C.

Afterward, treatments were removed and cells were washed with 200 µL of PBS three times and incubated for an additional 48 h.

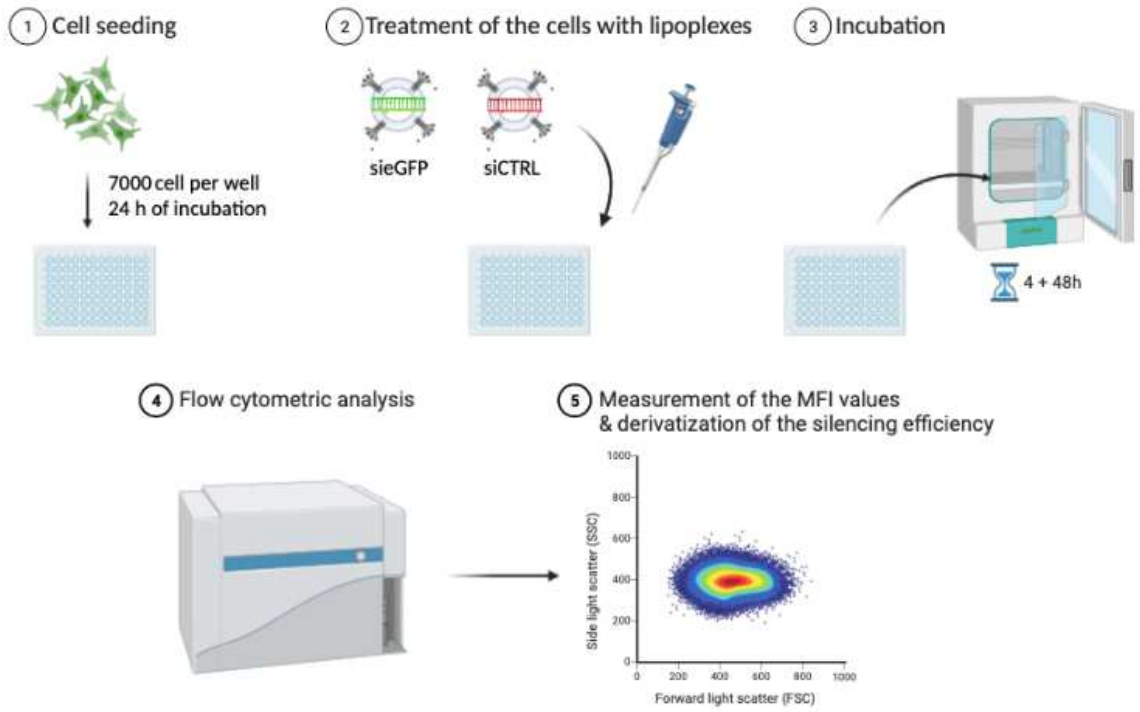

Figure 6.12. *Schematic representation of the procedure used for the quantification of the silencing efficiency by the lipoplexes on* eGFP-H1299 cells.

Cells were then washed with 200 µL of PBS and detached by incubation with 30 µL of trypsin for 5 min at 37 °C. The activity of trypsin was stopped by adding 120 µL of RPMI 1640 + 10% FBS. Cell suspensions were subsequently transferred to U-bottom 96 well plate and centrifuged for 5 minutes at 500g. The supernatant mixture was removed and cell pellets were resuspended in 80 µL of flow buffer (0.1% Sodium Azide, 1% Bovine Serum Albumin in PBS) for flow cytometry analysis. The samples were analyzed by laser irradiation at 488 nm and the fluorescent signal was detected with a 525 filter using a CytoFLEX plate reader flow cytometer (Beckman Coulter, Krefeld, Germany). FlowJo software was used to measure eGFP expression according to equation 6.5. The statistical analysis was performed using two-way ANOVA, *p < 0.05, **p < 0.01, ***p < 0.001.

Equation 6.5:

$$eGFP\ Expression\ (\%) = \frac{MFI\ of\ cells\ treated\ with\ siGFP - lipoplexes}{MFI\ of\ cells\ treated\ with\ siCTRL - lipoplexes}\ x\ 100$$

Silencing efficiency by confocal microscopy

The GFP knockdown efficiency of siGFP-loaded lipoplexes was also investigated by confocal microscopy after treatment of cells with the lipoplexes composed of 1:1 HSPC:DOPE with 4% OCE loaded with siGFP as shown in Figure 6.13. To this aim, H1299-eGFP cells were seeded in 35 mm 4-well CELLview microscopy dishes with glass bottom (Grainer Bio-One, Vilvoorde-Belgium) at a density of $5x10^4$ cells per well and were allowed to settle overnight. After the removal of the cell culture medium, the cells were treated with 1:1 HSPC:DOPE with 4% OCE lipoplexes loaded with siGFP for 4 hours at a 10-100 nM siRNA concentration range. After 4 hours, the treatments were replaced with the cell culture medium and the live-cell imaging was performed after 48 hours. Before the imaging, cells were washed with 1 mL/well of PBS, and nuclei were labeled by incubation with a Hoechst 33342 solution (0.02 mM in PBS) for 15 minutes. After the removal of the Hoechst treatment, cells were washed and maintained in phenol-free opti-MEM and transferred to the microscope stage, and maintained at 37 °C and 5% CO_2 to enable live-cell imaging at optimal conditions. Cells were imaged using lasers at 408 and 488 nm laser lines were used to detect Hoechst 33342 and eGFP proteins, respectively.

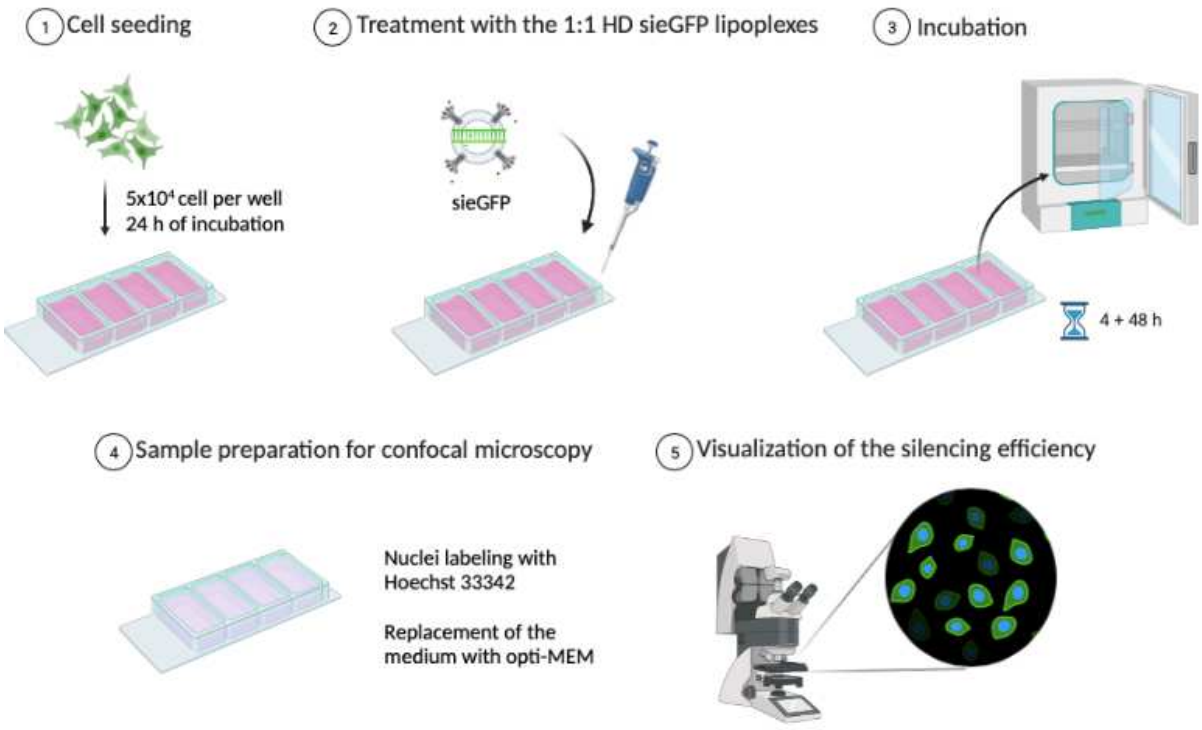

***Figure 6.13**. Schematic representation of the procedures used for the confocal microscopic analysis to detect silencing efficiency on cells treated by siGFP-loaded lipoplexes.*

6.2.6.5. Intracellular trafficking studies

Intracellular trafficking studies were performed to gain a better insight into the silencing process and the intracellular trafficking of the 1:1 HSPC:DOPE lipoplexes obtained with 4% OCE and loaded with cyanine 5 labeled siCTRL. To this aim, eGFP-H1299 cells, at a density of $5x10^4$ cells per well were seeded in 4-well chambers (35 mm) and then allowed to attach overnight. On the next day, cells were treated with 1:1 HSPC:DOPE lipoplexes obtained with 4% OCE and loaded with cyanine-5 labeled siRNA (cy5-siCTRL) at 100 nM siRNA concentration for 30 minutes in opti-MEM. Afterward, treatments were removed and cells were washed with 500 µL of PBS three times. Subsequently, cell nuclei were stained by incubation with 500 µL of a Hoechst 33342 solution (0.02 mM in PBS) for 15 minutes. After the removal of the treatment, cells were washed with 500 µL of PBS three times and lysosomes were stained by incubation with 500 µL of 100 nM Lysotracker red DND-99 solution in PBS for 15 minutes immediately before the confocal visualization at scheduled time points of 1, 2, 4, 6, and 8 hours. The co-localization of the cyanine-5 labeled siRNA with the lysosomes was derived by the Pearson Correlation Coefficient (PCC) using the JACoP plugin of ImageJ software.

7. RESULTS AND DISCUSSION

7.1. Synthesis of the oligocationic enhancer

Nucleic acid delivery represents a challenge for their biomedical application. Upon administration as free molecules, they suffer from a variety of extracellular limitations such as degradation by nucleases, glomerular filtration, and endothelial barrier crossing. Even provided that they can overcome these obstacles, to be effective, nucleic acids have two last barriers to cross: the cell membrane and cytosolic disposition[37]. Within this project, an oligocationic enhancer (OCE) (Figure 7.1) was synthesized as shown in Figure 7.2, and used in the development of the library of lipoplexes to both increase the nucleic acid loading into the lipoplexes and enhance the intracellular access of the carrier. The OCE developed in this thesis has a second-generation dendritic structure end tipped with 4 arginines. This design allows for a high density of cationic charges which is a feature found in natural cell penetration enhancers.

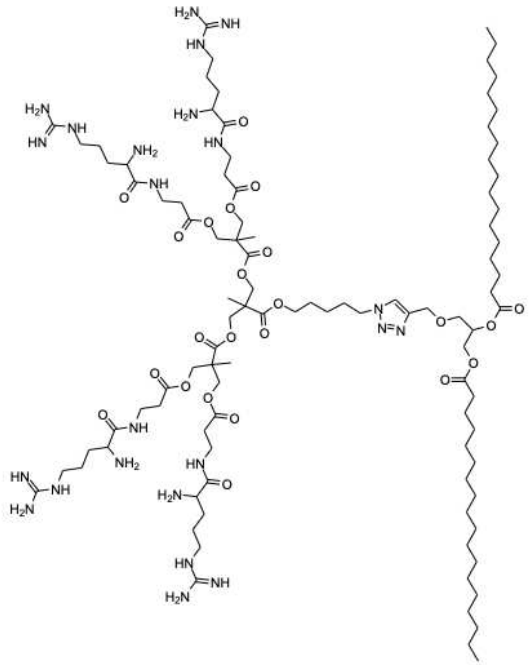

***Figure 7.1**. Chemical structure of the OCE functional component.*

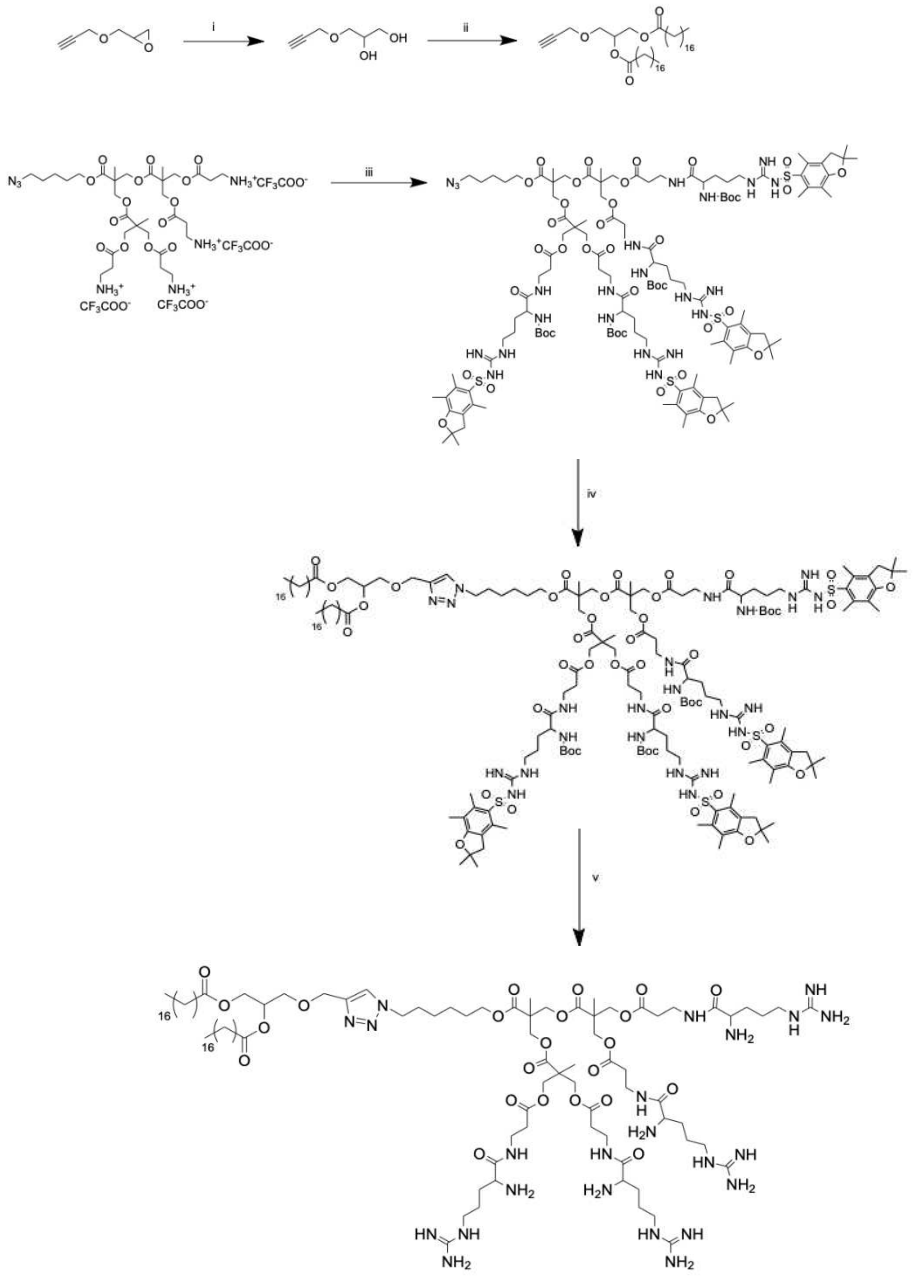

Figure 7.2. *Scheme of the synthesis of the oligocationic enhancer (OCE, ARG$_4$-DAG) functional component for the generation of the lipoplexes. Reagents and conditions: (i) H_2SO_4, $NaHCO_3$, RT, 1h; (ii) Et_3N, DMAP, stearoyl chloride, $CHCl_3$, 0°C, 1h; (iii) Boc-Arg(Pbf)-OH, DMAP, HOBT, HBTU, DMF, RT, 16h; (iv) 2,2-bipyridine, CuI, Sodium ascorbate, DCM, RT, 48h; (v) DCM/TFA 1:1 v/v, RT, 40 min*

The planned scheme of the synthesis of ARG_4-DAG involved 3 steps:

- Synthesis of the lipid anchor
- Synthesis of the arginine decorated dendron
- Huisgen cycloaddition of the lipid anchor to arginine decorated dendron and removal of the protecting groups

7.1.1. Synthesis of the lipid anchor

The surface decoration of the liposomes enables possible specific features and applications of liposomes including improved stability, active targeting, imaging agent delivery, and generation of the gene delivery systems. The surface modifications with functional components request the use of anchoring lipids to graft them. The use of anchoring lipids plays a significant role in coating agents' grafting density[183].

The choice of appropriate lipid anchors can affect several parameters of liposomal formulations, e.g., the sustained transport (or release) of a model cargo during extended circulation, or the durability of association of these molecules to the liposomal surface[184,185]. Dialkyl anchors of any tested length have previously been demonstrated to be more stably anchored to the liposomal membrane than cholesterol derivatives[186]. Furthermore, it was shown that dialkyl glyceryl lipids with a chain length of 18–20 methylene units are inherently stable in liposomal membranes, while those with 16 methylene units show some lipid exchange[187]. In our studies, dialkyl glyceryl lipids with alkyl chains of 18 methylene units were employed to anchor the arginine tipped dendron to liposomes since it is reported to confer noticeable anchor stability, and it also corresponds to the typical chain length founds in phospholipids of biological membranes.

To this aim, first, acid-catalyzed epoxide ring-opening of glycerol propargyl ether was achieved in the presence of H_2SO_4. Then, with the addition of the stearoyl chloride in the presence of the catalysts (DMAP and TEA), 1-(2-propanoxy)glycerol-2,3-distearate ether was obtained and purified with flash chromatography. ^1H NMR spectra of the glycerol monopropargyl ether and glycerol propargyl distearate are reported in Figures 7.3 and 7.4.

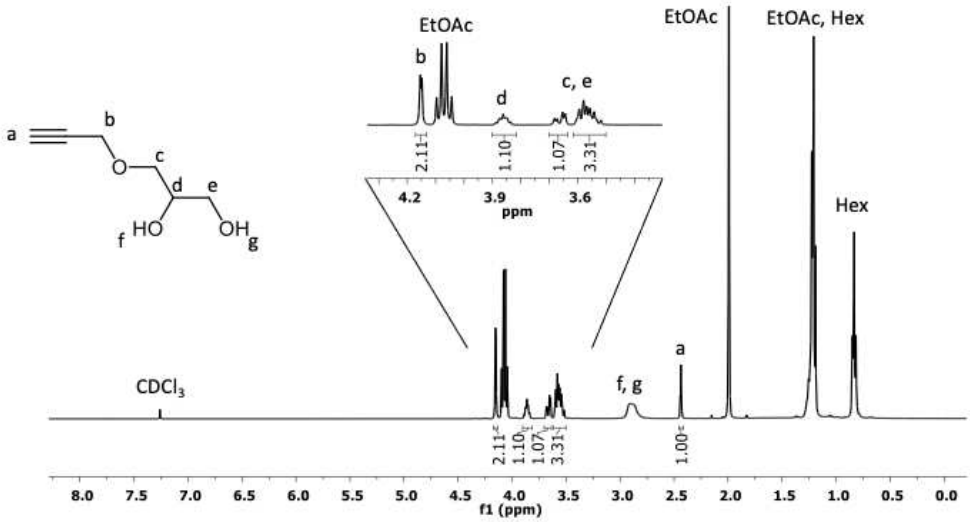

Figure 7.3. *^{1}H NMR spectra of glycerol monopropargyl ether in $CDCl_3$*

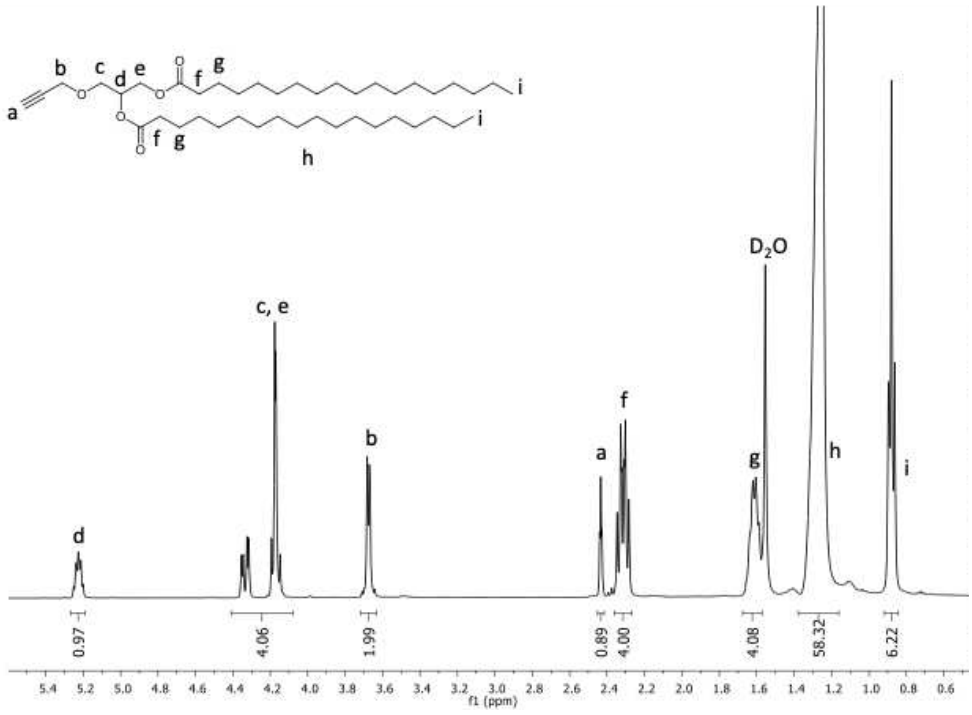

Figure 7.4. *^{1}H NMR spectra of the 1-(2-propanoxy)glycerol-2,3-distearate ether in $CDCl_3$*

7.1.2. Synthesis of the arginine decorated dendron

Dendritic structures, for being highly branched and homogeneous structures, have been investigated as a carrier or as a scaffold for a variety of compounds. The dendritic scaffold was chosen for its excellent biocompatibility, stability in physiological conditions, and biodegradability, already investigated by Feliu et al., which make it suitable for clinical applications. Furthermore, Sheldon reported that cell-penetrating peptides with dendritic architecture typically outperform their linear homologs in terms of cellular uptake[188, 189]. On the other hand, The natural TAT peptide possesses 6 arginines (sequence: GRKKRRQRRRPQ) and possesses 8 cationic charges[190], and the dendron we have designed, due to the presence of both the guanidyl and free ammino groups of arginines, possess 8 cationic charges at physiological pH. Thus, when comparing the charge number of the TAT peptide Use of the dendron comply the requirements for charge similarity.

The dendritic unit (((2-(((6-(4-((2,3-bis(stearoyloxy)propoxy)methyl)-1*H*-1,2,3-triazol-1-yl)hexyl)oxy)carbonyl)-2-methylpropane-1,3-diyl)bis(oxy))bis(carbonyl))bis(2-methylpropane-2,1,3-triyl) tetrakis(3-(2-((*tert*-butoxycarbonyl)amino)-5-(3-((2,2,4,6,7-pentamethyl-2,3-dihydrobenzofuran-5yl) sulfonyl)guanidino)pentanamido)propanoate) was synthesized as explained in Section 6.2.2.3 and identified by ^{1}HNMR analysis in $CDCl_3$ (Figure 7.4).

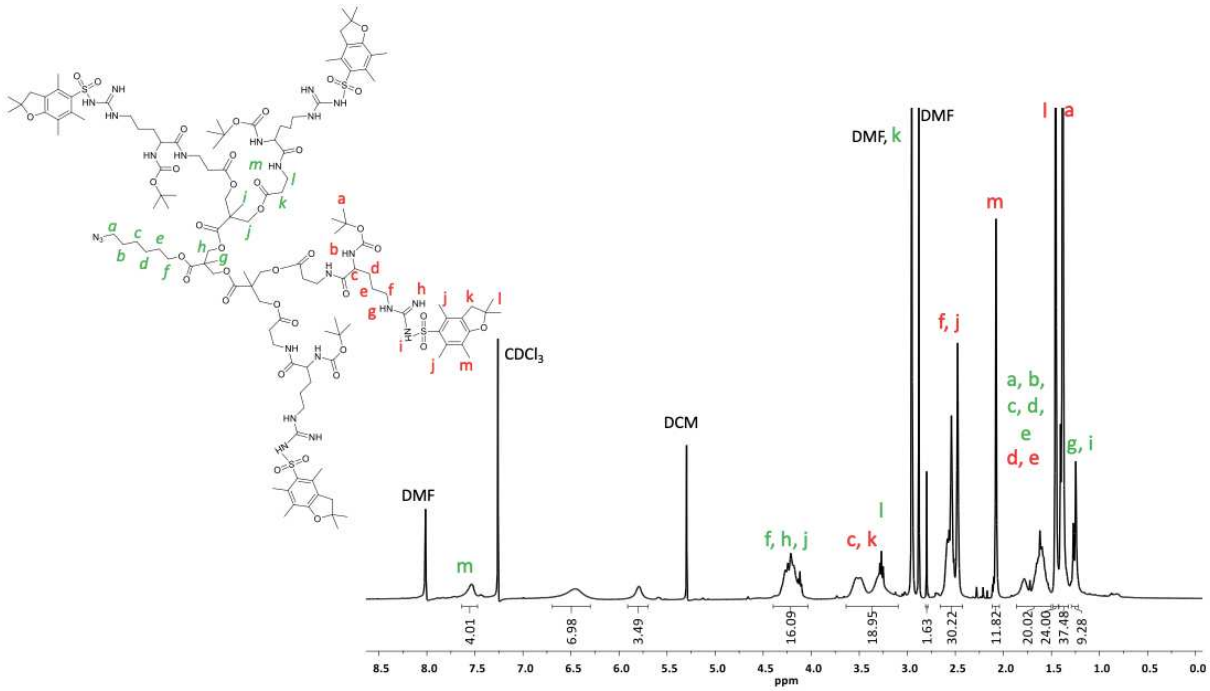

Figure 7.4. *^{1}H NMR spectra of the (((2-(((5-azidopentyl)oxy)carbonyl)-2-methylpropane-1,3-diyl)bis(oxy))bis(carbonyl))bis(2-methylpropane-2,1,3-triyl) tetrakis(3-(2-((tert-butoxycarbonyl)amino)-5-(3-((2,2,4,6,7-pentamethyl-2,3-dihydrobenzofuran-5-yl)sulfonyl)guanidino) pentanamido) propanoate) in $CDCl_3$*

7.1.3. Huisgen cycloaddition of the lipid anchor to arginine decorated dendron and removal of the protecting groups

The second-generation cell penetration enhancer Dendron, Arg_4-DAG, (Figure 7.1), is based on dendron unit (((2-(((6-(4-((2,3-bis(stearoyloxy)propoxy)methyl)-1*H*-1,2,3-triazol-1-yl)hexyl)oxy)carbonyl)-2-methylpropane-1,3-diyl)bis(oxy))bis(carbonyl))bis(2-methylpropane-2,1,3-triyl) tetrakis(3-(2-((*tert*-butoxycarbonyl)amino)-5-(3-((2,2,4,6,7-pentamethyl-2,3-dihydrobenzofuran-5yl) sulfonyl)guanidino)pentanamido)propanoate) and a 1-(2-propanoxy)glycerol-2,3-distearate ether anchoring unit for liposome association on the other side was synthesized by the Cu(I)-catalyzed Huisgen 1,3- dipolar cycloaddition ("click" reaction) between the alkyne terminated distearoyl propane anchoring unit and the azide terminated tetra-Boc-arginyl(Pbf) dendron followed by TFA mediated deprotection of the arginine protecting groups. The product before deprotection (((2-(((6-(4-((2,3-bis(stearoyloxy)propoxy)methyl)-1*H*-1,2,3-triazol-1-yl)hexyl)oxy)carbonyl)-2-methylpropane-1,3-diyl)bis(oxy))bis(carbonyl))bis(2-methylpropane-2,1,3-triyl) tetrakis(3-(2-((*tert*-butoxycarbonyl)amino)-5-(3-((2,2,4,6,7-pentamethyl-2,3-dihydrobenzofuran-5yl) sulfonyl)guanidino)pentanamido)propanoate) was identified by ^{1}HNMR analysis in $CDCl_3$. (Figure 7.5)

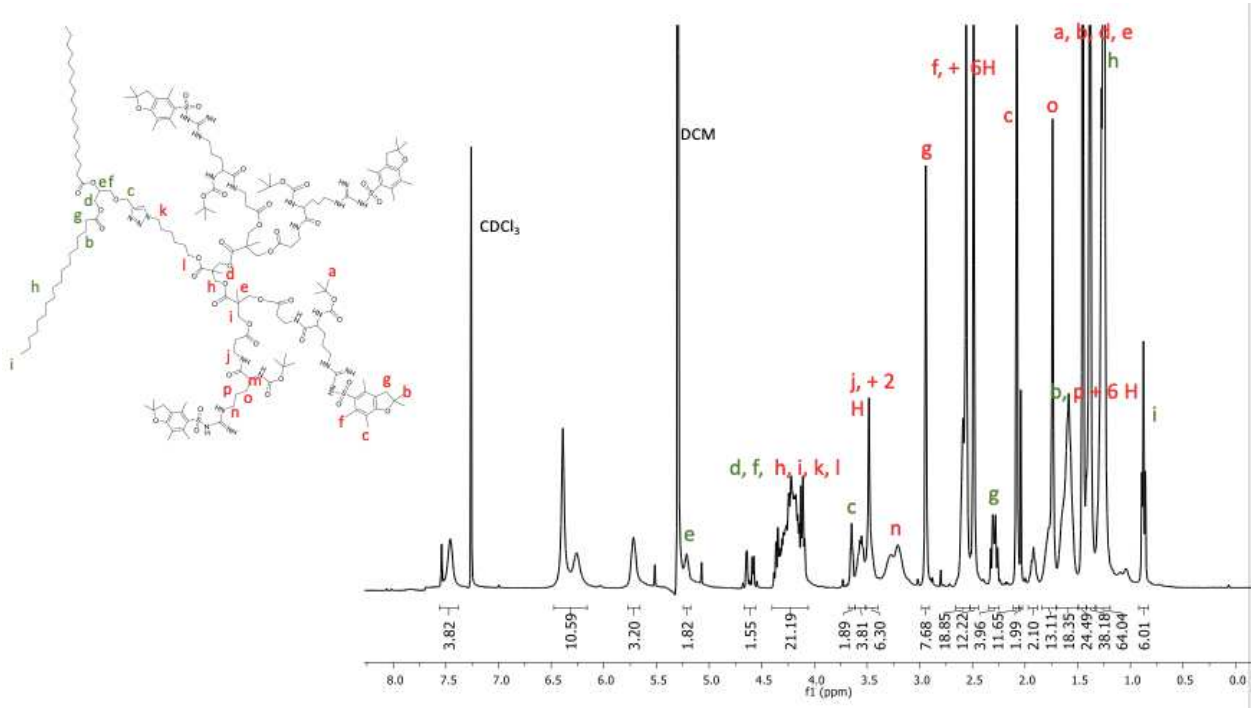

Figure 7.5. *^{1}H NMR spectra of the (((2-(((6-(4-((2,3-bis(stearoyloxy)propoxy)methyl)-1H-1,2,3-triazol-1-yl)hexyl)oxy)carbonyl)-2-methylpropane-1,3-diyl)bis(oxy))bis(carbonyl))bis(2-methylpropane-2,1,3-triyl) tetrakis(3-(2-((tert-butoxycarbonyl)amino)-5-(3-((2,2,4,6,7-pentamethyl-2,3-dihydrobenzofuran-5yl) sulfonyl)guanidino)pentanamido)propanoate)in $CDCl_3$*

The final alkylated oligo arginine dendron ((((2-(((6-(4-((2,3-bis(stearoyloxy)propoxy)methyl)-1*H*-1,2,3-triazol-1-yl)hexyl)oxy)carbonyl)-2-methylpropane-1,3-diyl)bis(oxy))bis(carbonyl))bis(2-methylpropane-2,1,3-triyl) tetrakis (3-(2-amino-5-guanidinopentanamido)propanoate)) was obtained with high purity, as proved by the ^{1}H NMR spectra (Figure 7.6, A) and the m/z signal at 516 of the [M+4H]4+ ion confirmed its identity (Figure 7.6, B).

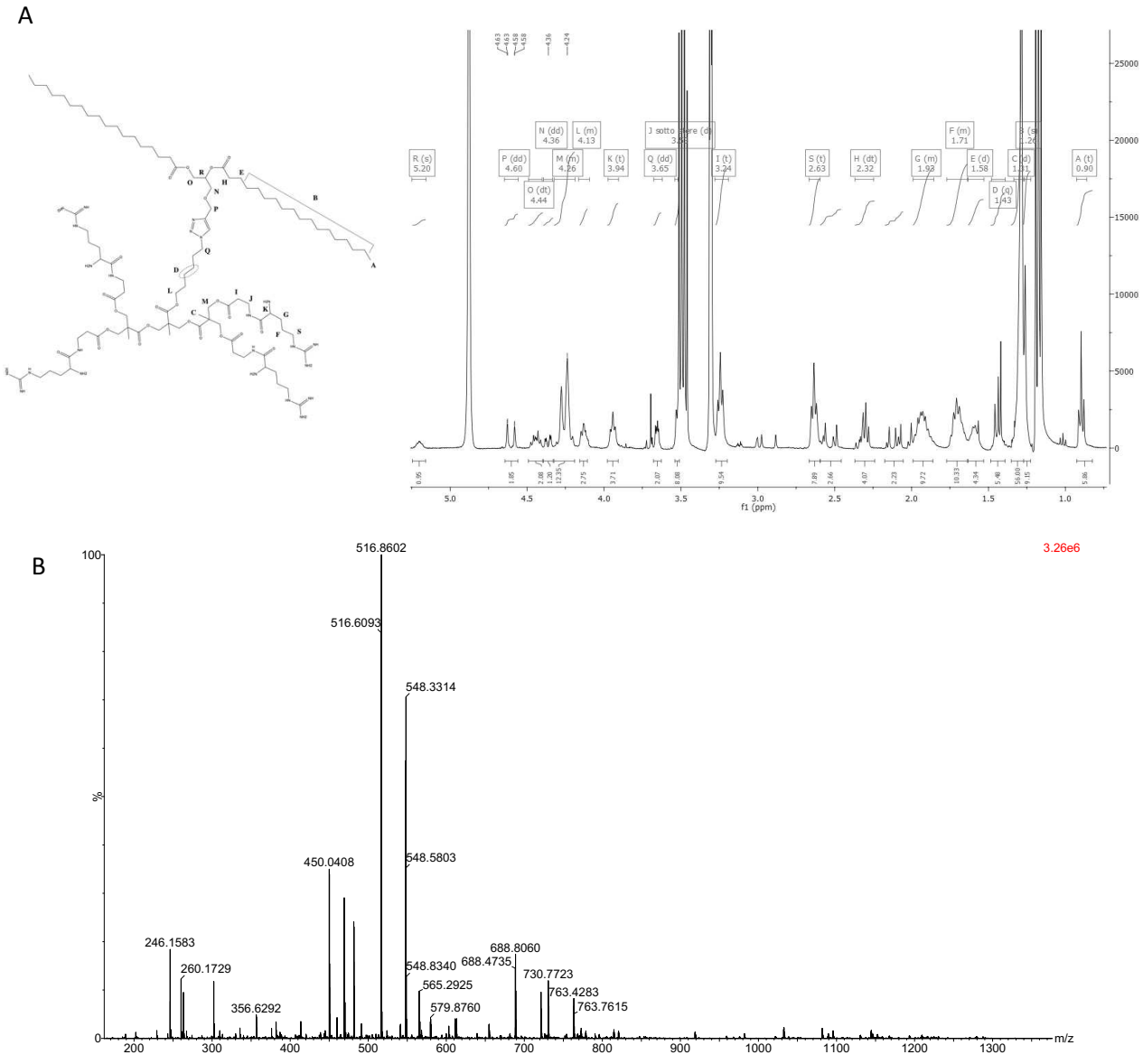

Figure 7.6. *^{1}H NMR (A) and ESI-TOF mass spectra (B) of the((((2-(((6-(4-((2,3-bis(stearoyloxy)propoxy)methyl)-1H-1,2,3-triazol-1-yl)hexyl)oxy)carbonyl)-2-methylpropane-1,3-diyl)bis(oxy))bis(carbonyl))bis(2-methylpropane-2,1,3-triyl) tetrakis (3-(2-amino-5-guanidinopentanamido)propanoate))*

7.2. Lipoplexes preparation

7.2.1. Selection of the OCE ratio

The optimum molar percentage of the oligocationic enhancer unit within the liposomal composition was first investigated. With this aim, liposomes were prepared by thin layer hydration method with 2:1 (mol/mol) HSPC/cholesterol composition including also the OCE at increasing molar ratios. The results of the characterization of liposomes are shown in Figure 7.7.

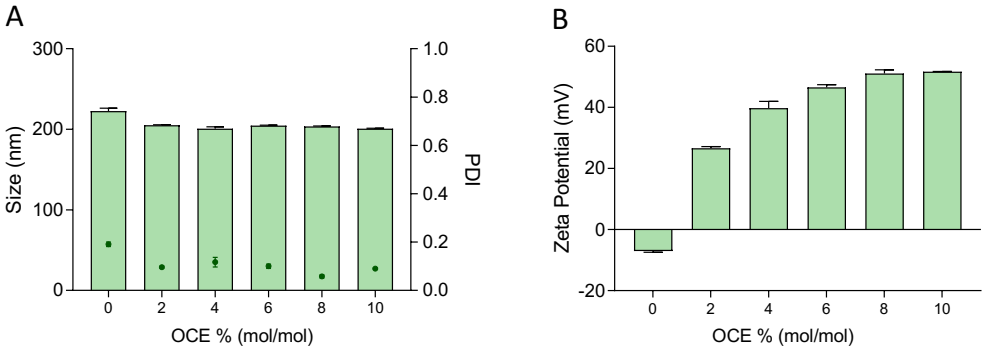

Figure 7.7. *Particle size, polydispersity index (A) and zeta potential (B) values of the cationic liposomes generated with 2:1 (mol/mol) HSPC/cholesterol composition and 0-10 % OCE molar ratios.*

The applications of nano-sized drug delivery systems require particle size control since it is a crucial feature. Although the average particle size of LNPs is typically between 100 and 400 nm, having a size below 200 nm is more desirable for systemic applications[191]. The results reported in Figure 7.7 show that the size of the 2:1 (mol/mol) HSPC/cholesterol liposomes generated by the thin layer hydration method with and without OCE was around 200 nm, which was expected since the extrusion of the liposomes was performed with a 200 nm cut-off membranes. A slight change in the sizes of the lipoplexes was observed. This behavior may be attributable to a different arrangement of the behavior as the density of the cationic OCE is introduced in the lipid bilayer. However, the mechanism of this effect must be further elucidated with dedicated studies.

The PDI value shows the degree of particle distribution with a range of 0 to 1. A PDI lower than 0.2 is frequently regarded as having a narrow size distribution, whereas most studies set a PDI value of less than 0.3 as the upper limit[191]. The measured PDI values for each liposomal formulation obtained with increasing were below 0.2, confirming the homogeneity of the samples.

The Zeta Potential (ZP) is a parameter that better reports the surface charge density of the particles. Typically ZP higher than +30 mV or lower than -30 mV is considered to be suitable to maintain colloidal

stability because of electrostatic repulsion[191]. The ZP analyses revealed that the surface charge of liposomes is positive and increases as the ratio of OCE added increases with respect to lipids, proving that the cationic lipid was successfully inserted in the liposomes bilayer. The increase of the zeta potential was reaching a plateau when OCE mol% fed into liposomes was at 8 mol%, having zeta potentials of about +51 mVs. The plateauing of the zeta potential may be attributed to a saturation of OCE of both sides of the lipid membrane of liposomes with a threshold of density that is achieved at about 8 mol% of fed OCE because of the electrostatic repulsions of the oligo-cationic OCE unimers.

During the selection of the OCE ratio within the liposomes, the OCE association efficiency to the lipid bilayer was also assessed. To this aim, the OCE associated with the liposomes was quantified after removal by centrifugation of the non-associated OCE using a calibration line generated with arginine. The results of the OCE insertion efficiency are reported in Figure 7.8.

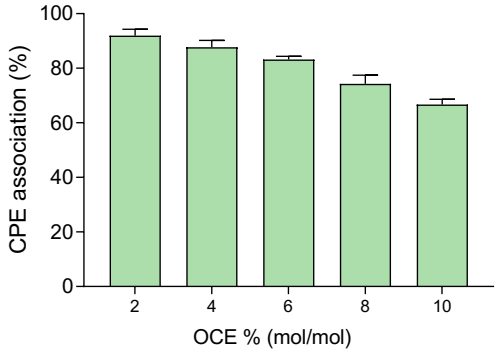

Figure 7.8. *OCE association efficiency (%) of the cationic liposomes was obtained with 2:1 (mol/mol) HSPC/cholesterol composition and 0-10 mol% fed OCE molar ratios.*

The results of the association assessment showed that when liposomes are generated with a 2 mol% fed ratio with respect to lipids, the association percentage is over 90 percent, and with the increasing fed percentage the association efficiency slightly decreased. Indeed, when OCE is fed at 10% in molar ratio, only 70 mol% of the OCE is associated with the lipid bilayer. The decrease in the association efficiency of the OCE can be due to the saturation of both the inner and outer surface of the liposome bilayer, as a result of electrostatic repulsion of the oligo-cationic macromolecule when in proximity. These results elucidate the plateau observed on the zeta potential profile as the OCE fed is increased. Based on the combined results of the zeta potential plateau and the association efficiency, 4 mol% OCE was selected for the production of the lipoplexes.

7.2.2. Selection of the lipid composition

To tailor the features of the liposomal surface and membrane layer, the lipids used to assemble the liposomes can be rationally selected and combined at different molar ratios. Phospholipids, the primary constituents of biological membranes, are also the lipids that are employed most frequently to formulate liposomes. These compounds have a glycerol core molecule connecting two hydrophobic alkyl acids to a hydrophilic polar head group with a phosphate group, making them amphipathic molecules[185]. It is well known that the degree of fatty acid chain saturation in the bilayer membrane structure regulates membrane fluidity and packing density[192]. The transition temperature of the majority of long-chain saturated fatty acids is higher than ambient or body temperature. This indicates that the fatty acid chains in the lipid bilayer are spatially organized either in a liquid-crystalline or crystalline state rather than being truly liquid[193]. Conversely to saturated lipid chains, unsaturated fatty acids generate voids between their alkyl tails, which results in fewer intermolecular interactions and greater membrane fluidity also at room and body temperature as a result of a lower transition temperature.

To investigate the effect of lipid saturation on the colloidal features, loading efficiency, and leakage of lipoplexes, the saturated phospholipid HSPC, and the unsaturated phospholipid EPC were employed. HSPC/Cholesterol (2:1 mol/mol) and EPC/Cholesterol (2:1 mol/mol) formulations were generated without DOPE. Then cholesterol was gradually replaced with the fusogenic lipid DOPE up to 75% (mol/mol) concerning total lipids to monitor also the effect of the DOPE on the colloidal features, loading efficiency, and leakage of lipoplexes. Lipoplexes were loaded with dsDNA at a 10:1 N/P ratio for this study. The formulations were characterized in terms of particle size, PDI, and zeta potential by DLS. The results of the DLS analysis are shown in Figure 7.9.

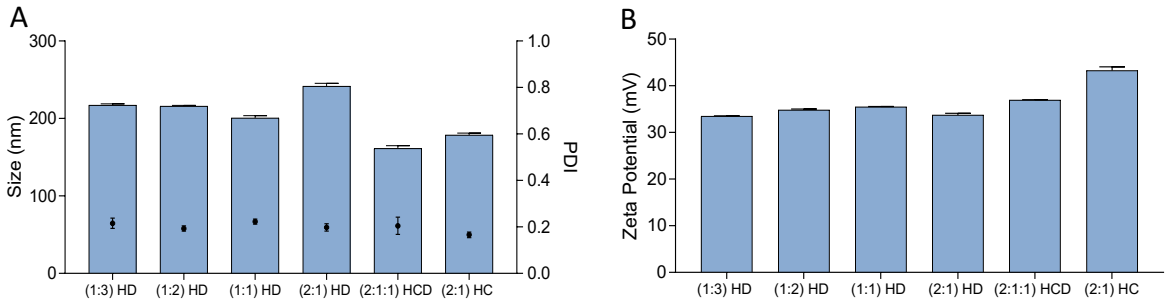

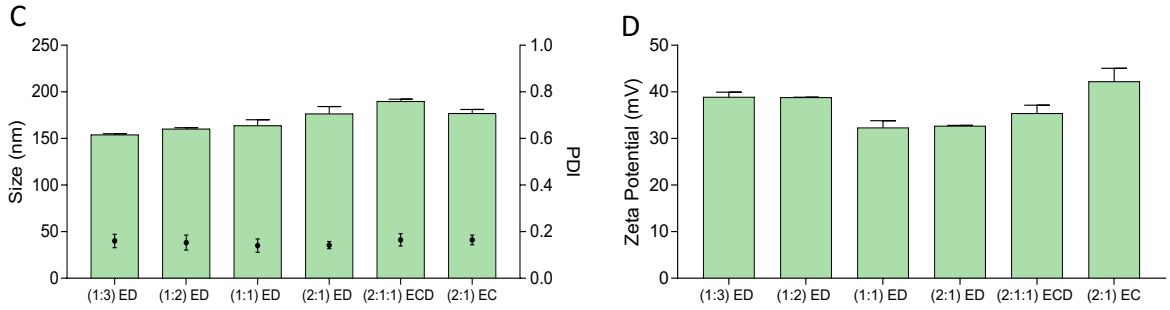

Figure 7.9. *Particle size, polydispersity index (A and C), and zeta potential (B and D) profiles of the HSPC (■) and EPC(■)-based lipoplexes obtained with 4 mol% of OCE and loaded with dsDNA 10:1 N/P ratio. Acronyms: (1:3) HD:HSPC/DOPE (1:3 mol/mol); (1:2) HD:HSPC/DOPE (1:2 mol/mol); (1:1) HD:HSPC/DOPE (1:1 mol/mol); (2:1) HD:HSPC/DOPE (2:1 mol/mol); (2:1:1) HCD:HSPC/Cholesterol/DOPE (2:1:1 mol/mol); (2:1) HC:HSPC/Cholesterol (2:1 mol/mol); (1:3) ED:EPC/DOPE (1:3 mol/mol); (1:2) ED:EPC/DOPE (1:2 mol/mol); (1:1) ED:EPC/DOPE (1:1 mol/mol); (2:1) ED:EPC/DOPE (2:1 mol/mol); (2:1:1) ECD:EPC/Cholesterol/DOPE (2:1:1 mol/mol); (2:1) EC:EPC/Cholesterol (2:1 mol/mol)*

The results reported in Figure 7.9, Panel A show that HSPC-based lipoplexes generated with 4 mol% OCE at a 10:1 N/P ratio have a size of about or lower than 200 nm, and no relevant difference in size was observed depending on the composition. Indeed, observed sizes were varying between 179 and 218 nm. Similar to HSPC-based lipoplexes, EPC-based lipoplexes with the same lipid ratios showed sizes lower than 200. The measured sizes varied between 154 and 189 nm. a slight difference in the size profiles of the HSPC and EPC-based lipoplexes were observed; in particular the EPC-based lipoplexes containing DOPE and without Cholesterol showed a slightly lower size with respect to their HSPC-based counterparts. This effect can be attributed to the difference in the saturation levels of the phospholipids employed in combination with the DOPE, which is also an unsaturated lipid. Indeed, phospholipids with saturated fatty acid chains are mostly observed in the gel phase, where the lipid acyl chains become straight and ordered, the lipid head groups are closely packed and bilayer thickness is increased[194].

The PDI profile of the libraries of lipoplexes showed that lipoplexes generated at a 10:1 N/P ratio by the thin layer hydration technique followed by extrusion through 200 nm cut-off membranes had a very low polydispersity (< 0.2) independent of their composition (Figure 7.9, Panels A and C).

The zeta potential measurement results showed that lipoplexes generated with 4 mol% OCE at a 10:1 N/P ratio present a high zeta potential (>30 mV) independent of the phospholipid used (i.e. saturated HSPC and unsaturated EPC phospholipids) and other lipids present in the composition (i.e. cholesterol and DOPE). This was expected since the only lipid with net cationic charge is the functional component OCE. Furthermore, the similar profile in terms of surface charge of the libraries of lipoplexes suggests that OCE is associated with all of the lipoplexes formulations. This was further confirmed by assessing

the OCE associated with each lipoplexes library component which confirmed that more than 90 % of the fed OCE was combined with the lipoplexes in agreement with results reported in Section 7.2.1, Figure 7.8.

The effect of lipid saturation on the loading efficiency and capacity of the lipoplexes was investigated on the same two libraries of lipoplexes reported above obtained either by HSPC or EPC, 4 mol% OCE and loaded with dsDNA at a 10:1 N/P ratio. After assembly, non-loaded dsDNA was removed by dialysis lipid and dsDNA concentrations were assessed. Loading efficiency was calculated after normalizing the dsDNA to the lipid recovery. Results of the loading efficiency and capacity profiles of the two lipoplexes libraries are reported in Figure 7.10

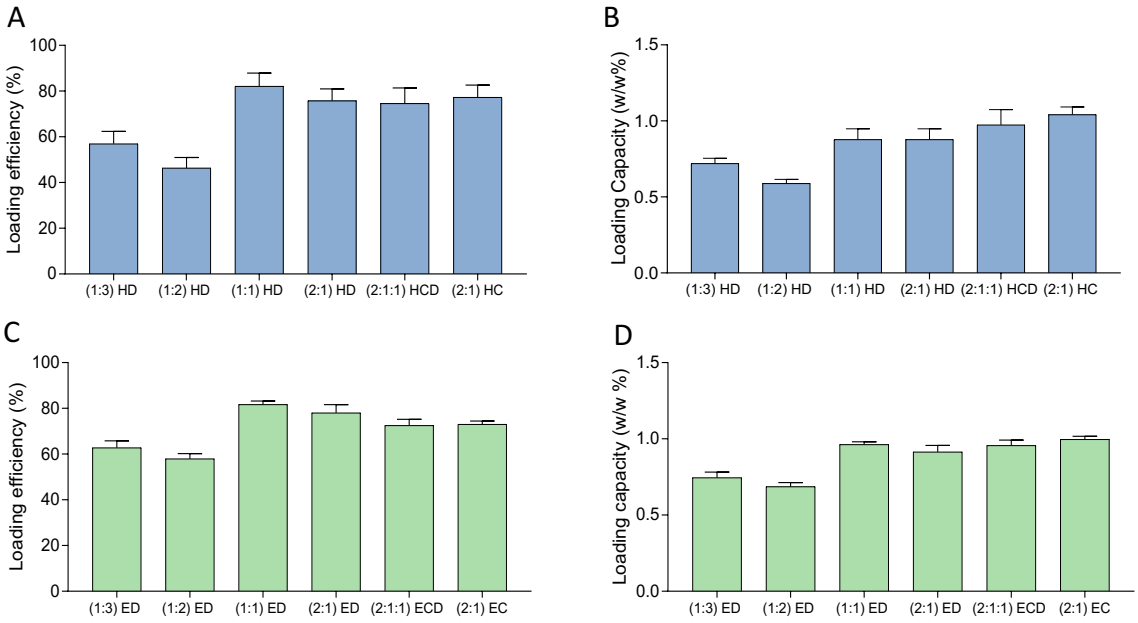

Figure 7.10. *Loading efficiency (A and C), and loading capacity (B and D) profiles of the HSPC (■) and EPC(■) based lipoplexes were obtained with 4 mol% of OCE and loaded with dsDNA A at a 10:1 N/P ratio. Acronyms: (1:3) HD:HSPC/DOPE (1:3 mol/mol); (1:2) HD:HSPC/DOPE (1:2 mol/mol); (1:1) HD:HSPC/DOPE (1:1 mol/mol); (2:1) HD:HSPC/DOPE (2:1 mol/mol); (2:1:1) HCD:HSPC/Cholesterol/DOPE (2:1:1 mol/mol); (2:1) HC:HSPC/Cholesterol (2:1 mol/mol); (1:3) ED:EPC/DOPE (1:3 mol/mol); (1:2) ED:EPC/DOPE (1:2 mol/mol); (1:1) ED:EPC/DOPE (1:1 mol/mol); (2:1) ED:EPC/DOPE (2:1 mol/mol); (2:1:1) ECD:EPC/Cholesterol/DOPE (2:1:1 mol/mol); (2:1) EC:EPC/Cholesterol (2:1 mol/mol)*

Figure 7.10, Panel A shows that HSPC-based lipoplexes generated with 4 mol% OCE at the 10:1 N/P ratio overall result in high loading efficiency which is attributed to the contribution of the cationic charges provided by the OCE that drive the electrostatic association with nucleic acids. All lipid compositions tested provided more than 50 % loading into the lipoplexes of the processed dsDNA. The lowest loading efficiency was observed for the lipoplexes generated with 1:2 HSPC/DOPE composition (52.3 ± 4.1%) while the highest loading efficiency was achieved by the lipoplexes

generated with 1:1 HSPC/DOPE composition by 82.14 ± 5.7%. Loading efficiency of the other formulations (1:3 HSPC/DOPE, 2:1 HSPC/DOPE, 2:1:1 HSPC/Cholesterol/DOPE, and 2:1 HSPC/Cholesterol) were included between 57 and 77%. A similar profile was observed for the EPC-based lipoplexes, overall showing loading efficiencies higher than 50%. The lowest loading efficiency was displayed by the 1:2 EPC/Cholesterol lipoplexes with 58.0 ± 2.2% and the highest efficiency was observed with the 1:1 EPC/Cholesterol lipoplexes with 81.7 ± 1.4%. The loading efficiency of the other formulations was in the 62-73% range. Eventually, we observed that the lipids with different saturation degrees (namely HSPC and EPC) did not affect the loading efficiency. This result confirms that the driving force for the loading of nucleic acid in lipoplexes is mostly attributed to OCE. However, within the same library of lipoplexes, we noticed that DOPE may have some detrimental effect on the loading efficiency since the formulations with the highest ratios of DOPE showed a decrease in loading either in lipoplexes obtained with HSPC or EPC. This may be due to a looser structure of the lipid bilayer at a high DOPE/phospholipids ratio resulting in a decrease in entrapment. Cholesterol did not alter the loading when replacing DOPE at the same ratio.

To investigate the effect of the phospholipid saturation on the release profile, a release study was performed using 1:3, 1:2, 1:1, 2:1 HSPC/DOPE, 2:1:1 HSPC/Cholesterol/DOPE, and 2:1 HSPC/Cholesterol lipoplexes and their counterparts obtained with EPC in place of HSPC, both at physiological pH (7.4) and endosomal pH (5.5). The results of the release studies of the HSPC-based lipoplexes are shown in Figure 7.11.

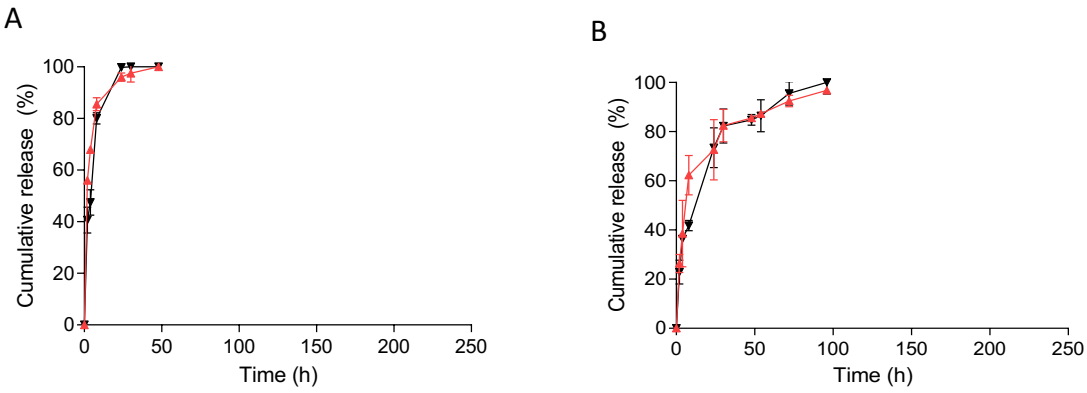

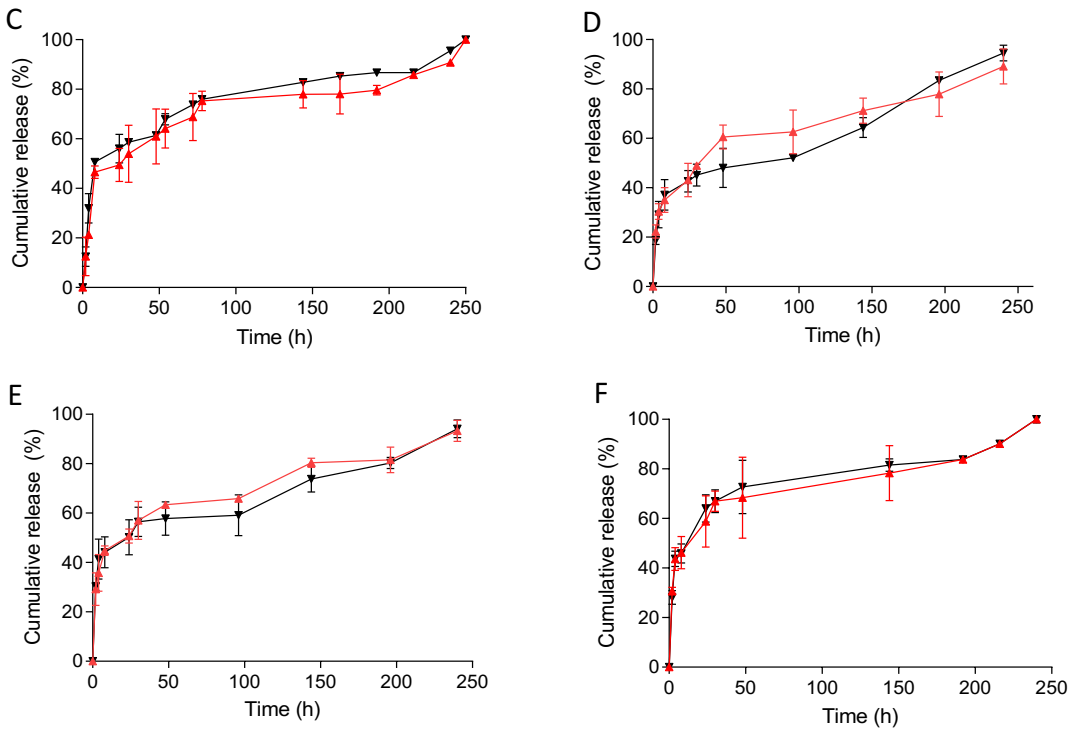

Figure 7.11. *Release profiles of cy3-dsDNA from the 1:3 HSPC/DOPE (A), 1:2 HSPC/DOPE (B), 1:1 HSPC/DOPE (C), 2:1 HSPC/DOPE (D), 2:1:1 HSPC/Cholesterol/DOPE (E) and 2:1 HSPC/Cholesterol (F) lipoplexes generated at 10:1 N/P ratio and with 4 mol% OCE in acetate buffer at pH 5.5 (—) and in HBS buffer pH 7.4 (—).*

As shown in Figure 7.11, the release of the dsDNA from the HSPC-based lipoplexes is prolonged for all formulations over 10 days under the two pH conditions used. Independently from the composition, lipoplexes have shown a burst release in the first 24 hours with a faster release for the two formulations containing the highest DOPE molar ratio; indeed, the release was 98.7 ± 1.6 % and 73.4 ± 8 % for the 1:3 and 1:2 HSPC/DOPE lipoplexes at pH 5.5 after 24 hours. The faster release of the formulations with higher DOPE molar ratio agrees with the lower loading and may be correlated to a looser structure of the lipid bilayer thus allowing faster diffusion of the encapsulated dsDNA. After 24 hours of release, lipoplexes have shown a slower release profile. After 10 days, over 90% of the loaded dsDNA was released for all of the formulations. A very similar release profile was observed in the studies conducted in pH 7.4 HBS. At the given time points, for each formulation, the difference in the amount of the released dsDNA in different buffers was found to be not significant and thus no effect of the environment pH was observed.

The results of the release studies of the 1:3, 1:2, 1:1, 2:1 EPC/DOPE, 2:1:1 EPC/Cholesterol/DOPE, and 2:1 EPC/Cholesterol lipoplexes are shown in Figure 7.12.

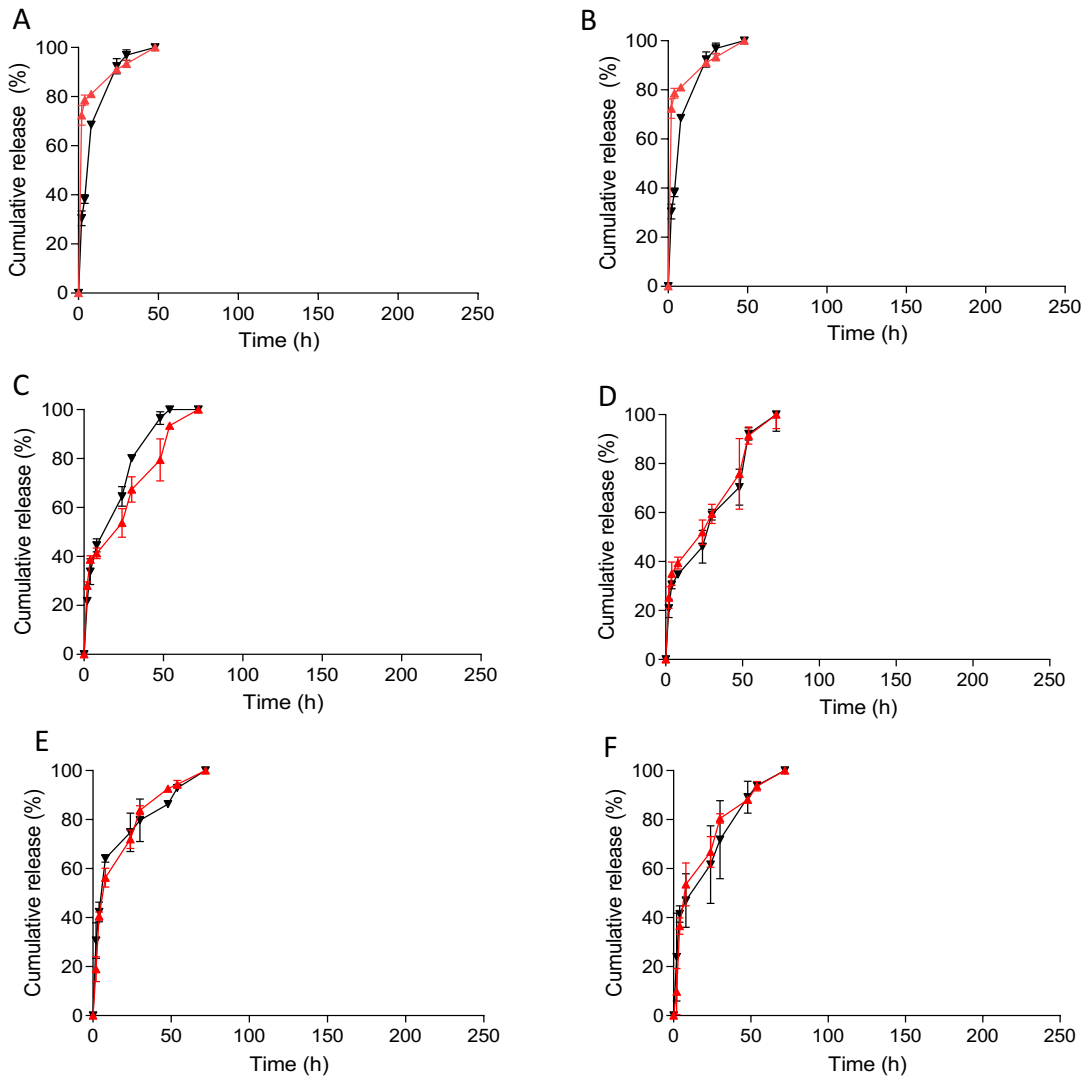

Figure 7.12. *Release profile of cy3-dsDNA from the 1:3 EPC/DOPE (A), 1:2 EPC/DOPE (B), 1:1 EPC/DOPE (C), 2:1 EPC/DOPE (D), 2:1:1 EPC/Cholesterol/DOPE (E) and 2:1 EPC/Cholesterol (F) lipoplexes generated at 10:1 N/P ratio with 4 mol% OCE in acetate buffer pH 5.5 (—) and HBS buffer in pH 7.4 (—).*

The release of the dsDNA from the EPC-based lipoplexes is about 3 times faster than that observed for the HSPC-based lipoplexes. Indeed, dsDNA is released from all formulations in 3 days. Also, this library of formulations presented a burst release within the first 6-10 hours and a lower release afterward. Similar to the HSPC-based library, the lipoplexes containing the highest molar ratio of DOPE release faster the nucleic acid payload: indeed, the release was 90.32 % and 91.08 % for the 1:3 and 1:2 EPC/DOPE lipoplexes at pH 5.5 after 10 hours showing that DOPE increases the permeability of the lipid bilayer of liposomes as observed for the HSPC counterparts. This can be explained by the

enhanced permeability of the phospholipid vesicle membranes when the temperature is near or above their transition temperature[195] due to the formation of grain boundaries between the gel and the fluid phases in the lipid bilayer[196]. Indeed, DOPE, EPC and HSPC are characterized by transition temperatures of -16, -7, and +50 °C, respectively.

The lipoplexes obtained with the highest DOPE molar ration (namely, 1:3 and 1:2 HSPC/DOPE molar ratios) were excluded from further studies since they provide the lowest loading efficiency with the library (lower than 56%) while all the other library members had loading efficiency above 74%. The library obtained with EPC was instead excluded from further studies since those lipoplex formulations release the nucleic acid about three times faster than the HSPC-based library at pH 7.4 with a burst release of about 40 % within the first 6-8 hours which showed its poorer biopharmaceutical features for therapeutic applications with respect to the HSPC based-lipoplex library.

7.2.3. N/P ratio effect on lipoplexes colloidal and biopharmaceutical features

The ratio of the positively-charged guanidyl (N) groups of the OCE to negatively-charged phosphate (P) groups (N/P ratio) of nucleic acids is possibly one of the key chemical features of gene delivery vehicles because the N/P ratio dictated the loading efficiency of nucleic acids and can affect many formulation properties such as surface charge, particle size, and stability[181]. Therefore, the identification of the ratio that provides vehicles with suitable colloidal and biopharmaceutical properties for gene delivery systems is crucial.

To this aim, the lipoplexes with 1:1 HSPC/DOPE, 2:1 HSPC/DOPE, 2:1:1 HSPC/Cholesterol/DOPE and 2:1 HSPC/Cholesterol composition were generated with 4 mol% of OCE at decreasing N/P ratios from 10:1 to 1:1. Control lipoplexes without OCE were also generated to derive information about the contribution of the OCE in the loading of lipoplexes at each N/P ratio tested. The particle size and polydispersity index of the generated formulations are shown in Figure 7.13.

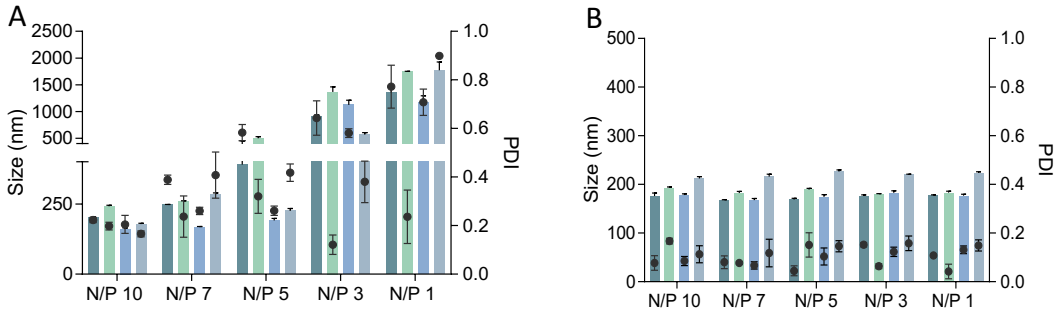

Figure 7.13. *Particle size and polydispersity index profiles of the lipoplexes generated with 4 mol % OCE (A) and liposomes generated without OCE (B) with 1:1 HSPC/DOPE (■), 2:1 HSPC/DOPE (■), 2:1:1 HSPC/Cholesterol/DOPE (■) and 2:1 HSPC/Cholesterol (■) compositions.*

The size and PDI analysis results showed that the lipoplexes generated with 4 mol% OCE at the N/P ratio of 10:1 possess a size of 200 nm and are homogeneous with low PDI (< 0.2). Higher N/P ratios than 7:1 resulted in lipoplexes sizes of about 200-250 nm while at lower N/P ratios the size tended to increase as a result of the electrostatic crosslinking of the cationic liposomes by the excess of nucleic acids Especially the lipoplexes composed of 1:1 HSPC/DOPE and 2:1 HSPC/DOPE the detected particle sizes at an N/P ratio of 5:1 were about 500 nm, while the size of the 2:1:1 HSPC/Cholesterol/DOPE and 2:1 HSPC/Cholesterol lipoplexes did not increase with respect to the formulation obtained at N/P ratio of 7:1. However, at N/P ratio below 5:1 all lipoplexes, regardless their composition, aggregates were observed with size above 600 nm and over 1 µm for N/P ratio 1:1 overall increase of the PDI values. Aggregation observed at low N/P ratios occurred independently from the lipoplexes composition. Similarly to lipoplexes generated with OCE, liposomes generated without OCE at the N/P ratio of 10:1 had a size of about 200 nm and low PDI (<0.2) but on the contrary, the decrease in N/P ratio did not affect the particle sizes. Indeed these liposomes do not have cationic surface charges that can be cross-linked by the presence of nucleic acids. Furthermore, the PDI value was also not affected by the change of the increasing dsDNA ratio with respect to lipids and for all the investigated N/P ratios, it remained lower than 0.2. Notably, these liposomes do not have the guanidyl groups of the OCE, and thus the N/P ratio was calculated by using an equivalent amount of lipids processed for the OCE containing lipoplexes.

Zeta potential measurement results of the lipoplexes and liposomes generated with the 1:1 HSPC/DOPE, 2:1 HSPC/DOPE, 2:1:1 HSPC/Cholesterol/DOPE and 2:1 HSPC/Cholesterol composition is reported in Figure 7.14.

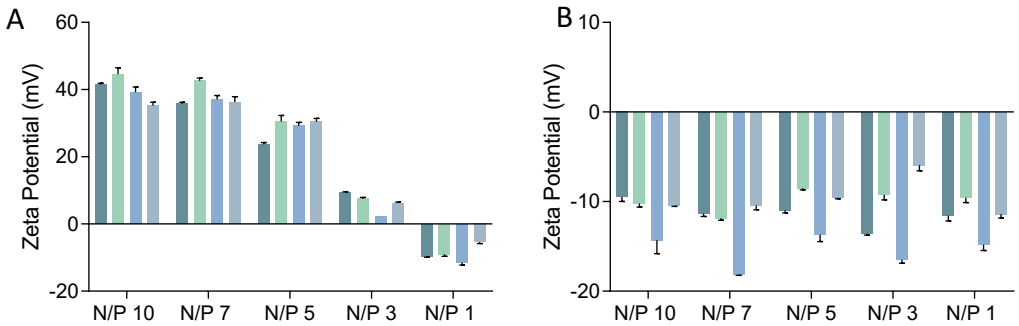

Figure 7.14. *Zeta potential profiles of the lipoplexes generated with 4 mol% OCE (A) and liposomes generated without OCE (B) in 1:1 HSPC/DOPE (■), 2:1 HSPC/DOPE (■), 2:1:1 HSPC/Cholesterol/DOPE (■) and 2:1 HSPC/Cholesterol (■) compositions.*

Figure 7.14 panel A shows that lipoplexes with 4 mol% OCE generated at 10:1 and 7:1 N/P ratios had a high zeta potential (~ 40 mV) as a result of the excess of cationic charges with respect to the nucleic acids The decrease of the N/P ratio of the lipoplexes since the negatively charged dsDNA in the lipoplexes quenches the OCE charges. The decrease of the ZP of lipoplexes as the N/P ratio decrease from 5:1 to 3:1 also explains the aggregation profile observed in Figure 7.13 since the quenching of the cationic charges of the OCE with dsDNA results in the decrease of repulsive electrostatic forces between nanoparticles which favor aggregation. On the other hand, liposomes generated without OCE showed a neutral surface charge at all of the N/P ratios investigated. Indeed, while the liposomes have also neutral zeta potential, they do not aggregate since the lack of cationic surface charges prevent the crosslinking by dsDNA as N/P ratios are decreased.

The loading efficiency and capacity of lipoplexes and liposomes generated with 1:1 HSPC/DOPE, 2:1 HSPC/DOPE, 2:1:1 HSPC/Cholesterol/DOPE and 2:1 HSPC/Cholesterol composition and with 4 mol% OCE was assessed to identify the conditions that minimize the loss percentage of non-loaded nucleic acid and high encapsulated nucleic acid to lipid ratio. Liposomes without OCE were tested as a control. Loading efficiency and capacity (w/w %) of the lipoplexes and liposomes generated are shown in Figure 7.15.

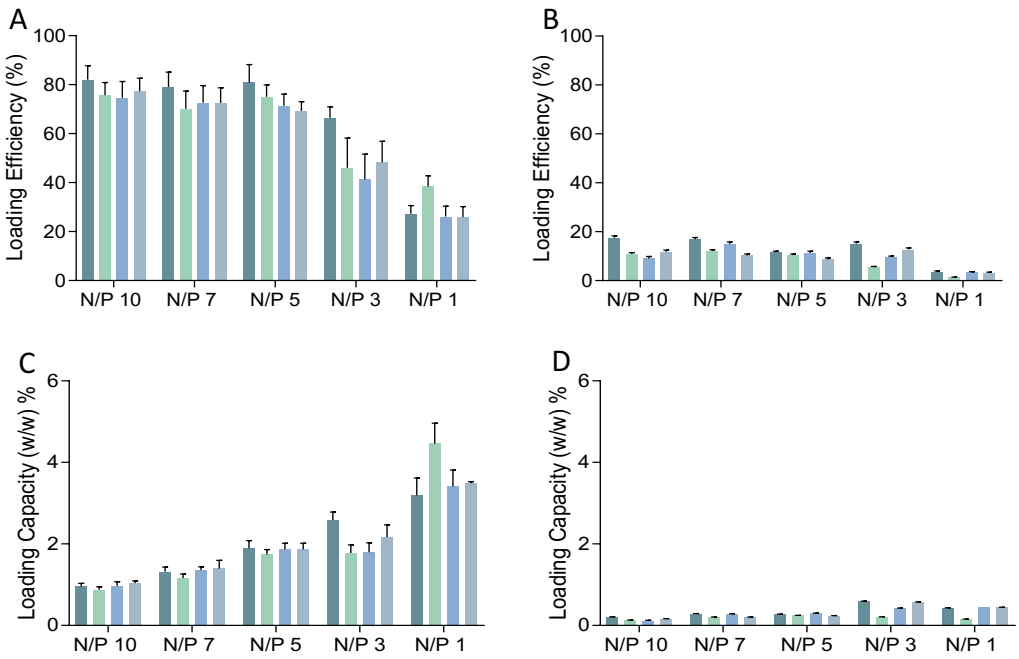

Figure 7.15. *Loading efficiency and loading capacity of the lipoplexes generated with 4 mol% OCE (A, C) and liposomes generated without OCE (B, D) with 1:1 HSPC/DOPE (■), 2:1 HSPC/DOPE (■), 2:1:1 HSPC/Cholesterol/DOPE (■) and 2:1 HSPC/Cholesterol (■) compositions at decreasing N/P ratio.*

The results of the loading study show that OCE is crucial to improving the loading of nucleic acids in liposomes at any given N/P ratio, as shown in Figure 7.15, panels A and B. Lipoplexes produced with a 10:1 N/P ratio did, in fact, exhibit very high loading efficiencies for all formulations regardless the lipid composition. The calculated LEs were about 80 %. with the 1:1 HSPC/DOPE lipoplexes showing the highest loading efficiency of the library (82.0 ± 5.7 %). The loading efficiency only slightly decreased as the N/P ratio was decreased to 5:1; at this N/P ratio the 1:1 HSPC/DOPE lipoplexes still showed the highest loading efficiency of the library of (80.9 ± 7.3), The calculated loading efficiency decreased at N/P ratios at and below 3:1 for all the lipoplex library, indicating lipoplexes loading saturation as the fed dsDNA was increased during assembly. Notably, the highest loading capacity was found on lipoplexes generated with a 10:1 N/P ratio: the 2:1 HSPC/Cholesterol lipoplex showed a loading capacity of 1.04 ± 0.05% (w/w).

On the other hand, liposomes generated without the OCE at a 10:1 NP ratio have shown limited loading efficiency below 18 % which was 4 to 9 times lower than that of the lipoplexes counterparts. Due to the lack of cationic charges, loading efficiency decreased also for control liposomes as the N/P ratio was decreased and the liposomes produced at a 1:1 N/P ratio had the lowest loading efficiency (<4%).

The efficiency of the complexation of the nucleic acids and the cationic carrier was also investigated by agarose gel retardation assay that mostly provides a qualitative evaluation of the efficiency of association of the nucleic acid to the carrier. The size and charge of the carriers and gel pore size affect how molecules migrate along the agarose gel. This technique relies on the migration of nucleic acid through a cross-linked agarose gel under exposure to electric current. The complexation of the NA with the positively charged carrier quenches the NA's overall charge and the move in the gel is prohibited for the fraction complexed, not for the non-complexed fraction that can run along the gel[197]. Therefore, we have used agarose gel electrophoresis to further investigate the effect of the OCE on the loading of the NA's and to help in the choice of the optimum N/P ratio. Results of the agarose gel electrophoresis are shown in Figure 7.16.

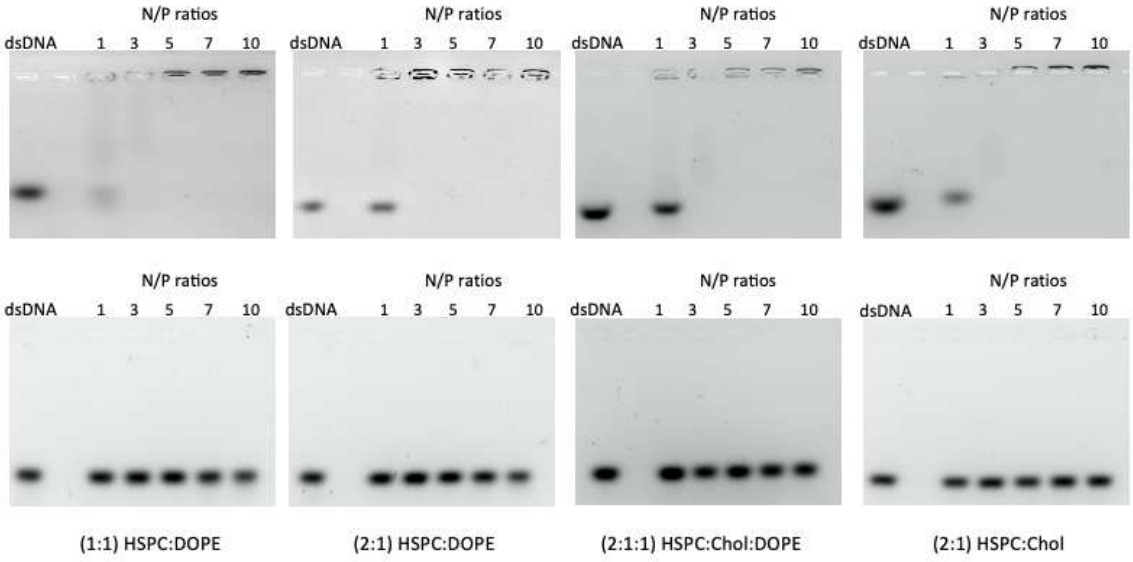

***Figure 7.16**. Electrophoretic mobility profiles of dsDNA loaded in lipoplexes (upper raw) and liposomes (lower raw) formulated within the 1:1-10-1 N/P ratios range.*

Results showed that OCE-containing formulations assembled at the 5:1 N/P ratio and lower yielded high complexation which results in the inhibition of the fed dsDNA run along the gel. On the contrary, the library of liposomes generated without OCE did not provide any complexation and dsDNA freely ran along the gel. These results are in agreement with the loading efficiency measured by the spectrofluorometric method discussed above (Figure 7.15).

The lipoplexes assembled using a 10:1 N/P ratio were selected for further studies since these lipoplexes have the lowest loss of fed dsDNA and, almost complete loading of the fed dsDNA (70-85 %), the highest loading capacity 1.04 ± 0.05 %, which is relevant since it dictates the dose per mg of lipids, and a low polydispersity showing no aggregation (PDI <0.2). Our results showed that the use of the fusogenic lipid DOPE did not affect the colloidal and biopharmaceutical features of the formulations namely particle size, zeta potential, and loading efficiency.

A competitive displacement assay was also performed to assess the strength of association of the dsDNA with the lipoplexes in the presence of competing polyanionic agents. Indeed, heparin is a biomacromolecule presents in the blood at 1 to 5 µg/mL[198] and in virtue of its polyanionic charges, it may compete for the association to the cationic charges of lipoplexes and displace the loaded oligonucleotides (Figure 7.17).

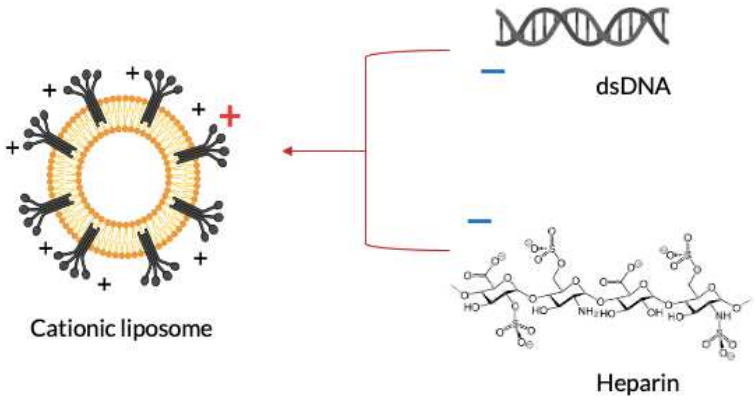

Figure 7.17. *Schematic representation of negatively charged dsDNA and heparin competition for binding to positively charged cationic liposomes*

The displacement study with competing for anionic polymers was performed by preincubating lipoplex formulations with increasing concentrations of heparin followed by gel electrophoretic analysis. Results of the agarose gel electrophoresis are given in Figure 7.18.

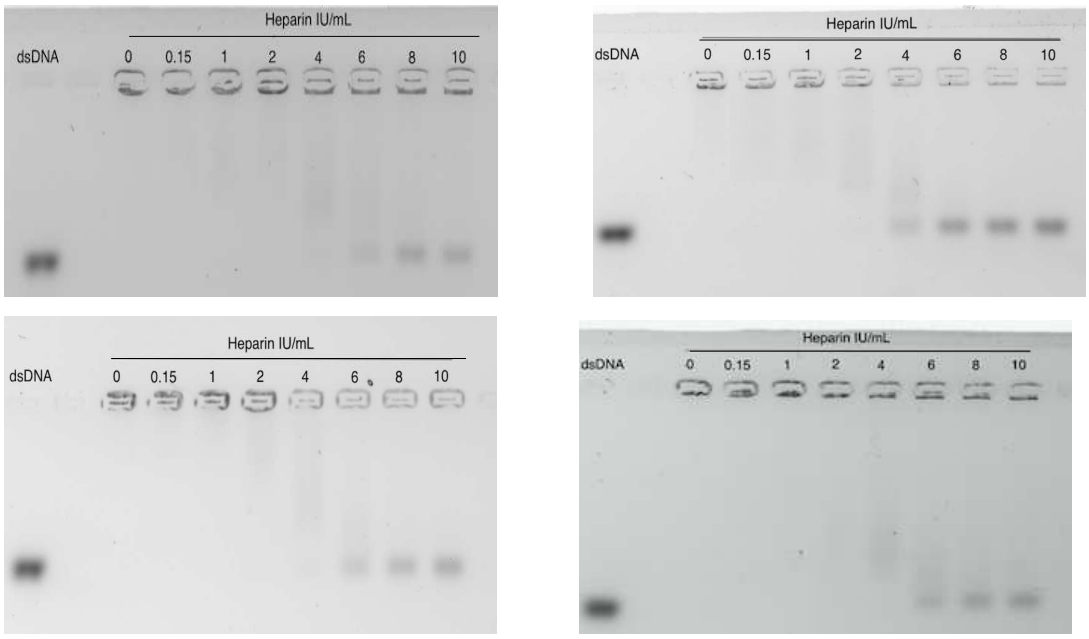

Figure 7.18*. Gel electrophoresis of the 1:1 HSPC/DOPE, 2:1 HSPC/DOPE, 2:1:1 HSPC/Cholesterol/DOPE and 2:1 HSPC/Cholesterol lipoplexes loaded with dsDNA and generated with 4 mol % of OCE at 10:1 N/P ratio, after incubation with increasing concentration of heparin for 15 minutes.*

The results of the heparin displacement assay showed lipoplexes generated with a 4 mol% OCE at a 10:1 N/P ratio possess great stability when exposed to the physiological heparin concentration (0.15 IU/mL). The dsDNA associated with the lipoplexes started to leak out of the system at high heparin concentrations (from 4 IU/mL) due to the heparin's competition with dsDNA for the OCE. In the absence of the heparin, lipoplexes did not show any leaking of dsDNA independently from their

composition, showing that the electric field applied to the system does not stress the formulation to the point of inducing the NA leaking.

Colloidal stability of the lipoplexes was evaluated in buffer (10 mM HEPES, 0.15 M NaCl, pH 7.4) at 37 °C. The results of the stability test is given in Figure 7.19.

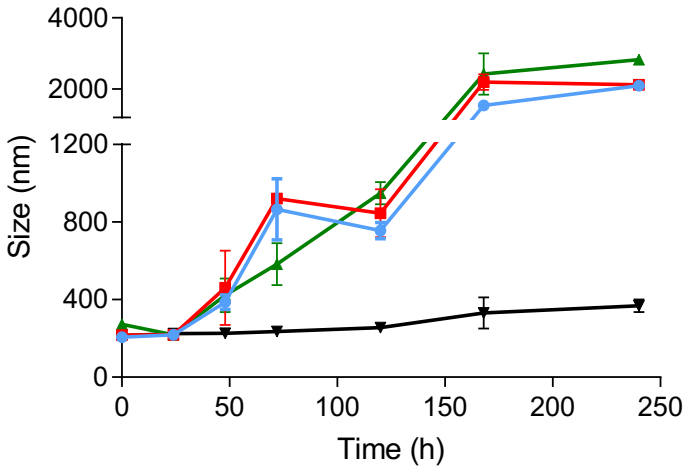

Figure 7.19 *Size profiles of 1:1 HSPC/DOPE (—), 2:1 HSPC/DOPE (—), 2:1:1 HSPC/Cholesterol/DOPE (—) and 2:1 HSPC/Cholesterol (—) lipoplexes loaded with dsDNA and generated with 4 mol % of OCE at 10:1 N/P ratio, in HEPES buffer at pH 7.4 and 37 °C.*

Lipoplexes generated N/P ratio of 10 were characterized by a size of 200 nm and low polydispersity. Independent of the lipid composition, lipoplexes maintained their size around 200 nm, after 24 hours of incubation. After 48 hours of incubation, size of the lipoplexes in 1:1 HSPC/DOPE, 2:1 HSPC/DOPE and 2:1:1 HSPC/Cholesterol/DOPE composition increased and reached to a value around 500 nm, while the lipoplexes in 2:1 HSPC/Cholesterol composition maintained its size around 200 nm. In the third day, aggregation was seen with the 1:1 HSPC/DOPE, 2:1 HSPC/DOPE and 2:1:1 HSPC/Cholesterol/DOPE lipoplexes, while the lipoplexes generated with 2:1 HSPC/Cholesterol showed high stability. These findings are not surprising since it has been well established that cholesterol is the most commonly used sterol in the liposomal compositions to enhance liposome membrane stability and to avoid liposome aggregation[199]. The relatively lower stability of the DOPE-containing lipoplexes can be explained by the tendency of the DOPE to create an inverted hexagonal phase rather than a lamellar bilayer[200]. However, it is worth noting that the inclusion of certain polymers such as PEG into the surface of the liposomes can improve the colloidal stability of liposomes and also the blood circulation time of the therapeutics[201].

7.2.4. siRNA-loaded lipoplexes: formulation and characterization

The formulation parameters investigated in previous chapters using model dsDNA were then transferred for the assembly of lipoplexes loaded with biologically active siRNA to test the therapeutic efficacy of the systems with in vitro cellular model. To this aim, lipoplexes were loaded with a sequence of siRNA inhibiting the expression of GFP in eGFP-expressing cells.

The HSPC-based lipoplex formulations with the composition selected in section 7.2.2 were obtained with the Arg_4-DAG unimer and their loading was achieved by hydration of the lipid mixture containing the Arg_4-DAG with sieGFP RNA aqueous solution at a 10:1 N/P ratio. Control lipoplexes were prepared with non-coding siRNA duplex (siCTRL),. Indeed, negative control siRNAs are most often a non-targeting siRNA to assess the possible non-specific effects of intracellular delivery of siRNA and for providing a baseline for the coding siRNA-treated samples. Therefore, its use is crucial to determine the biological effect and the efficiency of the system.

Particle size, polydispersity index, and zeta potential of the lipoplexes were assessed by DLS analysis and the results are shown in Figure 7.20.

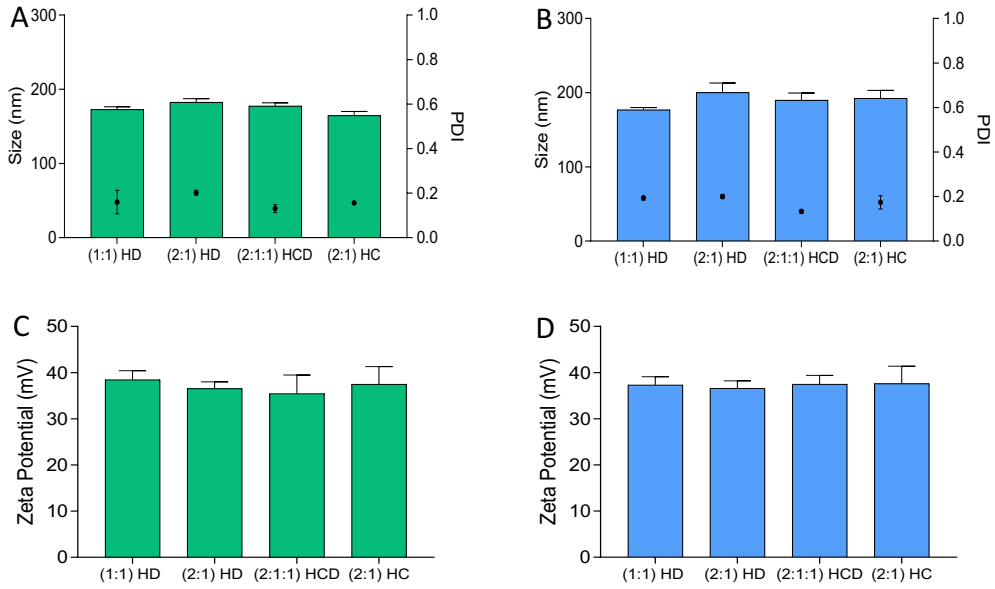

Figure 7.20. *Particle size, polydispersity index, and zeta potential of lipoplexes loaded with sieGFP (A and C) and siCTRL (B and D). Liposomes were generated with the following composition: 1:1 HSPC/DOPE, 2:1 HSPC/DOPE, 2:1:1 HSPC/Cholesterol/DOPE and 2:1 HSPC/Cholesterol*

Lipoplexes loaded with sieGFP and with the 4 different compositions, namely 1:1 HSPC/DOPE, 2:1 HSPC/DOPE, 2:1:1 HSPC/Cholesterol/DOPE and 2:1 HSPC/Cholesterol, were characterized by the sizes in the 165-182 nm range and PDI values in the 0.131-0.202 range. Overall, the library of lipoplexes

presents very similar colloidal features regardless of the composition. The sizes and the PDI of the lipoplexes loaded with siCTRL were in agreement with those of the sieGFP-loaded lipoplexes confirming that the sequence of siRNA does not affect the lipoplexes' colloidal features.

The zeta potentials of the sieGFP-loaded lipoplexes were in the 35-38 mV range and comparable values were found for the lipoplexes generated with siCTRL. Overall, the sizes (~200 nm), polydispersity index (<0.2), and zeta potential (~37 mV) were in fair agreement with the results of the lipoplexes generated with dsDNA with the same nitrogen to phosphate ratio.

Loading and encapsulation efficiency of the lipoplexes was quantified with the RiboGreen assay. Ribogreen is an ultrasensitive fluorescent nucleic acid stain. The Ribogreen assay is a simple and rapid procedure for quantifying RNA concentration in solution and is used in several molecular biology procedures. This test was used for quantification of the total amount of the siRNA associated with lipoplexes (Figure 7.21, Panel A) as well as the siRNA encapsulated inside the core of the lipoplexes (Figure 7.21, Panel B). Results of the loading and encapsulation efficiency of the lipoplexes are given in Figure 7.21, panel C.

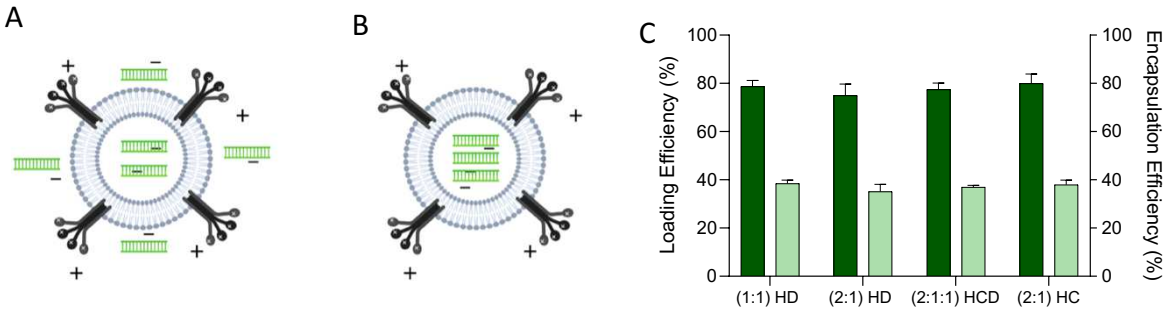

Figure 7.21. *Schematic representation of the loaded/associated (A) and encapsulated (B) siRNA in the lipoplexes. Loading (■, left axis) and encapsulation (■, right axis) efficiency of sieGFP in the 1:1 HSPC/DOPE, 2:1 HSPC/DOPE, 2:1:1 HSPC/Cholesterol/DOPE and 2:1 HSPC/Cholesterol formulations with respect to processed sieGFP (C).*

In agreement with lipoplexes loaded with dsDNA and discussed in the previous chapter, regardless of the lipoplex's lipidic composition, siRNA total loading efficiency was found to be about 80%, while the encapsulation efficiency, which represents the fraction of processed siRNA inside the lipoplexes was found to be about 40% (Figure 7.21, panel C). Each formulation of the lipoplexes library has very similar loading and encapsulation efficiencies which can be ascribed to the fact that the oligocationic lipid is the component mostly responsible for the siRNA loading within the formulation. Furthermore, oligocationic lipid was added to the lipid mixture before creating the lipid film. Upon the hydration of the lipid film with the siRNA solution, oligocationic lipid is available, reasonably, at the same density

on both sides of the lipid bilayers and thus the same electrostatic forces guide the condensation on both sides of the membrane. The comparable fraction of the siRNA that was found core encapsulated and surface complexed on the lipoplexes reasonably confirms this hypothesis.

The condensation of the siRNA within lipoplexes was also investigated by agarose gel retardation assay using a fluorescently labeled version of siRNA. The result of the agarose gel electrophoresis is shown in Figure 7.22.

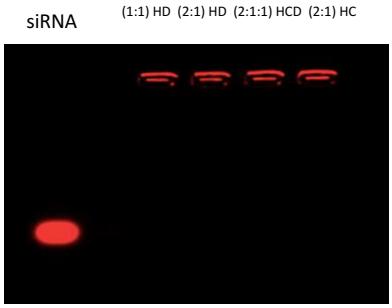

***Figure 7.22**. Agarose gel electrophoresis of 1:1 HSPC/DOPE, 2:1 HSPC/DOPE, 2:1:1 HSPC/Cholesterol/DOPE and 2:1 HSPC/Cholesterol lipoplexes formulated with siRNA-cy5*

The results showed that OCE-bearing formulations assembled at a 10:1 N/P ratio provide high complexation which prevents the cy5-siRNA migration along the gel, which confirms the tight association to lipoplexes of both the core encapsulated and also the surface associated fractions of siRNA.

7.3. Hemolysis assay

Nanoparticles intended for biomedical applications must undergo biocompatibility testing to receive regulatory approval for patient administration, just like any medical device or therapeutic treatment. One of the most common tests to assess blood toxicity as a consequence of the interaction of nanoparticles with blood components is the hemolysis assay[202]. Hemolysis is the disruption of red blood cell (RBC) membranes, which causes the release of iron-containing protein hemoglobin into plasma[203], and it can lead to several pathological conditions such as anemia and jaundice[202]. The role of NP surface chemistry in NP hemocompatibility and interactions with blood cells is unquestionable[204]. The erythrocyte surface is negatively charged, like the majority of cell membranes, and can easily interact with cationic NPs[205]. Since erythrocytes are devoid of phagocytic activity, the adsorption of cationic particles may translate into membrane destabilization. Therefore, it is crucial to assess the hemolytic profiles of lipoplexes to elucidate their biocompatibility for in vivo

applications. Figure 7.23 shows the hemolytic profiles of the 1:1 HSPC/DOPE, 2:1 HSPC/DOPE, 2:1:1 HSPC/Cholesterol/DOPE and 2:1 HSPC/Cholesterol lipoplexes.

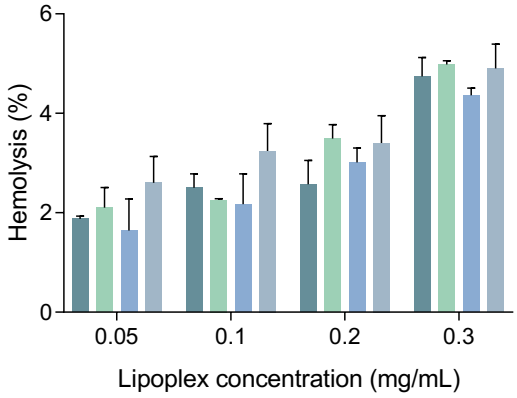

Figure 7.23. *Hemolytic profiles of 1:1 HSPC/DOPE(■), 2:1 HSPC/DOPE (■), 2:1:1 HSPC/Cholesterol/DOPE (■) and 2:1 HSPC/Cholesterol (■) formulations loaded with dsDNA and prepared at 10:1 N/P ratio at increasing lipid concentrations.*

Lipoplex formulations, namely, 1:1 HSPC/DOPE, 2:1 HSPC/DOPE, 2:1:1 HSPC/Cholesterol/DOPE and 2:1 HSPC/Cholesterol loaded with model dsDNA at 10:1 N/P ratio were incubated with RCBs at a lipid concentration in the 0-0.3 mg/mL range. The range concentration of the lipoplexes tested was selected to include the maximum dose used for the transfection studies corresponding to 0.125 mg/mL lipoplex concentration. The hemolytic activity of the lipoplex library is below 4.5% which is the threshold for a hemolytic reaction[206].

7.4. In vitro cellular studies

7.4.1. Cytotoxicity assessment by MTT assay

The positive charges associated with cationic carriers are crucial to condensate nucleic acids by electrostatic interaction with anionic nucleic acid cargo. The charge requirement to generate NA carriers has drawn significant effort into designing cationic components with enhanced condensation abilities. However, toxicities have always been the main obstacles in the application of cationic carriers[207]. The potential cytotoxic effect of the lipoplexes at increasing concentrations (equivalent to 50-100 nM siEGFP concentration range) and siRNA-free cationic liposomes at an equivalent lipid concentration (62.5-125 μg/mL) was investigated by MTT assay.

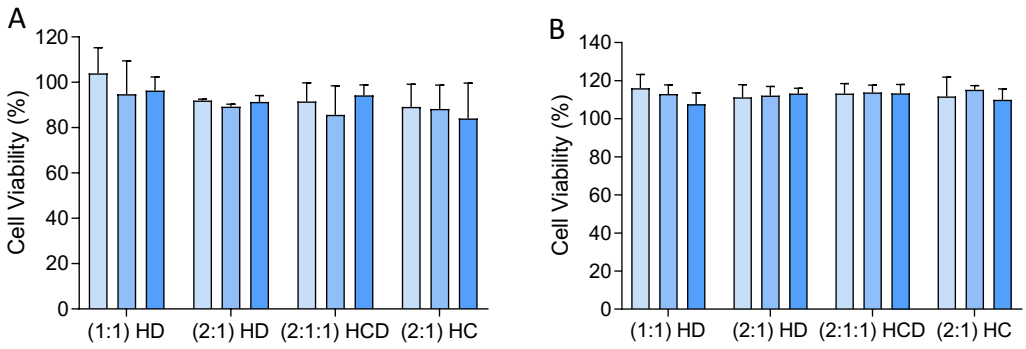

Figure 7.24. *Cytotoxicity profiles of the 1:1 HSPC/DOPE, 2:1 HSPC/DOPE, 2:1:1 HSPC/Cholesterol/DOPE and 2:1 HSPC/Cholesterol lipoplexes at sieGFP concentrations of 50 (□), 75 (■), and 100 nM (■) (A) and cytotoxicity profiles of the siRNA -free cationic liposomes at equivalent lipid concentrations of 0.0625 (□), 0.093 (■), and 0.125 (■) mg/mL (B) on H1299-eGFP cell line.*

The sieGFP-loaded lipoplexes did not show significant toxicity within the range of siRNA concentrations tested (Figure 7.24 A): cell viability remained in the 80-100% range. Cell viability above 80% is considered the range for not cytotoxic agents[208], thus the lipoplex formulations displayed a safe profile within the concentration range used in the studies.

No cytotoxicity was observed for the siRNA-free cationic liposomes at equivalent lipid concentrations and viability was in the 100-120% range for all formulations confirming that the vehicle per se is safe under the conditions used (Figure 7.24 B). The enhanced viability of cells treated with cationic liposomes is not surprising and it can be attributed to a positive effect on cell metabolism by long carbon chains (18 C) of the phospholipids of liposomes; indeed the integration of exogenous long-chain lipids into the cancer cell membrane was already reported to promote the proliferation process[209].

7.4.2. Membrane toxicity assessment by LDH assay

We also performed another cell viability test by assessing the effect of lipoplexes on cell membrane integrity. To this aim, the LDH released by cells was measured after 24 hours of incubation with lipoplexes. The spectrophotometric absorbance measured at the end of the LDH assay and the cell viability values are reported in Figure 7.25.

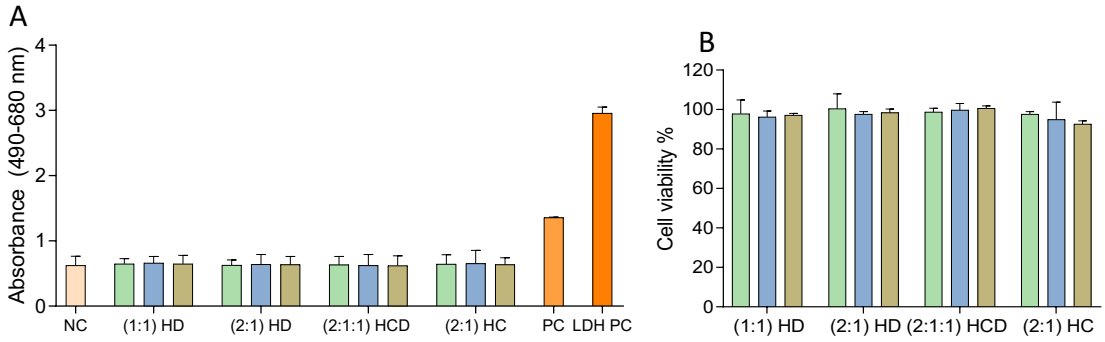

Figure 7.25. *Spectrophotometric absorbance of LDH released by H1299-eGFP cells (A) and cell viability (B) upon incubation 1:1 HSPC/DOPE, 2:1 HSPC/DOPE, 2:1:1 HSPC/Cholesterol/DOPE and 2:1 HSPC/Cholesterol lipoplexes at sieGFP concentrations of 50 (■), 75 (■), and 100 nM (■). NC: negative control; PC: positive control; LDH PC: LHD positive control*

The LDH assay was used to test cell viability because cationic nanocarriers are known to create or expand defects in the lipid bilayers of cells[210]. The toxic effect of the lipoplexes was found to be negligible after a 24-hour incubation time. Indeed, the difference between the LDH released by the non-treated cells and those treated with the lipoplexes was not statistically significant ($p > 0.05$, Figure 7.24 A). The viabilities of the lipoplexes treated cells were calculated with respect to nontreated and Triton-X100 treated cells (Figure 7.24 B). The calculated cell viability was found to be in agreement with the cell viability assessed by the MTT assay, suggesting that cell proliferation was not affected by the presence of the lipoplexes.

7.5.3. Cellular uptake

The negative charge and relatively high molecular weight of the siRNA hinder passive diffusion over the cell membrane and siRNA is generally encapsulated in nanovehicles to ensure intracellular delivery. To promote the intracellular delivery of the siRNA, we have encapsulated the siRNA into the cationic liposomes by endowing the condensing agent (namely the OCE) with cell penetration enhancement ability. The association of the engineered lipoplexes to H1299-eGFP cells was first evaluated by flow cytometry at increasing lipoplexes concentration (equivalent to 50, 75, and 100 nM cy5-siRNA) and DOT-plot profiles of the analysis is shown in Figure 7.26. Two different parameters were evaluated with the flow cytometer: the percentage of positive cells and mean fluorescence intensity (MFI).

Figure 7.26 shows the DOT-plot profiles of the flow cytometric analyses.

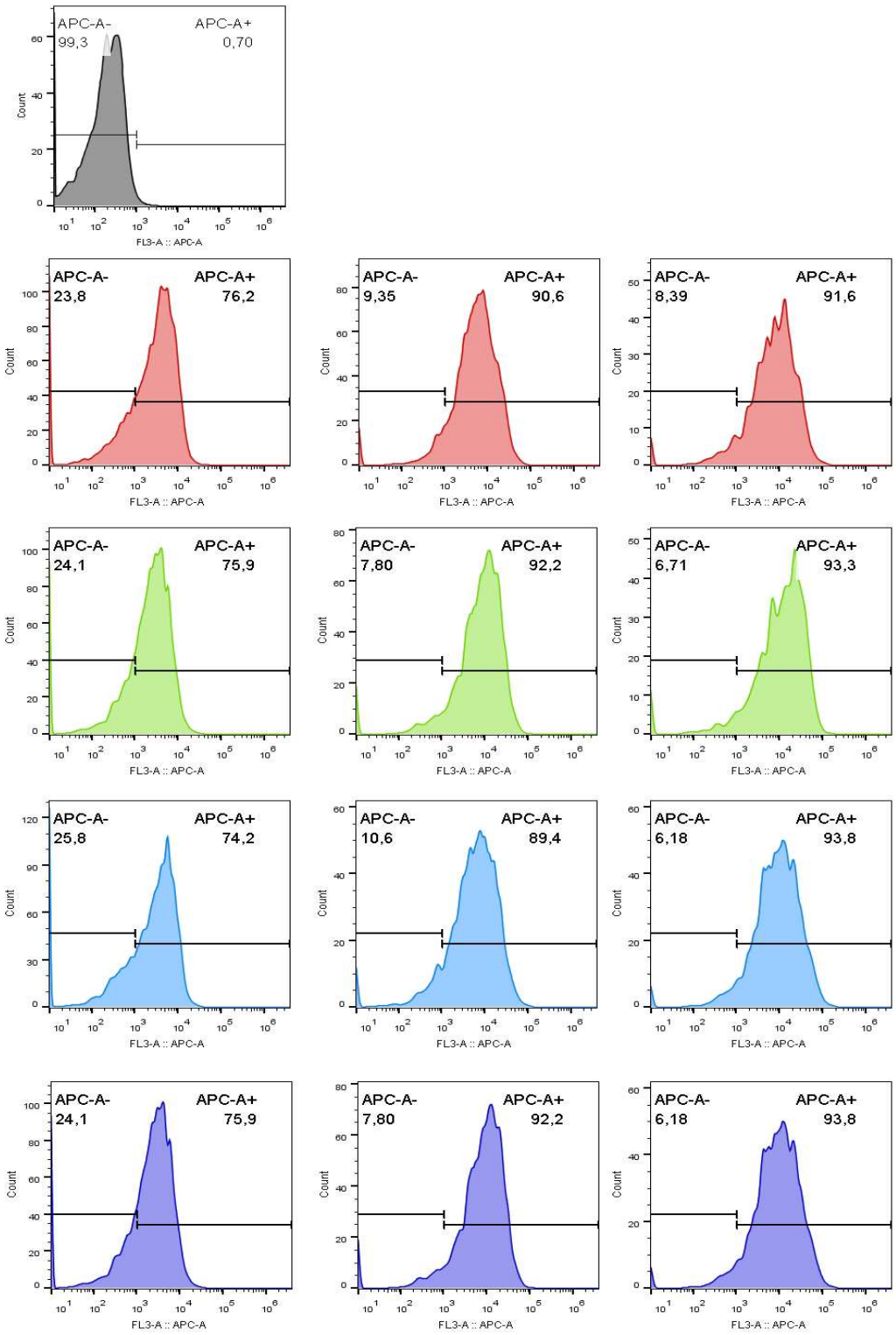

Figure 7.26. *Representative DOT-plot profiles of the H1299-eGFP cells without treatment (grey) and treated with 1:1 HSPC/DOPE lipoplexes (red), 2:1 HSPC/DOPE lipoplexes (green), 2:1:1 HSPC/Cholesterol/DOPE lipoplexes (blue) and 2:1 HSPC/Cholesterol lipoplexes (purple). DOT-plots for each lipoplexes composition are given for cy5-siRNA concentrations of 50, 75, and 100 nM (from left to right).*

The percentage of the cy5-siRNA positive cells and MFI were calculated by elaborating the data derived from the FACs data and the results are reported in Figure 7.27.

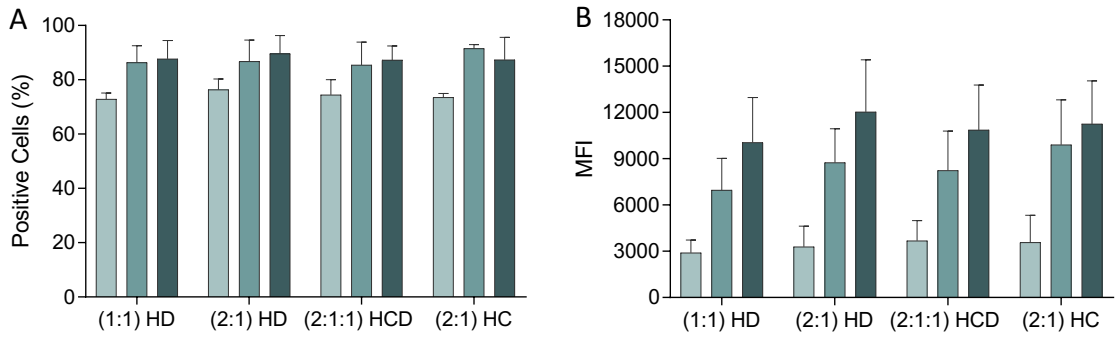

Figure 7.27. *Flow cytometric profiles of H1299-eGFP cells after 4 hours of incubation with HSPC/DOPE 1:1,HSPC/DOPE 2:1, HSPC/Cholesterol/DOPE 2:1:1 and HSPC/Cholesterol 2:1 lipoplexes at 50 (■), 75 (■) and 100 (■) nM cy5-siRNA concentration. Results were expressed as positive cells % (A) and Mean Fluorescence Intensity (MFI) % (B).*

Flow cytometric analysis demonstrated that, regardless of the lipid composition, all the formulations containing the Arg_4-DAG oligocationic lipid associate with cells to a great extent. Indeed, the positive cells' percentage was higher than 70% at a Cy-siRNA concentration of 50 nM, and the value was found to be about 90% when the Cy-siRNA concentration of the lipoplexes was 75 nM. Notably, with the further increase in the sRNA concentration to 100 nM, the percentage of the positive cells only slightly increased above 90%, while the MFI values increased by about 90 % with respect to the values of the cells treated with lipoplexes at 75 nM CysiRNA concentration, suggesting that even though the large majority of the cells had already the lipoplexes associated, the association of lipoplexes to cells and likely the uptake was further increased by increasing the lipoplexes concentration. The results confirmed that the cationic charges of the lipoplexes endowed by the exposure of the OCE on their surface are very efficient to mediate electrostatic association with cells. On the other hand, cytotoxicity studies also proved that this association does not translate into toxic effects on cell membranes.

7.5.4. Gene silencing by flow cytometric analysis

Gene silencing is a specific therapeutic approach by which the expression of one or more of an organism's gene expressions is suppressed. Gene silencing has a therapeutic interest: indeed, the silencing of the expression of selected proteins relevant to the cell cycle allows for to reduction of tumor growth. Silencing studies are commonly used to assess the function or role of a given gene/protein and also investigate the efficiency of the siRNA delivery system. Within this study, the effect of the lipoplex composition on the intracellular delivery and endosomal escape of the lipoplex cargo, and ultimately on the therapeutic efficiency, was investigated by silencing studies. Lipoplexes were loaded with siRNA duplex targeting the green fluorescent protein (sieGFP), and the H1299-eGFP cell line was involved. Representative flow cytometry DOT-plots of cells treated with 1:1 HSPC/DOPE lipoplexes are shown in Figure 7.28.

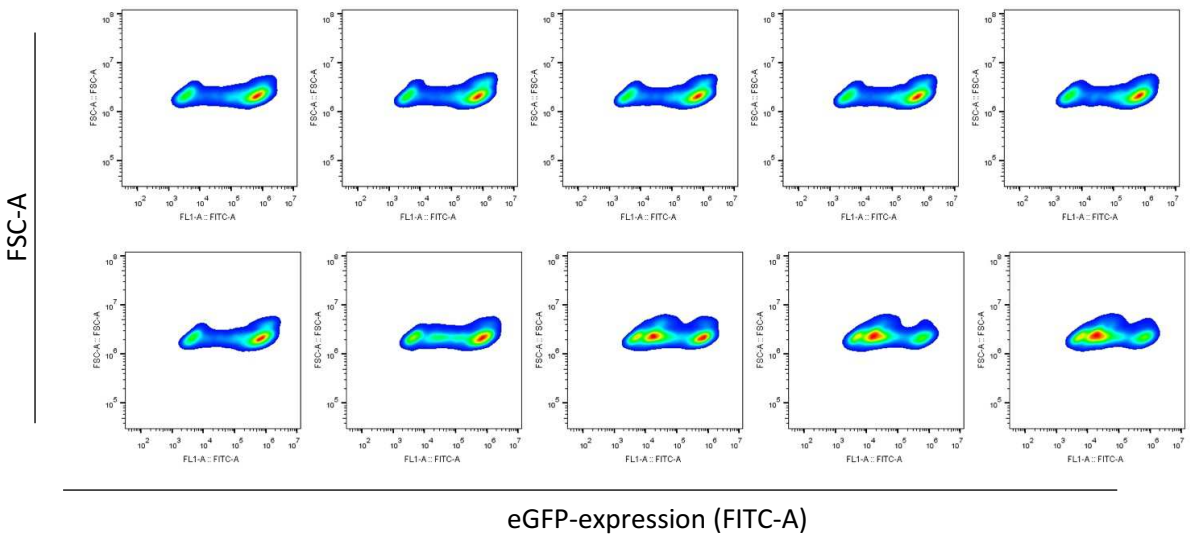

Figure 7.28. *Representative flow cytometric DOT-plots of H1299-eGFP cells treated with siCTRL loaded 1:1 HSPC/DOPE lipoplexes (upper panel) and si-eGFP loaded lipoplexes (lower panel) at the siRNA concentrations of 10, 25, 50, 75 and 100 nM (from left to right).*

The representative DOT-plot obtained with cells incubated with si-eGFP 1:1 HSPC/DOPE lipoplexes (Figure 7.28) shows a clear cell population fluorescence decrease, while the cell population fluorescence of cells treated with the siCTRL loaded lipoplexes did not change. Indeed, the measured MFI values of the cell samples treated with siCTRL loaded 1:1 HSPC/DOPE lipoplexes reported in figure 7.27 were about $5x10^5$, while the MFI value decreased to $1.65x10^5$ after the treatment with the 100 nM sieGFP loaded 1:1 HSPC/DOPE lipoplexes, resulting in a silencing efficiency of 65%.

Lipoplexes-mediated eGFP silencing was quantified from the flow cytometric analysis of cells incubated with the complete library of lipoplexes and correlated to the lipoplexes composition and concentration as reported in Figure 7.29.

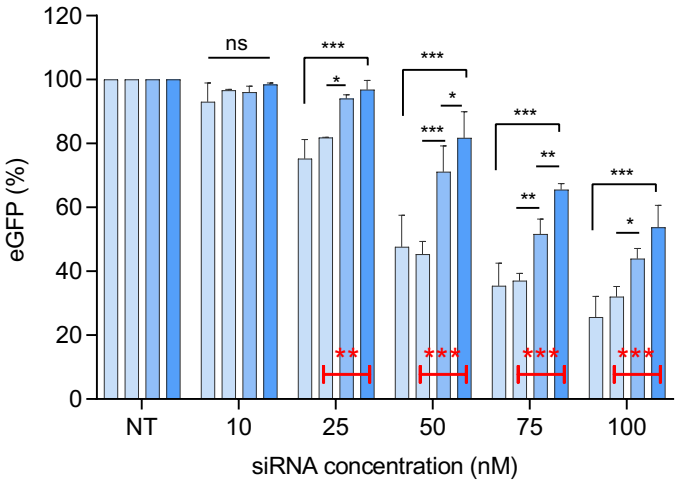

Figure 7.29. *eGFP silencing efficiency by the 1:1 HSPC/DOPE ( ), 2:1 HSPC/DOPE ( ), 2:1:1 HSPC/Cholesterol/DOPE ( ) and 2:1 HSPC/Cholesterol ( ) lipoplexes on H1299-eGFP cells. Cells were treated with lipoplexes with 10, 25, 50, 75 and 100 nM equivalent sieGFP concentrations. Statistical analysis: *p < 0.05, **p < 0.01, ***p < 0.001.*

The lowest concentration of the sieGFP employed in the study (10 nM) did not induce a significant difference in eGFP expression with respect to untreated cells for all the formulations tested. At this concentration, the eGFP expression of cells treated with the lipoplexes was over 90%. As the sieGFP concentration increased, an overall eGFP expression decrease was observed with different performances of the formulations tested. The lowest silencing efficiency was observed with the 1:1 HSPC/Cholesterol formulation. This formulation yielded 1.5, 3.2, 18.2, 34.6 and 46.2 % silencing efficiency at the sieGFP concentrations of 10, 25, 50, 75 and 100 nM, respectively. The formulation implemented with DOPE, namely 2:1:1 HSPC/Cholesterol/DOPE showed that the inclusion of the DOPE is significantly increasing the eGFP silencing when siRNA concentration is equal to or higher than 50 nM. The highest silencing efficiency was observed with both lipoplexes composed of 1:1 and 2:1 HSPC/DOPE molar ratios. In these formulations, the cholesterol was replaced with DOPE at 50 and 33 mol% concerning total lipid, respectively. The relatively higher silencing efficiency of the DOPE-containing formulations with respect to the 2:1 HC formulation is attributed to DOPE's fusogenicity to endosomal vesicles[211] resulting in the cytosolic disposition of biologically active sieGFP where the molecular target RISC complex is located. On the other hand, cholesterol does not prohibit the endosomal escape of lipoplexes, but its exchange with DOPE at the same lipid ratio results in a remarkable access of the cargo to the cytosol.

Interestingly, no significant silencing efficiency difference was observed in cells treated with the 1:1 and 2:1 HSPC/DOPE formulations even at the highest siRNA concentration. The measured silencing efficiency for both of these lipoplexes compositions was about 10, 20, 50, 65 and 70 percent at the sieGFP concentrations of 10, 25, 50, 75, and 100 nM, respectively. This result can be attributed to DOPE behavior Indeed, DOPE tends to assemble into inverted hexagonal micelles rather than a flat bilayer[212], and its inclusion in the lipid composition at different percentages can result in different supramolecular structures[211,213] which does not necessarily further translate in better cytosolic release and higher silencing efficiency. Nevertheless, this hypothesis may be supported by the small angle X-ray scattering (SAXS) measurements of each liposomal composition.

7.5.5. Visualization of the gene silencing by confocal microscopy

The silencing efficiency of the lipoplexes was also investigated by confocal imaging. H1299-eGFP cells expressing eGFP were incubated with the best performing formulation identified by the cytofluorimetric study, namely the 1:1 HSPC/DOPE lipoplexes, in the 10-100 nM si-eGFP concentration range and imaged by confocal microscopy. The resulting images are shown in Figure 7.30.

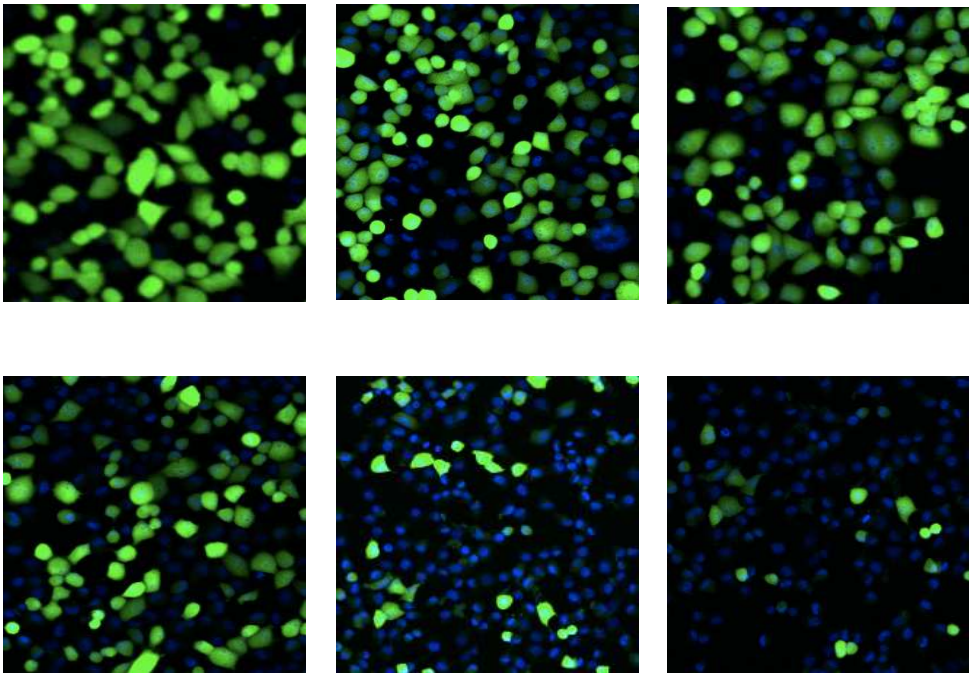

Figure 7.30. *Representative confocal images of H1299-eGFP cells after incubation with the 1:1 HSPC/DOPE lipoplexes at sieGFP concentrations of 0, 10, 25 (upper panel, from left to right) and 50, 75, and 100 (lower panel, from left to right).*

The qualitative results from the imaging study are in agreement with the flow cytometric results performed for the quantification of the silencing efficiency. The lipoplexes concentration-dependent decrease of the number of the eGFP-expressing cells and the intensity of fluorescence confirm the intracellular delivery of sieGFP and its biological activity as a proxy for the therapeutic outcome that this delivery system can have once used to silence disease correlated intracellular proteins. The reason why the eGFP expression is quenched more in some cells rather than others may be ascribed to their different endocytic activity correlated to their cell cycle.

7.5.6. Intracellular trafficking

The endocytic pathway is the primary process for intracellular access to hydrophilic bio-macromolecules such as DNA, siRNA, proteins, and other biological agents. These therapeutic agents get trapped in endosomes upon endocytosis which is detrimental when their targets are in the cytosol since they are digested by specific lysosomal enzymes. Therefore, facilitating endosomal escape and ensuring cytosolic delivery of the therapeutics is a mandatory need to achieve an effective biologics-based therapy[214]. To facilitate the endosomal escape, the library of formulations we have designed included a lipid helper, namely DOPE, which is well known for facilitating the escape. Based on the silencing study, the 1:1 HSPC/DOPE formulation was selected and the effect of DOPE on the endosomal escape was comparatively tested to the control formulation devoid of DOPE by looking at the relative disposition into endosomes over time. Hence, confocal images were captured from at least three fields of the same glass slide for each time point with at least 10 cells/field. The co-localization of the cy5-siRNA within lysosomes was investigated for 8 hours to derive information about intracellular trafficking. Pearson Correlation Coefficient (PCC) values for each time point and representative images are presented in Figures 7.31 and 7.32.

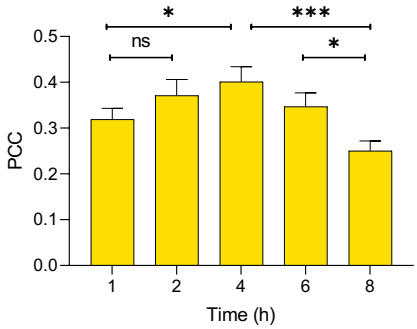

Figure 7.31. *The calculated PCC values at each time point. Statistical analysis: *p < 0.05, **p < 0.01, ***p < 0.001.*

Yellow spots were identified as a result of the siRNA/acid organelles colocalization, as shown in Figure 7.32.

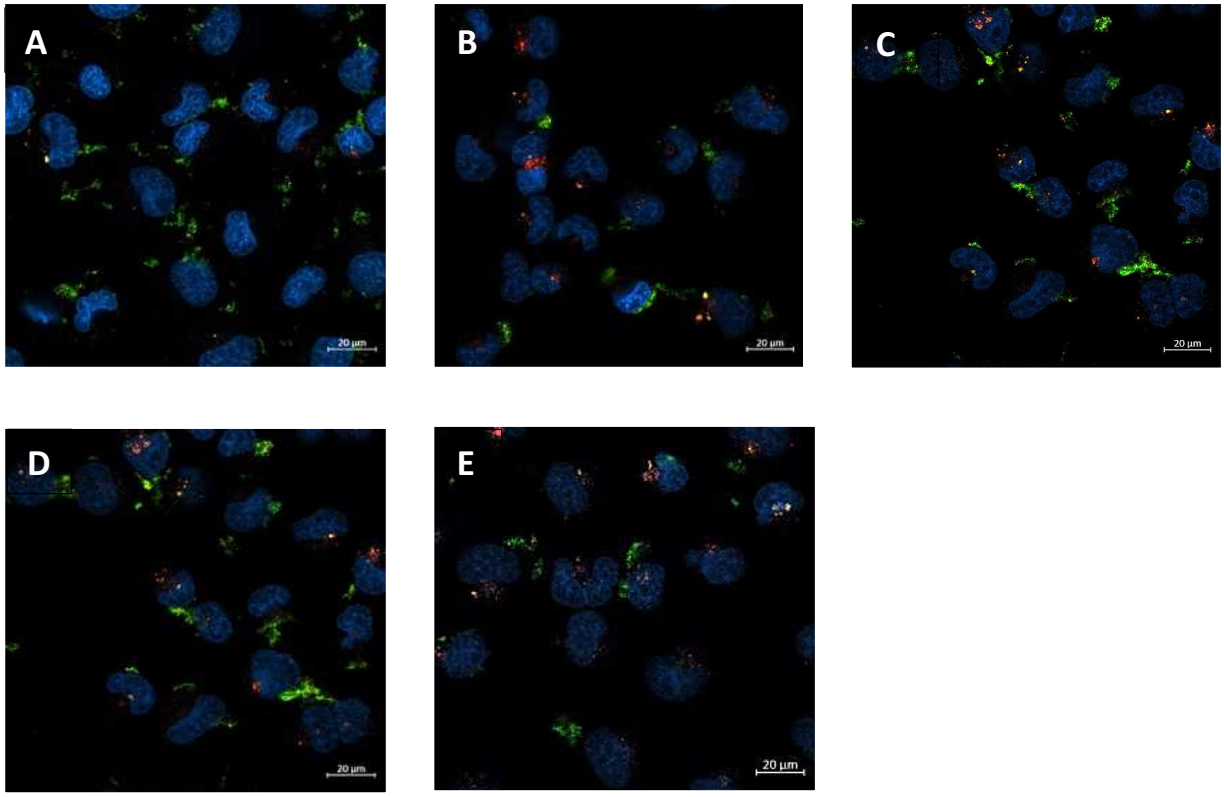

Figure 7.31. *Representative confocal images of H1299-WT cells treated with 1:1 HD lipoplexes; images were captured 1, 2, 4, 6, and 8 hours after the incubation with lipoplexes. Cell nuclei are labeled with Hoecst 33342 (represented in blue), siRNA was labelled with cy-5 (represented in green) and lysosomes were labelled with lysotracker red (represented in red).*

The Pearson Correlation Coefficient (PCC) is a parameter that refers to the colocalization of intracellularly delivered molecules with endosome/lysosome. PCC is a statistical test that measures the relationship or association between two continuous variables and values. PCC ranges from -1 to +1, where +1 indicates a strong linear correlation (meaning colocalization) and values close to 0 indicate no correlation (no colocalization) and -1 shows a negative correlation. The results of the colocalization of the cy5-siRNA within endosomes/lysosomes are time-dependent and show that following the endocytosis of DOPE-containing lipoplexes, after 1 hour cy5-siRNA only slightly colocalized in acidic compartments such as late endosome or lysosome, resulting in very low PCC value of about 0.33 as expected. The colocalization of cy5-siRNA within the acids compartment slightly increases over the timecourse of three hours after pulse contact, resulting in a slight increase of PCC to 0.41. The colocalization value increase is attributed to the trafficking of the lipoplexes towards more acidic compartments such as lysosomes that are labeled efficiently by the Lysotracker Red. The

colocalization value was found to be noticeably dropping after 4 hours and reached a value of only 0.25 after 8 hours. Indeed, the PCC decrease at 8 hours was statistically significant with respect to its maximum value at 4 hours. Altogether, the quite low maximum achieved PCC value and its decrease after 4 hours prove that the DOPE lipid is indeed triggering the endosomal escape of the lipoplexes resulting in the silencing activity provided by the released sieGFP in the cytosol as discussed in the previous chapter.

8. CONCLUSIONS

This thesis project was aimed at the development of a liposomal carrier system decorated with a synthetic oligocationic enhancer to overcome the barriers related to intracellular nucleic acid delivery. OCE is a novel cationic lipid, synthesized by our group and employed in the lipoplexes composition both to promote nucleic acid complexation and to enhance intracellular access of the carrier. Common fusogenic helper lipid DOPE was introduced to the liposomal composition to advance endosomal barrier crossing.

Employing the OCE, to investigate the effect of the lipid saturation on the lipoplexes, saturated phospholipid HSPC or unsaturated phospholipid EPC were employed. Even though EPC-based lipoplexes have shown a similar particle size, polydispersity index, zeta potential and loading efficiency, they were excluded from the study for their very fast release profile.

Lipoplexes generated in HSPC/DOPE (1:1 and 2:1 mol/mol), HSPC/Cholesterol/DOPE (2:1:1 mol/mol), HSPC/Cholesterol (2:1 mol/mol) lipid compositions with 4% OCE and formulation optimization resulted in small particle size, low polydispersity index and positive surface charge. Owing to the presence of the OCE, lipoplexes have shown high oligonucleotide complexation efficiency, compared to their counterparts devoid of OCE. Moreover, independently from the composition, lipoplexes have shown high stability in the presence of heparin and displayed quite low hemolytic activity.

In-vitro cytotoxicity studies showed that siRNA-loaded lipoplexes induced negligible toxicity within the concentration range used in the studies. Cellular association studies revealed that the inclusion of the OCE significantly increases the association of the lipoplexes. Silencing efficiency as a proxy for the therapeutic activity of the siRNA-loaded lipoplex library was measured and showed the inclusion of the fusogenic lipid DOPE significantly increases the eGFP silencing. Finally, intracellular trafficking studies showed that lipoplexes generated in 1:1 HSPC/DOPE composition show a limited accumulation in the acidic compartments such as late endosomes and lysosomes within 8 hours, suggesting that DOPE is triggering the endosomal escape of the lipoplexes that is resulting in high silencing efficiency.

In conclusion, our findings suggest that the combinational use of the OCE and the fusogenic lipid DOPE can be a promising approach to ensure the delivery of nucleic acids across cell barriers.

2 | Microfluidic manufactured solid lipid nanoparticles for oral exenatide delivery

CONTENT

	106
1. ABBREVIATIONS	**109**
2. ABSTRACT	**111**
3. RIASSUNTO	**113**
4. INTRODUCTION	**115**
4.1. PEPTIDE THERAPEUTICS: OVERVIEW	115
4.2. GLUCAGON-LIKE PEPTIDE 1 (GLP-1) AND EXENATIDE	118
4.3. ROUTES OF PEPTIDE DELIVERY	121
4.3.1. Non-parenteral delivery methods	121
4.3.1.1. Nasal route	121
4.3.1.2. Pulmonary route	122
4.4. ORAL DELIVERY OF PEPTIDE THERAPEUTICS	124
4.4.1. Transport mechanisms in the gastrointestinal tract	124
4.4.2. Barriers to effective oral delivery	126
4.4.3. Strategies for successful oral delivery	128
4.4.3.1. Chemical modifications	128
4.4.3.2. Employment of the drug delivery systems	129
4.5. SOLID-LIPID NANOPARTICLES	132
4.5.1. Conventional methods for SLN preparation	136
4.5.2. Innovative microfluidic techniques	137
4.5.3. Lyophilization of nanoparticles	140
4.6. ENTERIC COATING OF ORAL DOSAGE FORMS	142
5. AIM OF THE PROJECT	**144**
6. MATERIALS AND METHODS	**145**
6.1. MATERIALS	145
6.1.1. Reagents	145
6.1.2. Scientific equipment	146
6.2.1. Analytical methods	147
6.2.1.1. Exenatide concentration assessment by RP-HPLC	147
6.2.1.2. Phospholipid assessment by Stewart Assay	148
6.2.1.3. Validation of the ethanol removal from the SLNs suspension	149
6.2.1.4. Validation of the non-loaded EXEN removal from the SLNs	149
6.2.2. Interaction between DOTAP and EXEN	149
6.2.2.1. ITC Analysis	149
6.2.2.2. Exenatide adsorption on SLNs surface	151
6.2.3. Formulation of the SLNs	152
6.2.3.1. Selection of the lipid mixture concentration	152
6.2.3.2. Selection of the microfluidics process parameters	153
6.2.3.3. Effect of buffer concentration and DOTAP/EXEN molar ratio on SLNs' features	153
6.2.3.4. Selection of the EXEN/total lipid feed and DOTAP/EXEN ratios	154
6.2.3.5. PEGylation of the SLNs	155
6.2.3.6. Lyophilization of the SLNs	155
6.2.4. Characterization of the SLNs	156
6.2.4.1. Particle size and zeta potential measurement	156
6.2.4.2. Loading efficiency and capacity assessment	156
6.2.4.3. Release studies	157

6.2.4.4. Stability studies 157
6.2.4.5. Morphological investigation of the SLNs 157
6.2.4.6. Mucin diffusivity of the SLNs by FRAP analysis 158
6.2.5. Stability of exenatide 159
6.2.5.1. Conformational stability 159
6.2.5.2. Chemical stability 160
6.2.6. Preparation of the enteric-coated capsules 160
6.2.7. In vitro cellular studies 162
6.2.7.1. Cytotoxicity studies 162
6.2.7.2. Cellular association studies 163
7. RESULTS AND DISCUSSION 165
7.1. CALIBRATION AND VALIDATION OF THE ANALYTICAL METHODS 165
7.1.1. Phospholipid assessment by Stewart Assay 165
7.1.2. Ethanol removal validation 166
7.1.3. Validation of non-loaded EXEN removal process 168
7.2. INTERACTION BETWEEN DOTAP AND EXEN 168
7.2.1. ITC analysis 168
7.2.2. Exenatide adsorption on SLNs surface 172
7.3. FORMULATION OF THE SLNS 174
7.3.1. Selection of the lipid mixture concentration 174
7.3.2. Selection of the microfluidics process parameters 176
7.3.3. Selection of the DOTAP/EXEN precomplexation buffer concentration 179
7.3.4. Selection of the EXEN/total lipid feed ratio and DOTAP/EXEN molar ratio 182
7.3.5. PEGylation of the SLNs 185
7.3.6. Lyophilization of the SLNs 187
7.4. RELEASE STUDIES 190
7.5. COLLOIDAL STABILITY STUDIES 192
7.6. MORPHOLOGICAL INVESTIGATION 195
7.7. MUCIN DIFFUSION BY FRAP ANALYSIS 195
7.8. STABILITY OF EXENATIDE 197
7.8.1. Conformational stability 197
7.8.2. Chemical stability 198
7.9. ENTERIC-COATING OF THE CAPSULES 200
7.10. IN-VITRO CELLULAR STUDIES 201
7.10.1. Cytotoxicity studies 201
7.10.2. Cellular association studies 203
8. CONCLUSIONS 206
9. REFERENCES 207

1. ABBREVIATIONS

AUC	Area Under the Curve
CH_3OH	Methanol
Chol	Cholesterol
CMC	Critical Micelle Concentration
Da	Dalton
DDS	Drug Delivery System
DLS	Dynamic Light Scattering
DM	Diabetes Mellitus
DOTAP	1,2-dioleoyl-3-trimethylammonium-propane
DSPE	1,2-Distearoyl-sn-Glycero-3-Phosphoethanolamine
EPR	Enhanced Permeation and Retention
Et al.	Et alii
Et-OH	Ethanol
EXEN	Exenatide
FBS	Fetal Bovine Serum
FDA	Food and Drug Administration
FRR	Flow Rate Ratio
GIT	Gastrointestinal Tract
GLP-1	Glucagon Like Peptide-1
HEPES	4-(2-hydroxyethyl)-1-piperazine ethane sulfonic acid
HIP	Hydrophobic Ion Pairing
HSPC	Hydrogenated Soybean Phosphatidyl Choline
ITC	Isothermal Titration Calorimetry
MeCN	Acetonitrile
MFI	Mean Fluorescence Intensity
MHF	Microfluidic Hydrodynamic Focusing
mM	Millimolar

MW	Molecular Weight
MWCO	Molecular Weight Cut-Off
NLC	Nanostructured Lipid Carrier
nM	Nanomolar
LC	Loading Capacity
LE	Loading Efficacy
PBS	Phosphate Buffer Saline
PDI	Polydispersity Index
PEG	Polyethylene Glycol
PFA	Paraformaldehyde
PMDS	Poly(dimethylsiloxane)
P/S	Penicillin/Streptomycin
Re	Reynolds Number
RES	Reticulo Endothelial System
RP-HPLC	Reverse Phase High-Performance Liquid Chromatography
Rpm	Revolution Per Minute
SD	Standard Deviation
SHM	Staggered Herringbone Mixer
SIF	Simulated Intestinal Fluid
SLN	Solid Lipid Nanoparticle
TEM	Transmission Electron Microscopy
TFR	Total Flow Rate
Tm	Melting Temperature
TV	Total Volume
UV-Vis	Ultraviolet-visible
WGA-AF 633	Wheat Germ Agglutinin Alexa-Fluor 633
ε_M	Molar Extinction Coefficient

2. ABSTRACT

Diabetes mellitus (DM) is a chronic metabolic disorder that can be caused by deficient insulin release by the pancreas (Type 1, T1DM) or insulin resistance in the peripheral tissues (Type 2, T2DM)[215]. The treatment of T2DM relies on several options. GLP-1, the naturally occurring hormone secreted from the intestine, is one of the most effective options to provide for blood glucose control, with the benefits of preserving beta-cell function, weight loss, and increased insulin sensitivity[216]. Exenatide (EXEN), the first approved GLP-1 analogue[217], shares a 50% sequence homology with the native GLP-1 with the replacement of Arg with Gly providing a longer half-life with respect to the native peptide[218]. Administration of the peptides are commonly performed through the parenteral route. However, frequent injections have many disadvantages. Desired administration option would be the oral route for better patient compliance[219] and minimization of infections. However, peptides bioavailability upon oral administration is strongly limited. In this thesis project, we aimed at contributing to the oral delivery strategies of therapeutic peptides by developing EXEN-loaded solid lipid nanocarriers by microfluidic technology. The hydrophobic ion pairing (HIP) approach was systematically investigated to enhance the loading of EXEN into the lipid matrix[220].

To gain physicochemical information on the hydrophobic ion pairing between EXEN and DOTAP, isothermal titration calorimetry (ITC) was exploited. At pH 8 where EXEN is negatively charged, the titration of DOTAP-liposomes with EXEN generated an exothermic enthalpic variation confirming the ionic association of EXEN with the cationic liposomes.

Preliminary studies were conducted to select the lipid mixture concentration in ethanol that will be fed into the microfluidic system to generate solid lipid nanoparticles (SLN) and 35 mg/mL was selected for providing small and homogeneous SLNs suspension. The optimal microfluidic process parameters were identified by generating SLNs at different Flow Rate Ratios (FRR= 3:1 and 5:1) and Total Flow Rates (TFR= 3, 6, 9, and 12) using 5% (w/w) EXEN/total lipid feed ratio and 6:1 DOTAP/EXEN molar ratios. The process parameters of 3:1 FRR and 12 mL/min TFR were selected in virtue of the small (<100 nm) and homogeneous size distribution (PDI < 0.2) of the resulting SLNs. Studies using a 5 % (w/w) EXEN/total lipid ratio were performed to select the buffer concentration on the aqueous phase to be fed into the microfluidic system that ensures the highest loading, small and homogenous SLNs. 1 mM HEPES at pH 8 resulted in particle size of about 120 nm, and PDI of about 0.13.

A library of SLNs was produced by processing 5-15% (w/w) EXEN/total lipid feed ratio. Each set of formulations was produced with pre-complexation of the EXEN at an increasing DOTAP/EXEN molar ratio in the 0:1 to 18:1 range. SLNs obtained with 10% (w/w) EXEN/total lipid feed ratio and 12:1 DOTAP/EXEN molar ratio showed the most desirable features in terms of size, PDI, and loading

efficiency. Indeed, the nanoparticles had a particle size of 123.7 ± 2.5 nm, PDI of 0.136 ± 0.01, the zeta potential of 53.09 ± 2.7, loading efficacy of 94.3 ± 0.4%, and a loading capacity of 9.6 ± 0.2%. Therefore, this formulation was selected for further characterization. The release of the EXEN from SLNs in simulated intestinal fluid (SIF) at pH 6.8 and in phosphate-buffered saline (PBS) at pH 7.4 mimicking the extracellular conditions, respectively, showed burst release was observed in the first 8 hours followed by a prolonged release of 10 days. SLNs colloidal stability of SLNs in SIF and PBS was remarkable; low increase in particle size and PDI have been noticed after 4 days. The storage stability studies revealed that over 4 weeks freshly prepared SLNs remain stable at 4°C.

The positive charges of SLNs were masked by a post-assembly decoration with DSPE-PEG_{2kDa} at 2-30 % (w/w) and 10 and 30% w/w ratios were selected as mean and high PEG density. TEM imaging showed a spherical morphology of SLN with size in agreement with the results provided by DLS analysis. No sign of collapsed structures typical of the liposomes under vacuum conditions of the TEM analysis was observed. Fluorescence recovery after photobleaching (FRAP) analysis was conducted to investigate the SLNs' mobility in the mucin and results showed that the diffusion of the cationic particles is quite limited but it can be modulated by PEG surface coating.

SLNs were converted into lyophilized powder for loading in enteric-coated capsules. A lyoprotectant mixture of trehalose and mannitol (1:1 w/w) at 2% (w/v) concentration was selected for ensuring the redispersion of the SLNs without aggregation and also for providing good cake integrity.

The stability of EXEN throughout the formulation process (i.e. microfluidics and freeze-drying) was investigated by circular dichroism and mass spectroscopy which showed that the conformation and the chemical structure of the peptide were conserved.

The biocompatibility study of the EXEN-free and EXEN-loaded SLNs (decorated with 0, 10, and 30 % w/w DSPE-PEG_{2kDa}) with human intestinal Caco-2 cells showed a safe profile with cell viability of over 80% in every condition. Finally, the cellular association of the SLNs to Caco-2 cells investigated by flow cytometric analysis and confocal microscopy, showed over 50% association efficiency of the not PEGylated SLNs while the 10 and 30 percent w/w DSPE-PEG_{2kDa} coating decreased, as expected, the cell association.

Finally, hard gelatine capsules were filled with rhodamine b/starch mixture and were coated with Eudragit L100 aqueous solution. Capsules showed high integrity for 2 h in 0.1 M HCl pH 1.2 where the gastric conditions are simulated, while in simulated intestinal fluid a rapid disintegration of the capsule and release of over 80% of the content in 1 hour was observed. On the contrary, not-coated capsules showed an immediate disintegration in the simulated gastric fluid.

3. RIASSUNTO

Il diabete mellito (DM) è una malattia metabolica cronica che può essere causata da un rilascio insufficiente di insulina da parte del pancreas (Tipo 1, T1DM) o da una resistenza all'insulina nei tessuti periferici (Tipo 2, T2DM)[214]. Il trattamento del T2DM si basa su diverse opzioni. Il GLP-1, l'ormone naturale secreto dall'intestino, è una delle opzioni più efficaci per il controllo della glicemia, con i vantaggi di preservare la funzione delle cellule beta, la perdita di peso e una maggiore sensibilità all'insulina[215]. Exenatide (EXEN), il primo analogo del GLP-1 approvato[216], condivide un'omologia di sequenza del 50% con il GLP-1 nativo con la sostituzione di Arg con Gly fornendo un'emivita più lunga rispetto al peptide nativo[217]. La somministrazione dei peptidi viene comunemente eseguita per via parenterale. Tuttavia, le iniezioni frequenti presentano molti svantaggi. L'opzione di somministrazione desiderata sarebbe la via orale per una migliore compliance del paziente e la riduzione al minimo delle infezioni[218]. Tuttavia, la biodisponibilità dei peptidi dopo somministrazione orale è fortemente limitata. In questo progetto di tesi, abbiamo mirato a contribuire alle strategie di somministrazione orale di peptidi terapeutici sviluppando nanocarrier lipidici solidi caricati con EXEN mediante la tecnologia microfluidica. L'approccio dell'accoppiamento ionico idrofobico (HIP) è stato sistematicamente studiato per migliorare il carico di EXEN nella matrice lipidica[219].

Per ottenere informazioni fisico-chimiche sull'associazione ionica idrofobica tra EXEN e DOTAP, è stata sfruttata la calorimetria isotermica di titolazione (ITC). A pH 8 dove EXEN è caricato negativamente, la titolazione dei liposomi DOTAP con EXEN ha generato una variazione entalpica esotermica confermando l'associazione ionica di EXEN con i liposomi cationici. Sono stati condotti studi preliminari per selezionare la concentrazione della miscela lipidica in etanolo che verrà immessa nel sistema microfluidico per generare nanoparticelle lipidiche solide (SLN) ed è stato selezionato 35 mg/mL per fornire una sospensione di SLN piccola e omogenea. I parametri di processo microfluidici ottimali sono stati identificati generando SLN a diversi rapporti di portata (FRR= 3:1 e 5:1) e portate totali (TFR= 3, 6, 9 e 12) utilizzando il 5% (p/p) EXEN/rapporto lipidico totale e rapporti molari DOTAP/EXEN 6:1. I parametri di processo di 3:1 FRR e 12 mL/min TFR sono stati selezionati in virtù della distribuzione dimensionale piccola (<100 nm) e omogenea (PDI < 0.2) degli SLN risultanti. Sono stati eseguiti studi utilizzando un rapporto EXEN/lipidi totali del 5 % (p/p) per selezionare la concentrazione di tampone sulla fase acquosa da immettere nel sistema microfluidico che garantisce il carico più elevato, SLN piccoli e omogenei. HEPES 1 mM a pH 8 ha prodotto una dimensione delle particelle di circa 120 nm e una PDI di circa 0.13.

Una libreria di SLN è stata prodotta elaborando il 5-15% (p/p) di EXEN/rapporto di alimentazione lipidica totale. Ciascun set di formulazioni è stato prodotto con pre-complessazione dell'EXEN a un rapporto molare DOTAP/EXEN crescente nell'intervallo da 0:1 a 18:1. Gli SLN ottenuti con il 10% (p/p)

di EXEN/rapporto lipidico totale e rapporto molare DOTAP/EXEN di 12:1 hanno mostrato le caratteristiche farmaceutiche più desiderabili in termini di dimensioni, PDI ed efficienza di caricamento. In effetti, le nanoparticelle avevano una dimensione di 123,7 ± 2,5 nm, PDI di 0,136 ± 0,01, potenziale zeta di 53,09 ± 2,7, efficacia di caricamento di 94,3 ± 0,4% e una capacità di carico di 9,6 ± 0,2%. Pertanto, questa formulazione è stata selezionata per un'ulteriore caratterizzazione. Il rilascio dell'EXEN dagli SLN nel fluido intestinale simulato (SIF) a pH 6,8 e in soluzione salina tamponata con fosfato (PBS) a pH 7,4 che imitano le condizioni extracellulari, rispettivamente, ha mostrato che il rilascio di burst è stato osservato nelle prime 8 ore seguite da un prolungato rilascio di 10 giorni. La stabilità colloidale degli SLN degli SLN in SIF e PBS è stata notevole; dopo 4 giorni è stato notato un basso aumento della dimensione delle particelle e della PDI. Gli studi sulla stabilità allo stoccaggio hanno rivelato che per 4 settimane gli SLN rimangono stabili a 4°C.

Le cariche positive degli SLN sono state mascherate da una decorazione post-assemblaggio con DSPE-PEG2kDa al 2-30% (p/p) e i rapporti del 10 e 30% p/p sono stati selezionati come densità media e alta di PEG. L'imaging TEM ha mostrato una morfologia sferica di SLN con dimensioni in accordo con i risultati forniti dall'analisi DLS. Non è stato osservato alcun segno di strutture collassate tipiche dei liposomi in condizioni di vuoto dell'analisi TEM. Gli SLN sono stati convertiti in polvere liofilizzata per il caricamento in capsule con rivestimento enterico. È stata selezionata una miscela lioprotettiva di trealosio e mannitolo (1:1 p/p) a una concentrazione del 2% (p/v) per garantire la ridispersione degli SLN senza aggregazione e anche per fornire una buona integrità della torta.La stabilità di EXEN durante tutto il processo di formulazione (cioè microfluidica e liofilizzazione) è stata studiata mediante dicroismo circolare e spettroscopia di massa che hanno mostrato che la conformazione e la struttura chimica del peptide erano conservate.Lo studio di biocompatibilità degli SLN privi di EXEN e caricati con EXEN (decorati con 0, 10 e 30 % p/p di DSPE-PEG2kDa) con cellule Caco-2 intestinali umane ha mostrato un profilo sicuro con vitalità cellulare superiore all'80% in ogni condizione. Infine, l'associazione cellulare degli SLN alle cellule Caco-2 studiata mediante analisi citofluorimetrica e microscopia confocale, ha mostrato un'efficienza di associazione superiore al 50% degli SLN non PEGilati mentre il rivestimento DSPE-PEG2kDa al 10 e 30% p/p è diminuito, come previsto , l'associazione cellulare.Infine, capsule di gelatina dura sono state riempite con una miscela di rodamina b/amido e sono state rivestite con una soluzione acquosa di Eudragit L100. Le capsule hanno mostrato un'elevata integrità per 2 ore in HCl 0,1 M pH 1,2 dove sono simulate le condizioni gastriche, mentre nel fluido intestinale simulato è stata osservata una rapida disintegrazione della capsula e il rilascio di oltre l'80% del contenuto in 1 ora. Al contrario, le capsule non rivestite hanno mostrato una disintegrazione immediata nel liquido gastrico simulato.

4. INTRODUCTION

4.1. Peptide therapeutics: overview

Since the isolation of insulin in the early 1920s, the modern pharmaceutical industry has been reshaped by peptide and protein drugs. Over the last two decades, about 30 peptide drugs have been approved to treat numerous diseases including cancer, genetic, immunological, infectious, musculoskeletal, pulmonary, respiratory diseases, and many others[221 222].

Peptides are specific sequences of amino acids with 2 to 50 residues that are linked by peptide bonds. Peptides can be classified based on the number of amino acids in their structure. Peptides including 10-20 amino acids are classified as oligopeptides, while when a peptide contains more than 20 amino acids, it is classified as polypeptide[223]. The structure of proteins and peptides is hierarchical (Figure 4.1). The primary structure is defined as the ordered sequence of amino acids connected by peptide bonds between their N and C terminals. Secondary structure refers to the spatial arrangement of polypeptide chains, which might take the shape of helixes, sheets, or random coils. The tertiary structure is referred as the three-dimensional arrangement resulting from hydrophobic and ionic interactions or disulfide bonds. A protein complex results from tertiary structures self-combine to form a quaternary structure. The most stable structure under physiological conditions is the native state, in which a protein is biologically active. Keeping a protein in its native state is very important to maintain its functionality[187, 224].

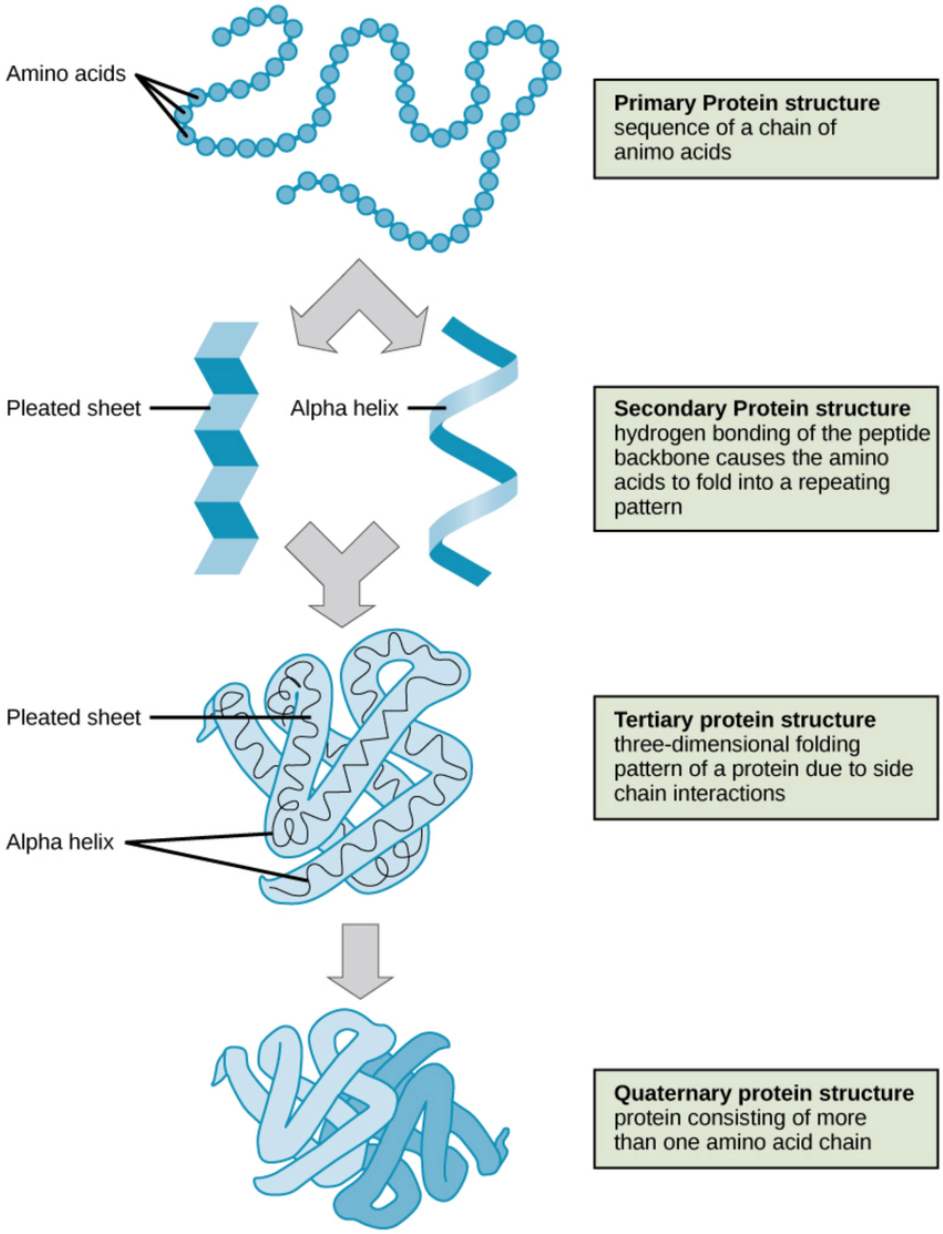

Figure 4.1. *Schematic representation of the hierarchy of protein structure*[225]

Peptide drugs have several advantages over small-molecule drugs. They possess specific and complex functions that small molecules cannot mimic which causes low interference with normal biological processes, and thus low adverse effects due to their high selectivity. They are well tolerated because they are made by the same components of the proteins of the body, and have high chemical and biological diversity, high efficacy, and low tissue accumulation. However, peptides' therapeutic use is limited because of their high production cost, short half-life and stability, chemical and enzymatic instability, and poor membrane permeability[222,226]. Protein aggregation is a common indicator of protein instability, and it's one of the biggest barriers to possible therapeutic development. Physical

aggregation occurs when molecules associate without changing their primary structure, whereas chemical aggregation occurs when new covalent bonds cause cross-linking. Both pathways can result in the formation of insoluble aggregates in water. Proteins can undergo dimerization, trimerization, and other oligomerization, which causes loss of function and activation of the immune system. Insulin, for example, may aggregate both physically and chemically. Chemical aggregation caused by the formation of disulfide bonds can result in soluble peptide dimers or insoluble aggregates, whereas physical aggregation can result in the creation of even more complex structures such as soluble hexamers or insoluble fibrils[227].

Peptide therapeutics are gaining interest since the vasopressin analog, Lypressin®, was approved by FDA in 1970[228]. Following this, with the approval of insulin in 1982, the development of peptide and protein therapeutics grew significantly[229]. Despite the challenges of scaling up and licensing peptide products, their vast clinical potential is reflected in the 60 or so peptide-based therapeutics currently on the market, as well as the 500 derivatives in the development pipeline[230]. Although this growing market encourages the further investigation of peptide therapeutics, it should be noted that the majority of the peptide drugs are either structurally modified or delivered by drug delivery systems. Amino acid substitution and backbone modification are two examples of peptide modification. Atazanavir® is an oral azapeptide in which the carbon in the amino acid of the peptide is replaced by nitrogen and is used as an HIV protease-1 inhibitor[231]. Another example is albiglutide, a glucagon-like peptide-1 (GLP-1) analogue in which an amino acid substitution and fusion of the resulting product with human albumin renders the product resistant to proteolytic degradation by dipeptidyl peptidase-IV (DPP-4) which is the enzyme that cleaves GLP-1[232]. To increase the circulating half-life and targeting of novel therapeutic protein drugs, a variety of protein engineering technologies are used, such as protein conjugation (e.g. albumin fusion), or polymer derivatization (e.g. PEGylation)[233]. By steric hindrance, the hydrated PEG chain protects the conjugated compound from access to proteases and peptidases, reducing nonspecific degradation. PEGasys® by Roche and PegIntron® by Schering-Plough are examples of pegylated proteins on the market that are used in the treatment of hepatitis B and C[234].

Many drug delivery systems have also been employed in the successful delivery of current peptide therapeutics and have shown superior properties both in preclinical and clinical studies compared to naked peptides. Exanatide® LAR is a biodegradable microsphere formulation of GLP-1 analog that extends the peptide's half-life to approximately 2 weeks by controlling the release upon the subcutaneous injection[232]. Examples of successful development of polymer-based peptide delivery

systems are Lupron Depot®, Sandostatin LAR®, and Trelstar® in which leuprolide, octreotide, and triptorelin are encapsulated in PLGA-based microparticles[235].

Even though alternative routes such as oral, pulmonary, transdermal, buccal, and nasal delivery are being explored, injectable dosage forms, such as subcutaneous, intravenous, and intramuscular injections, remain the main route of administration for peptide and protein therapeutics[236].

4.2. Glucagon-like peptide 1 (GLP-1) and Exenatide

Diabetes mellitus (DM) is a chronic metabolic disorder that can be attributed to deficient insulin release from the pancreas as a result of autoimmune eradication of the beta cells (Type 1, T1DM) or insulin resistance in the peripheral tissues (Type 2, T2DM). Today, T1DM accounts for 5-10% of diabetic patients, while about 90% suffer from T2DM[215]. Other causes of diabetes are (1-2% of the patients) endocrine disorders such as acromegaly, gestational diabetes mellitus, exocrine pancreas diseases such as pancreatitis, and use of medications (e.g., glucocorticoids, pentamidine, niacin).

T2DM is characterized by hyperglycemia which is a consequence of the decreased insulin response and insulin resistance. In such a case, insulin secretion is spontaneously increased to preserve glucose homeostasis. However, insulin production is exhausted over time, causing T2DM. Microvascular (nephropathy, neuropathy, retinopathy) and especially macrovascular (cardio- and cerebrovascular) complications cause the majority of the co-morbidity and mortality associated with type 2 diabetes[237]. T2DM is increasing all over the world, as a result of rising urbanization, aging populations, obesity, and declining levels of physical activity[238].

Adults over 45 years old are suggested to perform screening for T2DM every 3 years. Diagnostic criteria of DM are: casual plasma glucose concentration $\geq$ of 200 mg/dL, fasting plasma glucose $\geq$ of 126 mg/dL, or 2-hour glucose level $\geq$ of 200 mg/dL during an oral glucose tolerance test. According to American Diabetes Association (ADA), the blood glycemic targets of the treatment are Hemoglobin A1C level < 7%, preprandial plasma glucose level between 90 to 190 mg/dL, and postprandial plasma glucose level lower than 180 mg/dL[239]. First treatments when DM is diagnosed start with body exercise and diet. If glycemic targets are not achieved, pharmacological monotherapy is initiated. Commonly used oral antidiabetic agents are: sulfonylureas (i.e. glyburide, glipizide,glimepiride), meglitinides (i.e. repaglinide, nateglinide), biguanides (i.e. metformin), thiazolidinediones (i.e. troglitazone, rosiglitazone) and alpha-glucosidase inhibitors (i.e. acarbose and miglitol). In case a single-agent treatment does not provide glycemic control, combination therapies are used[240].

GLP-1 (glucagon-like peptide-1) is a 30 residue 'incretin' hormone that is secreted by intestinal L-cells located in the small and large intestine[241]. Different G protein-coupled receptors (GPCRs) present in the intestinal epithelial cells that serve as chemosensors immediately sense nutrients and metabolites at the luminal side of the L cell, which causes exocytosis of granules containing GLP-1 at the basolateral side of the cell (Figure 4.2). GLP-1 can also control physiological responses in neighboring and/or distant tissues and cell types, but to do that can activate endocrine, paracrine, and neural pathways. For such reason, robust and ubiquitous expression of the GLP-1 receptor is found[242].

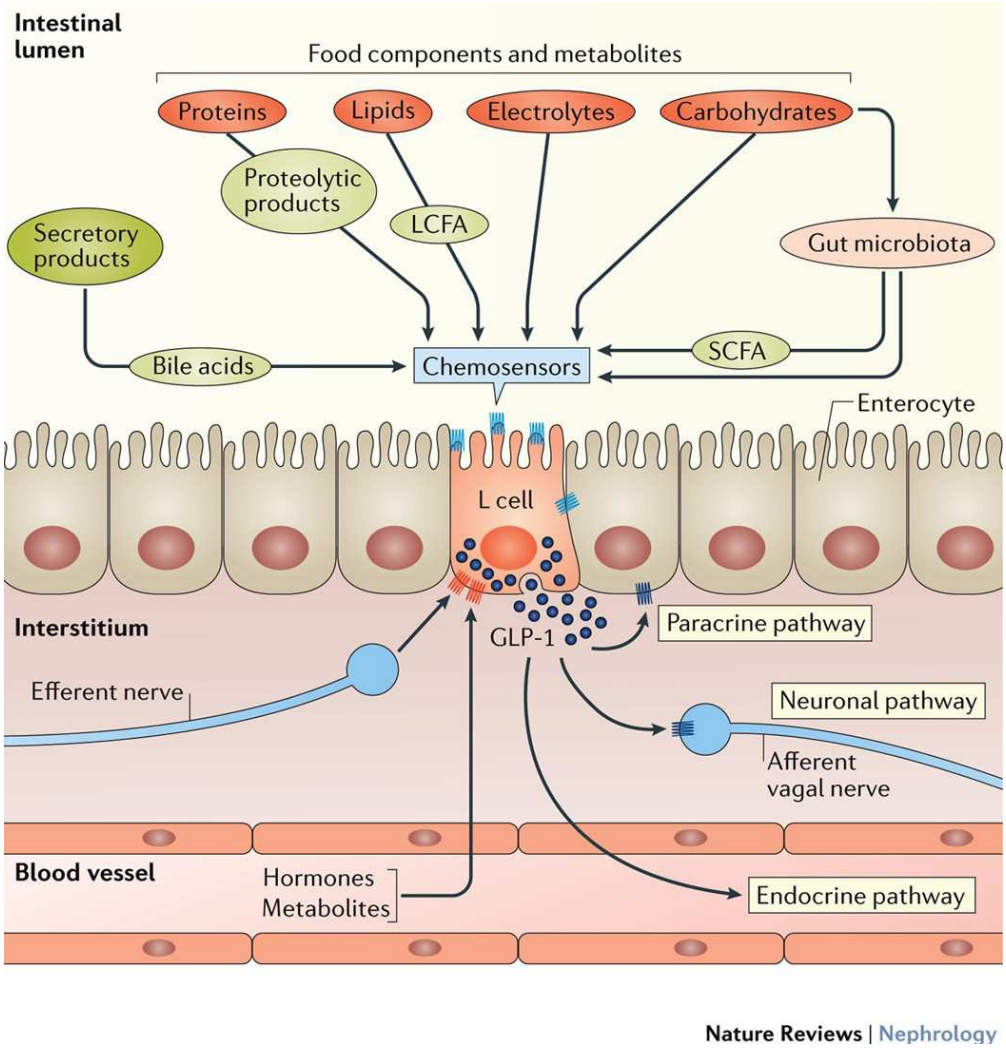

***Figure 4.2**. The secretion of glucagon-like peptide 1 (GLP-1) by L cells in the intestinal epithelium is regulated by chemosensors. (Long-chain fatty acids are LCFAs, while short-chain fatty acids are SCFAs) [242].*

The GLP-1 regulates glucose metabolism by controlling insulin and somatostatin (SMS) production through the GLP-1 receptor (GLP-1R), which is expressed on islet β and δ cells, respectively. Through the somatostatin-2 receptor, SMS in turn prevents islet α cells from secreting glucagon (SSTR2). Additionally, GLP-1 inhibits beta-cell death and promotes its proliferation and expansion. Notably, activation of the GLP-1R signaling increases the production and secretion of insulin field[243].

Because of the hormone's essential function in post-prandial insulin secretion, as well as its additional actions including inhibition of stomach emptying, inhibition of glucagon secretion, and reduction of food intake, the GLP-1 receptor (GLP-1R) has become a prominent target for the prospective therapy of diabetes[244]. Indeed, employment of the GLP-1 receptor agonists is a good strategy for T2DM patients who have failed to respond to metformin, when oral combination therapy with metformin and sulfonylurea is ineffective and a simultaneous loss of body weight is a therapeutic goal or when hypoglycemia must be avoided.

In 2005, Exenatide (Byetta) was approved by FDA as the very first GLP-1 receptor agonist[245]. Exenatide is a synthetic 39-amino-acid peptide (Figure 4.3) that has incretin properties similar to the human incretin hormone glucagon-like peptide 1. (GLP-1). Exenatide shares 53% of the amino acid sequence with human GLP-1 but unlike GLP-1, exenatide is resistant to mammalian dipeptidyl peptidase-IV (DPP-4) in-vivo proteolytic degradation and has a much longer elimination half-life[237]. Indeed, while the half-life of GLP-1 is 2 minutes, exenatide has a half-life of 3.3 to 4 hours after subcutaneous administration[246].

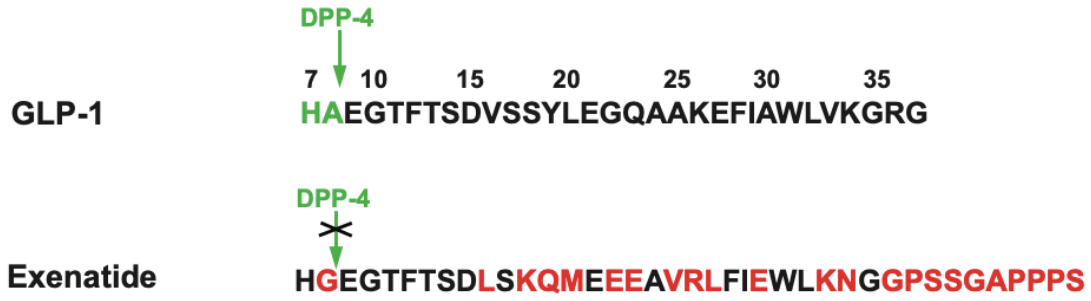

Figure 4.3. *Structures of native GLP-1 and Exenatide. Dipeptide "HA" in the GLP-1 structure is the proteolytic cleavage site for DPP-4. Due to the change of alanine (A) with glycine (G) at the N terminus, exenatide is not a substrate to DPP-4 thus showing higher stability against degradation. Red letters indicate the changes on the exenatide sequence with respect to GLP-1*[247]*.*

Exenatide improves glycemic control in type 2 diabetes patients through a variety of acute and chronic glucoregulatory mechanisms such as enhancement of glucose-dependent insulin secretion and inhibition of inappropriately high glucagon secretion for acute treatment and reduction of food intake, body weight, and enhancement of insulin sensitivity for chronic treatment[237].

Exenatide holds 6 acidic and 4 basic amino acids in its structure which results, according to its isoelectric point, in 2 negative charges at the physiologic pH (Figure 4.4). These characteristics of exenatide can be exploited for the electrostatic interactions with other negatively or positively charged polymers or surfactants in the formulative studies[220, 248, 249]

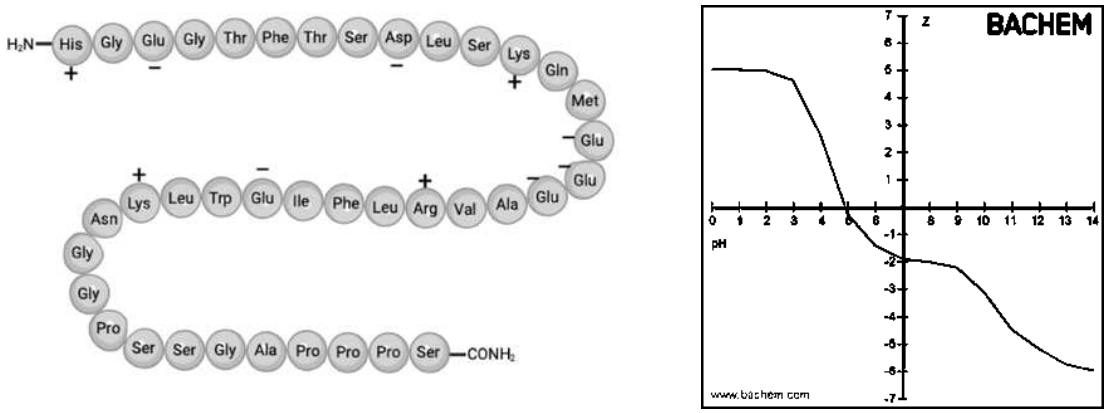

***Figure 4.4**. The amino acid sequence of exenatide shows acid and basic amino acids (A)[220] and the net charge of the exenatide at different pH values (B).*

4.3. Routes of peptide delivery

Peptide and protein therapeutics have become crucial due to their widespread therapeutic applications; however, their physicochemical properties limit their exploitation for therapeutic applications. Their high molecular weight and hydrophilicity, for example, result in low bioavailability, poor biological membranes crossing by diffusion, and low bloodstream stability. Some of these issues can be overcome by employing the parenteral route[250]. When the administration frequency is low or as a one-time dose to a patient, parenteral administration is considered acceptable. Non-parenteral delivery routes, on the other hand, would be preferred for products that are administered frequently or daily (e.g., insulin for diabetics) for being less invasive, painful, and having higher patient compliance[251].

Commonly investigated alternative non-parenteral delivery routes include nasal, pulmonary, transdermal, and oral routes.

4.3.1. Non-parenteral delivery methods

4.3.1.1. Nasal route

The nasal cavity has several advantages as a site for systemic peptide and protein delivery, including the nasal epithelium's high permeability, which allows for a higher molecular mass threshold for permeation, as well as the rapid drug absorption rate, which has been shown to be comparable, at some extent, to that of intravenous injections for some drugs[252]. Moreover, intranasal delivery of the peptides, proteins, monoclonal antibodies, and oligonucleotides via the nose-to-brain route provides

a potential approach for evading the blood-brain barrier and enabling new treatments for neurological diseases such as Alzheimer's and Parkinson's disease[253,254]. Table 4.1 lists some of the intranasal peptides/proteins that are currently on market and also under development[255,256, 257].

Table 4.1. *Examples of peptide/protein-based drugs on the market or under development*

Peptide/protein and brand names	Therapeutic use	Status
Salmon calcitonin Miacalcin®, Fortical®	Osteoporosis	On market
Desmopressin Minirin®, Stimate®	Management of diabetes insipidus Hemophilia A, moderate von Willebrand disease (vWD)	On Market
Buserelin Suprefact®, Profact Nasal®	Prostate cancer Endometriosis	On market
Oxytocin Syntocinon®	Lactation stimulation	On market
Exenatide	Type 2 diabetes	Under development
Human growth factor	Growth failure	Under development

Mucociliary clearance, which continuously clears the drug from the absorption site and reduces the time available for direct transport into the systemic bloodstream from the nasal mucosa, limits the success of systemic drug delivery from the nasal cavity. Because of the limited contact time of small drug or drug formulations with the nasal mucosa, as well as their low permeation and absorption, alternative strategies to improve nasal bioavailability have been investigated[258]. In particular, permeation enhancers are employed to increase the transport of the peptide/protein drugs through the nasal mucosa, while muco/bioadhesive agents are used to increase the retention time at the application site and drug delivery systems are exploited to improve the absorption by encapsulation and surface modification[253].

4.3.1.2. Pulmonary route

The absorption of therapeutic macromolecules such as proteins and peptides administered via the pulmonary route has gotten a lot of attention in recent years. The advantages of pulmonary delivery for drug absorption are numerous: the lung of an adult has a large surface area (approximately 100 m^2) for drug absorption, it is highly vascularized, has quick membrane permeability, and shows low enzymatic activity[259]. Regardless of the advantages that the pulmonary route offers, peptide and protein absorption via the lung is still hampered by specific physicochemical limitations, such as mucus

layer thickness (1-10 μm), mucociliary clearance, alveolar epithelium permeability features, pulmonary enzymes, and presence of macrophages, lymphocytes and other cells[260]. In addition to the limitations posed by the lungs, peptides' hydrophilic nature and high molecular size lower their passage by diffusion across the epithelium[261].

The respiratory tract includes the conducting and respiratory areas. The nasal cavity, nasopharynx, bronchi, and bronchioles make up the conducting area while the respiratory area, including the airways proximal to the bronchioles and the alveoli, represents the surface area where fast solute exchange with blood occurs. The access of micronized or aerosolized drug formulation to the respiratory area is restricted by a very important aerodynamic parameter, namely the particle size of the particles/aerosol. Inhaled particles have to be produced in a size range of 1-5 μm to ensure their access to the alveoli. The particles smaller than 1 μm are mostly exhaled with breathing and the ones larger than 6 μm are mostly accumulating in the oropharynx[262].

In addition to the advantages of the pulmonary route for systemic administration, this route of administration is exploited for the treatment of local diseases. In this case, systemic absorption has to be prohibited. Some examples of protein/peptides for both therapeutic applications are given in Table 4.2[263]

***Table 4.2**. Examples of the commonly studied peptides and proteins for local and systemic administration*

Peptide/protein	Therapeutic use	Application
Interleukin-1 receptor Interleukin-4 Lactoferrin Vasoactive intestinal peptide	Asthma	Local
rhDNAase (Pulmozyme®) Secretin α-1-Antitrypsin	Cystic fibrosis	Local
Cyclosporin A	Lung transplant	Local
Erythropoietin	Anemia	Systemic
Exendin-4 Insulin Glucagon-like peptide	Diabetes Mellitus	Systemic
Calcitonin Parathyroid hormone	Osteoporosis	Systemic

Pulmonary delivery will become a convenient administration route for proteins and peptides in the future, particularly for local delivery, as knowledge in this field continues to advance.

4.4. Oral delivery of peptide therapeutics

The majority of peptide/protein drugs available in the market are administered by the parenteral route. Peptidic drugs, cytokines, and monoclonal antibodies are typically used to treat chronic illnesses, and frequent injections have clear disadvantages. In contrast to this drawback, the oral route provides the benefits of self-administration, avoidance of discomfort and possible infections associated with injection, and hence improved patient compliance. Moreover, the manufacturing cost of oral medications is usually lower than parenteral ones, since the sterilization step and procedures to avoid pyrogens are not needed[219]. Furthermore, the large surface area of the small intestine enables the drug interaction and absorption for the oral route provided that the drug is stable enough and can exploit one of the mechanisms of absorption[264]. Together with being the most preferable route of drug administration for patient compliance, peptide oral administration can offer additional advantages. EXEN is one of those peptides that mostly can benefit from oral administration according to a peculiar physiological rationale; indeed, its intestinal absorption would mimic the physiological GLP-1 secretion by the intestinal L cells to the systemic circulation[265].

4.4.1. Transport mechanisms in the gastrointestinal tract

Paracellular, transcellular, membrane transporter-mediated and receptor-mediated routes are the four basic mechanisms for drugs to cross through the intestinal epithelium (Figure 4.5). Physical properties of the drug or the carrier, such as hydrophilicity, molecular size and weight, shape, pH stability, and ionization constants, affect passage through each pathway[266].

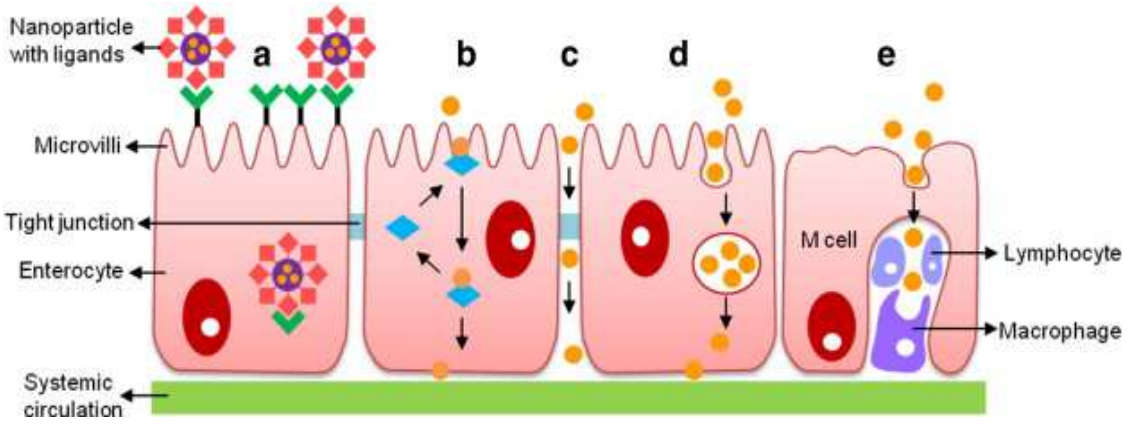

Figure 4.5. *Schematic representation of the transport mechanisms in the intestinal lumen, a) Receptor-mediated, b)* membrane transporter-mediated*, c) Paracellular, d) Transcellular and e) M-cell mediated transport [266].*

- Receptor-mediated transport is often exploited to increase the bioavailability of protein drugs by modification with receptor-specific ligands. This mechanism of transport is a multi-step process: the first step involves the binding of the ligand to a specific cell receptor, followed by receptor clustering and internalization through coated vesicles into the endosomal compartment. This mechanism, in principle, can be exploited for protein chimeras, or nanocarriers coated with ligands[267]. The physical and chemical properties of the protein chimeras or the formulation control the absorption process to the systemic circulation. Hydrophilic constructs/carriers are carried to the liver and then they reach the systemic circulation. On the other hand, highly lipophilic constructs/carriers are transported by the intestinal lymphatic drainage bypassing the first-pass metabolism.

- Membrane transporter-mediated transport occurs only for small hydrophilic molecules such as sugars and amino acids. The membrane transporter recognizes the molecules and transports them across the membranes against the concentration gradient.

- Paracellular transport is a passive mechanism and is regulated by diffusion across the intestinal epithelium. The transport occurs through tight junctions. The section of the paracellular space is on the order of 10 Å. This suggests that solutes with a molecular radius over 15 Å (3,5 kDa) cannot be transported via this route.

- Transcellular transport occurs through intestinal epithelial cells by transcytosis, which is a cellular active mechanism. Endocytosis takes place at the apical membrane of the cell. Then, the vesicles migrate through the cells and are released on the basolateral side. Enterocytes and M cells are the primary intestinal cells for transcellular transport. M cells are important for the delivery of proteins and nanocarriers from the lumen to the lymphoid tissues. Indeed, transported exogenous proteins may then be also processed by the immune system and induce an immune response. M cells possess a high transport capacity for peptides, proteins, and nanoparticles[266].

There is a consensus that transcytosis increases with the decrease of particle size. Indeed, previous studies showed that nanoparticle size has a negative correlation with the oral bioavailability of the drugs[268]. For example, a study performed using Caco-2/HT-29 cells has shown that cellular uptake of nanoparticles decreased by the increase of the particle size (50 nm-200 nm-500 nm-1000 nm) [269]. In another study, Hu et al showed that the size decrease of the SLNs from 328.8 to 89.3 nm increased the oral bioavailability of retinoic acid by three-fold[270]. Studies on polystyrene latex showed that maximum particle absorption occurred with particles sized between 50-100 nm, meanwhile, particles of 1 μm size were trapped in the Peyer's patches. This result was in agreement with the literature since several studies show that particles below 1 μm are taken up by M cells but remain trapped in

Peyer's patches showing that the optimal size for a nanoparticle to be transcytosed by an M cell should be below 1 μm, with highest absorption performance below 200 nm[268].

4.4.2. Barriers to effective oral delivery

Oral delivery provides advantages over other types of delivery in terms of disease management. However, its exploitation for peptide therapeutics is limited due to the peptides' poor water solubility, low membrane permeability, and poor chemical and biological stability. In addition to these, physiological obstacles such as pH, efflux transporters, and metabolic enzymes, can limit their absorption (Figure 4.6)[264, 271].

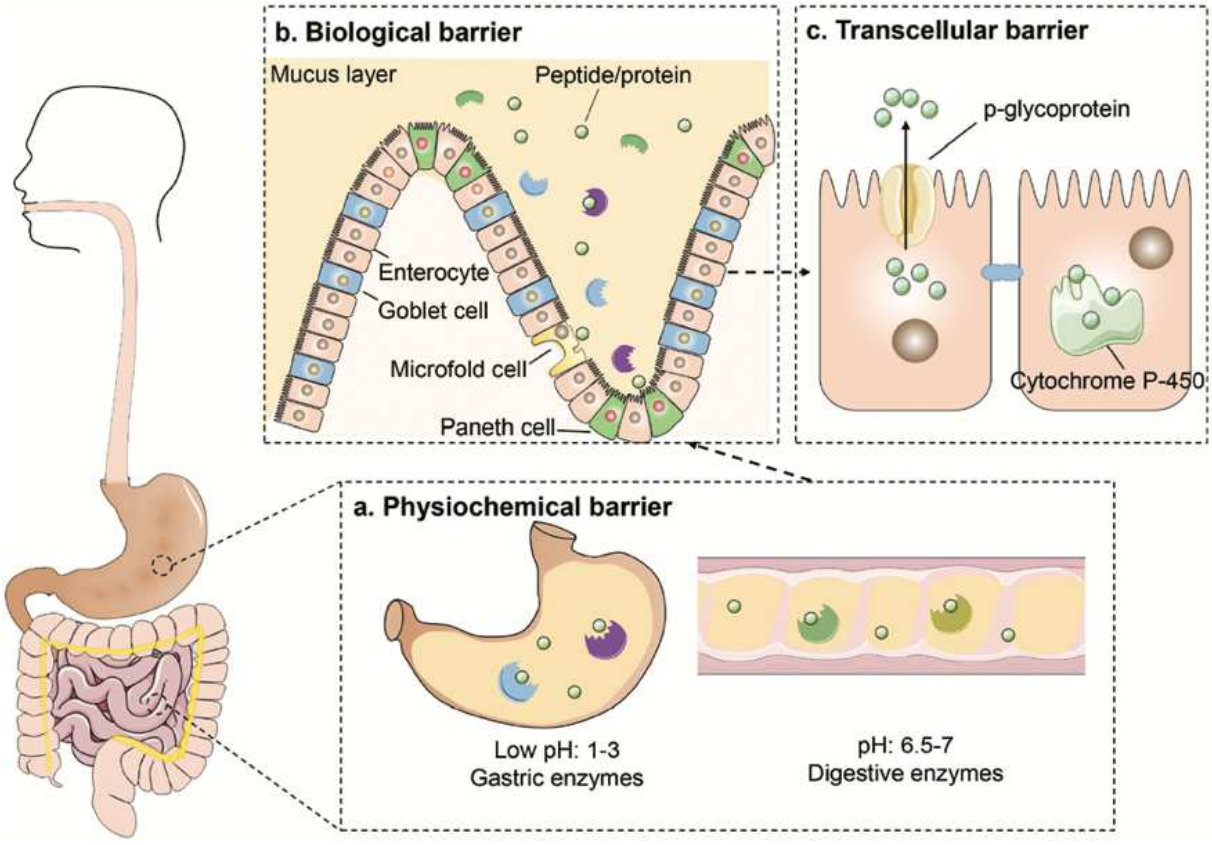

Figure 4.6. *Main gastrointestinal barriers in oral peptide delivery. (a) Physicochemical barriers (b) Biological barriers (c) Transcellular barriers*[271]*.*

- *Physicochemical barriers:* The main physicochemical barriers found in the gastrointestinal tract are represented by the stomach's acidic pH (1-3) and sharp pH increase (7-8) in the intestinal lumen and enzymatic degradation of the peptides in the stomach and intestinal lumen[272]. Peptides are susceptible to enzyme-catalyzed hydrolysis[273] into small peptides or amino acids by pepsin activity

in the stomach. Later on, since peptides are amphoteric electrolytes containing positively and negatively charged amino acids, with a sudden change of the pH in the intestinal lumen, peptide's conformation and stability can be affected negatively, resulting in degradation and cleavage by enzymes secreted by the pancreas into the gut. The serine endopeptidases trypsin, -chymotrypsin, and elastase, as well as the exopeptidases carboxypeptidase A and B, are the most important pancreatic proteases. The pre-systemic breakdown of peptides is also aided by contact with enterocyte-associated enzymes found in the brush border membrane, cytoplasm, and lysosomes. It is crucial that peptide drugs are protected and/or resistant to proteolysis in this harsh environment to ensure their pharmacological activity[274].

- *Biological barriers:* The epithelium of the intestinal lumen contains a single layer of columnar cells: enterocytes, goblet, endocrine, and Paneth cells which are connected by tight junctions[275]. Tight junctions have pores of 3-10 Å and selective permeability to small hydrophilic molecules; they tightly limit protein/peptide diffusion into the systemic circulation, lowering the oral bioavailability and penetration efficiency[276].

Goblet cells, which are accounting for 10 to 20% of the total cells, are responsible for the mucus secretion that exert a role in intestinal epithelium protection. It has been shown that mucus restricts the access of peptides to the epithelial surface[277]. Glycoproteins (mucins) are the main components of the mucus gel layer, and these high-molecular-weight macromolecules may operate as a barrier to drug absorption by maintaining in place a water layer or through interactions between diffusing molecules and mucus layer components[278]. Mucus's composition, ionic strength, shape, viscoelastic features, net charge, and concentration of drugs and particles all affect how they diffuse through the mucus[279]. Large molecules' mobility may be decreased by the network's brush-like topology and mesh space, which function as a size exclusion filter. The development of several non-covalent interactions may immobilize a drug or particle in the mucus network, adding another crucial interaction component to mucus in addition to this steric barrier. Drugs can interact hydrophobically with the non-glycosylated portions of the mucin protein backbone and the lipids associated with the mucins, which reduce mucus diffusion rates (Figure 4.7).

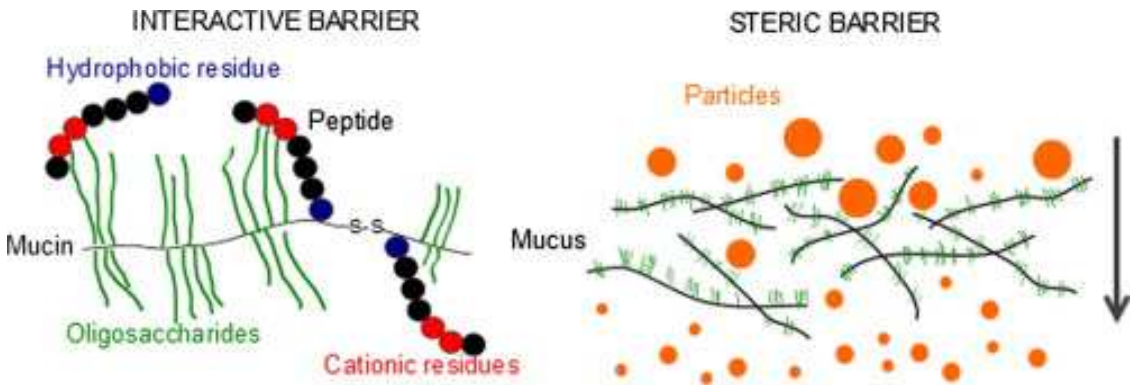

Figure 4.7. *Schematic representation of the interactive and steric barriers faced in the mucus layer upon oral delivery*[280].

- *Transcellular barriers:* After overcoming the mentioned obstacles, peptide/protein therapeutics must still cross transcellular barriers such as cytochrome P-450 (CYP450) metabolization and a p-glycoprotein (p-gp) efflux pump before entering the bloodstream. Efflux pumps such as P-gp commonly found in epithelial cells' apical membranes may, in fact, lower the bioavailability[271]. P-gp transfers substrates from the cell to the apical side of the cell and influences their pharmacological action. The function of the P-gp differs depending on the location. Intestinal P-gp lowers the oral bioavailability of the drugs by preventing their absorption from the intestinal lumen and decreasing the blood concentration. P-gp is a significant hurdle to the oral delivery of medicines in this scenario and limits their therapeutic applications[281].

4.4.3. Strategies for successful oral delivery

To overcome the limitations and increase the bioavailability of orally administered peptides, a variety of approaches have been investigated. Using anatomical, histological, physiological, and biochemical features of the gastrointestinal tract (GIT) and combining the drug with advanced drug delivery systems or devices, successful delivery of peptides by oral route can be achieved.

4.4.3.1. Chemical modifications

As mentioned earlier, a peptide's physicochemical properties determine its absorption route in the intestinal lumen through the epithelium. Therefore, the structural modifications open up several possibilities to enhance the absorption properties of the peptides while also affecting their pharmacokinetic and pharmacodynamic profile[282].

The physicochemical properties of peptides or proteins such as solubility, hydrophilicity, and hydrophobicity may be obstacles to oral absorption. To overcome low solubility, covalent

modifications with polyethylene glycol (PEG) or low molecular weight chitosan are frequently used. Enzymatic stability in the GIT is often improved by the same modifications, as the hydrophilic PEG/chitosan shields the molecule's surface from enzymatic degradation[283]. Hexyl-insulin monoconjugate-2 (HIM2) is a PEG-conjugated insulin version that was one of the first orally delivered insulin forms to show acceptable bioavailability (5%) and adequate glucose-lowering effects. Studies on HIM-2 showed the PEG conjugation to Hexyl-insulin has provided better solubility, absorption, and stability in the presence of enzymes. In a case study, it was also found to maintain a stable blood glucose level compared to the formulation without PEG in type-1 diabetic patient'[284]. Insulin Tregopil (Biocon Lt.) is a new PEGylated insulin analogue that has been modified for oral administration. Similar to HIM-2, the solubility and stability of insulin were increased with the PEG conjugation. The efficiency and safety of Tregopil were examined on type-2 diabetic patients in 2019, but results have not been published yet[285].

Another method for increasing the bioavailability of orally administered proteins is protein lipidization. Polypeptides conjugated with fatty acids have better transport across biological membranes, are more stable, and have longer plasma half-lives. However, conventional lipidization of the polypeptides faces several limitations, such as incompatibility of peptide and lipid with reaction media, solubility decrease of the peptide due to the lipid conjugation, and, as a result, a decrease of bioavailability. To avoid these issues, a reversible aqueous lipidization (REAL) method has been developed[286]. In a study conducted on rats, salmon calcitonin (sCT) was lipidated using the REAL method; absorption and AUC of lipidated sCT were found to be 19-fold higher compared to free sCT[287]. Other promising chemical modifications include the cyclization[288], B12 conjugation[289], N-acetylation[290] and prodrug approaches[291].

4.4.3.2. Employment of the drug delivery systems

Drug delivery systems (DDS) are defined as formulations or devices that enable the drug to be delivered to target tissues, organs, cells, and subcellular organs. The main purpose of the employment of DDSs is to improve the pharmacological activities of therapeutic drugs and to overcome problems such as low solubility, drug aggregation, low absorption and bioavailability, poor biodistribution, lack of selectivity, and fast degradation; furthermore, DDS are developed to reduce dosing frequency, side effects of therapeutic drugs and thus improve patient compliance[292, 293]. In many cases, DDS are nano-sized products loaded with a drug that are generated to improve the drug characteristics in diverse ways. These systems are engineered in such a way that they can lead to prolonged circulation, improved drug disposition, improved drug efficacy, etc.[294]. A most significant example of nanocarriers are[295] :

- *Polymeric nanoparticles (PNPs):* due to their favorable characteristics, polymeric nanoparticles are widely used as biomaterials in virtue of their good biocompatibility, a broad variety of structures, and noticeable bio-mimic characteristics. PNPs can also be used for other purposes, such as tissue engineering, besides the applications for drug delivery[296].

- *Polymeric micelles:* spherical, colloidal, supramolecular nano-constructs are assembled using amphiphilic copolymers at a concentration above their critical micelle concentration (CMC). Polymeric micelles exhibit several advantages, such as solubilization of the poorly water-soluble or hydrophobic drugs and extension of the circulation in the blood by evading the mononuclear phagocytic system in the liver, provided that they are sufficiently colloidally stable in the blood stream[297].

- *Dendrimers:* dendrimers are highly branched three-dimensional macromolecules with highly controlled structures, a large number of 'peripheral' controllable features, and a tendency to possess a globular form. They are used in drug delivery to entrap drugs among the dendritic branches and to conjugate drug molecules onto the terminal ends of the branches[298].

- *Core-shell systems:* particles build up from different materials, such as metals, metal oxides, and polymers; they may be efficiently stabilized and their surface properties can be modulated. They can be used as contrast agents depending on their composition, size, and shape[299, 300].

- *Lipid-based nanocarriers:* In virtue of the enhancement of drug bioavailability, protection of the active molecules from chemical degradation, and their higher biocompatibility and lower toxicity compared to polymeric nanoparticles, increased attention is given to lipid-based nanocarriers as drug delivery systems[301]. Several routes of administration are being investigated for lipid-based nanocarriers, such as parenteral[302, 303], ocular[304], topical[305], pulmonary[306] and oral[307, 308] routes. Lipid-based carriers can be obtained with different compositions, formulation processes, and morphology (Figure 4.8)

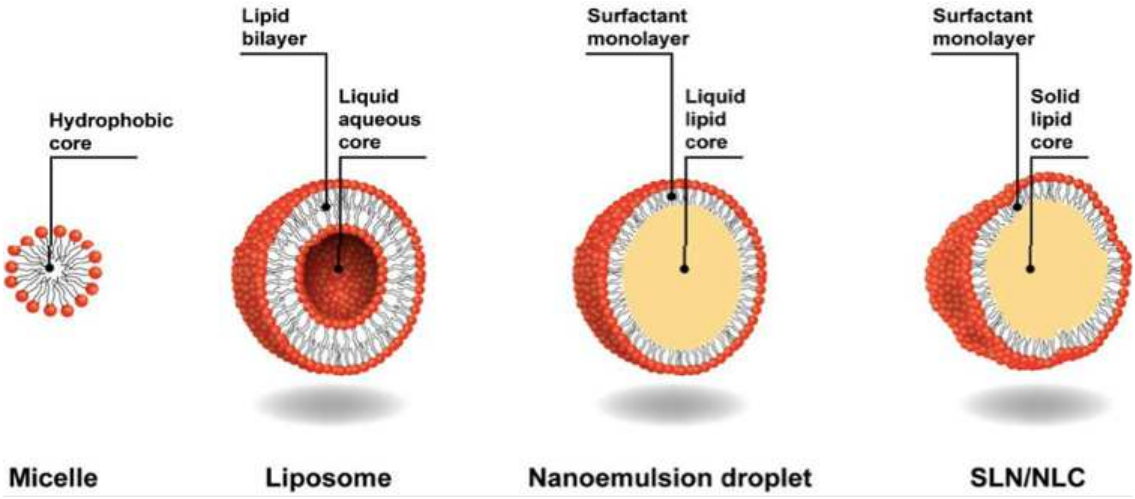

Figure 4.8. *Schematic representation of some of the lipid-based nanocarriers[309].*

Classical examples of different lipid-based formulations include "liposomes", which consist primarily of phospholipids, the major components of biological membranes. In virtue of their unique composition, liposomes are developed to encapsulate both hydrophilic drugs in their aqueous core (hydrophilic region), and lipophilic drugs in their phospholipid bilayer (Figure 4.8). Liposomes can be classified by their lamellarity (unilamellar liposomes contain a single bilayer of phospholipids, while multilamellar liposomes consist of multiple liposomal membranes), size (small liposomes [100 nm], intermediate liposomes [100-250 nm], large liposomes [250 nm] or giant liposomes [> 1 um]), and surface charge (anionic, cationic, or neutral).

Liposomes have been extensively used since their first description by Prof. A.D. Bangham as a drug delivery system, in biomedical applications and several liposomal drug delivery systems are already used in the clinical practice[310, 311].

However, conventional liposomes obtained by mixtures of phospholipids and cholesterol have limited efficacy in oral delivery applications mostly due to poor stability in the gastrointestinal content which may induce instability and dissociation. Enhanced bilayer stability, shielding payload from enzymatic degradation, improved retention and mucus penetrating abilities of drug-loaded liposomes in the intestinal tract, and receptor-mediated transcytosis are some of the strategies proposed to improve the stability and bioavailability of liposomes under GI tract conditions[312].

Solid lipid nanoparticles (SLNs) are lipid nanocarriers with a solid core that can carry mostly hydrophobic drugs. They can be made with biocompatible lipids. SLNs are considered one of the most popular drug delivery systems. Surface modifications of SLNs may also provide them with unique properties such as mucoadhesiveness or targeting ability. Notably, the lipid solid matrix allows a controlled release of drugs mostly by erosion; furthermore, SLN possesses higher stability than

liposomal that stem from the hydrophobic interactions of lipids that occur within the whole matrix and not only on the lipid bilayer as in liposomes[313, 314].

4.5. Solid-lipid nanoparticles

Solid lipid nanoparticles (SLNs) were first described in 1991, as an alternative to the traditional carrier systems such as nanoemulsions, liposomes, and polymeric nanoparticles. SLNs are made up of a solid core made up of lipids with high melting temperatures (above 37 °C) that's been coated with phospholipids or surfactants (Figure 4.9). The main difference between SLNs and other lipid-based carriers (i.e. liposomes) is that SLNs have a solid core instead of a liquid core[315].

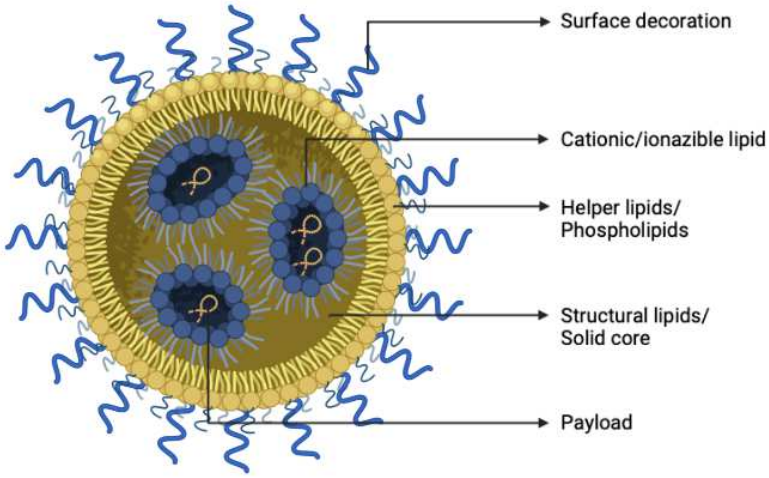

Figure 4.9. *Schematic representation of solid lipid nanoparticles with their components.*

Triglycerides, partial glycerides, fatty acids, steroids such as cholesterol (Figure 4.10, A), and waxes are commonly used lipids for SLN production. The components used to assemble SLN are selected to reduce the risk of acute and chronic toxicity, which is a clear advantage of SLN[316]. The solid core of SLN with respect to the liquid core of nanoemulsion has been shown to improve the stability of chemically-sensitive lipophilic ingredients and provide better control over the release kinetics of the loaded drugs. This can be explained by: i) mobility decrease of the drugs in the solid matrix and delay of the chemical degradation, ii) prevention of the drug accumulation on the surface of the nanoparticle thus avoiding possible degradation, and iii) slow lipid digestion in virtue of the solid core with respect to the liquid core allowing for more sustained release of the loaded drug[317]. Emulsifiers and water are also present in SLNs. Phospholipids, poloxamer, and polysorbate are emulsifiers that are used to stabilize the lipid suspension and prevent agglomeration, indeed it has been shown that with the increasing emulsifier concentration particle size is decreased[318]. This is a consequence of the

higher surface that the surfactant can coat as a result of decreasing size at steady total particle volume. Soy lecithin, egg lecithin, and hydrogenated soy phosphate lecithin are the most common phospholipids used in the formulation (HSPC). HSPC is a phospholipid that has a longer aliphatic chain and a high melting temperature (Figure 4.10, B).

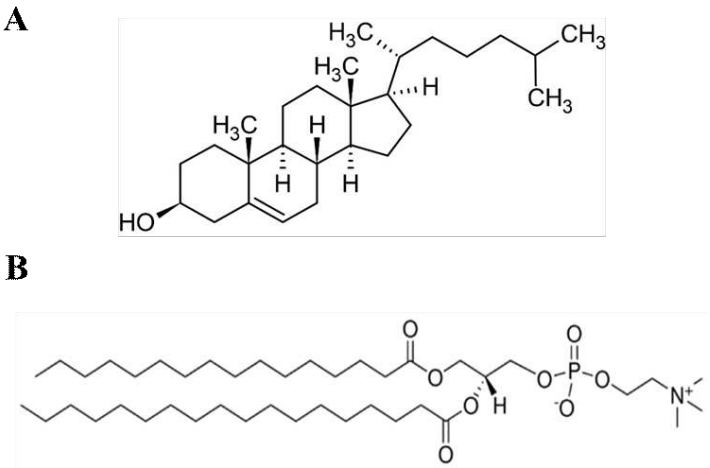

Figure 4.10. *Chemical structure of Cholesterol (A) and Hydrogenated Soy Phosphatidyl Choline (B)*

The ease of large-scale production, biocompatibility, biodegradability or clearance of components, and the ability to target drugs are all significant advantages provided by SLN. Solid lipid nanoparticles may have some drawbacks as well. Indeed, due to the crystalline structure of the matrix, there is a risk of drug expulsion during the crystallization process. However, when compared to other traditional carriers, the advantages outweigh the disadvantages[319].

Hydrophobic drugs have a higher encapsulation than hydrophilic drugs because SLNs are made up of a solid lipid matrix. The hydrophobic ion pairing (HIP) technique is one strategy that has been suggested to enhance the loading efficiency of hydrophilic molecules such as peptides, proteins, and DNA into SLNs[54]. The lipophilicity of these drugs is increased as a result of the formation of the pairs, while the extent of burst release and rate of drug release from the SLN is decreased. Because the positive charge of surfactants can cause electrostatic interaction with the negative phosphate charges of nucleic acids, the HIP has also been widely used in gene therapy[320]. Because of the presence of quaternary ammonium in its structure, 1,2-dioleoyl-3-trimethylammonium-propane (DOTAP) has been one of the most widely used lipids for this purpose (Figure 4.11). DOTAP possesses a permanent positive charge that participates in the formation of rather stable complexes with the anionic counterparts.

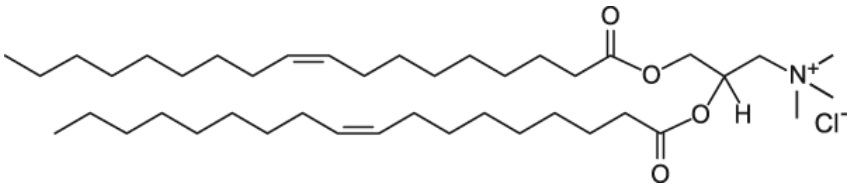

Figure 4.11. *Chemical structure of 1,2-dioleoyl-3-trimethylammonium-propane (DOTAP).*

Dumont et al. previously investigated the potential of the HIP with SLNs and nanostructured lipid carriers (NLCs) to enhance peptide transport across a simulated intestinal barrier. The anionic docusate was used to enhance the lipophilicity of Leuprolide (cationic), which was encapsulated in SLNs and NLCs with encapsulation efficacy of 84 and 89 percent, respectively. The carriers had a size about 110 nm, and both were tested for cytotoxicity, intracellular uptake, and intestinal transport in Caco-2 and co-cultures of Caco-2 and HT29-MTX cells. SLNs did not affect cell viability, whereas NLCs were found to be toxic to the cells suggesting that the water-insoluble surfactant in the formulation increases toxicity and influences intracellular uptake. Confocal microscopy was used to examine the uptake profile of the formulations, and the results revealed the presence of both types of nanoparticles in both cell monolayers, even in the presence of mucus. Flow cytometry confirmed these findings, with SLN and NLC internalization rates of 82 percent and 98.8 percent on Caco-2 cells, respectively[321]. In another study performed by Phan et al, the cationic exenatide has been ionically paired with anionic n-octadecyl sulfate (SOS) and anionic docusate (DOC) to improve its oral bioavailability. The generated formulations, self-emulsifying drug delivery system (SEDDS) with a liquid core, showed improved ex vivo permeation, and relative bioavailability vs subcutaneous injection of 19.6 and 15.2 % for SOS and DOC-based formulations, respectively[249].

The particle size and surface properties of nanoparticles dictate a variety of behaviours including cellular uptake, absorption, pharmacokinetic profile, and biodistribution in the organism [322]. Depending on the type of drug and its biological target, intact drug-loaded nanoparticles are absorbed by the intestinal epithelium, or they can be used as adhered reservoir releasing the drug in the proximity of the epithelium. For the ones absorbed, the toxicological issue has to be considered, while those that remain in the gastrointestinal tract will be excreted. The precise delivery mechanism of particles depends on composition, size, surface features, and other variables. Thus, it remains unclear if the improvement of drug efficacy observed when drugs are administered with nanoparticles is ascribable to an increase in residence time close to the absorptive epithelium or if the absorption of the drug-loaded nanoparticles is required. Understanding how nanoparticles interact with the intestinal epithelium is essential to adjust the properties of nanocarriers and improve efficacy and safety to accelerate their clinical translation[268].

The role of nanoparticle size in oral delivery using carboxylated polystyrene particles was investigated by Banerjee et al. The cellular model for in vivo studies has demonstrated a great influence on the results. Both the Caco-2 monolayer and co-culture of Caco-2 and HT-29 (similar to mucus-producing goblet cells) had no significant transport of particles: a maximum transport of 0.3-0.4% was observed after 5 hours for 50 nm-sized particles. Inclusion of Raji-B cells, which induce M cell type phenotype when co-culture with Caco-2 cells, improved the transport up to 25% in 5 hours with slight but not significant difference between 50 nm and 200 nm particle size. In the same culture, the transport of 500 nm and 1000 nm-sized particles was significantly lower, with a maximum of 15% after 5 hours[269]. Similar results were obtained by Bandi et al., employing polystyrene nanoparticles. The mucus permeation of nanoparticles across rabbit intestinal mucus also showed a size-dependent profile. Particles with a 50 nm diameter had the greatest permeation through the mucus, reaching the 100% of loaded particles permeated across the mucus membrane in 2 hours. Their permeation profile during the time had no significant difference with particles of 100 nm size, while a significant difference was found with 200 nm diameter particles (p<0.01) and with 500, 750, and 1000 nm diameter particles (p<0.05). In particular, only 2% of total loaded particles with a size higher than 200 nm permeated through mucus. In the same study, some data regarding the effect of surface functional groups were also reported. Diffusion of particles could be compromised by mesh spacing size between mucin fibers, smaller particles can penetrate rapidly through mucus layers and prolong retention of drug molecules[323].

The effect of surface charge on the bioavailability and absorption of polymeric nanoparticles after oral administration was investigated by Du et al. PEG-PLA nanoparticles were modified with three different lipids containing positive, negative, or zwitterionic charges. In a Caco-2 model, using the confocal laser scanning microscopy (CLSM) and fluorescence-activated cell sorting (FACS) analysis, the results suggested that positively charged nanoparticles facilitated the cellular uptake and transport of nanoparticles. This can be related to the multiple internalization pathways, such as clathrin, lipid raft (caveolae)-dependent endocytosis, and micropinocytosis, that involve mainly the positively charged nanoparticles compared with zwitterionic and negatively charged nanoparticles. On the other hand, the surface charge doesn't affect exocytosis. In male C57BL/6J mice a stronger interaction of positively charged nanoparticles with both the epithelial surface and lamina propria compared with other nanoparticles was also observed. This result can be ascribed to the electrostatic interaction with the glycocalyx[324]. On the other hand, the mucus contains negatively charged glycoproteins that can reduce the mobility of positively charged NPs with respect to negatively charged nanoparticles that diffuse 20-30 times faster[325]. Thus, the surface of nanoparticles for oral administration must be rationally

engineered to exploit a combined effect of fast diffusion across the mucus while ensuring significant electrostatic interaction with epithelial cells of the intestine.

4.5.1. Conventional methods for SLN preparation

The formation of a pre-emulsion with or without the use of organic solvents, followed by size reduction, is the most common method for SLN preparation. The selection of preparation method of the SLNS is based on the drug of interest, the desired size of the particles, polydispersity index, administration route, composition, and many other parameters[326].

High-pressure homogenization is a technique in which a high-pressure homogenizer (100-2000 bar) is used. This procedure can be carried out under hot or cold conditions. Hot homogenization involves heating lipids to a temperature above their melting point, then mixing them with a hot aqueous phase containing the emulsifier to set up an emulsion. After passing the emulsion through a high-pressure homogenizer, the sample is cooled to or below room temperature while being stirred which induces the solidification and crystallization of lipids and the generation of SLN. Cold homogenization is achieved by milling the drug dispersion in the bulk lipid melt, which is then rapidly cooled and dispersed in a cold surfactant aqueous solution. This method, rather than hot homogenization, ensures a homogeneous distribution of the drug within the matrix by minimizing hydrophilic drug loss to the water phase. Furthermore, because the drug is not molecularly dissolved in melted, cold homogenization reduces temperature-induced drug degradation. On the other hand, cold homogenization produces larger particles with a wider size distribution[327]. Since peptides are known to easily unfold by high shear stress/pressure and high temperatures, the process parameters to generate peptide-loaded SLNs should be carefully selected[328].

Another method to prepare SLNs is “emulsion solvent evaporation”, which involves dissolving the lipophilic material in a water-immiscible organic solvent followed by emulsification in an aqueous phase. Evaporation of the solvent causes the lipid to phase separate in water. The major advantage of this technique is that it does not require high temperature and thus no thermal stress is applied. However, it requires the use of organic solvents that can present incompatibility with drugs and can remain in the final formulation as residual contaminations. This technique was commonly applied for the loading of the peptides, such as lysozyme[329], leuprolide[330], recombinant human growth hormone[331], and BSA[332]. Peptide encapsulation efficiency of the generated carriers was found to be poor. Furthermore, due to various factors such as high shearing forces and exposure to a large interface between the aqueous and organic phases, protein drugs tend to undergo denaturation and form aggregates[333].

4.5.2. Innovative microfluidic techniques

Many efforts are made to develop drug delivery systems to identify those with easy up-scale fabrication methods with low batch-to-batch variability to advance the translation from research to clinic. The microfluidic approach has shown that it is possible to produce nanoparticles with improved loading and scalable formulation volumes to achieve this goal. It's a cutting-edge technique that allows for the creation of miniaturized microscale devices with a variety of chambers and microchannels with precise fluid mixing control. When compared to traditional methods, it allows for the production of smaller nanoparticles with a lower size distribution, and higher encapsulation efficacy [334]. This technology also improves mixing process controllability, reduces batch-to-batch variation, reduces reagent consumption, and saves time by replacing multi-step procedures with just one step [335].

A supersaturation condition is achieved by rapidly mixing two phases, one containing a solute and the other an antisolvent. This causes nanoprecipitation, which causes solute nucleation and particle growth. This procedure produces smaller nanoparticles with uniform size because microfluidic systems mix solvents in microseconds to milliseconds (ms), which is faster than the typical timescale for lipid aggregation (between 10 and 100 ms)[336]. Furthermore, the choice of mixer geometry and flow results in a change in supersaturation conditions and, thus, thus modulation of particle properties.

Laminar and turbulent flows have been identified as the two possible interactions of two fluids (Figure 4.12). Different types of flow can be generated along the microfluidic chambers with different levels of order and mixing profiles. The type of flow depends on Reynolds number (Re), a dimensionless number calculated as

$$Re = \frac{\rho u D}{\mu}$$

where:

- ρ is the fluid density (kg/m^3)
- u is the mean fluid velocity (m/s)
- D is the hydraulic diameter of the channel of the mixer (m)
- μ is dynamic viscosity (kg/m*s)

Along a microchannel, when the Reynolds number is relatively high (Re > 4000) a turbulent flow occurs, which is characterized by an irregular fluctuation and continual mixing in both direction and magnitude. A laminar flow occurs when the Reynolds number is less than 2100, and fluids flow in

parallel layers with no opposing directions to the main flow. The majority of microfluidic devices use this type of flow.

The flow is dictated by the mixer geometry when the Reynolds number is between 2100 and 4000[337].

The microfluidic equipment consists of a microreactor with two pumps and a micromixer made up of tubes or channels that can quickly mix reagents due to the high surface area-to-volume ratio.
Micromixers are divided into two types: active and passive micromixers. Passive micromixers rely only on the geometry of microchannels to achieve mixing: T-junction mixing, microfluidic hydrodynamic focusing (MHF), and staggered herringbone mixing (SHM). Active micromixers are based on an externally applied disturbance to the fluid flow and this disturbance is caused by moving the components inside the micromixer, such as magnetically activated stirrers or the applications of external forces, e.g. pressure, ultrasound, acoustic and so on[338].

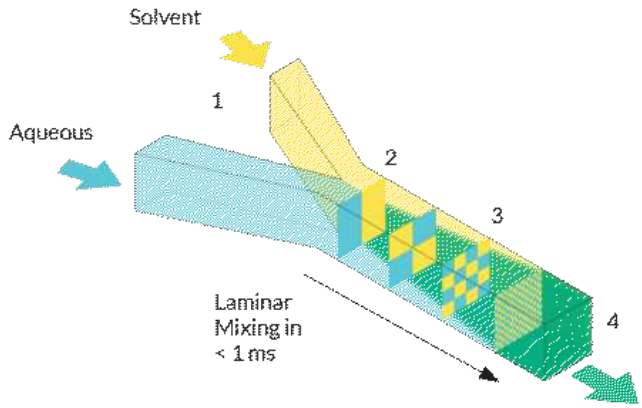

Figure 4.12. *Diagram depicting two fluids mixing under laminar flow in a microfluidic mixer. 1) Fluids (solvent and aqueous phase) entering the channel. 2) Mixture of the channels in a controlled, non-turbulent way. 3) Mixture of the fluids while running through the system. 4) Fluids leave the system completely mixed[339].*

One of the earliest geometric designs of microfluidic devices for passive mixing is the T-junction, where the two phases meet in an orthogonal way (Figure 4.13, panel A). The geometry can be modified to form a Y-like shape, where the two inlets form a sharp angle (< 90°). On the main channel surface, the mixing occurs.
MHF exploits a convective-diffusive mixing in which the organic solvent containing lipids is hydrodynamically focused by an aqueous phase (Figure 4.13, panel B).
The SHM is an innovative microchannel design developed in 2002, which consists of a channel with herringbone grooves that cause turbulent flow in the channel and transversal vortices repeatedly changing as a consequence of the asymmetric geometry (Figure 4.13, panel C). This mixing system

leads to more refined and faster mixing performances and homogenous particle sizes. It is employed by Precision Nanosystem™ with NanoAssembler® instrument that was used to develop SLN in this thesis project. However, this design does not allow to achieve the high speeds that would be required by Good Manufacturing Practice (GMP) standards. To reach high fluid speeds up to 20 Liter/hour, Toroidal Mixer (TM) also known as bifurcating mixers, has been developed by Precision Nanosystem™ that consists of circular structures within the microflow path (Figure 4.13, panel D)[336].

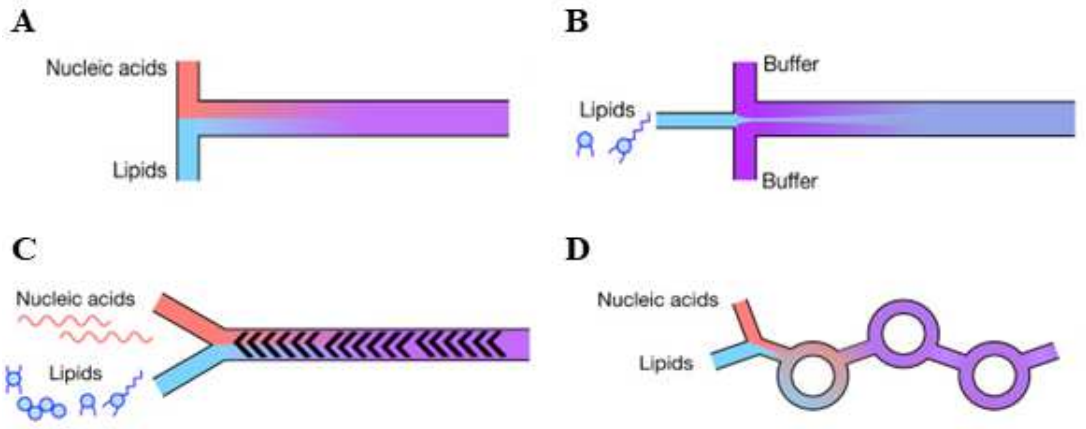

Figure 4.13. *Schematic illustration of microfluidic mixing morphology for nanoparticles formulation: A) T-junction mixing, B) Microfluidic Hydrodynamic Focusing (MHF), C) microfluidic Staggered Herringbone Micromixer (SHM), D) microfluidic bifurcating mixer*[36].

The size and polydispersity index of nanocarriers generated by microfluidic techniques are strongly controlled by two process parameters: Total Flow rate (TFR), expressed in mL/min, and the Flow Rate Ratio (FRR), which is the ratio between the aqueous and the organic phase. These operating parameters have a role in the control of size and PDI because they govern the mixing between the organic and the aqueous phase[340].

A microfluidic method to produce siRNA-containing lipid nanoparticles was exploited by Chen et al. exploited. Cationic lipid and other lipids, dissolved in ethanol, were rapidly mixed with an aqueous siRNA solution: water decreases the solubility of lipid and promotes their self-assembly into lipid nanoparticles, entrapping negatively charged siRNA as a consequence of the electrostatic interaction with the cationic lipids. The effect of mixing on the particle size was investigated: the diameters of nanoparticles tended to decrease at total higher flow rates, from 100 nm to 70 nm. This behavior can be explained by the theory of vesicle formation under non-equilibrium conditions. When rapid dilution of ethanol happens at a high total flow rate, the lipids have limited time to assemble before an ordered organization into closed vesicles is achieved, resulting in smaller particles. Conversely, low flow rates favoring stabilization and growth of intermediate fragments lead to larger lipid nanoparticles[341, 342].

The research conducted by the scientists of the Precision Nanosystem™ also demonstrated the utility of the NanoAssembler® Benchtop instrument for formulating lipid-based nanoparticles and ease of the size tuning by changing the system parameters, namely FRR (Figure 4.14, Panel A) and TFR (Figure 4.14, Panel B)[339].

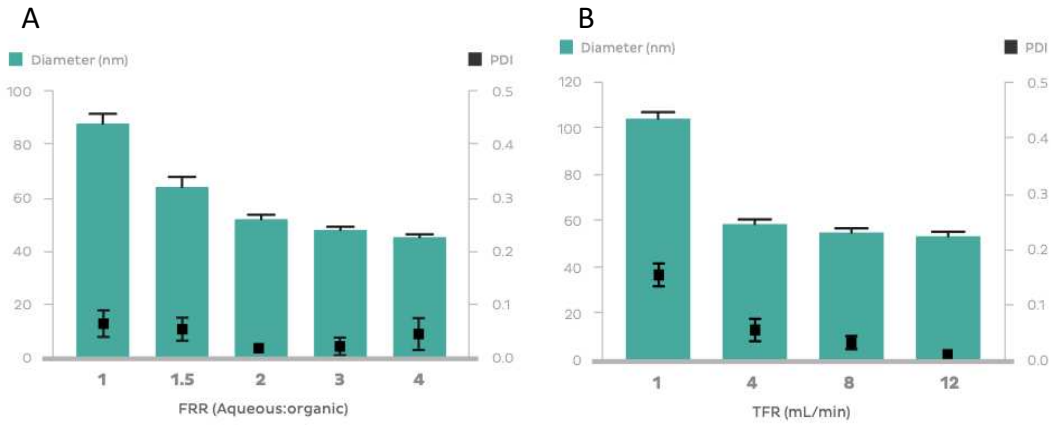

Figure 4.14. *Liposome size tuning by FRR (A) and TFR(B). A higher aqueous:organic flow rate ratio reduces the size asymptotically of the liposomes and increasing TFR increases the mixing speed and reduces the liposome size generated in POPC/Cholesterol/DSPE-PEG$_{2kDa}$ (52:45:3 mol%) composition.*

4.5.3. Lyophilization of nanoparticles

Lyophilization, also called freeze-drying, is a technique exploited to improve the long storage stability and shelf-life of various lipid or polymer-based systems, peptides and proteins, and many other macromolecules for pharmaceutical use[343]. Indeed, lipid nanocarriers such as SLNs could undergo agglomeration and oxidation during long-term storage, or the aqueous medium where they are dispersed may undergo microorganism contamination and growth.

Freeze-drying is a low-temperature dehydration method that uses sublimation to remove water from the final product. There are three stages to performing this process: freezing, primary drying, and secondary drying. Water is first solidified at low temperatures resulting in ice crystals. Then, to induce sublimation, the pressure is reduced below the triple point of water while the sublimation heat is provided by the freeze-drying equipment. The residual water that is associated with the lyophilized material is then removed from the formulation during the secondary drying step[344].

The freeze-drying process may be responsible for a few physical stresses, conditions such as low temperatures, and mechanical pressures created by ice crystals, which might cause particle aggregation. Indeed, lyophilization without a lyoprotectant may result in a significant agglomeration of the colloidal systems dispersed in water that is maintained even after regeneration of the dispersion and is responsible for the increase of particle size[345]. For such reason, lyoprotectants are frequently

used to preserve the physio-chemical properties of nanoparticles and improve the final product's quality. Trehalose, mannitol, sucrose, and glucose are the most common sugars used as cryoprotectants[345]. The mechanism by which they preserve colloids from aggregation during freeze drying is mostly related to their ability to create a glassy matrix that prevents nanoparticles from mechanical stress caused by ice crystals and isolates individual particles in the unfrozen fraction[346]. Indeed, Lin Niu showed very nicely the effect of the lyoprotectant on nanoparticle aggregation by cryo-SEM imaging (Figure 4.15)[347].

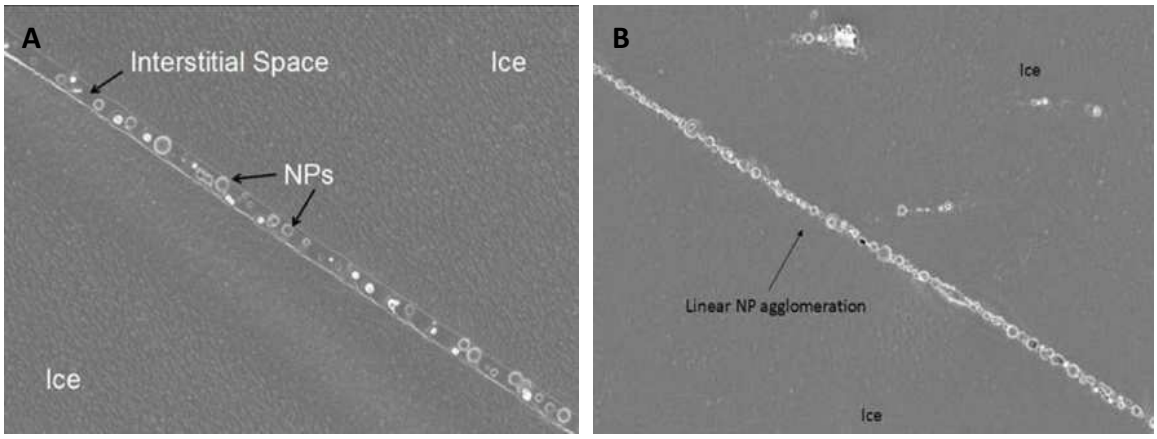

***Figure 4.15**. Cryo-SEM image of an aqueous 30 mg/mL PLGA NP dispersion, after dry ice-induced freezing in the presence of 3% sucrose (A) and the absence of cryoprotectant (B).*

Lyoprotectants are commonly used when protein solutions have to be freeze-dried to provide protection from stress denaturation and preserve their biological activity. Several sugars can be used to this aim. The underlying mechanisms of protein stabilization during freeze dying are based on the replacement of hydrogen bonds with water by saccharides thus preventing destabilization and lyoprotectants amorphous structure generation and prevention of physical phase separation[348]. In particular, trehalose has been demonstrated to be more efficient to this aim with respect to sugars, since it has no internal hydrogen bond, low chemical reactivity, high glass transition temperature (Tg), and low hygroscopicity[349].

SLNs have been lyophilized in few studies by including different lyoprotectants in the aqueous medium, namely, glucose, sorbitol, and fructose in a range from 5 and 10% (w/w). Insulin-loaded SLNs were prepared by a modified solvent emulsification-evaporation method. Particle size before freeze-drying was 400 nm with a low polydispersity (0.17). After freeze-drying, the particle size of the SLNs

with the lyoprotectants after dispersion regeneration was preserved, except for sorbitol, which increased by 100 nm with a broad size distribution. Insulin's native conformation was protected independently from the presence of the lyoprotectant, which was related to the protecting activity of the lipid matrix of the SLNs[350]. In another study, trehalose and mannitol were employed for the freeze-drying of SLNs. The research group of C. Schwarz studied the effect of these lyoprotectants on the colloidal features of the SLNs at an increasing concentration of up to 15% (w/v). Trehalose was proved to be highly effective as a lyoprotectant of SLNs as previously reported for liposomes[351].

4.6. Enteric coating of oral dosage forms

Enteric coating of dosage forms is a commonly used technique to endow oral pharmaceutical formulations with a controlled release profile. This approach ensures the stability of the loaded drug in acidic gastric conditions and provides its release in the intestinal lumen where the environment is close to neutrality and the enzymatic digesting activity is reduced (Figure 4.16). This can be accomplished by using pH-sensitive poly-anionic polymers that are insoluble at acidic pH but soluble at intestinal pH. Among the polymers frequently used to create enteric coatings are hydroxypropyl methylcellulose phthalate, methacrylic acid copolymers, and cellulose acetate phthalate[352].

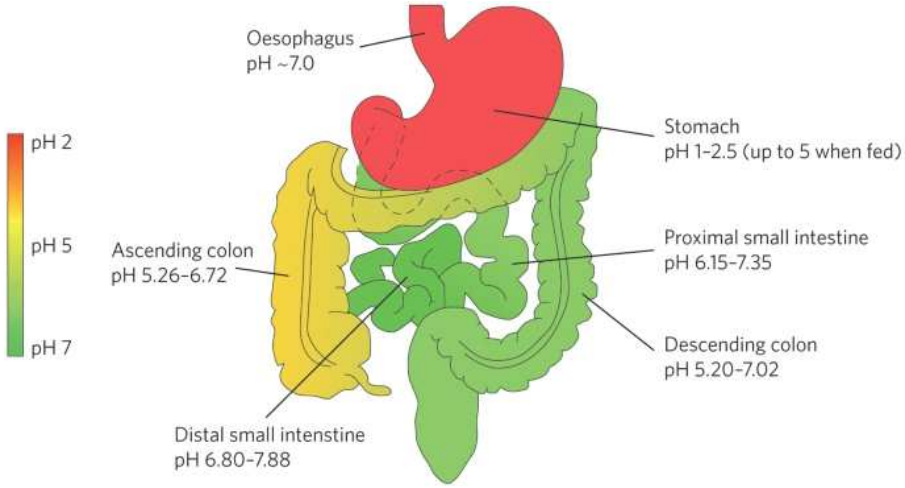

Figure 4.16. *pH values in different sections of the gastrointestinal tract[353].*

Polymethacrylates are polymers that may be polymerized using chemically different methacrylates monomers in different ratios and are produced by using free radical addition polymerization[354]. A wide variety of copolymers based on polymethacrylates are marketed primarily by Evonik Industries in Germany under the trade name Eudragit. In 1953, Rohm & Hass GmbH, Darmstadt first introduced Eudragit as an alkaline soluble, acid-resistant drug coating material. Today various kind of Eudragit is available for targeting different parts of the intestinal tract[355].

The most commonly used Eudragit grades include Eudragit L100, which dissolves when the environmental pH is over 6. The enteric effect of this polymer can be explained by the presence of carboxylic groups: at acid pH, the carboxylic groups result in protonated and neutral, which reduce the polymer solubility and the polymer creates a water-insoluble film that is resistant to gastric juice [356]; on the contrary, they are deprotonated to the anionic carboxylate in the 5–7 pH range of and the polymer convert into the polyanionic water-soluble version. Being regarded as a non-toxic functional excipient, Eudragit L derivatives are commonly used in marketed products such as Claversal, Salofalk, Mesasal, Calitofalk, and Apriso, all carrying Mesalazine as the active ingredient for the treatment of inflammatory bowel disease[355].

5. AIM OF THE PROJECT

The delivery of biotechnological drugs via non-invasive routes remains a great challenge. In particular, the oral administration of peptides, while providing high patient compliance, offer several drawbacks including instability in the gastrointestinal environment due to acidic pH and proteases activity which induces rapid degradation. Furthermore, the low diffusion of biologics across the intestinal barrier due to their hydrophilicity and molecular weight also represents a limitation to absorption. Taken all together, these drawbacks result in low absorption and bioavailability.

The aim of this thesis project was the development of an engineered multicomponent therapeutic system for the oral administration of the antidiabetic agent, exenatide (Figure 5.1). The therapeutic system consists of exenatide-loaded solid lipid nanoparticles (SLN) encapsulated into gastroprotected capsules. To this aim, the physico-chemical features of the peptide were exploited for hydrophobic ion pairing mediated loading into SLN. The loading efficiency and the colloidal features of SLN were maximized by screening a library of SLN with different component ratios and different microfluidic assembly parameters. After surface modification with PEG for cationic charge shielding to modulate SLN diffusion through intestinal mucus and facilitate absorption, SLNs underwent lyophilization to generate a solid version which was encapsulated into hard gelatine capsules. Enteric coating of the capsules was performed to provide gastric protection and SLNs release in the intestinal lumen for absorption.

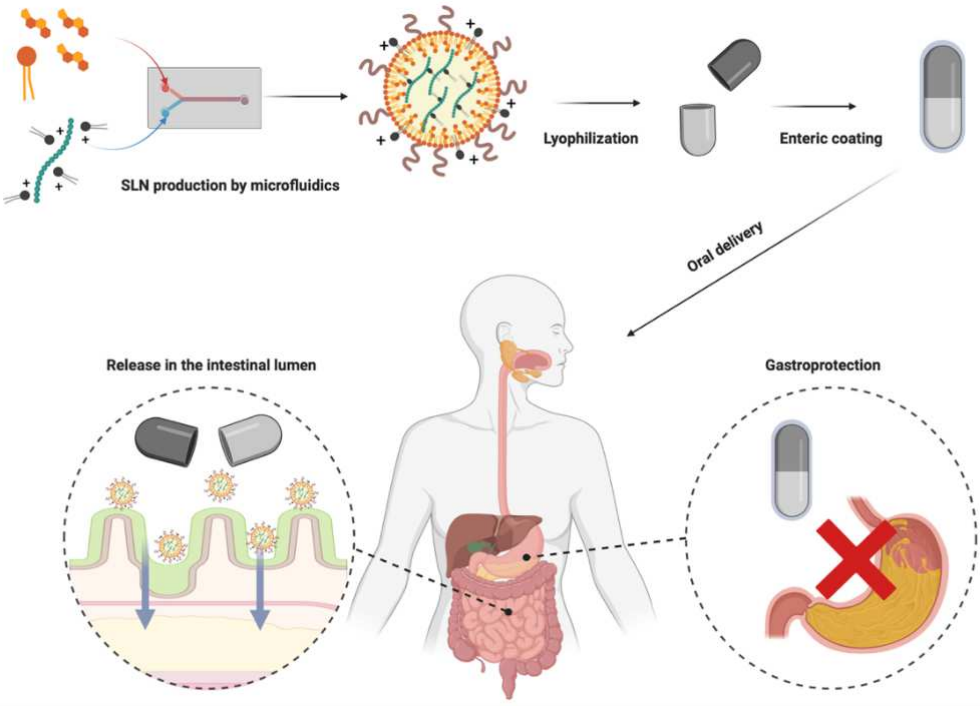

***Figure 5.1**. Schematic representation of the formulation of enteric-coated capsules filled with EXEN-loaded SLNs.*

6. MATERIALS and METHODS

6.1. Materials

6.1.1. Reagents

- Hydrogenated Soybean Phosphatidyl Choline (HSPC) was purchased from Lipoid (Ludwigshafen, Germany).
- 1,2-dioleoyl-3-trimethylammonium-propane (DOTAP) and 1,2-distearoyl-sn-glycero-3-phosphoethanolamine-N-[methoxy(polyethylene glycol)-2000] [$mPEG_{2kDa}$-DSPE] was provided by Avanti lipids (Alabama, USA).
- Cholesterol, ferric chloride hexahydrate ($FeCl_3 \cdot 6H_2O$), ammonium thiocyanate (NH_4SCN), D-(+)-Trehalose dihydrate, sodium citrate dihydrate ($Na_3C_6H_5O_7 \bullet 2H_2O$), sodium chloride (NaCl), potassium chloride (KCl), disodium hydrogen phosphate (Na_2HPO_4), Rhodamine B were provided by Sigma-Aldrich (St. Louis, MO, USA).
- Acetonitrile (MeCN), chloroform ($CHCl_3$), ethanol (EtOH), and methanol (CH_3OH) were provided by Honeywell Riedel-de-Haën TM (Morris Plains, NJ, USA).
- 2-[4-(2-hydroxyethyl)piperazin-1-yl]ethanesulfonic acid (HEPES) and 2,2'-bipyridine were provided by Thermo Fischer SCIENTIFIC (Waltham, MA, USA).
- Water for reactions was "ultrapure" water (Milli-Q grade, 0.06 Siemens cm^{-1}) generated with the Millipore Milli-Q® purification system (Merck, MA, USA).
- Citric Acid ($C_6H_8O_7$) was provided by Carlo Erba (Rodano, Milano)
- Potassium dihydrogen phosphate (KH_2PO_4) and starch were provided by Merck KGA, (Merck, MA, USA)
- Polyethylene Glycol – 400 (Peg400) was provided by A.C.E.F (Italy)
- Eudoragit L100 was provided by Evonik (Germany)
- Exenatide (Exendin-4) was purchased from CliniSciences (Guidonia Montecelio, Italy).
- All cell culture materials such as PBS, Dulbecco's Modified Eagle's Medium (DMEM), Foetal Bovine serum (FBS), penicillin, streptomycin, L-glutamine, trypsin, and 3-(4,5-Dimethylthiazol-2-yl)-2,5-diphenyl tetrazolium bromide (MTT) were purchased from Sigma-Aldrich (St. Louis, USA).
- Caco-2 cell line (HTB-37) was provided by the American Type Culture Collection (ATCC) (Virginia, USA).

6.1.2. Scientific equipment

- Solid lipid nanoparticles (SLNs) were prepared using NanoAssemblr® Benchtop, Precision Nanosystem™ Inc. (Vancouver, BC, Canada).
- Dynamic Light Scattering (DLS) measurements were performed by Zetasizer UltraZS from Malvern Instrument LTD (Malvern, UK).
- Solvents were evaporated using Büchi Rotavapor R100 equipped with Büchi Vacuum pump V-100, Büchi Heatingbath B-100, Büchi interfaces I-100 and Recirculating
- Chiller F-305 from Büchi from BÜCHI Labortechnik AG (Postfach, Switzerland).
- Dialysis was performed using 500-1000 Da MWCO and 50-100 kDa MWCO Spectra/Por® Float-A- Lyzer® from Spectrum Labs, Inc (Rancho Dominguez, CA, USA).
- pH measurements were carried out with pH-meterSevenEasy S20-K Mettler Toledo with electrode Mettler Toledo Inlab Expert Pro-ISM (Schwarzenbach, Switzerland).
- UV-Vis Spectrophotometric analysis was performed using UV-Vis spectrophotometer Evolution 201 from Thermo Scientific (Madison, WI, USA)
- High-Performance Liquid Chromatography (HPLC) analyses were performed with an HPLC system from Jasco (Tokyo, Japan) provided with two pumps PU-1580, UV detector Jasco UV-1575 and Borwin chromatography software program for the peaks integrations. C18 Luna Column 4.6 x 250 mm (Phenomenex, Torrance, USA) was used for RP-HPLC.
- Ultrasound sonicator Powersonic 410 of Hwashin Technology (Seoul, Korea).
- Liposomes were extruded with a mini-extruder provided by Avanti Polar Lipid (Alabaster, AL, USA), using 200 nm membrane filters provided by Whatman (Clifton, NJ, USA).
- Malvern MicroCal, LLC VP-ITC microcalorimeter system (Worcestershire, UK)
- Samples were centrifuged with Z300 Hemle Labortechnik (Wehingen, Switzerland) and on a Sigma 1-14 Laborzentrifugen from Sigma Aldrich (Saint Louis, MO, USA).
- Samples were kept under stirring with Heating Rotating stirrers of VELP Scientifica (Usmate Velate, MB, Italy) and Vetrotecnica (Padua, Italy).
- A rotary stirrer was provided by ASAL s.r.l. Cernusco s/N (MI, Italy)
- Lyophilization of the nanoparticles was performed with Ha etossic HETO Lab Equipment freeze-dryer (Birkerod, Denmark)
- Spectrofluorimetric measurements were performed using a Jasco FP-6500 (Tokyo, Japan) apparatus.

- ^{1}H NMR spectra were recorded on a Bruker Spectrospin AMX 300 MHz and Bruker DPX400 Ultrashield (Fallanden, Switzerland). All NMR data were processed using MestreNova 6.2.1 software.
- Transmission Electron Microscopy images were collected on a Tecnai G2 microscope instrument (FEI, Hillsboro, USA).
- Measurements at the Circular Dichroism were carried out on a J-810 Jasco spectropolarimeter (Tokyo, Japan).
- Flow cytometric analysis was performed using BD FACScanto II, Biosciences (San Jose, Canada).
- Confocal microscopy images were recorded on a Leica TCS SP5 confocal laser-scanning microscope (Leica microsystems, Mannheim, Germany), on spinning disc confocal 3I Marianas (Intelligent Imaging Innovation, Göttingen, Germany) or Zeiss LSM 800 (Jena, Germany).

6.2.1. Analytical methods

6.2.1.1. Exenatide concentration assessment by RP-HPLC

To assess the precise EXEN concentration, a stock solution was prepared in Milli-Q water and the concentration was assessed by UV-Vis spectrophotometry at 280 nm ($\varepsilon_{M280}(H_2O)$ = 5500 L· mol^{-1}·cm^{-1}). The stock solution was then used to generate dilutions in the 5-80 µg/mL concentration range in 40% (v/v) ACN/milli-Q water. The diluted samples were analyzed by RP-HPLC using a Jasco system (Easton, MD, USA) equipped with a C18 (2) Luna 5 µm, 100 Å (250x4.60 mm) column from Phenomenex (Torrance, CA, USA) was eluted with water added of 0.05 % TFA (eluent A) and acetonitrile (MeCN) added of 0.05 % TFA (eluent B) in a gradient mode.

The gradient profile was the following:

- 0-3 minutes with the acetonitrile/water ratio (v/v) of 30%
- 3-18 minutes with the acetonitrile/water ratio (v/v) increasing from 30% to 90%
- 18-21 minutes with the acetonitrile/water ratio (v/v) of 90%
- 21-24 minutes with the acetonitrile/water ratio (v/v) decreasing from 90% to 30%

Eluents for the mobile phase were prepared and degassed by sonicating for 30 minutes before use. UV-detector was set at 220 nm and exenatide concentration was correlated to the AUC of each dilution to obtain the calibration curve shown in *Figure 6.1*.

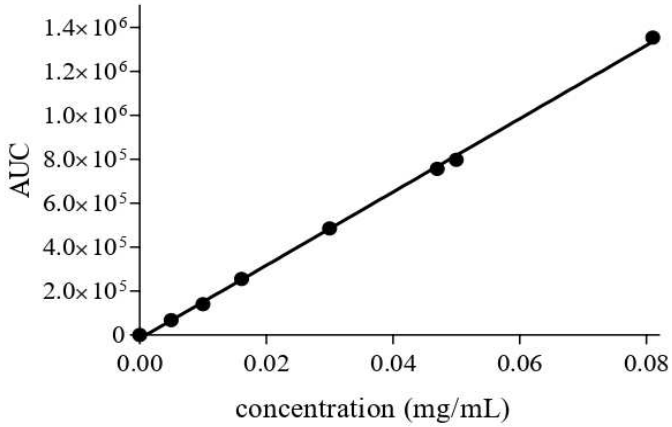

Figure 6.1. *RP-HPLC calibration line of EXEN was obtained by analyzing EXEN solutions at different known concentrations. The equation of the calibration line obtained was: y = 16.705.211,621x - 15.401,030 (R^2 = 0,999).*

6.2.1.2. Phospholipid assessment by Stewart Assay

The hydrogenated soybean phosphatidyl choline (HSPC) of SLNs formulation was quantified by Stewart assay as reported in the literature[357]. 0.1 M (27 g/L) ferric chloride ($FeCl_3 \cdot 6H_2O$) and 0.4 M (30 g/L) ammonium thiocyanate (NH_4SCN) were used to prepare the Stewart reagent. The solution is stable and was stored at room temperature. 50 µL of SLN suspension were mixed with 1950 µL of chloroform ($CHCl_3$) to disaggregate the particles and dissolve the lipidic components. Then, 2 mL of Stewart reagent was added. Samples were vortexed for 30 seconds and, after organic/water phase separation, were centrifuged for 10 min at 1,000 rpm. The complex between the negative phosphate groups of HSPC molecules and the Stewart reagent was detected by analyzing spectrophotometrically the organic phase at 485 nm.

The absorbance of the chloroform phase is linearly correlated to HSPC concentration in samples. DOTAP was found to interfere with this correlation, thus, different calibration lines were prepared following the DOTAP/lipids weight ratio in the lipid mixture used to formulate SLNs. Briefly, HSPC and cholesterol were dissolved in ethanol, and DOTAP was added at an increasing weight ratio. The DOTAP/lipids weight ratios in the mixture was 0%, 1.7%, 5%, 10%, 15%, 20%. A concentration range of 0-0.05 mg/mL of the lipid mixtures was used for all the calibration lines.

The calibration lines were used to assess the lipid recovery after SLN assembly and processing. HSPC concentrations in SLNs formulations were assessed using the calibration lines obtained by the Stweart assay that account for DOTAP/lipids weight ratio and total lipid recovery was derived considering the HSPC/cholesterol molar ratio used to prepare SLNs (*Equation 6.1*).

Equation 6.1:

$$Lipid\ recovery\ \% = \frac{HSPC/Chol\ assesed\ (mg/mL)}{HSPC/Chol\ fed\ (mg/mL)} * 100$$

6.2.1.3. Validation of the ethanol removal from the SLNs suspension

The ethanol removal process by the dialysis method was validated and the minimum time required for the dialysis was identified using SLNs formulations prepared as described in section 6.2.3.4 dialyzed in 500-1000 Da Spectra/Por® Float-a-Lyzer versus 2 L of 1 mM HEPES buffer pH 8 at room temperature. 100 µL of the SLNs aliquots were withdrawn from the Float-a-Lyzer at scheduled time points and added of 500 µL of a 12 mg/mL of 2,5-Dyhydroxybenzoic acid (internal standard) in deuterated water. The internal standard alone in deuterated water and the samples added of the internal standard were analyzed by ^{1}H NMR and the signal area of EtOH (1.17 ppm) was assessed with respect to the signal area of the internal standard (dd, 1H, 6.82 ppm; dd, 1H, 7 ppm; dd, 1H, 7.19 ppm).

6.2.1.4. Validation of the non-loaded EXEN removal from the SLNs

The method to remove non-loaded EXEN from SLN was validated and the time required for the complete removal of the non-loaded EXEN was identified. To this aim, firstly, Float-A-Lyzers were conditioned in 1 mM HEPES at pH 8. A stock EXEN solution was diluted to the final concentrations of 0.44 mg/mL, 0.88 mg/mL, and 1.31 mg/mL with 1 mM HEPES buffer pH 8, which corresponds to the concentration of EXEN in the freshly prepared SLN when produced using 5, 10 and 15% (w/w) EXEN with respect of total lipids. These solutions were transferred each into a 50-100 kDa Spectra/Por® Float-A-Lyzer and dialyzed versus 2 L of 1 mM HEPES buffer pH 8. At scheduled time points, 20 µL aliquots were withdrawn from the Float-A-Lyzers, diluted ten times in Milli-Q water, and then analyzed by RP-HPLC according to the procedure reported in section *6.2.1.1.*

6.2.2. Interaction between DOTAP and EXEN

6.2.2.1. ITC Analysis

ITC analysis was performed to investigate the electrostatic interaction between EXEN and cationic lipid DOTAP. Liposomes were used as a model that provide an ordered exposure of the quaternary ammonium group of DOTAP on their surface thus allowing to assess the energy involved in the

interaction with the negatively charged EXEN. Two conditions of pH were selected to perform the analysis: pH 8, where the EXEN is negatively charged, to demonstrate the electrostatic interaction that occurs between EXEN and DOTAP; and pH 3.5, where EXEN is positively charged, which was used as a negative control. Liposomes without DOTAP were also used as a control, to identify if non-specific interactions occur between EXEN and the surface of neutral liposomes under the same pH conditions. The study was performed according to 3 steps: liposome preparation, dialysis, and ITC analysis.

Liposome preparation

Liposomes with and without DOTAP were produced by the thin-layer hydration method. Liposomes with 10% DOTAP (w/w) were prepared by mixing 4.71 µmol of HSPC and 2.35 µmol of cholesterol in chloroform and 0.72 µmol of DOTAP in ethanol in a 10 mL round bottom flask. Control DOTAP-free liposomes were prepared by mixing in a 10 mL round bottom flask 5.23 µmol of HSPC and 2.62 µmol of cholesterol dissolved in chloroform. Organic solvents were removed from each round bottom flask at 40 °C using a rotatory evaporator. The resulting thin lipid films were hydrated with 1 mL Milli-Q water. The liposomes were extruded 11 times through a 200 nm polycarbonate membrane to achieve a homogenous dispersion. Size, PDI, and zeta potential were assessed by dynamic light scattering using Zetasizer UltraZS from Malvern Instrument LTD (Malvern, UK). The final concentration of lipids was assessed by the Stewart assay.

Dialysis

In order to have liposomes dispersion and EXEN solution in the same medium, dialysis of liposomes and EXEN was separately performed in two different pH conditions: pH 8, where EXEN has a net charge of -2, and pH 3.5, where EXEN has a net charge of +3 (Figure 4.4, Panel B). Under both pH conditions, liposome surface charge is insensitive to pH since DOTAP has a quaternary ammonium group that is positively charged in all pH scale ranges. To this aim, DOTAP-free liposomes and liposomes containing 10% (w/w) DOTAP with respect to total lipids were first diluted to 1 mM with 1 mM HEPES pH 8 or with 1 mM citrate buffer pH 3.5. EXEN stock solution was diluted to 1 µM with 1 mM HEPES pH 8 or with 1 mM citrate pH 3.5.

Then the 10% (w/w) DOTAP-liposome dispersions at pH 3.5 were transferred in 50-100 kDa Float-A-Lyzer, while exenatide solution at pH 3.5 was transferred in 500-1,000 Da Float-A-Lyzer and they were dialyzed versus 1 liter of 1 mM citrate pH 3.5 for 8 hours.

Liposomes with and without 10% (w/w) DOTAP at pH 8 were transferred in 50-100 kDa Float-A-Lyzer, while exenatide solution at pH 8 was transferred in 500-1000 Da Float-A-Lyzer and both were dialyzed versus 1 liter of 1 mM HEPES pH 8 for 8 hours.

Before and after the dialysis, the size, PDI, and zeta potential of liposomes were measured by DLS and EXEN concentration was assessed by analyzing 30 µL of exenatide solution by RP-HPLC using the procedure described in section *6.2.1.1*.

ITC analysis.

ITC measurements were performed using a MicroCal VP-ITC instrument. Before loading, the samples were degassed at reduced pressure to avoid bubbles, which can disturb the analysis. The reference cell was filled with previously degassed 1 mM citrate buffer at pH 3.5. The background of the microcalorimetric analysis was recorded by injecting aliquots of 1 mM DOTAP-free liposome or 1 mM 10% (w/w) DOTAP-liposome at pH 3.5 in the calorimetry cell (V_{cell}=1.42 mL) filled with the dialysis buffer (1 mM citrate at pH 3.5). Then the titrations of 1 µM EXEN at pH 3.5 in the calorimetry cell were performed by injecting 1 mM DOTAP-free liposomes or 1 mM 10% (w/w) DOTAP-liposomes at pH 3.5 acetate buffer. The same procedure was applied for the titration in 1 mM HEPES pH 8.

Each titration run consisted of 20 injections of 10 µL each, every 5 minutes at 25 °C, and a stirring speed of 394 rpm. The first 2 µL injection was discarded from the analysis because it is prone to artifacts. Data were analyzed with the software Origin 7.

6.2.2.2. Exenatide adsorption on SLNs surface

In order to investigate the EXEN electrostatic interaction with DOTAP, the adsorption of the peptide to DOTAP containing EXEN-free SLN was investigated by looking at their size increase when combined with EXEN. To this aim, EXEN-free SLN containing 10% (w/w) DOTAP was formulated. 1:3 HSPC/cholesterol molar ratio was dissolved in ethanol to a final 31.50 mg/mL concentration. DOTAP was firstly dissolved in ethanol at the concentration of 20 mg/mL and then diluted in Milli-Q water at the final concentration of 1.17 mg/mL. 4 mL of the aqueous DOTAP phase was processed with 1.5 mL of the ethanolic lipid solution using the NanoAssemblr® Benchtop system. 4.5 mL of 8.75 mg/mL EXEN-free 10% (w/w) DOTAP-SLNs were formulated using TFR: 12 mL/min and FRR of 3:1.

SLNs dispersion was dialyzed using 50-100 kDa Float-A-Lyzer versus 2 L of Milli-Q water for 8 hours to remove ethanol. Then, 2 mL of SLNs suspension was dialyzed overnight using 50-100 kDa Float-a-Lyzer against 1 L of 1 mM citrate pH 3.5 or 1 mM HEPES pH 8 to set the pH of SLNs dispersion. Lipid recovery was assessed by Stewart assay using the calibration line generated with 10% (w/w) of DOTAP with respect to total lipid.

Meanwhile, 1.2 mL of 0.44 mg/mL EXEN solution was set to pH 3.5 with 0.1 M HCl or to pH 8 with 0.1 M NaOH under gentle stirring. 600 µL of SLNs at pH 8 or 600 µL of SLNs pH 3.5 were mixed in glass

vials with 600 µL of exenatide solution at pH 8 or pH 3.5, respectively. The size, PDI, and zeta potential of SLNs were measured by DLS before mixing and after 2 hours of incubation.

6.2.3. Formulation of the SLNs

Lipids with high transition temperatures, namely HSPC and cholesterol, were employed in this project to generate solid lipid nanoparticles. These lipids can generate a solid nanosized matrix at room and body temperature, yet show high solubility in ethanol at room temperature, allowing the dissolution in this organic solvent and be processed at room temperature to minimize the impact on the stability of the EXEN. Different formulation parameters have been investigated to maximize loading and optimize the colloidal features (size, polydispersity, zeta potential).

6.2.3.1. Selection of the lipid mixture concentration

The most suitable lipid mixture concentration in ethanol for the microfluidic process to generate SLNs with small size and low polydispersity was identified by preparing a small library of formulations at increasing lipid concentrations of the ethanolic solution: i. 11.9 mg of HSPC (15.61 µmol) and 18.1 mg (46.83 µmol) of cholesterol were dissolved in 1 mL of EtOH resulting in 30 mg/mL lipid at 1:3 HSPC/cholesterol molar ratio; ii. i 13.9 mg of HSPC (18.2 µmol) and 21.1 mg (54.6 µmol) of cholesterol were dissolved in 1 mL of EtOH resulting in 35 mg/mL lipid at 1:3 HSPC/cholesterol molar ratio; iii. to generate a lipid mixture at 40 mg/mL, 15.86 mg of HSPC (20.81 µmol) and 24.11 mg (62.43 µmol) of cholesterol were dissolved in 1 mL of EtOH resulting in 1:3 HSPC/cholesterol molar ratio. A higher concentration of HSPC/Cholesterol than 40 mg/mL could not be considered because of the solubility limit.

Before processing the lipids to prepare EXEN-free SLNs with NanoAssemblr® Benchtop, the two channels of the cartridge were conditioned by running 1 mM HEPES buffer at pH 8 and EtOH in each of the inlets. The system parameters used for the conditioning and for cleaning after the formulations were the following: Total Volume (TV) = 1.2 mL, Flow Rate Ratio (FRR) = 5:1, Total Flow Rate (TFR) = 4 mL/min, and auto-switch off. This procedure was performed before every SLN production process.

After initial conditioning, the right syringe was filled with 200 µL of the lipid mixture solution in EtOH, and the left syringe with 1 mL of 1 mM HEPES buffer at pH 8. The two syringes were set in the proper slots of the instrument. The heating block was set at 25 °C, and SLNs were produced at total volume (TV)= 1.2 mL, FRR= 5:1, TFR= 4 mL/min, start waste= 150 µL, and end waste 50 µL.

SLN suspension was placed into 500-1000 Da Spectra/Por® Float-A-Lyzer and dialyzed against 2 L of 1 mM HEPES buffer (pH 8) for 8 hours for ethanol removal. SLNs then were characterized in terms of size and polydispersity index by DLS. Lipid recovery after dialysis was calculated by Stewart Assay. The morphology of the SLNs was imaged with transmission electron microscopy (TEM).

6.2.3.2. Selection of the microfluidics process parameters

Preliminary studies were undertaken to assess the effect of the process parameters, namely total flow rate (TFR) and flow rate ratio (FRR) on SLNs' size, polydispersity, zeta potential, and loading efficiency and select the ones that are more suitable for in vivo applications. The effect of the aqueous to organic phase ratio was investigated employing FRRs 5:1 and 3:1. For both FRRs tested, formulations were generated at different total flow rates, namely, 3, 6, 9, and 12 mL/min. EXEN and DOTAP were also included in the formulation for the investigation of the effect of the process parameters on the loading efficiency of the SLNs. A 5% (w/w) EXEN/total lipid feed ratio and 6:1 (mol/mol) DOTAP/EXEN ratio was employed for this preliminary investigation. SLNs were produced at total volume (TV)= 1.2 mL.

Formulations with FRR 5:1 were prepared by loading one syringe with 200 μL of lipid mixture (1:3 HSPC: Cholesterolmol/mol ratio, 35 mg/mL) in EtOH, while the second syringe was filled with 1 mL of 6:1 DOTAP:EXEN mol/mol ratio in 1 mM HEPES (pH=8); formulations with FRR=3:1 were prepared by loading one syringe with 300 μL of the lipid mixture (1:3 HSPC:Cholesterol mol/mol ratio, 35 mg/mL) in EtOH and the second syringe with 0.9 mL of 6:1 DOTAP/EXEN mol/mol ratio solution in 1 mM HEPES (pH=8).

After processing the two solutions, SLN suspensions were collected and dialyzed for 22 hours using 50 KDa Spectra/Por® Float-a-Lyzer versus 2 L of 1 mM HEPES (pH 8) to remove EtOH and non-loaded EXEN. After the dialysis, SLNs were characterized in terms of particle size, polydispersity index, and zeta potential by DLS. The concentration of the SLNs was assessed by the Stewart assay and loading efficiency was quantified by RP-HPLC.

6.2.3.3. Effect of buffer concentration and DOTAP/EXEN molar ratio on SLNs' features

Three sets of SLN were generated by processing DOTAP/EXEN mixture dissolved either in Milli-Q water or 1 or 10 mM HEPES at pH 8 to study the possible effect of buffer concentration on colloidal features, loading efficacy, and capacity of SLN formulations. Each set was prepared by processing a 5% (w/w) EXEN/total lipid feed ratio and five different DOTAP/EXEN molar ratios, namely 0:1, 2:1, 6:1, 12:1, and 18:1. The total lipid concentration in the ethanolic solution was kept constant among all formulations; thus, when the DOTAP/EXEN ratio increased, HSPC and cholesterol amounts were decreased by the same weight ratio.

The aqueous phase was prepared by diluting 2 mg/mL EXEN stock solution with Milli-Q water, or 1 mM or 10 mM HEPES buffers. The pH of the exenatide solution in Milli-Q water was adjusted to 8 by using 0.1 M NaOH.

DOTAP solutions in ethanol (20 mg/mL) were added to each EXEN solutions to achieve 0.19 mg/mL, or 0.58 mg/mL or 1.17 mg/mL or 1.75 mg/mL DOTAP concentration providing 2:1, 6:1, 12:1 and 18:1 DOTAP/EXEN molar ratio. Solutions were gently stirred for 30 seconds.

The aqueous phase containing DOTAP/EXEN mixtures was then processed with the ethanolic 1:3 HSPC/cholesterol mol/mol ratio solution at 35, 34.81, 34.42, 33.83, and 33.25 mg/mL using the NanoAssemblr® Benchtop system to generate the SLNs at 0:1, 2:1, 6:1, 12:1 and 18:1 DOTAP/EXEN ratios, respectively. EXEN-loaded SLNs were formulated at total volume (TV)= 1.2 mL, FRR=3:1 and TFR=12 mL/min. The final EXEN concentration in the just processed formulations resulted to be 0.44 mg/mL, and the total lipid mixture (including DOTAP) was 8.75 mg/mL. The samples were dialyzed as reported in sections 6.2.1.3. and 6.2.1.4. to remove ethanol and non-loaded exenatide, respectively. After the dialysis, SLN formulations were stored at 4 °C[30]. Particles were then analyzed by DLS to derive size, polydispersity index, and zeta potential. Lipid recovery was measured by Stewart assay, and loading efficiency was assessed by RP-HPLC.

6.2.3.4. Selection of the EXEN/total lipid feed and DOTAP/EXEN ratios

The effect of the EXEN/total lipid feed weight ratio and the DOTAP/EXEN feed molar ratios on the loading of SLN was investigated by generating formulations with increasing EXEN/total lipid feed ratios of 5, 10, and 15 % (w/w) and increasing DOTAP/EXEN feed molar ratios, namely, 0:1, 2:1, 6:1, 12:1, and 18:1 for all three EXEN/lipid feed weight ratios.

- SLN formulations with 5% EXEN feed w/w ratio were prepared by diluting a 2 mg/mL EXEN stock solution in 1 mM HEPES buffer at pH 8 to the final concentration of 0.58 mg/mL then a volume of 20 mg/mL DOTAP in EtOH was added to yield 0.19 mg/mL, or 0.58 mg/mL or 1.17 mg/mL or 1.75 mg/mL under gentle stirring for 30 seconds resulting in samples at 2:1, 6:1, 12:1 and 18:1 DOTAP/ EXEN molar ratios.

- SLN formulations with 10% EXEN feed w/w ratio were prepared by diluting 2 mg/mL EXEN stock solution to the final concentration of 1.17 mg/mL in 1 mM HEPES buffer at pH 8, then 20 mg/mL DOTAP in EtOH was added to yield 0.39 mg/mL, or 1.17 mg/mL, or 2.34 mg/mL or 3.50 mg/mL under gentle stirring for 30 seconds resulting in samples at 2:1, 6:1, 12:1 and 18:1 DOTAP/EXEN molar ratios.

- SLNs formulated with 15% (w/w) EXEN feed ratio were prepared by diluting 2 mg/mL EXEN stock solution to the final concentration of 1.75 mg/mL in 1 mM HEPES at pH 8, then 20 mg/mL DOTAP in EtOH was added to yield 0.58 mg/mL, or 1.75 mg/mL, or 3.50 mg/mL or 5.26 mg/mL under gentle stirring for 30 seconds resulting in samples at 2:1, 6:1, 12:1 and 18:1 DOTAP/ EXEN molar ratios.

The aqueous DOTAP/EXEN mixtures were mixed with the ethanolic lipid solution composed of a 1:3 HSPC/cholesterol molar ratio using the NanoAssemblr® Benchtop system. The microfluidic system was run at TV= 1.2 mL, FRR=3:1 and TFR=12 mL/min to generate formulations at 0.44 mg/mL, 0.88 mg/mL and 1.31 mg/mL EXEN concentration, using 5, 10 and 15% EXEN feed w/w ratio, respectively, and a final concentration of total lipid, including DOTAP, of 8.75 mg/mL.

After the formulation, dialysis was performed to remove the ethanol and non-loaded exenatide. Particles were then analyzed by DLS to derive size, polydispersity index, and zeta potential. Lipid recovery was measured by Stewart assay, and loading efficiency was assessed by RP-HPLC.

6.2.3.5. PEGylation of the SLNs

SLN formulations obtained with a 10% EXEN/total lipid feed w/w ratio and 12:1 DOTAP/EXEN molar ratio were selected for the PEGylation process. A 114 µL of 8.75 mg/mL SLN suspensions were diluted with 1 mM HEPES pH 8 to 500 µL and a final SLN concentration of 2 mg/mL. Then 20-300 µg from a 2 mg/mL DSPE-PEG_{2kDa} solution in Milli-Q water was added to the SLN samples to achieve DSPE-PEG_{2kDa}/SLN w/w ratios in the 2-30 % (w/w). SLN suspensions with DSPE-PEG_{2kDa} were briefly vortexed and incubated at 37 °C and at scheduled timepoints of 5, 10, and 15 minutes the samples were tested by DLS to derive size, polydispersity index, and zeta potential to estimate the effect of the incubation time with the PEGylating component. Zeta potential was considered as an indicator of the shielding of the cationic charges on the SLN surface. Lipid concentration was measured by the Stewart assay and the loading efficiency and capacity of the formulation were calculated by RP-HPLC.

6.2.3.6. Lyophilization of the SLNs

The lyophilization process was investigated to generate solid formulations to be transferred into gastro-protected gelatin capsules. At increasing concentrations, the lyoprotectants, namely, trehalose, mannitol, and trehalose-mannitol mixtures (4:1, 2:1, and 1:1 w/w ratios) were investigated for the lyophilization of the SLNs dispersions. Stock lyoprotectant solutions were generated at 25 w/v % in milli-Q-water. The single trehalose or mannitol solutions were added to 0.75 mL of 3.0 mg/mL SLN suspension to provide lyoprotectant concentrations in the 0.5-10% (w/v) range, while trehalose

mannitol mixtures in the weight ratios of 4:1, 2:1, and 1:1 were added to the SLN suspension at final concentrations of 1.25, 1.5 and 2 % (w/v), respectively.

The SLN suspensions added of lyoprotectant were frozen at -20°C for 2 hours, then, at -80 °C for 4 hours. Frozen samples were then transferred to the freeze-dryer and freeze-dried for 24 hours. After lyophilization, SLNs dry samples were re-suspended in 0.75 mL of Milli-Q-water, and size and zeta potential analyses were performed.

6.2.4. Characterization of the SLNs

6.2.4.1. Particle size and zeta potential measurement

The mean hydrodynamic size, the polydispersity index, and the zeta potential of the SLNs were assessed by Dynamic Light Scattering (DLS) using Zetasizer UltraZS from Malvern Instrument LTD (Malvern, UK). SLNs formulations were diluted in Milli-Q water to 0.35 mg/mL before analysis. Measurements were carried out in triplicate. The size data (nm) were recorded in intensity.

6.2.4.2. Loading efficiency and capacity assessment

Freshly prepared SLNs were dialyzed as reported in *section 6.2.1.5.* After the removal of the non-loaded exenatide, 30 µL of the SLNs formulation was withdrawn from the Float-A-Lyzer, diluted ten times with acetonitrile, and sonicated for 10 minutes to dissociate solid lipid nanoparticles and dissolve lipids. The EXEN concentration was then analyzed by RP-HPLC under the conditions described in *section 6.2.1.1*. The concentration of encapsulated exenatide was derived by integrating the eluted peak area and referring to the calibration curve in Figure 6.1. The lipid concentration was assessed by Stewart assay (*section 6.2.1.2.*).

The loading efficiency % (LE%) and loading capacity % (LC%) were calculated using the following equations.

Equation 6.2:

$$LE\% = \frac{loaded\ EXEN\ (mg)}{fed\ EXEN\ (mg)} * 100$$

Equation 6.3:

$$LC\% = \frac{loaded\ EXEN\ (mg)}{total\ lipid\ in\ SLNs\ (mg)} * 100$$

6.2.4.3. Release studies

EXEN-loaded SLNs produced with a 10% EXEN/total lipid feed w/w ratio and 12:1 DOTAP/EXEN molar ratio were employed for the release studies. A 1.5 mL of SLNs suspension at 3.5 mg/mL was transferred into the Float-A-Lyzers with a cut-off of 50-100 kDa and dialyzed versus 2 L of different buffers:

a) simulated intestinal fluid (SIF) constituted by 50 mM KH_2PO_4, pH 6.8;

b) phosphate-buffered saline (PBS) constituted by 0.137 M NaCl, 2.7 mM KCl, 10 mM Na_2HPO_4, 1.8 mM KH_2PO_4 at pH 7.4

The release was investigated over 14 days, and the release buffer was changed once per day to ensure sink conditions. At scheduled time points, 10 µL of each sample was withdrawn from the Float-A-Lyzer, diluted ten times with acetonitrile, sonicated for 10 minutes, and then analyzed by RP-HPLC according to the procedure reported in *section 6.2.1.1*.

6.2.4.4. Stability studies

EXEN-loaded SLNs produced with a 10% EXEN/total lipid feed w/w ratio and 12:1 DOTAP/EXEN molar ratio were employed for the colloidal stability studies in SIF (pH 6.8), PBS (pH 7.4), and in PBS with 10 % (v/v) FBS. To this aim, SLNs were first diluted in the buffers at a concentration of 0.35 mg/mL and incubated in a thermomixer at 37 °C under mild shaking (300 rpm). At scheduled time points, aliquots were withdrawn and the size distribution of the SLNs was analyzed by DLS.

6.2.4.5. Morphological investigation of the SLNs

Transmission electron microscopy (TEM) is an efficient technique that allows to derive information about the morphology of particles and understand the possible crystallization of drugs on the particle surface.

EXEN-free or EXEN-loaded SLNs with and without PEG were analyzed by Transmission Electron Microscopy (TEM). To this aim, SLNs have first diluted in 1 mM HEPES buffer pH 8 to 10 µg/mL SLN concentration. The suspensions were deposited on a carbon-coated copper grid. Samples were stained with 1 % w/v uranyl acetate in distilled water. TEM images were recorded using a Tecnai G2 microscope (FEI™, Hillsboro, USA).

6.2.4.6. Mucin diffusivity of the SLNs by FRAP analysis

Fluorescence recovery after photobleaching (FRAP) is a fluorescence microscopic technique that quantify the diffusion of nanoparticles in a mucin solution. In FRAP test, fluorescently labelled nanoparticles are dispersed in a mucin solution, that is then irradiated by laser to bleach a restricted area and the fluorescence recovery is measured over time and correlated to diffusivity of the particles.[358]. Within this project, FRAP analysis was used to study the diffusivity of the EXEN-loaded SLNs through mucin to gain insight into the mobility SLNs in the gastroinsteinal mucus.

With this aim, EXEN-loaded SLNs were produced with a 10% EXEN/total lipid feed w/w ratio and 12:1 DOTAP/EXEN molar ratio, and labeled with 0.3% (mol/mol) Fluorescein-DHPE with respect to total lipids. Particles without DSPE-PEG_{2kDa} coating and particles decorated with 10 an 30% w/w DSPE-PEG_{2kDa} were prepared as explained in section 6.2.3.5.

Mucin solution at 10% w/w was prepared by adding 500 mg of dry mucin from porcine stomach (type II) into 5 mL of SIF and overnight mixing in the rotational shaker (ASAL SRL, Model 708, Italy).

Then, 800 µL of Fluorescein-labeled SLNs (with 0, 10, and 30% w/w DSPE-PEG_{2kDa} coating) at 2 mg/mL concentration were mixed with 200 µL of 10% (w/w) freshly prepared mucin solution resulting in a 2% mucin concentration. As a control, 200 µL of 10% w/w mucin solution was mixed with 800 µL of 1 mM HEPES at pH 8 without SLNS. The mixtures were then placed on ice and mildly shaken (200 rpm) for 2 hours to disperse the particles homogeneously[359]. 500 µL of the mixtures were then placed into a glass bottom 4-well cell culture chamber (Sarstedt, Germany) and sealed with the lid. After 15 minutes of equilibration, FRAP analysis was performed employing a Zeiss LSM800 confocal microscope (Carl Zeiss, Jena, Germany) equipped with a 40x objective.

A rectangular shaped (60×60 µm) region of interest (ROI) for each condition was chosen and scanned for 30 seconds at low laser intensity (1%) to obtain reference images before the bleaching process was started and subsequently bleached for 90 seconds with the 488 nm line of a solid state laser with a laser intensity of 100%. The post-bleaching fluorescence recovery was measured for 600 seconds at 30 frames per minute with a laser transmission set at 1%. The scans were recorded every 2 seconds to prevent bleaching. Recorded data were normalized and analyzed in FIJI/ImageJ software. The fluorescence intensity before and after bleaching was defined as one and zero, respectively[360], and the intensities ratios were calculated by diving each intensity value by the difference between pre- and post-bleaching intensity values (Plugins>Stowers>Create Spectrum jru v1>Normalize Trajectories jru v1 min-max). Data were further normalized by subtracting the fluorescence recovery of the control (mucin solutions, No particles) from the fluorescence recovery of the SLN containing -mucin solutions.

Statistical analysis was performed using a two-way ANOVA (GraphPad Software): *p< 0.05, **p < 0.01, ***p < 0.001.

6.2.5. Stability of exenatide

6.2.5.1. Conformational stability

Circular dichroism (CD) is a spectroscopic analysis based on the differential absorption of left-handed and right-handed circularly polarized light. The phenomenon is due to the structural asymmetry of macromolecules absorbing light which can be related to specific structural chirality or an asymmetric environment. The CD spectrum registered in the near-UV region (250-350 nm) provides information about the chirality around aromatic amino acids and disulfide bonds, while the far-UV region (<250 nm) is dominated by the absorption of peptide bonds characterized by two electronic transitions: an n→π* with a weak absorption at 220 nm and stronger absorption at 190 nm of the π→π* transition. Different secondary structure conformations have characteristic CD spectra profiles due to different absorption of the amides of the polypeptide backbone.

Within this project, CD analyses have been performed to investigate the conformational stability of the EXEN along with the SLN production, and freeze-drying processes,

With this aim, the effect of the microfluidics process was first assessed: EXEN in milli-Q-water at a concentration of 1.5 mg/mL (0.9 mL) was injected into the left inlet of the microfluidic cartridge and processed with ethanol under the same conditions used for SLN production process (FRR: 3:1, TFR: 12 mL/min TV: 1.2 mL) resulting in a final mixture of 25% of ethanol/water (v/v). To remove the organic solvent, the EXEN solution was dialyzed for 8 h against 2 L of Milli-Q water using a Spectra/Por® Float-A-Lyzer® with an MWCO 500-1,000 Da.

The effect of the SLN production process and lyophilization processes on the conformational stability of EXEN, the SLNs formulations (at 3 mg/mL concentration) after production, and those after lyophilization and redispersion were left under rotational shaking (ASAL SRL, Model 708, Italy) for 2 days at room temperature and then transferred in 50 kDa MWCO Amicon® Ultra-15 centrifugal filter units and centrifuged at 2,000 x g for 1 hour at 4 °C. The released EXEN from SLNs was collected at the bottom of the centrifugal filter. The concentration of the exenatide solutions was assessed using RP-HPLC and diluted in MilliQ water to 0.1 mg/ml before CD analysis.

CD analyses of the exenatide solutions were performed using a Jasco J-810 spectropolarimeter (Tokyo, Japan) in the far UV (195-260 nm) at 25 °C with a 0.1 cm cell path-length quartz cuvette. The

measurements were performed in triplicate and the data were reported as mean residue ellipticity [θ] mrw (deg cm dmol-1), using the equation:

Equation 6.4:

$$[\theta]\mathrm{mrw} = \frac{\theta\mathrm{obs} * \mathrm{MRW}}{10 \times \mathrm{c} \times \mathrm{l}}$$

where θ_{obs} is the observed ellipticity in degree, MRW is the Mean Residue Weight (calculated according to the equation MRW= M/(N-1); M is the molecular mass of the polypeptide in Da, N is the number of amino acids in the EXEN sequence, c is the concentration of EXEN in mg/mL and l is the cell path-length in cm.

6.2.5.2. Chemical stability

Chemical degradation of the peptides includes many pathways such as deamidation, isomerization, oxidation, hydrolysis, and disulfide bond break or formation and may result in the change of conformation and biological activity[361]. Since it is well known that instabilities may occur at any stage of the peptide processing including purification and formulation, and storage, within this study, the chemical stability of the EXEN was analyzed by electrospray ionization-time of flight mass spectrometry (ESI-TOF MS)[362]. Using the Applied Biosystem Mariner ESI-TOF mass spectrometer (Monza-Italy), the analysis was run with 50:50 (v/v) water/acetonitrile with 1% (v/v) formic acid. Native and processed EXEN solutions were prepared as in section 6.2.6.1., briefly the SLNs formulations after production and those after lyophilization and redispersion were left under rotational shaking that was followed by the centrifuge for the collection of the released EXEN.

6.2.6. Preparation of the enteric-coated capsules

SLNs were produced to develop an oral dosage form. To this aim, therefore, EXEN-loaded SLNs were planned to encapsulate into hard gelatine capsules and enteric-coated to protect the EXEN from the acidic environment of the stomach.

The enteric coating of the hard gelatin capsules was performed using Eudragit L100 polymer. The coating solution was prepared as reported in the literature[363] with a slight modification. Briefly, 12.5% (w/v) solutions of the Eudragit L100 in acetone/water mixture (97:3 v/v) were prepared. 2.5% (w/v) polyethylene glycol 400 was added to these solutions as a plasticizer.

The coating of the capsule was validated. To this aim gelatine capsules filled with 200 mg of rhodamine B/starch mixture (1:1000 w/w) were coated by dipping three times at 3 hours time intervals, which was followed by drying overnight at room temperature (Figure 6.4). Gelatine capsules filled with 200 grams of rhodamine B/starch mixture (1:1000 w/w) without coating are employed as the negative control.

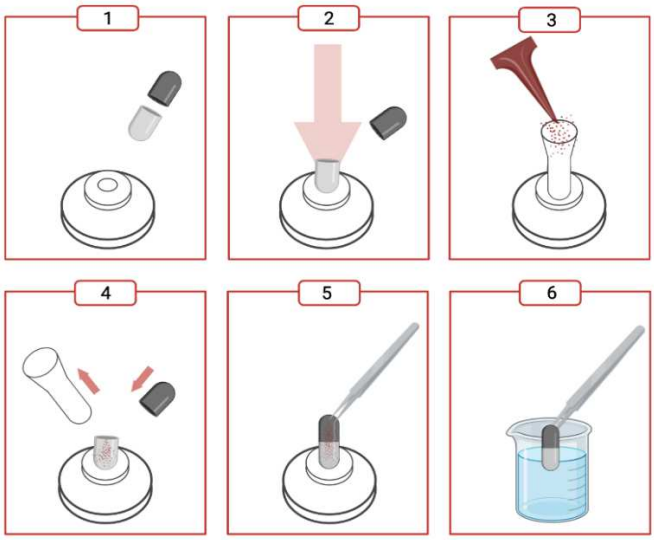

***Figure 6.4**. Schematic representation of the encapsulation of the rhodamine B/starch mixture into hard gelatine capsules and enteric coating processes.*

The enteric protective efficacy of Eudragit L100 was tested in simulated media. The Eudragit L100 coated and not coated capsules were immersed in 50 mL of 0.2 M HCl pH 1.2 as dissolution medium and placed in an incubator at 37 ± 2 °C, under mild shaking (300 rpm). After 2 hours the medium was replaced with simulating intestinal fluid (50 mM KH_2PO_4, pH 6.8) and kept in the shaking incubator for 2 hours at 37 ± 2 °C. At scheduled time points (0.5, 1, 2, 2.5, 3, and 4 hours), 500 µL of dissolution medium was withdrawn an equal amount of pre-heated medium was added to the dissolution medium. The concentration of the released rhodamine B was measured by spectrofluorometric analysis with an excitation wavelength of 546 nm and an emission of 580 nm. The concentration of rhodamine B was derived from the calibration curve obtained by serial dilutions of a Rhodamine stock solution (10 µM) in milli-Q water ($y=32.540x-8.053$, $R^2=0.997$). The released Rhodamine was reported as a percentage with respect to the fed Rodamine in the capsules.

6.2.7. In vitro cellular studies

6.2.7.1. Cytotoxicity studies

Biocompatibility studies of EXEN-loaded SLN were carried out on immortalized human intestinal epithelium Caco-2 cell line using a protocol reported in Figure 6.5. The Caco-2 cells were grown in DMEM supplemented with 10 % (v/v) FBS, 1% (v/v) L-Glutamine, 1% (v/v) penicillin/streptomycin at 37 °C in an atmosphere of 5 % CO_2 (v/v). The medium was replaced every other day and passaged every 2-3 days when they reached ~80 % confluency.

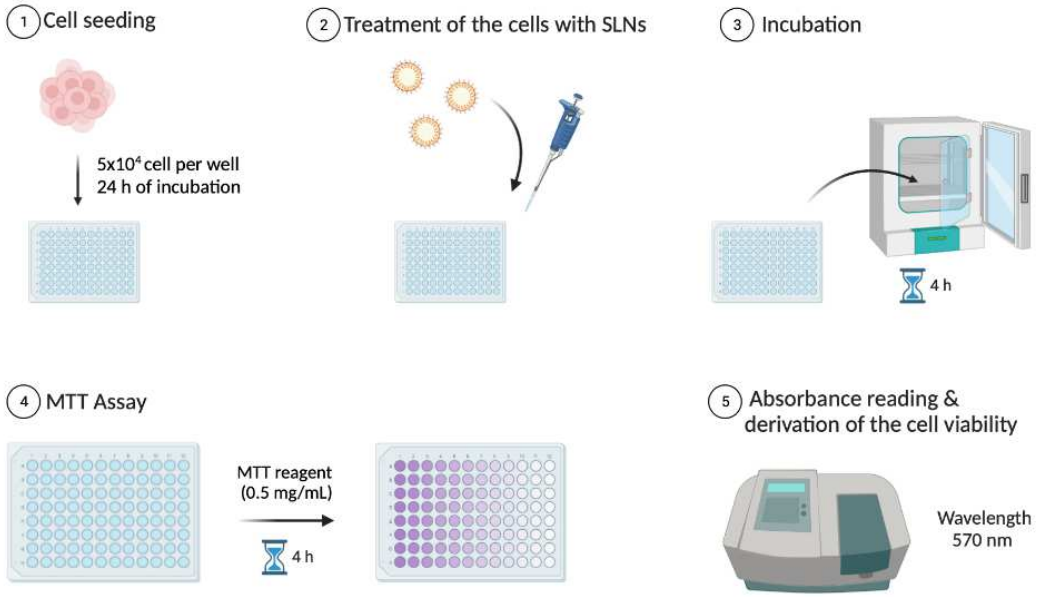

Figure 6.5. *Schematic representation of the in-vitro cytotoxicity assay performed by incubating Caco-2 cells with EXEN-loaded SLN.*

Caco-2 cells were seeded in a 96-well plate at the density of $5x10^4$ cells/well in 200 µL/well of complete medium. After 24 hours of incubation at 37 °C and 5% of CO_2, the medium was discharged and cells were treated with 200 µL of EXEN-loaded SLN suspension (decorated with 0, 10, and 30 % w/w DSPE-PEG_{2kDa}) in DMEM without FBS at an EXEN equivalent concentration of 1, 2, 4, 6, 8 and 10 µg/mL[364]. Untreated cells were incubated with 200 µL of DMEM without FBS, and used as the negative control, while cells treated with 0.1% (v/v) Triton X-100 were used as the positive control of cytotoxicity.

After 4 hours of incubation[365], treatments were removed, and cells were washed with PBS 3 times before adding 200 µL of 0.5 mg/mL MTT solution in 1:9 PBS/DMEM (v/v). Cells were incubated for four hours at 37 °C to allow the formation of the formazan salts. Then the medium was discharged and replaced with 200 µL/well of DMSO. Finally, the plate was mildly shaken for 10 minutes to allow

the dissolution of formazan crystals, and the spectrophotometric absorbance was read using the plate reader at a wavelength of 570 nm. The absorbance values were used to calculate the cell viability as a percentage using the following equation:

Equation 6.6:

$$Cell\ Viability\ (\%) = \frac{Absorbance\ of\ test\ sample - Absorbance\ of\ positive\ control}{Absorbance\ of\ negative\ control - Absorbance\ of\ positive\ control}\ x\ 100$$

6.2.7.2. Cellular association studies

Association of SLN to cells by flow cytometry analysis

The cellular association of the SLNs was investigated with flow cytometric analysis as shown in Figure 6.6. To this aim, Caco-2 cells were seeded in a 48-well plate at the density of 10^5 cells/well in 400 µL/well[366] of complete medium. After 24 hours of incubation at 37°C and 5% of CO_2, the medium was discharged and cells were treated with 500 µL of EXEN-loaded fluorescein-DHPE labeled SLNs (decorated with 0, 10, and 30 % w/w DSPE-PEG_{2kDa}) suspension in DMEM without FBS at EXEN concentrations of 6, 8 and 10 µg/mL.

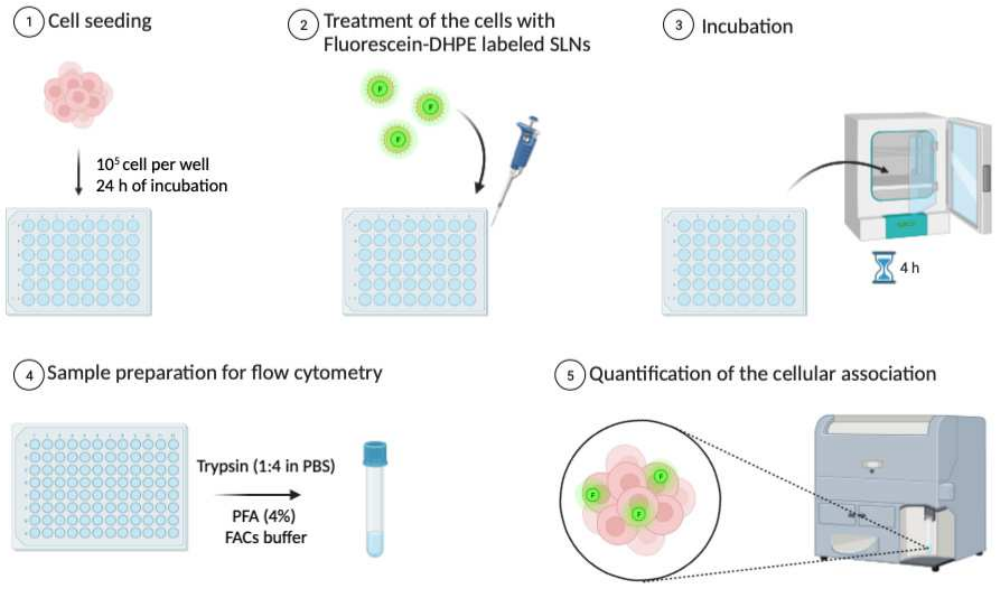

Figure 6.6. *Schematic representation of the flow cytometric analysis of Caco-2 cells incubated with EXEN-loaded SLN.*

After 4 hours of incubation, the medium was removed and the cells were washed three times with PBS to remove plastic-bound SLNs; finally, cells were detached by treatment with 200 µL/well of 0.125

mg/mL trypsin solution in PBS for 4 min at 37 °C and subsequently mixed with 100 µL of 4 w/v % PFA (fixing agent) in PBS buffer and 100 µL of FACs buffer (PBS, 1% bovine serum albumin, 0.1 % sodium azide). Afterward cell suspensions were transferred in flow cytometric tubes and analyzed by a flow cytometer (BD FACScanto II, Biosciences, San Jose, Canada) to assess the cell association of SLNs. Cell samples were stored in the dark on an ice bath before analysis. The mean fluorescence intensity (MFI) of cell samples and the percentage of the positive cells were analyzed using FlowJo Software.

Visualization of the cellular association with the confocal microscopy

The visualization of SLN disposition within Caco-2 cells was investigated by confocal microscopy. Caco-2 cells were seeded in 4-well cell culture chambers with a glass bottom (Sarstedt, Germany) at a density of 10^5 cells per well and were allowed to settle overnight. The next day, after the removal of the cell culture medium, the cells were incubated with 500 µL of EXEN-loaded fluorescein-DHPE labeled SLNs suspension (decorated with 0, 10, and 30 % w/w DSPE-PEG_{2kDa}) in DMEM without FBS at EXEN concentrations of 10 µg/mL.

After 4 hours, the treatments were removed. Before imaging, cells were washed and nuclei were labeled with Hoechst 33342 (0.02 mM in PBS) and followed by the cell membrane labeling with Wheat Germ Agglutinin Alexa-Fluor 633 (WGA-AF 633) conjugate (10 µg/mL in PBS) with 15 minutes of incubations. After the removal of the WGA-AF633 treatment, cells were washed and maintained in phenol-free opti-MEM and transferred to the stage of the confocal microscope The cell samples were imaged using a Zeiss LSM 800 confocal microscope (Carl Zeiss, Jena, Germany) equipped with a 40x objective and a ZEN 2.1, blue edition software (Carl Zeiss, Jena, Germany) and an incubator to enable live-cell imaging at optimal conditions (5% CO_2 and 37 °C). The lasers with emission wavelengths at 408, 488, and 640 nm were used to detect Hoechst 33342, Fluorescein, and WGA-AF633, respectively.

7. RESULTS AND DISCUSSION

7.1. Calibration and validation of the analytical methods

7.1.1. Phospholipid assessment by Stewart Assay

Stewart assay is a colorimetric method used for the quantification of phospholipids. It exploits the ability of the phosphate group of phospholipids to form a complex with ammonium ferrothiocyanate in an organic solution. Ammonium ferric thiocyanate is insoluble in chloroform; however, the complex ferric thiocyanate/phospholipids are soluble in chloroform. When a solution of chloroform containing phospholipids is mixed with ammonium ferric thiocyanate, a colored complex is formed in the chloroform phase that can be spectrophotometrically detected.

In this project a lipid mixture containing DOTAP was used, thus, the spectrophotometric absorbance of the chloroform phase generated in the Stewart assay will increase linearly to the HSPC concentration in the sample, but DOTAP was found to increase the absorbance of the chloroform phase, which has to be taken into account when quantifying HSPC in the formulations.

To take this into account, different calibration lines were prepared with increasing ratios of DOTAP with respect to total lipids, as explained in section *6.2.1.2*. A two-way ANOVA analysis was performed to compare the absorbances at the same HSPC concentration (0.015-0.05 mg/mL) with an increasing ratio of DOTAP. Absorbance for each HSPC concentration was significantly different for each DOTAP ratio with respect to the mixture without DOTAP. Indeed, *Figure 7.1* shows that the higher the ratio of DOTAP the higher the absorbance.

As an example, the absorbance provided by the Stewart assay when testing a solution at 0.05 mg/mL of HSPC/cholesterol mixture was 67% higher in the presence of 20 w/w% DOTAP with respect to the HSPC solution devoid of DOTAP (Figure 7.1). Thus, to more precisely assess the lipid concentration in samples, the calibration line obtain with the corresponding DOTAP/lipid percentage used to prepare the SLNs was adopted.

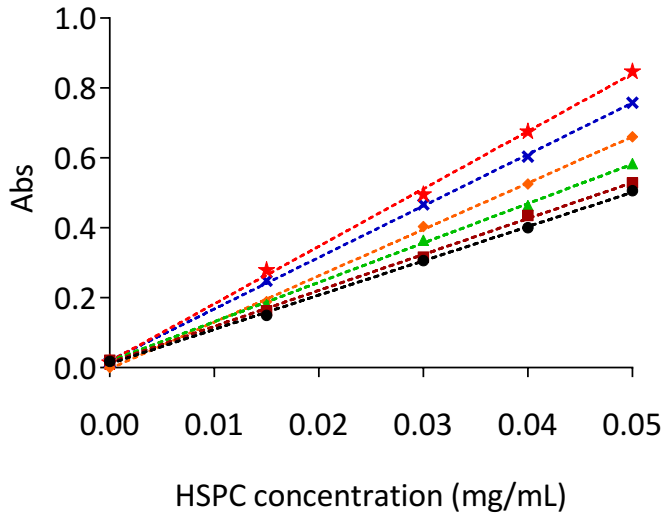

Figure 7.1. *HSPC concentration calibration line obtained by Stewart assay in chloroform at increasing weight percent of DOTAP in lipid mixture. The obtained calibration lines equations were: 0 w/w% DOTAP, y=9,801x+0.012 (R^2=0,999) (●); 1.7 w/w% DOTAP, y=10,284x+0,015 (R^2=0,999) (■); 5 w/w% DOTAP, y=11,268x+0,019 (R^2=0,999) (▲); 10 w/w% DOTAP, y=13,266x-,003 (R^2=0.999) ( ); 15 w/w % DOTAP, y=14,743x+00,020 (R^2=0,999) (x); 20% DOTAP, y=16,454x+0,018 (R^2=0,999) (★).*

7.1.2. Ethanol removal validation

The removal of the organic solvent after microfluidic preparation of SLNs is a crucial step that ensures the safety and stability of the formulation. In this study, ethanol was used as an aqueous miscible organic solvent during microfluidic mixing and it was removed by dialysis after SLN production. To validate the method of removal and identify the suitable time for dialysis, samples of freshly prepared SLNs suspension were analyzed by ^{1}H-NMR spectroscopy during dialysis.

A representative ^{1}H-NMR spectrum of suspension after 2-hour dialysis is shown in *Figure 7.2*. The signal of the methyl group of ethanol at 1.17 ppm (t, -CH_3) was integrated and related to the internal standard.

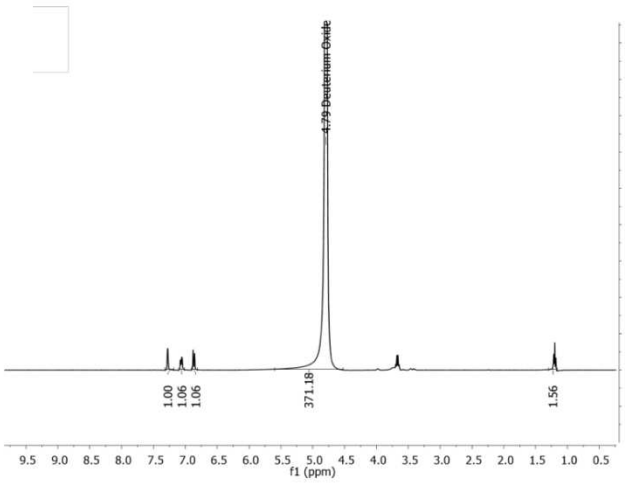

Figure 7.2. *^{1}H-NMR spectrum (400 MHz, in D_2O) of SLNs after 2 hours of dialysis.*

The percentage of residual ethanol in the sample was calculated by comparing the signal area of ethanol protons (t, -CH_3, 3H, 1.17 ppm) to the signal area of the aromatic protons of internal standard 2,5-Dihydroxybenzoic acid (dd, 1H, 6.82 ppm), (dd, 1H, 7 ppm) and (dd, 1H, 7.19 ppm). The residual percentage (v/v %) of ethanol in the formulation was plotted versus dialysis time. As reported in *Figure 7.3*, the residual percentage (v/v %) resulted to be 5.9, 2.2, 0.3, and 0.1% after 2, 4, 6, and 8 hours of dialysis, respectively.

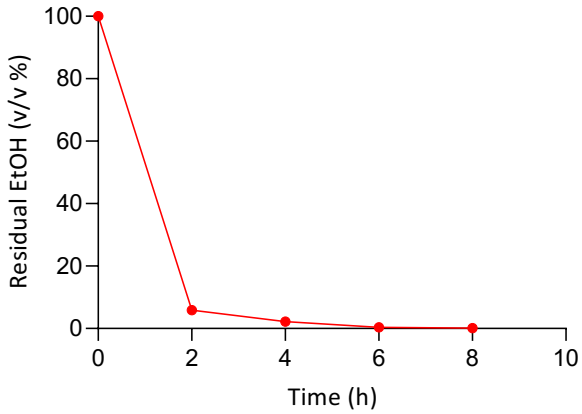

Figure 7.3. *Residual ethanol (v/v %) in SLNs formulation at different dialysis time points.*

After 8 hours of dialysis, the residual ethanol was less than 0.1% in volume; which is acceptable according to the guidelines for ethanol in pharmaceutical products for oral administration[367]. According to the result, the time selected for extensive removal of ethanol from freshly prepared SLNs was 8 hours.

7.1.3. Validation of non-loaded EXEN removal process

The EXEN loading efficiency in the SLNs was assessed by a direct quantification as described in section *6.2.4.2.* Before the quantification, dialysis is performed to remove the non-loaded EXEN from SLNs suspension. The method was validated by investigating the kinetic profile of EXEN diffusion from 50-100 kDa Spectra/Por® Float-A-Lyzer (Figure 7.4), which allowed to choose the minimum time required for the complete removal of the non-loaded EXEN. Three concentrations were selected based on the concentration of EXEN in freshly prepared SLN dispersion produced using 5, 10, and 15% (w/w) EXEN/total lipid feed.

After 8 hours, the EXEN solution with an initial concentration of 0.44 mg/mL shows that almost complete diffusion of the EXEN from the Float-A-Lyzer occurs (97% diffusion). The EXEN solution with the initial concentration of 0.88 mg/mL showed a slower diffusion than the previous condition. Indeed, after 8 hours about 77% of the EXEN diffused from the device. The slowest release profile was identified for peptide solution with an initial concentration of 1.32 mg/mL. These results are reasonable because they show that the higher the concentration of exenatide in solution, the longer the time required for its complete diffusion, even though the diffusion rate increases with increasing gradient. After 22 hours, free EXEN is completely diffused from the Float-A-Lyzer in all three samples.

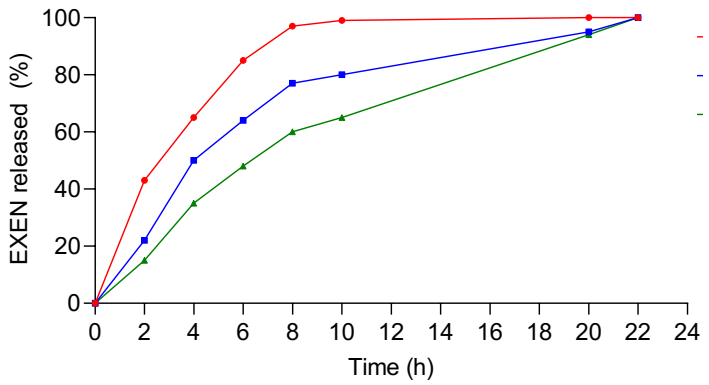

Figure 7.4. *Kinetic profile of* EXEN *diffusion from Float-A-Lyzer with 50-100 kDa cut-off to release buffer (1 mM HEPES, pH 8).* EXEN *samples in 1 mM HEPES pH 8 had initial concentration of 0.44 mg/mL (■) and 0.88 mg/mL (■) and 1.31 mg/mL (▲).*

7.2. Interaction between DOTAP and EXEN

7.2.1. ITC analysis

The thermodynamics of the electrostatic interaction between DOTAP and the EXEN, which leads to precomplex formation, was studied by the use of calorimetric analysis as reported in the literature[368,

[369]. Isothermal titration calorimetry (ITC) is a well-established technique that measures the variation of enthalpy that occurs when two species, generally a ligand and a protein, interact. In the system under investigation, an exothermic event is expected when the interaction between DOTAP and EXEN occurs. Since the charge of EXEN is pH-dependent, we proved the electrostatic interaction that leads to the complexation between the two molecules at pH 8 where the EXEN is anionic (2 anionic charges) and DOTAP cationic (1 cationic charge). We also measured the interaction between the two molecules at pH 3.5 as a negative control condition, where an electrostatic repulsion should occur since both molecular partners possess cationic charges.

DOTAP is a cationic lipid that is highly soluble in ethanol, but it has a lower solubility in water. We decided to first solubilize it in ethanol and then dilute it in water for the electrostatic interaction with exenatide; however, the presence of ethanol in the samples provides an analytical bias since it tends to contribute to the heat of dilution when ITC measurement is involved. Moreover, the low molecular weight of DOTAP does not allow run dialysis to remove ethanol before the analysis since it would be dialyzed together with ethanol. This step is usually recommended to minimize the subtle composition differences that may occur between the solutions of the two analytes in the syringe and the one in the sample cell. For all such reasons, liposomes were used as a scaffold to introduce DOTAP and expose its quaternary ammonium cationic charge to the surface of liposomes for electrostatic interaction with the EXEN.

DOTAP liposomes possess a size of almost 180 nm, and they exposed the cationic charge of DOTAP at the surface as confirmed by their zeta potential which was +52.7 ± 1.7 mV (in Milli-Q water) while the zeta potential of control liposomes formulated without DOTAP was -5.8 ± 2.8 mV.

The dialysis of the liposome sample and the EXEN sample was performed in the same beaker containing buffer. In both pH conditions, the presence of the buffer salts affected slightly the zeta potential of liposomes. The zeta potential of liposomes after dialysis in 1 mM HEPES pH 8 and in 1 mM citrate pH 3.5 decreased to +39.0 ± 1.5 mV +35.0 ± 1.9 mV, respectively. Also, the control liposomes produced without DOTAP and dialyzed against 1 mM HEPES pH 8 underwent a slight decrease of zeta potential to -14.3 ± 0.9 mV. However, the size of all liposomes remained at about 180 nm.

The ITC titration was run by titrating the EXEN in the cell sample with 10% (w/w) DOTAP-liposome at pH 8. As reported in *Figure 7.5, Panel A,* a significant change of enthalpy was generated after the first injection of 10 µL of liposome solution. Then, the change of enthalpy decreased for each following injection. The ITC profile resulting from the calorimetric titration is related to the saturation of the binding site of the exenatide by the 10% (w/w) DOTAP-liposomes. Thus, the exothermic reaction occurs by virtue of the electrostatic interaction between the positive charge of DOTAP on the surface

of the liposomes and the negative charges present in the EXEN. Usually, the constant of association (Ka) between the two interacting partners can be calculated from the slope at the inflection point of the sigmoid, but since a sigmoid was not obtained, a Ka value was not defined.

As reported in *Figure 7.5, Panel B,* we have fitted the integrated heat pulses with a curve to define the stoichiometry (N) of the interaction and the variation of enthalpy (ΔH). The N value was 3.2 ± 0.4, which corresponds to the number of DOTAP molecules, contained in 10% (w/w) DOTAP-liposomes (100 µM), bound to EXEN, whereas ΔH is 0.913 ± 0.103 kcal/mol.

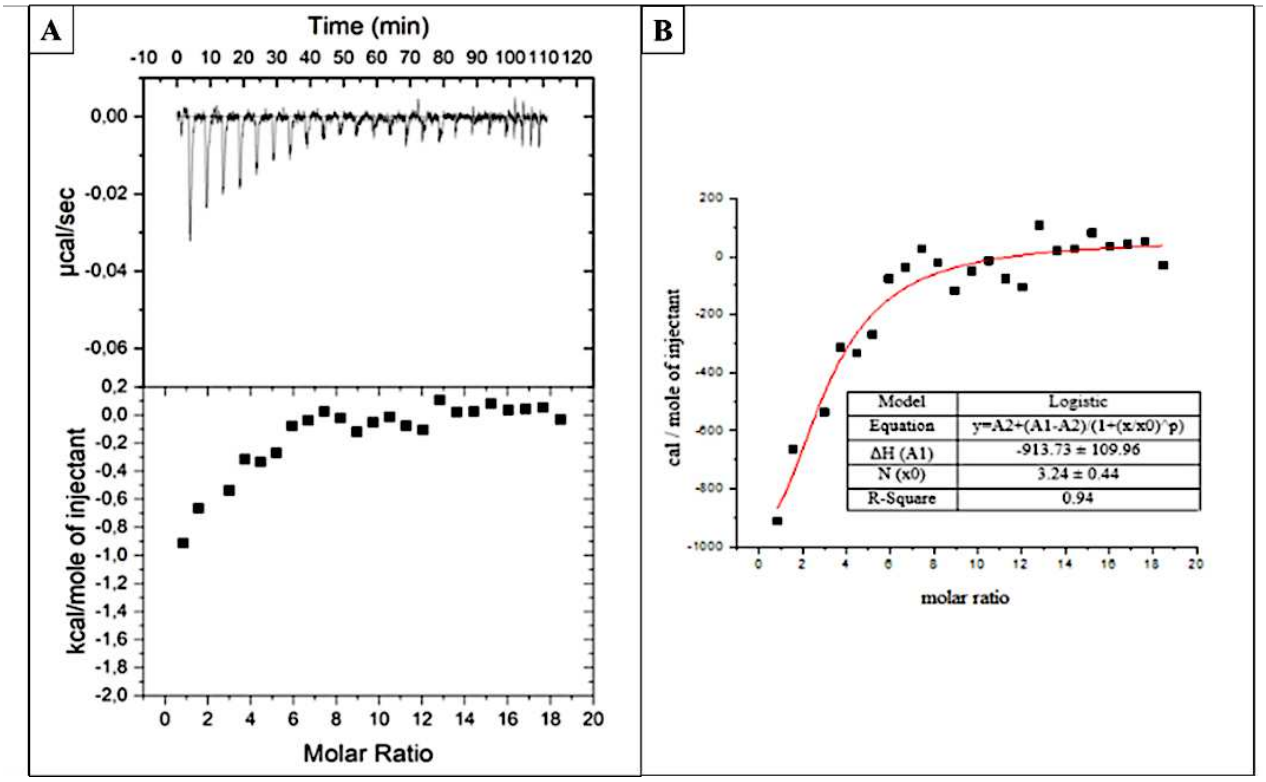

Figure 7.5. *A) Microcalorimetric titration profile of 1 µM EXEN solution in 1 mM HEPES pH 8 with 1 mM liposomes containing 100 µM DOTAP in 1 mM HEPES pH 8 injected. The top graph shows raw data of the heat per unit of time-released after each injection of 10% DOTAP-liposome into EXEN solution. The bottom graph shows the integrated heat pulses, normalized per mol of injected DOTAP as a function of the molar ratio. B) The red curve represents the best fit of the integrated heat pulses obtained with a logistic model.*

Taking into account the amino acids sequence of the EXEN containing 5 glutamic acids (pKa 4.2) and 1 Aspartic acid (pKa 3.8), it is expected that their carboxylic groups should be, on average, deprotonated at pH 8 and their negative charges contribute to the electrostatic interaction with DOTAP. Based on the stoichiometry of the binding sites, we can derive that only 3 out of the 6 binding sites, namely the 6 -COOH groups of glutamic and aspartic acids, are involved in the interaction. This

can be reasonably explained by the steric hindrance provided by the curvature of the liposomes that limit the occupation of all negatively charged sites of the EXEN by the DOTAP embedded in the lipid bilayer.

The ITC titration was also performed at pH 3.5 where both the DOTAP and EXEN possess cationic charges, thus it was selected as a negative control. No trend of heat changes was detected along the titration of the EXEN by 10% DOTAP-liposomes, as reported in *Figure 7.6*. The heat generated after every injection was quite low and it was referred to as the heat of dilution of liposomes in the sample cell. Indeed, when the background analysis was subtracted from the analysis, the variation of enthalpy was negligible, about 0.1 kcal/mol for all the injections.

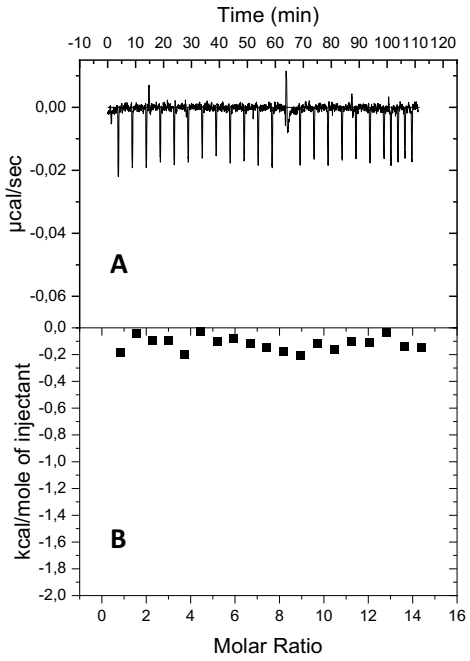

Figure 7.6. *Microcalorimetric titration profile of 1 µM EXEN solution in 1 mM citrate pH 3.5 with 1 mM liposome containing 100 µM DOTAP in 1 mM citrate pH 3.5. Panel A shows raw data of the heat released per unit of time after each injection of the 10% DOTAP-liposome into an exenatide solution. Panel B shows the integrated heat pulses, normalized per mol of injectant as a function of the molar ratio.*

Additional control was also tested using DOTAP-free liposomes. DOTAP-free liposomes injected into the sample cell containing EXEN solution in 1 mM HEPES at pH 8 did not elicit changes of heat by the single liposome injection as reported in *Figure 7.7*, The heat by each injection remained constant and the variation of enthalpy was found to be close to 0 kcal/mol which reflects the heat of dilution. Thus no titration of the EXEN with neutral liposomes was derived confirming the interaction of EXEN with DOTAP only.

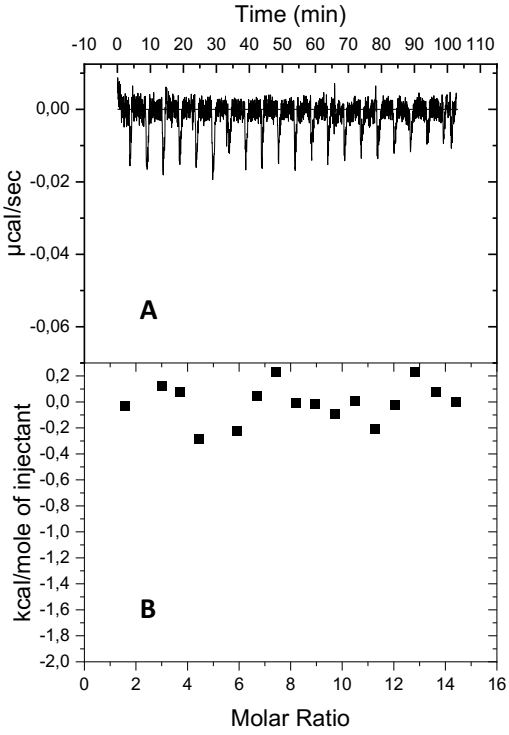

Figure 7.7. *Microcalorimetric titration profile of 1 mM DOTAP-free liposome in 1 mM HEPES pH 8 injected into 1 µM EXEN solution in 1 mM HEPES pH 8. Panel A shows raw data of the heat released per unit of time after each injection of 1 mM DOTAP-free liposomes into 1µM exenatide solution. Panel B shows the integrated heat pulses, normalized per mol of injectant as a function of the molar ratio.*

7.2.2. Exenatide adsorption on SLNs surface

The EXEN adsorption study on SLN further confirmed the electrostatic interaction between the peptide and DOTAP. Since the ionization of the EXEN is pH-dependent, we ran the adsorption test at pH 8, where DOTAP has a cationic charge and EXEN has an excess of 2 negative charges at this pH condition. A test condition at pH 3.5 was also used as a negative control because EXEN and DOTAP are both positively charged and repulsion occurs.

The EXEN-free 10% DOTAP-SLNs were incubated for 2 hours with EXEN. The DOTAP included in the SLN composition is expected to display its cationic quaternary charge on the particle surface which resulted in a significant increase in the size of SLNs upon incubation with the EXEN at pH 8 as shown in *Figure 7.9 Panel A*. Indeed, particles increased from 61.8 ± 4.5 nm to 122.9 ± 19.7 nm after the incubation. It can be hypothesized that when the EXEN is adsorbed on the particle surface in virtue of the electrostatic interaction with DOTAP, the coating of SLN provide an increase in their hydrodynamic size. However, despite the size increase, the PDI of SLNs remained quite monodisperse (*Figure 7.9*

Panel B) which may prove homogeneous peptide adsorption on the particle surface and no aggregation.

On the contrary, at pH 3.5, SLNs' size did not change in the presence of EXEN (54.80 ± 1.1 nm and 56.0 ± 3.2 before and after incubation with exenatide, respectively). Conceivably, no adsorption of EXEN occurred on particle surfaces due to electrostatic repulsion at pH 3.5.

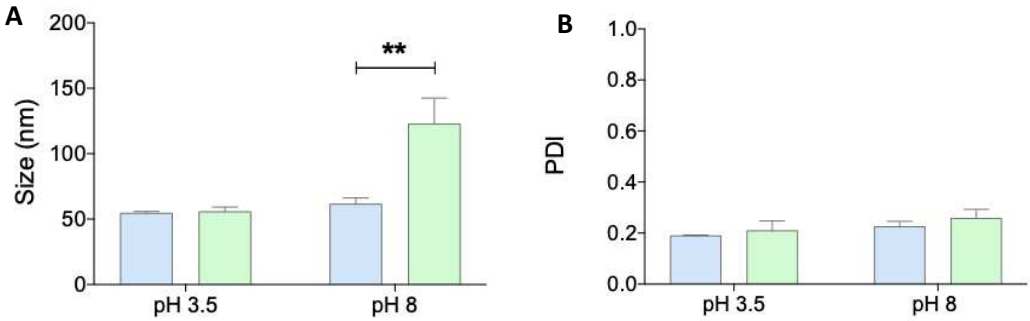

Figure 7.9. *Size (A) and PDI (B) were measured before (■) and after (■) the incubation of DOTAP containing EXEN-free SLNs (10% DOTAP (w/w) with respect to total lipids), with EXEN at pH 3.5 and pH 8. Data are reported as mean ± SD. (**: p<0.01)*

As reported in *Figure 7.10, the* zeta potentials of EXEN-free SLN before the incubation with EXEN were similar at pH 8 and pH 3.5.

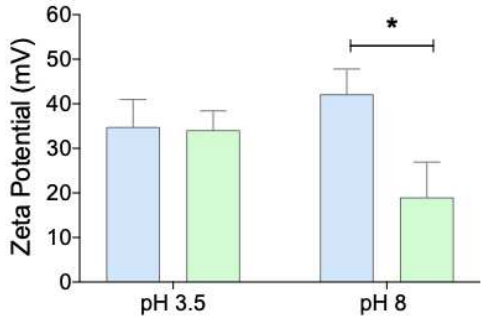

Figure 7.10. *Zeta potential of DOTAP containing* EXEN*-free SLNs (generated with 10% DOTAP (w/w) with respect to total lipids) before (■) and after (■) incubation with* EXEN *at pH 3.5 and pH 8. Data are reported as mean ± SD. (*: p<0.05)*

After the incubation of DOTAP-containing SLN with the free EXEN at pH 8, the zeta potential decreased from +42.1 ± 5.7 mV to +19.0± 8.0 mV. On the contrary, the zeta potential of DOTAP-containing SLN remained unchanged before (+34.8 ± 6.2 mV) and after (+34.1 ± 4.3 mV) incubation with EXEN at pH 3.5. When EXEN is adsorbed on the particle surface, it shields the charge provided by DOTAP and this leads to a decrease in the overall zeta potential of cationic SLNs. The outcomes obtained from the zeta

potential analysis are in agreement with the size analysis results and further prove the electrostatic interaction of the EXEN with DOTAP cationic charge exposed on SLN surfaces.

7.3. Formulation of the SLNs

7.3.1. Selection of the lipid mixture concentration

SLNs were prepared by the microfluidic process. The most suitable lipid mixture concentration to generate SLNs with small size and low polydispersity was selected by looking at the effect of 1:3 HSPC/Cholesterol mol/mol ratio lipid concentration in ethanol on the SLN colloidal features. SLNs were generated as explained in section 6.2.3.1.

The formulation obtained by processing an ethanolic lipid mixture at 40 mg/mL showed a size of 103.58 ± 25.03 nm and a PDI value of 0.272 ± 0.120 (Figure 7.11, panel A), while the formulation obtained by processing an ethanolic lipid mixture at 35 mg/mL showed a size of 87.04 ± 2.39 nm and a PDI value of 0.229 ± 0.062 (Figure 7.11, panel B). Finally, the formulation obtained by processing an ethanolic lipid mixture at 30 mg/mL showed a size of 92.42 ± 7.00 nm and a PDI value of 0.214 ± 0.046 (Figure 7.11, panel C).

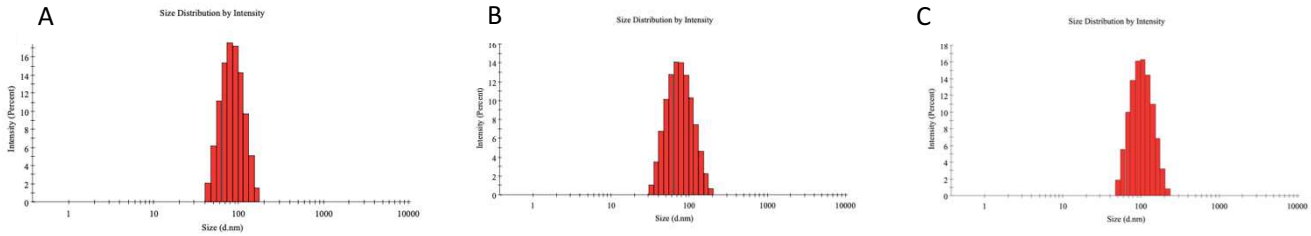

Figure 7.11. *Size distribution of the SLNs produced by processing ethanolic 1:3 HSPC/Cholesterol mol/mol ratio mixtures at 40 (A), 35 (B), and 30 (C) mg/mL*

The standard deviation is a parameter that identifies the batch-to-batch differences and was relatively lower for the SLNs obtained processing the lipid mixture in EtOH at 35 mg/mL, than the formulations obtained with 30 and 40 mg/mL of lipid concentration. The polydispersity index values for each formulation were quite low, showing a quite homogeneous SLN distribution in terms of size. However, while the formulations obtained with 35 and 40 mg/mL showed a low standard deviation, processing 30 mg/mL of lipid mixture resulted in a higher standard deviation for the polydispersity index (Figure

7.12). Based on this result, the lipid mixture concentration of 35 mg/mL was selected to further investigate the formulation parameters of SLN assembly.

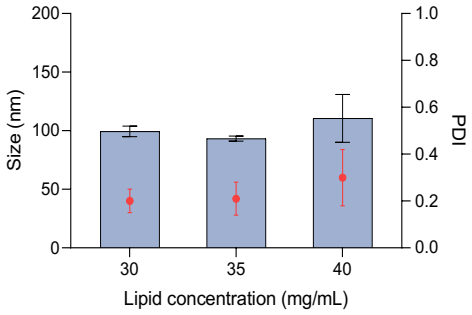

Figure 7.12. *Particle size (grey bars refer to the left vertical axis) and PDI (red symbols refer to the right vertical axis) of the EXEN free and SLNs generated by processing 30, 35, and 40 mg/mL of 1:3 HSPC/Cholesterol mol/mol ratio lipid mixtures.*

The recovery of the lipids after processing by the microfluidic system and dialysis was quantified by Stewart Assay. The recovery of lipids in the SLN after assembly and dialysis was 94, 93, and 95% when the 30, 35, and 40 mg/mL lipid mixture in ethanol were processed, respectively, suggesting a very limited lipid loss during the SLN production and dialysis processes.

To have a deeper insight into the features of the core of particles assembled with lipids, a morphologic analysis was undertaken by transmission electron microscopy. Indeed, TEM can provide information concerning the 3D arrangement of the lipids, either in a vesicular system, which would appear as ”condom-like” structures under the vacuum conditions of TEM imaging, or in a hardcore lipid particle, which would appear as a sphere. SLNs to be imaged by TEM were generated by processing a 1:3 HSPC/Chol molar ratio at 35 mg/mL in EtOH as the organic phase and 1 mM HEPES (pH 8) as the aqueous phase and the results of the TEM analysis are shown in *Figure 7.13*.

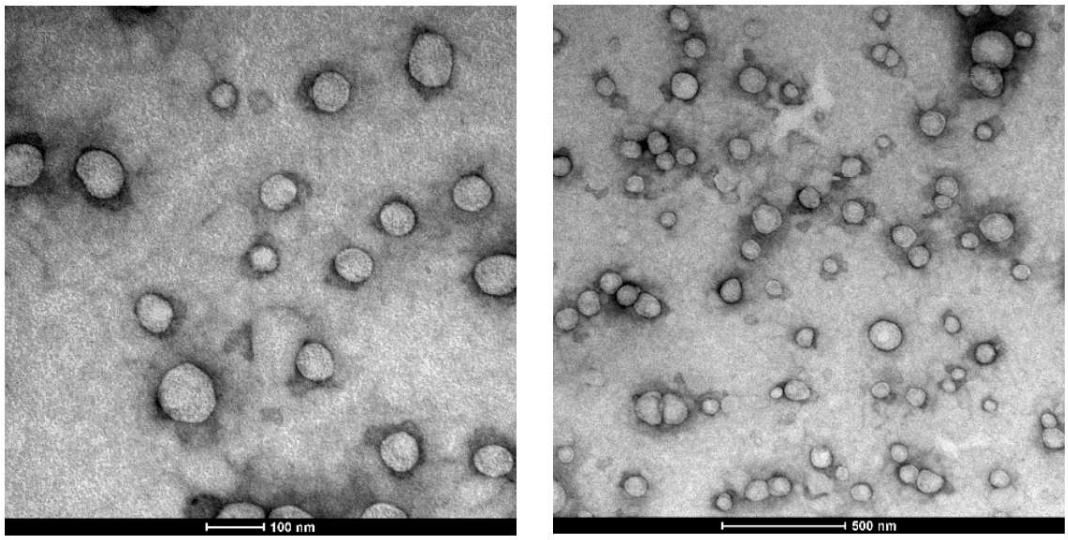

Figure 7.13. *Transmission electron microscopic images of exenatide-free SLN formulation. Scale bar: 100 nm (left panel) and 500 nm (right panel).*

As shown in Figure 7.13, TEM results demonstrated that the colloidal system obtained possesses spherical shapes with dense content without signs of the collapsed structure. The size of the particles appears homogeneous and no aggregates were detected. The size observed with the TEM analysis was in agreement with the size obtained by the DLS analysis.

7.3.2. Selection of the microfluidics process parameters

Preliminary studies were performed to select the optimal microfluidic instrument settings including the total flow rate (TFR) and flow rate ratio (FRR) in order to generate lipidic particles with homogeneous size, possibly in the 100-200 nm. Indeed, particles with size in this range were found to provide better drug bioavailability upon oral administration with respect to bigger particles. Furthermore, this size is also desired for better diffusion across the intestinal mucus[277,278,279].

Studies reported in the literature showed that FRR can affect particle size[340,370]. Moreover, the water volume must exceed the organic phase because this is required for the lipids to be exposed to an increase of medium polarity resulting in supersaturated conditions which cause the assembly of lipids in solid nanoparticles[371-373]. On the contrary, when the water volume is comparable to that of the organic solvent upon mixing, it is more likely that lipids tend to organize in bilayers resulting in vesicles, namely liposomes[374-376]. For this reason, we selected two FRRs, 3:1 and 5:1. TFR is also reported to affect the final features of the formulation. A high total flow rate results in a rapid increase in the polarity of the medium which causes the solution to quickly reach a state of high lipid monomer

supersaturation throughout the entire mixing volume, leading to the quick and uniform nucleation of nanoparticles[371].

In order to select the microfluidic conditions, preliminary formulation studies were carried out using only 5% (w/w) EXEN/total lipid feed ratio and 6:1 (mol/mol) DOTAP/EXEN ratio. SLNs were produced by changing the flow rate ratio (FRR = 5:1; 3:1), total flow rate (TFR = 3, 6, 9, 12 mL/min) while the total volume (TV) of the formulation was set at 1.2 mL, the start and end waste were 150 and 50 µL, and operating temperature of 25 °C. In total, a small library of 8 formulations was generated. After the production, SLN suspensions were dialyzed in order to remove EtOH and non-loaded EXEN and colloidally characterized. Size distribution and PDI of the library are reported in *Figure 7.14*.

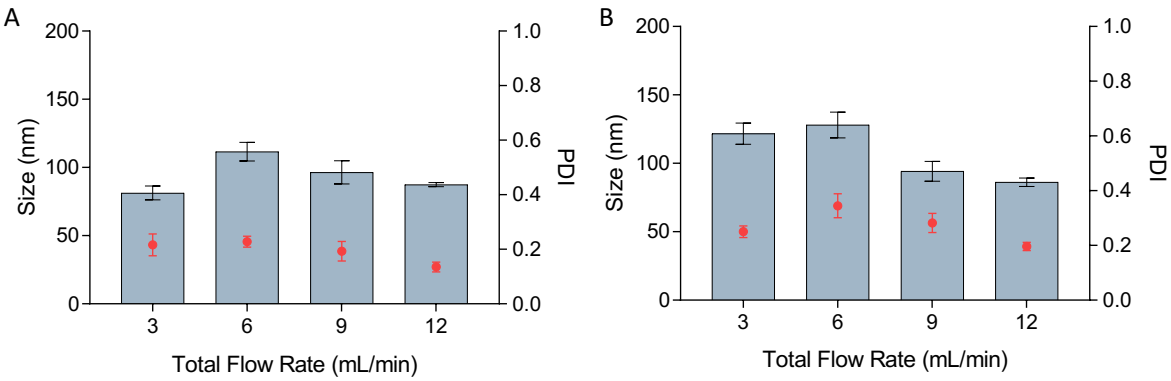

Figure 7.14. *Particle size (grey bars refer to the left vertical axis) and PDI (red symbols refer to the right vertical axis) of the EXEN-loaded SLNs generated with FRR 3:1 (A) and FRR 5:1 (B) at increasing TFRs (3, 6, 9 and 12 mL/min).*

The FRR was not significantly affecting the colloidal properties. Assembly with FRR of 3:1 and 5:1 resulted in SLN with size in the 80-130 nm range and PDI of about 0.2 for most formulations. The size tended to decrease when increasing TFR for FFR 3:1, which was not evident for FFR 5:1. Smaller and more homogeneous SLN with lower PDI and standard deviation were obtained with both FRRs tested at the highest TFR of 12 mL/min.

EXEN loading efficiency and capacity of the formulations are shown in *Figure 7.15*.

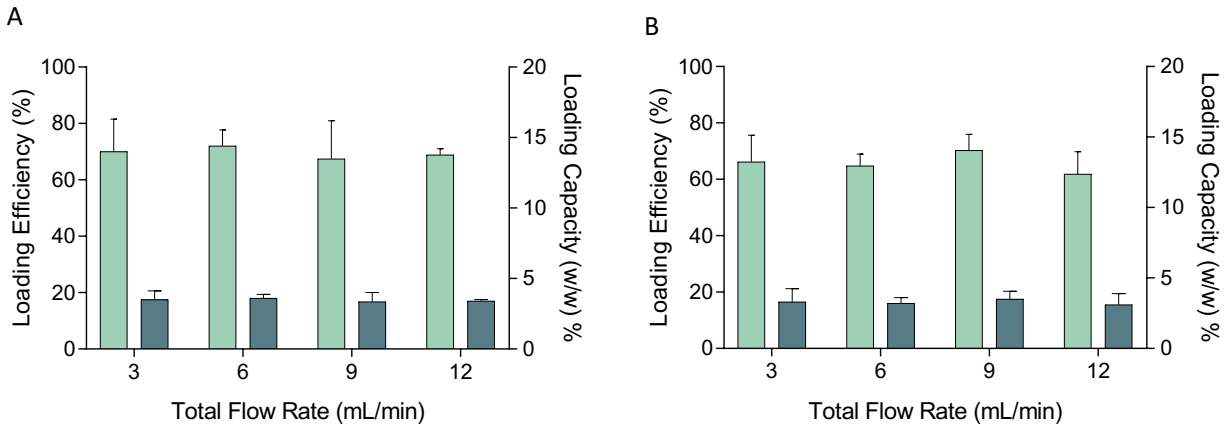

Figure 7.15. *Loading efficiency (■, left axis) and loading capacity (■, right axis) of the EXEN loaded SLNs generated with FRR 3:1 (A) and FRR 5:1 (B) at increasing TFRs (3, 6, 9, and 12 mL/min).*

The results showed that there are no remarkable differences between formulations in terms of loading efficiency (LE) and loading capacity (LC) both for the formulations generated with FRR of 3:1 and 5:1. Indeed, LE was found to be in the range of 60-70% and LC was between 3.1-3.6 w/w% with respect to lipids for every formulation.

Given that, no significant differences in terms of size, PDI, and EXEN loading were observed when changing the FRR, other considerations were made to choose the microfluidic process settings for SLN production. The formulation setting with FRR 3:1 and TFR = 12 mL/min was selected for further studies. Indeed, this condition allows for smaller and homogeneous particles: the mean size was found to be 87.4 ± 1.47 nm and the PDI is 0.35 ± 0.018 while the loading efficiency was comparable to that of other formulations obtained with different microfluidic settings but the standard deviation was lower. LE and LC were 68.91 ± 2.13 % and 3.4 ± 0.1 %, respectively. Furthermore, the formulation condition using FRR at 3:1 was preferred over FRR at 5:1 because the SLN suspension is obtained with a lower dilution with the former with respect to the latter, namely 8.75 mg/mL lipid and 5.83 mg/mL, respectively. Related to this point, we also took into account that since SLNs are planned to be administered via the oral route, they will be lyophilized before being transferred inside hard gelatin capsules. Thus, lower FRR also results in a lower volume of residual water to be removed by lyophilization, which reduces the process costs.

7.3.3. Selection of the DOTAP/EXEN precomplexation buffer concentration

The effect of buffer ionic strength on the colloidal features and loading of EXEN to SLNs was investigated. The complexation between EXEN and DOTAP relies on the electrostatic interaction of the six anionic amino acids, and the quaternary amino group of DOTAP. This association increases the hydrophobic character of hydrophilic EXEN, thus favoring its loading into a lipophilic carrier matrix, i.e. SLNs.

The net charge of the EXEN is dictated by its isoelectric point and the aqueous medium pH. Since EXEN can be safely exposed to mild basic conditions[89], pH 8 was chosen to ensure the anionic state of EXEN while avoiding extreme conditions. At pH 8 EXEN possesses a net charge of -2 (Figure 4.4).

The pH of the EXEN solution was adjusted according to two different procedures that we have here investigated to assess their effect on the loading efficiency. Firstly, 0.1 M NaOH was added to the exenatide aqueous solution to adjust the pH value to 8. This strategy is reported in the literature to obtain Hydrophobic Ion Pairing (HIP) between peptides and a hydrophobic anion[89,90]. After the combination of DOTAP with EXEN, the pH was set to 8.

Secondly, the pH for DOTAP/EXEN electrostatic complexation was set using two different buffer concentrations. Indeed, HEPES is a zwitterionic sulfonic buffering agent that may interfere with the electrostatic interaction between DOTAP and EXEN; if this occurs, a buffer concentration effect would be expected. Thus, HEPES buffer at pH 8 was employed at 1 mM or 10 mM to set the pH of the DOTAP/EXEN mixture. Both buffers were able to maintain the pH of the mixture when DOTAP was added to the EXEN solution. In terms of operating procedures, the use of buffer is more reliable concerning the use of NaOH to set the DOTAP/EXEN solution pH.

Since EXEN has a net charge of -2 at pH 8 and DOTAP has one positive permanent charge the lowest DOTAP/EXEN molar ratio selected was 2:1 to provide for a 1:1 charge ratio. A library of formulations was generated by increasing DOTAP/EXEN molar ratios up to 18:1 to shift association equilibria toward complexation. Particles without DOTAP were also generated as a negative control.

The particle sizes, polydispersity index (PDI), and zeta potential of the SLNs produced by ion-pairing of DOTAP and EXEN in three different buffer conditions (0, 1, and 10 mM HEPES buffer, pH 8) are reported in *Figure 7.16.*

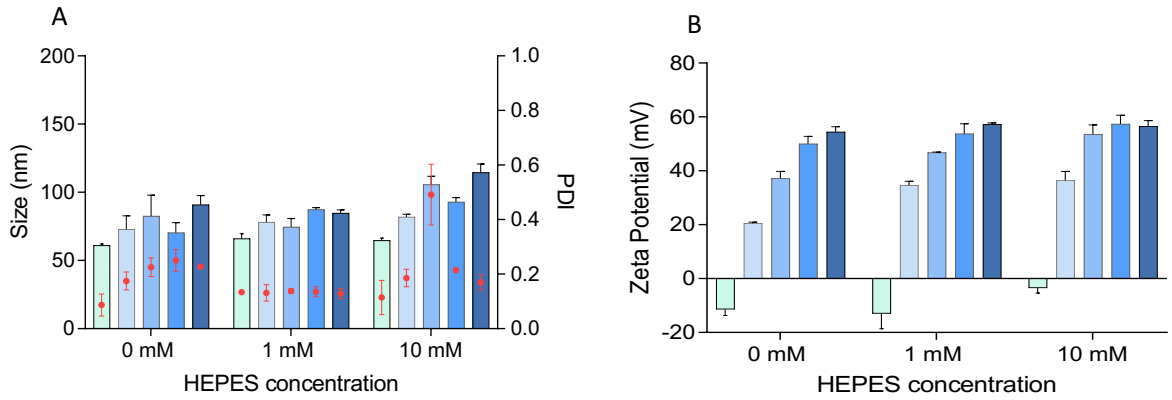

Figure 7.16. *Particle size, PDI (A), and zeta potential (B) of the EXEN-loaded SLNs produced by ion pairing of DOTAP and EXEN in 0, 1, 10 mM HEPES pH 8 by processing 5% EXEN/total lipid (w/w) feed ratio and 0:1 (▫), 2:1 (▫), 6:1 (▫), 12:1 (▫) and 18:1 (▫) DOTAP/EXEN molar ratios.*

The size of EXEN-loaded SLNs resulted in a range of 60-115 nm. Indeed the particles without DOTAP showed the lowest mean size of about 60 nm for all buffer conditions used for the DOTAP/EXEN pre-complexation. It is reasonable to believe that the hydrophilic EXEN in the absence of DOTAP may have quite limited loading, thus it does not affect the arrangement of the SLN and thus their size. The size of all formulations obtained with 0 mM HEPES (pH 8 adjusted with NaOH) and with 1 mM HEPES pH 8 is below 100 nm; a slight and very similar trend of size increase was observed for both buffer conditions as the DOTAP/EXEN ratio increased.

The SLNs generated by pre-complexation of DOTAP and EXEN in 10 mM HEPES pH 8 showed a higher size trend increase with respect to the counterpart obtained with 0 and 1 mM HEPES. The size increased up to 114.6 ± 6.2 nm for formulation with an 18:1 DOTAP/EXEN molar ratio. In terms of PDI, formulations generated without the use of buffer showed a trend in which, the increase of the DOTAP/EXEN molar ratio resulted in a PDI increase from 0.09 ± 0.04 for the formulation without DOTAP to 0.25 ± 0.04 for the formulation with 12:1 DOTAP/EXEN molar ratio. Notably, the formulation processed with 1 mM HEPES showed a very constant PDI of about 0.13 for all the various DOTAP/EXEN molar ratios, with a low standard deviation. The PDI was slightly higher in SLNs produced using 10 mM HEPES at increasing DOTAP/EXEN molar ratio with respect to the ones produced with 1 mM HEPES and multiple size populations occurred in SLNs generated using 6:1 DOTAP/EXEN molar ratio, which resulted in a higher PDI value of 0.49 ± 0.11.

The results from zeta potential measurement showed an expected trend under all three buffer conditions used for DOTAP/EXEN precomplexation; as the processed DOTAP/EXEN molar ratio increased in the formulations, the zeta potential also increased (Figure 7.16, Panel B). The zeta potential values of the particles generated with increasing DOTAP/EXEN molar ratio with 1 mM HEPES

pH 8 were comparable to the counterparts produced with 10 mM HEPES pH 8. On the other hand, the values of zeta potential of particles formulated with 0 mM HEPES were slightly lower than their counterparts produced with HEPES which was most evident for the SLN obtained with 2:1 and 6:1 DOTAP/EXEN molar ratio.

Slightly negative zeta potential was detected in EXEN-loaded formulations obtained without DOTAP (0:1 DOTAP/EXEN molar ratio). The zeta potential values of these formulations were in the -13.0 / -3.4 mV depending on the buffer condition for precomplexation. This negative zeta potential was attributed to the fraction of EXEN associated with the SLN surface which is in agreement with its negative charge.

The highest zeta potentials were detected when the highest ratio of DOTAP/EXEN was processed. In particular, the SLN obtained with 18:1 DOTAP/EXEN molar feed ratio showed zeta potential of +54.5 ± 1.9 mV, +57.3 ± 0.5 mV, +56.5 ± 2.1 mV when 1 mM and with 10 mM HEPES buffer were used for precomplexation, respectively. Based on zeta potential data, high colloidal stability is expected for these SLNs. Guidelines classify nanoparticle dispersion with zeta potential values in the ± 0-10 mV as unstable, while the ones with zeta potential values equal to or higher than ± 30 mV are highly stable.

Since the cationic lipid DOTAP was employed to generate a precomplex that decreases the hydrophilicity of the EXEN and promotes loading, we thus assessed the loading efficiency and capacity of the SLNs under different pre-complexation buffer conditions. Results are given in the *Figure 7.17*.

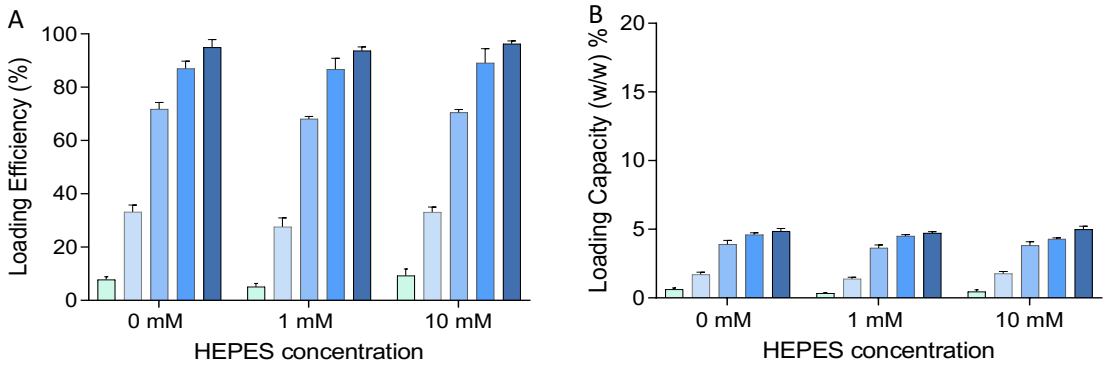

Figure 7.17. *Loading efficiency (A) and capacity (B) of the EXEN-loaded SLNs produced by precomplexation of DOTAP and exenatide in 0 mM, 1 mM, 10 mM HEPES pH 8 by processing 5% EXEN/total lipid (w/w) feed ratio and 0:1 (), 2:1 (), 6:1 (), 12:1 () and 18:1 () DOTAP/EXEN molar ratios.*

Figure 7.17 shows that the profile of LE and LC at increasing DOTAP/EXEN molar ratios were comparable for the different sets of SLN at different buffer concentrations used. Indeed, statistical analysis (Two-way ANOVA analysis) was performed to evaluate the effect of buffer concentration on LE and LC by comparing the formulations obtained with the same DOTAP/EXEN molar ratios at

different buffer concentrations. From the analysis, in terms of loading efficiency and capacity, no significant difference was detected.

A clear trend of EXEN loading as the DOTAP/EXEN molar ratio increases was observed. The LE shifted from a negligible value at 0:1 DOTAP/EXEN to almost 100% of encapsulation at 18:1 DOTAP/EXEN molar ratio. Indeed, in the absence of DOTAP (0:1 DOTAP/EXEN molar ratio), under the three buffer conditions, the LE of SLN was between 5 and 9% and increased in a range of 3-5 times for the formulations obtained with 2:1 DOTAP/EXEN molar ratio, 8-13 times for the formulations obtained with 6:1 DOTAP/EXEN molar ratio, 9-17 for the formulations obtained with 12:1 DOTAP/EXEN molar ratio, and 10-18 for the formulations obtained with 18:1 DOTAP/EXEN molar ratio. Except for the formulations created with the 12:1 and 18:1 DOTAP/EXEN molar ratios, where loading efficacy reaches a plateau, a significant difference between each DOTAP/EXEN molar ratio and the next higher ratio was found through statistical analysis.

Since the precomplexation buffer did not affect the loading process, we selected the buffer based on its effect on the colloidal features. Indeed, differently from the other two buffer conditions, the DOTAP/EXEN precomplexation in 1 mM HEPES pH 8 results in EXEN-loaded SLN with colloidal homogeneity and minimal size and PDI alterations as the DOTAP/EXEN molar ratio increase. Thus this buffer was selected as the preferable buffer condition to formulate the SLNs by microfluidics.

7.3.4. Selection of the EXEN/total lipid feed ratio and DOTAP/EXEN molar ratio

After the selection of the buffer concentration that ensures the good pharmaceutical quality of SLNs in terms of size, PDI and loading, the effect of the EXEN/lipid feed ratio was investigated in the 5-15% (w/w) range with respect to total lipid by looking at pre-complexing DOTAP/EXEN molar ratio range of 0:1- 18:1. Formulations were first characterized in terms of size, PDI and zeta potential and the results are given in *Figure 7.18*.

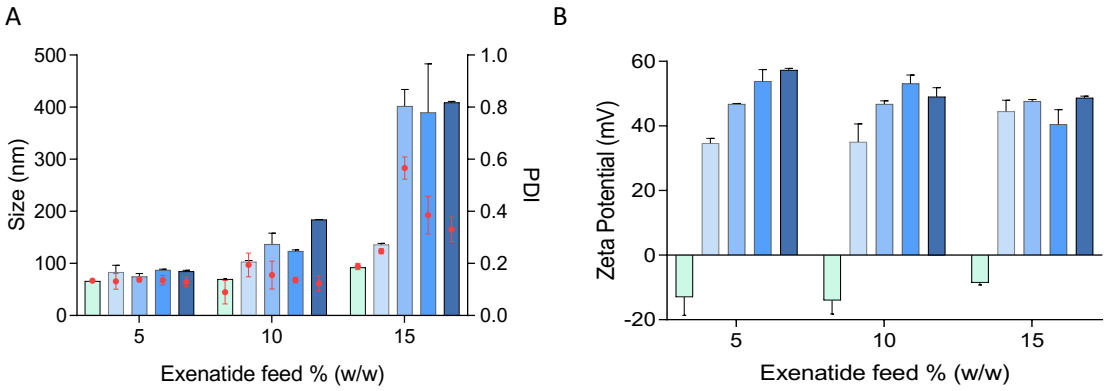

Figure 7.18. *Particle size, PDI (A), and zeta potential (B) of the EXEN-loaded SLNs produced by precomplexation of DOTAP and EXEN in 1 mM HEPES pH 8 by processing 5, 10, and 15% EXEN/total lipid (w/w) feed ratio and 0:1 (), 2:1 (), 6:1 (), 12:1 () and 18:1 () DOTAP/EXEN molar ratios.*

The size of the formulations generated with a 5% (w/w) EXEN/total lipid feed ratio was below 100 nm, while the of sizes formulations generated with a 10% (w/w) EXEN/total lipid feed ratio was slightly above 100 nm, and those generated with 15% (w/w) EXEN/total lipid feed ratio were remarkably bigger than 100 nm, except the nanoparticles without DOTAP. As shown in *Figure 22A,* the formulations without DOTAP showed the size of about 65 nm for the formulations processed with a 5 and 10% (w/w) EXEN/total lipid feed ratio, whereas the size of the formulations produced with a 15% (w/w) EXEN/total lipid feed ratio was 92.4 ± 1.6 nm.

SLNs obtained with 10% (w/w) EXEN with respect to lipids with a DOTAP/EXEN molar ratio of 12:1 showed higher quality in terms of colloidal properties than all other conditions. Indeed, these particles had a particle size of 123.7 ± 2.5 nm and a PDI of 0.136 ± 0.01. When DOTAP /peptide molar ratio was further increased the particle size increased to 184.1 ± 0.1 nm.

Evident phenomena of aggregation and heterogeneity systems occurred when SLNs were generated with a 15% (w/w) EXEN/total lipid feed ratio for the formulations generated at DOTAP/EXEN above 2:1 molar ratio. Particle sizes of these formulations were above 400 nm, and the suspension was polydisperse (PDI > 0.4). We concluded that a high EXEN feed ratio in combination with a higher ratio of DOTAP leads to non-ordered aggregation rather than a controlled assembly of components during microfluidic processing.

As shown in *Figure 7.18, panel B*, an increase of zeta potential as DOTAP increased with respect to EXEN (and consequently with respect to total lipids) was observed for the SLNs obtained by processing 10% (w/w) EXEN/total lipid feed ratio, similarly to what observed for the SLN obtained by processing 5% (w/w) EXEN/total lipid feed ratio. The highest zeta potential for the SLN obtained with 10% (w/w)

EXEN/total lipid feed ratio was measured with the 12:1 DOTAP/EXEN molar ratio; zeta potential was +53.1 ± 2.7 mV which was comparable to the zeta potential measured when a 5% (w/w) EXEN/total lipid feed ratio was processed (+53.8 ± 3.6 mV), even if the formulations have a different percentage of DOTAP with respect to lipids. A higher ratio of DOTAP did not further increase the zeta potential of nanoparticles. As expected, SLNs without DOTAP had a slightly negative charge (-14.0 ± 4.2 mV), comparable to that detected for the SLN obtained with a 5% (w/w) EXEN/total lipid feed ratio (-13.0 ± 5.6 mV).

Different zeta potential profile was observed for the SLN generated by processing 15% (w/w) EXEN/total lipid feed ratio with respect to the trend of zeta potential increase observed for SLN obtained by processing 5 and 10 % (w/w) EXEN/total lipid feed ratios at increasing DOTAP/EXEN molar ratio. Indeed, the increasing trend of zeta potential was not observed for the SLN generated with a 15% (w/w) EXEN/total lipid feed ratio. The SLNs obtained with a 2:1 DOTAP/EXEN molar ratio contained a higher ratio of DOTAP with respect to the SLNs counterpart obtained with 5% or 10% (w/w) peptide/lipid feed ratio, resulting in a higher zeta potential (+45 mV). Zeta potential did not significantly increase as the DOTAP/EXEN ratio increased which can be attributed to the interference of the particle aggregation as discussed above.

The effect of the EXEN/lipid feed ratio on the loading of SLNs was evaluated to identify the condition that provides for the highest loading capacity of the resulting particles. Also, within each EXEN/lipid feed ratio, a library was generated at increasing DOTAP/EXEN molar ratios. The loading efficacy and capacity of the formulations are reported below (Figure 7.19).

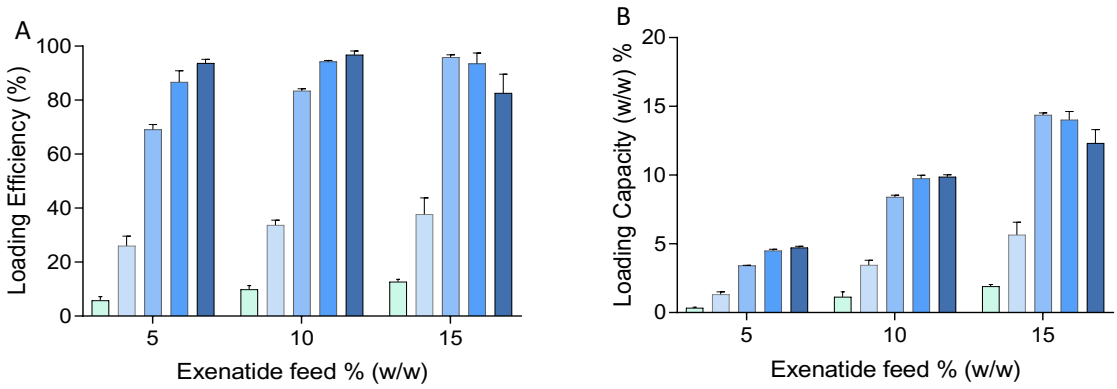

Figure 7.19. *Loading efficiency (A) and capacity (B) of the EXEN-loaded SLNs produced by precomplexation of DOTAP and EXEN in 1 mM HEPES pH 8 by processing 5, 10, and 15% EXEN/total lipid (w/w) feed ratio and 0:1 (□), 2:1 (□), 6:1 (□), 12:1 (□) and 18:1 (□) DOTAP/EXEN molar ratios.*

SLNs without DOTAP showed a low LE: 5.8 ± 1.4%, 9.9 ± 1.4 % and 12.7 ± 0.9 % at 5, 10 and 15% (w/w) EXEN/total lipid feed ratio, respectively. The low loading of exenatide into SLNs in the absence of

DOTAP confirms the hypothesis that DOTAP guides the loading of the EXEN by hydrophilic ion pairing which allows only a small fraction of peptide to be entrapped into the lipid matrix by microfluidic mixing of the aqueous solution with the organic phase.

The loading efficiency profile was quite comparable for the three sets of formulations obtained processing 5, 10, 15 w/w% EXEN/total lipid feed ratio at increasing DOTAP/EXEN molar ratio and almost complete loading was achieved for the three sets at DOTAP/EXEN molar ratio above 6:1. The LE profiles dictated the resulting LC, the highest being for SLN obtained by processing a 15% (w/w) EXEN/total lipid feed ratio at DOTAP/EXEN molar ratio above 6:1. However, these conditions did not provide good colloidal quality of nanoparticles in terms of size and PDI, and the high loading capacity may be caused by the aggregation of particles and entrapment of peptide within the aggregated. Thus, the nanoparticles obtained by processing 15% (w/w) EXEN/total lipid feed ratio were excluded for further investigation.

SLNs formulated with a 10% (w/w) EXEN/total lipid feed ratio and 18:1 DOTAP/EXEN molar ratio encapsulated almost all the EXEN processed. Indeed, LE increased up to 98.8 ± 1.4 % with the increase of DOTAP/EXEN molar ratio and LC was 9.9 ± 0.1 %, but these SLNs also possess a size above 150 nm (180 nm) with respect to those of the same set obtained at lower DOTAP/EXEN molar ratio.

On the other hand, SLNs obtained by processing 10% (w/w) EXEN/total lipid feed ratio and 12:1 DOTAP/EXEN molar ratio also showed a very high LE of 94.8 ± 0.4 % and LC of 9.6 ± 0.2 %, thus it can be concluded that 12:1 DOTAP/EXEN molar ratio is sufficient to provide quantitative encapsulation while using a lower DOTAP/lipids w/w ratio. Importantly, their size was smaller (around 120 nm) than the ones obtained with an 18:1 DOTAP/EXEN molar ratio and the particles resulted in monodispersed. Indeed, particle size is one of the factors that affect permeation through mucus and cellular uptake. Thus, 10% (w/w) EXEN/total lipid feed ratio and 12:1 DOTAP/EXEN molar ratio were selected to generate the SLN formulation for further investigations.

7.3.5. PEGylation of the SLNs

The mucus can trap pathogens, ultrafine particles, and particle-based drug delivery systems from exposed organs such as small intestines which may be followed by digestion. This limits drug absorption at mucosal surfaces. Many approaches are investigated to engineer nanoparticles that can easily diffuse across mucus to enhance particle adhesion to the underlying epithelium and improve particle absorption across the mucosa[377]. The mucin present in the mucus can especially capture cationic particles because of its negative charge and high glycan density[378]. Given that, EXEN-loaded SLNs selected in the previous chapter possess a high cationic surface charge (zeta potential > 50 mV),

SLNs were decorated with PEG_{2kDa} to shield the cationic charge, thus modulating the electrostatic association to mucin.

To this aim, SLNs generated by processing 10% (w/w) EXEN/total lipid feed ratio and 12:1 DOTAP/EXEN molar ratio were decorated, after the assembly, with DSPE-PEG_{2kDa} at a weight range of 2-30 %. size, polydispersity index, and zeta potential values of PEGylated SLNs are shown in *Figure 7.20*.

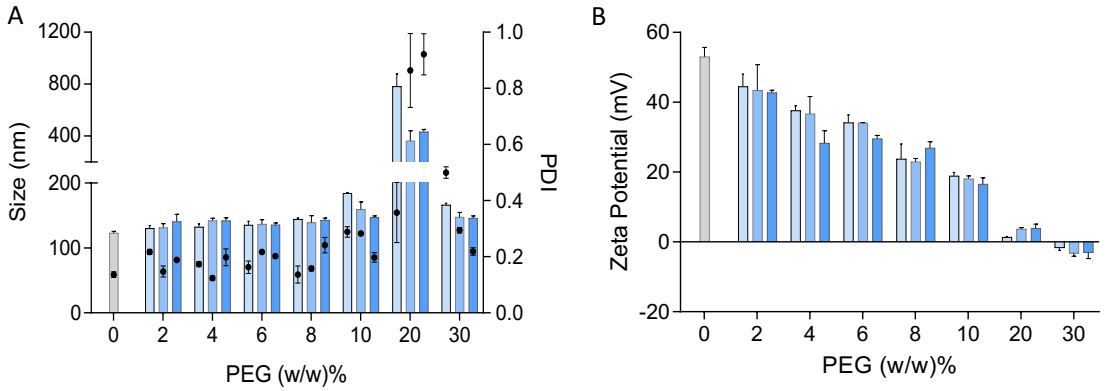

Figure 7.20. *Particle size, PDI (A), and zeta potential (B) of the EXEN-loaded SLNs before PEGylation (■) and after 5 (■), 10 (■), and 15 (■) minutes incubation with* DSPE-PEG_{2kDa} *in the 2-30 w/w%.*

Our findings from the PEGylation study demonstrated a progressive decrease of the SLNs' zeta potential as the DSPE-PEG_{2kDa} w/w % increase, which appear already at the lowest percentage (2 percent w/w%) at any tested incubation time. Nanoparticles with zeta potentials greater than +30 mV are considered strongly cationic[379]. Low zeta potential was reached with the 10% w/w PEG/total lipid ratio (~20 mv). Neutral zeta potential was first achieved at a 20 % w/w PEG/total lipid ratio; however, under this PEGylation condition, significant aggregation of SLN was noticed which may result in large surface charge shielding in the core of the aggregates (Figure 7.20 A). The particle coating with a 30% w/w PEG/lipid ratio resulted in SLNs with neutral zeta potential (~ -2mV) and small size (146-166 nm). Indeed PEGylation only slightly affected the particle size as expected by virtue of the polymeric coating that slightly expands the hydrodynamic volume of SLN.

In this study, the incubation time was tested for post-assembly PEGylation. Size and zeta potential were not significantly different for the SLN incubated for 5, 10, or 15 minutes with DSPE-PEG_{2kDa}. However, the 15 Iminutes incubation provided particles with lower PDI with respect to 5 and 10 minutes and this condition was selected for further studies.

Loading capacity of the SLNs after PEGylation was assessed and the results are displayed in *Figure 7.21.*

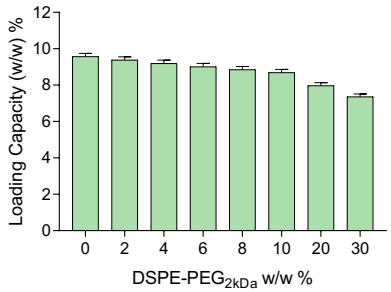

Figure 7.21. *Loading capacity of the EXEN-loaded SLNs before and after incubation with* DSPE-PEG_{2kDa} *in the weight range of 2-30%.*

The loading capacity results showed that the PEG coating of the EXEN loaded SLN slightly decrease the loading capacity by about 23 % with respect to the non-PEGylated particles with the highest decrease observed for SLNs decorated with 30 w/w% DSPE-PEG_{2kDa} (7.3 w/w %). The decreased loading capacity can be attributed to some displacement of the surface-associated peptide as the DSPE is inserted within the lipid matrix of the SLN.

Based on the zeta potential results we decided to PEGylate SLN by 15 minutes of incubation with 10 and 30 w/w% DSPE-PEG_{2kDa} to generate particles with low positive zeta potential and neutral particles to be used for further studies. Indeed, low zeta potential, while slowing the diffusion across the mucus, may promote interaction with intestinal epithelium and absorption.

7.3.6. Lyophilization of the SLNs

This thesis project was aimed at producing EXEN-loaded SLNs for oral administration. In order to do that, SLNs have to be protected from the harsh acidic condition of the stomach and be delivered to the intestine, therefore a gastro-protected formulation must be set up. To this aim, we further processed the SLN suspension in order to lyophilize them and transfer the powder into hard gelatine enteric-coated capsules. Hence, SLNs obtained by processing 10% (w/w) EXEN/TOTAL lipid feed ratio and 12:1 DOTAP/EXEN molar ratio undergo the freeze-drying process. Different cryoprotectants such as trehalose, sucrose, glucose, glycerol, and mannitol can be used to decrease SLN aggregations during freeze-drying and facilitate the redispersion in water. In this project, mannitol and trehalose were employed for the freeze-drying process. Mannitol is used for acts by crystallizing within the matrix, which prevents macroscopic collapse of the bulk during drying. Trehalose was chosen because of its high glass transition temperature (Tg: (100-115 °C)[380], which generates a stable glassy matrix where particles can be embedded.

To this aim, first, freshly prepared SLNs were diluted to the lipid concentration of 3 mg/mL, and mannitol or trehalose solutions were added to SLNs suspension to yield a concentration in the 0.5-10% (w/v) range. After the freeze-drying SLN were resuspended for colloidal characterization as reported in *Figure 7.22.*

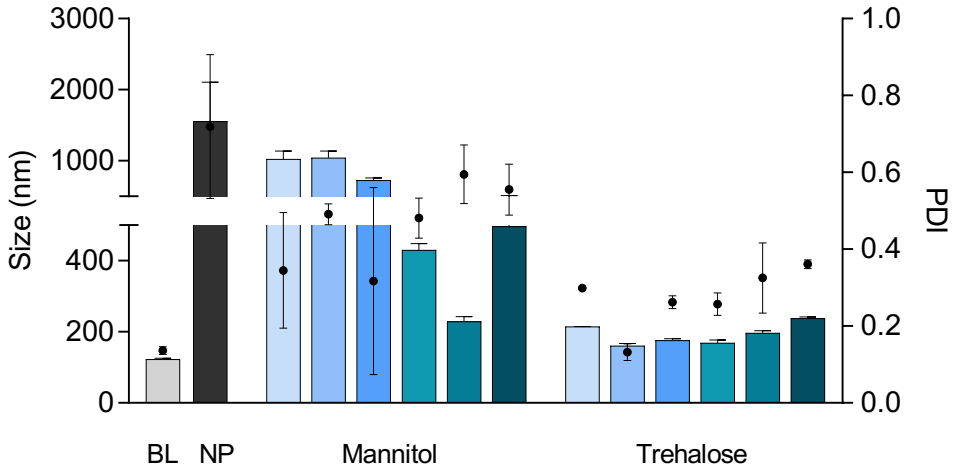

Figure 7.22. *The size and PDI profiles of the EXEN-loaded SLNs obtained processing 10% (w/w) EXEN/total lipid feed ratio and 12:1 DOTAP/EXEN molar ratio before (BL, ■) and after lyophilization without lyoprotectant (NP ■), and with 0.5 (■), 1 (■), 2.5 (■), 5 (■), 7.5 (■) and 10 (■) w/v% mannitol and trehalose concentrations.*

The quality of the lyophilization process can be derived by looking at several features such as cake integrity of the formulations, cake homogeneity and thickness, reconstitution time of the lyophilizate, and most importantly, size and PDI values of the particles after redispersion. Upon redispersion in the same volume of water where particles were dispersed before lyophilization, lyophilized SLN samples without lyoprotectant and with mannitol showed poor reconstitution in water, while the SLN samples with trehalose showed high reconstitution and were resuspended immediately.

SLNs lyophilized without lyoprotectants redispersed with visible aggregates with a size of about 1.5 µm. Results showed that by adding mannitol before lyophilization, particles aggregate after redispersion decreased in size as mannitol increased in concentration. The best performance for mannitol was obtained with 7.5 w/w% which provided a mean size of redispersed SLN of 229.6 ± 13.2 and the PDI was 0.595 ± 0.076. However, the size after redispersion was almost double with respect to the size of SLN before lyophilization. Furthermore, the polydispersity of the formulation was quite high and demonstrated a non-homogenous product. Even though the use of the mannitol did not ensure the same colloidal features of particles after redispersion, the use of mannitol provided good cake integrity. Indeed, mannitol facilitates freeze-drying and the elegant appearance of the freeze-dried products, thus commonly used in lyophilization as a bulking agent[381].

Trehalose showed better performance in terms of colloidal features of SLN when used as the lyoprotectant. This can be explained by the ability of the trehalose to form a glassy state outside of the SLNs by hydrogen bonding with the lipid head groups[382]. Except for the lowest and highest concentrations tested (i.e. 0.5 and 10%), the mean size of redispersed SLN was below 200 nm. The size and PDI values upon redispersion of SLN closest to the ones of SLN before lyophilization were obtained with 1 (w/v) % trehalose. The mean size was 161.0 ± 6.13 and the PDI was 0.13 ± 0.09. Although this lyophilization condition allowed for particle size below 200 nm and high colloidal homogeneity, a collapse of the cake integrity was observed. Indeed cake integrity is crucial to handle the lyophilized product for capsule filling. To this aim, the lowest trehalose concentration that provides SLN with a small size upon redispersion (1% w/v) was selected, while mannitol was included in the lyophilization process at 4:1, 2:1, and 1:1 trehalose/mannitol (T/M) weight ratios, resulting in total lyoprotectants concentrations of 1.25, 1.5 and 2 % w/v. Results of the particle size and PDI measurements of the SLNs after the freeze-drying and redispersion are reported in *Figure 7.23.*

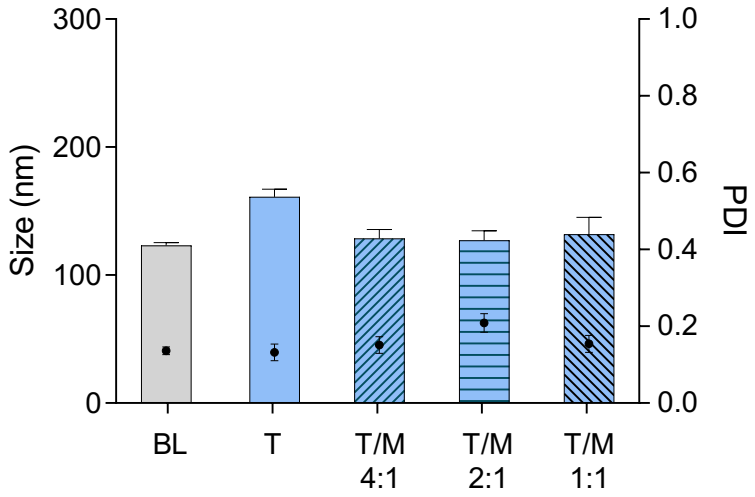

Figure 7.23. *The size and PDI profiles of the EXEN-loaded SLNs obtained processing 10% (w/w) EXEN/total lipid feed ratio and 12:1 DOTAP/EXEN molar ratio before (BL, ■) and after lyophilization with 1 w/v % trehalose(■) and with trehalose/mannitol (T/M) at 4:1 (▨), 2:1 (▤) and 1:1 (▧) w/w ratios.*

The measured particle sizes of SLN after redispersion in water were about 110 nm and very similar for the different trehalose/mannitol ratios. Measured PDI values for each condition were lower than 0.2. Although the size and PDI values of the redispersed SLNs were very close to those of SLN before lyophilization when 4:1 and 2:1 trehalose/mannitol ratios were used for lyoprotection, poor cake integrity was observed, while the 1:1 trehalose/mannitol ratio provided good cake integrity. Therefore, for the freeze-drying process, 1 w/v of 1:1 trehalose/mannitol ratio was selected as lyoprotectant for the freeze-drying of the SLNs generated with 10% (w/w) EXEN/TOTAL lipid feed ratio

and 12:1 DOTAP/EXEN ratio and of those decorated with 10 and 30 % (w/w) DSPE-$PEG_{2kDa.}$ Results of the particle size and PDI analysis are shown in *Figure 7.24.*

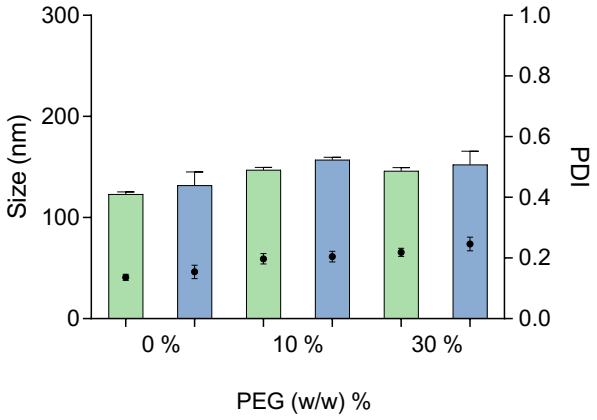

Figure 7.24. *The size and PDI of the EXEN-loaded SLNs with 0, 10 and 30 % (w/w)* DSPE-PEG_{2kDa} coating *before (■) and after (■) lyophilization with 1 % w/v of 1:1 w/w trehalose/mannitol ratio.*

SLNs before freeze drying had sizes of 123, 147, and 146 nm with 0, 10, and 30 % (w/w) PEGylation, respectively, and no significant change was observed. The results of the lyophilization study conducted on the SLNs with 0, 10 and 30 % (w/w) PEG showed that the use of the 2% w/v lyoprotectant composed of 1:1 w/w trehalose/mannitol ratio protects the colloidal features of all three formulations during the freeze-drying process.

7.4. Release studies

Release studies were performed on the selected SLN formulation prepared by processing a 10% (w/w) EXEN/total lipid feed ratio and 12:1 DOTAP/EXEN molar ratio. Release studies at 37 °C were carried out under two different conditions: in SIF at pH 6.8 to simulate the intestinal conditions and in PBS at pH 7.4 to simulate the microenvironmental extracellular interstitial conditions occurring after particles are absorbed through the intestinal epithelium.

The release profile of exenatide in SIF is reported in *Figure 7.25.*

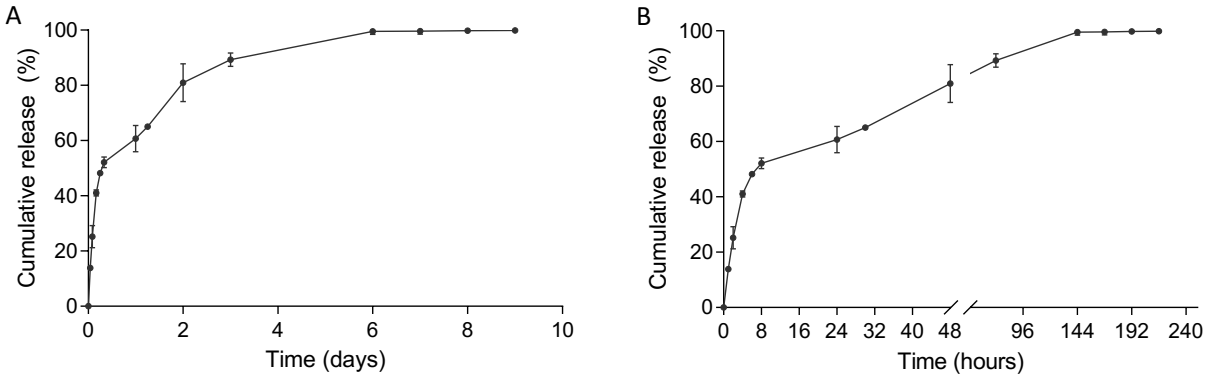

Figure 7.25*. The release profile of EXEN from SLNs obtained processing 10% (w/w) EXEN/total lipid feed ratio and 12:1 DOTAP/EXEN molar ratio. The release was carried out in SIF at pH 6.8 (A). Panel (B) shows the magnification of the release profile in the first 48 h.*

As reported in *Figure 7.25,* burst release occurred in the first 8 hours, with almost 50% of the exenatide released. After 48 hours the cumulative exenatide release achieved 80% and prologued slow release was observed afterward. After 144 hours (6 days) 100% of the exenatide was released from SLNs.

The kinetic release profile of EXEN from SLN in PBS is reported in *Figure 7.26*.

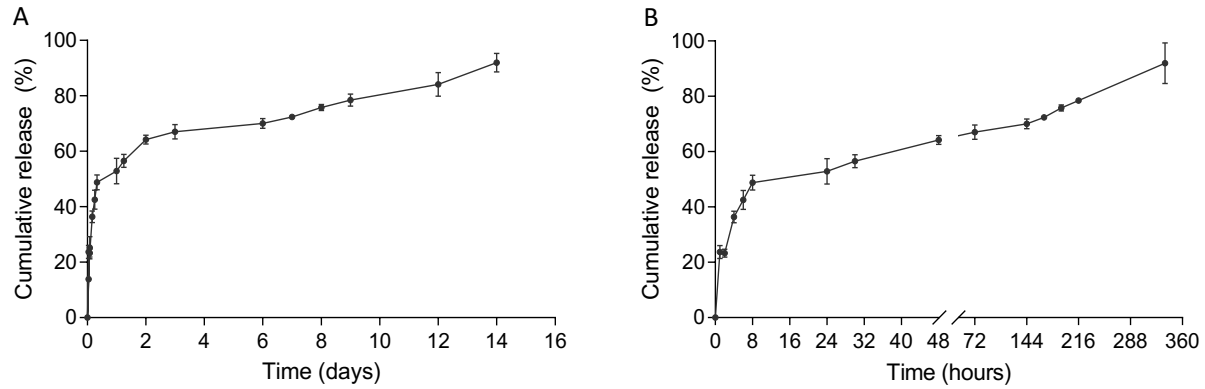

Figure 7.26. *The release profile of EXEN from SLNs obtained processing 10% (w/w) EXEN/total lipid feed ratio and 12:1 DOTAP/EXEN molar ratio. The release was carried out in PBS at pH 7.4 (A). Panel (B) shows the magnification of the release profile in the first 48 h.*

Similar to SIF, in PBS a burst release occurred and after 8 hours the release of EXEN was about 50%, followed by a slower release with respect to SIF. After 48 hours, the cumulative release reached 64% and after 216 hours (9 days) the release was not concluded as observed in SIF. Indeed, the residual 20% of the loaded EXEN was released over 5 additional days. On the 14th day, the amount of the EXEN released from SLNs was over 90%.

The burst release occurring under both pH conditions in the first 8 hours may be ascribable to the fraction of EXEN that is associated with the particle surface, and it is independent of the pH and

electrolytic conditions of the release environment. Indeed, the release profile in the two mediums used are overlapping during the first 8 hours. After 8 hours the two profiles slightly differed: in SIF at pH 6.8 the release was faster than in PBS at pH 7.4. It can be assumed that with the lipid matrix erosion, EXEN loaded in the lipid matrix dissociated from DOTAP and was released. While exenatide and DOTAP form a complex based on electrostatic interactions, the differences in pH and salt contents in the two conditions may dissociate differently the DOTAP/EXEN complexes. Indeed, at more acid conditions (pH 6.8) EXEN is closer to its isoelectric point and neutral charge which reduces interaction with the DOTAP within the SLN matrix, which may explain the faster release at pH 6.8 with respect to pH 7.4.

7.5. Colloidal stability studies

The colloidal stability of the EXEN-loaded SLNs produced with a 10% (w/w) EXEN/total lipid feed ratio and 12:1 DOTAP/EXEN molar ratio were investigated at 37 °C in SIF (pH 6.8), PBS (pH 7.4) and in PBS with 10 % (v/v) FBS. The size and PDI profile are reported in *Figure 7.27.*

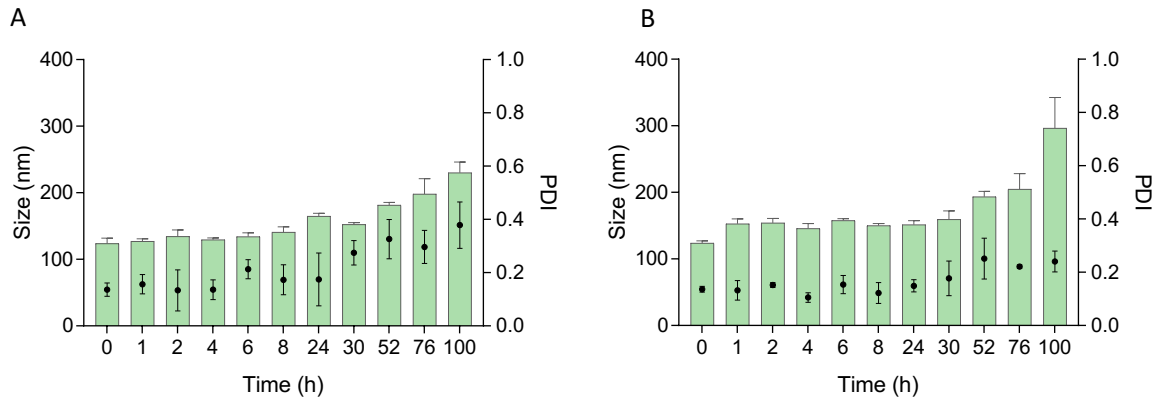

***Figure 7.27**. Size and PDI profiles of EXEN-loaded SLNs obtained processing 10% (w/w) EXEN/total lipid feed ratio and 12:1 DOTAP/EXEN molar ratio. The stability studies were carried out in SIF (A) and PBS (B) at 37 °C.*

In SIF, SLNs showed high stability over time. The size of the SLNs was 123.7 ± 2.5 nm and they had a PDI of 0.136 ± 0.01. After 24 hours, particle size and PDI values were slightly increased to 164.7 ± 4.2 nm and 0.174 ± 0.09, respectively. After 52 hours, size and PDI increase were more evident, indeed, the measured particle size was 181 ± 3.8 nm and PDI value was 0.32 ± 0.07, reaching a size of 230.2 ± 15.9 and PDI of 0.37 ± 0.08 after 100 hours. Similar to SIF, SLNs showed high stability in PBS. After 24 hours, particle size and PDI values of the SLNs were 151.5 ± 5.8 nm and 0.149 ± 0.02, respectively. After 30 hours, a gradual increase in particle size was observed. After 100 hours, the measured particle size in PBS was 296.5 ± 46 nm, and the PDI value was 0.24 ± 0.03. Under both experimental conditions,

particles were colloidally stable for about 30 h. The high colloidal stability of the SLNs can be attributed to their zeta potential which prevents aggregation by electrostatic repulsion.

Stability was also tested at a temperature mimicking a conventional storage condition, namely 4 °C. Freshly prepared SLNs were diluted with 1 mM HEPES buffer to a concentration of 0.35 mg/mL and stored at 4°C. The size distribution and PDI over time are reported in Figure 7.28.

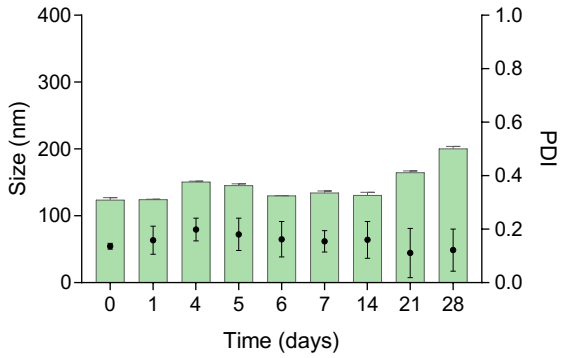

Figure 7.28. *The size and PDI profiles of the EXEN-loaded SLNs obtained processing 10% (w/w) EXEN/total lipid feed ratio and 12:1 DOTAP/EXEN molar ratio. The stability studies were carried out at 1 mM HEPES at 4 °C.*

The storage stability studies of the SLNs showed that solid lipid nanoparticles generated using lipids with a high transition temperature (HSPC and cholesterol) maintain their stability for a longer period of time at a temperature below their melting point compared to a temperature near their melting point even though this is an approximation being the medium different in term of buffer composition and concentration (Figure 7.27). This result can be attributed to their solid and partially crystalline state at the given conditions. Indeed a partially crystalline structure can lead to the coalescence and fusion of particles, while complete solid cores of particles prevent aggragation[383].

SLN stability was also tested in the presence of FBS to better understand their behavior in case of their biodistribution to the lymphatic drainage and the blood compartment after intestinal absorption. SLNs' stability can be altered upon the adsorption of biomolecules present in the biological fluids. The adsorption of proteins onto nanoparticles' surfaces is described as a “corona” formation[384]. The results of the colloidal stability in the presence of FBS are reported in *Figure 7.29*.

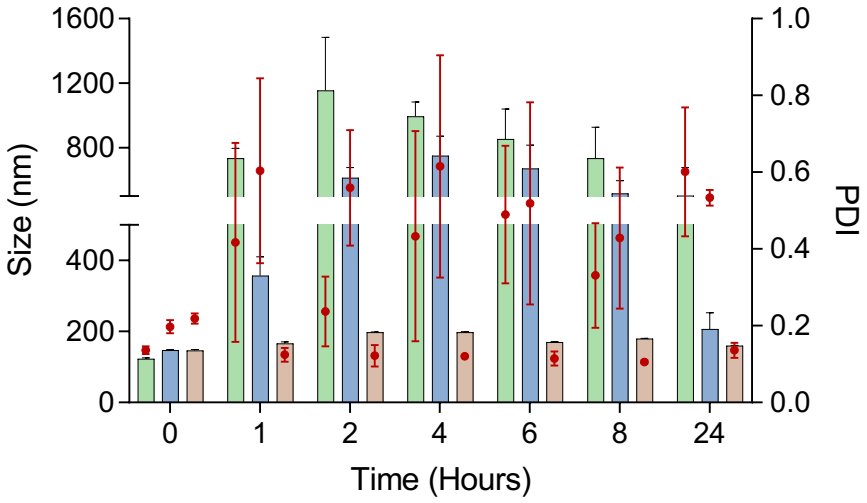

***Figure 7.29**. The size and PDI profiles of the EXEN-loaded SLNs obtained processing 10% (w/w) EXEN/total lipid feed ratio, 12:1 DOTAP/EXEN molar ratio and decorated with 0 ( ), 10 ( ) and 30 ( ) % w/w DSPE-PEG$_{2kDa}$. The stability studies were carried out in 10 % v/v FBS in PBS at 37 °C.*

As expected, the mean size of the non-PEGylated particles increased soon after contact with FBS, due to the adsorption of the negatively charged serum proteins on the surface of positively charged nanoparticles. Gessner et al showed that, due to favored electrostatic interactions, positively charged particles adsorb predominantly proteins with pI < 5.5, such as albumin[89].

Before the addition of the FBS to the nanoparticle suspension, the size of the SLNs was 123.7 ± 2.5 nm and they had a PDI of 0.136 ± 0.01. One hour after the addition of the FBS, the measured size was over 500 nm and became more than 1 µm after 2 hours. At this time point measured PDI was around 0.4, suggesting a disordered macro aggregation of the particles. Similar to the non-PEGylated SLNs, formulations decorated with 10% DSPE-PEG$_{2kDa}$ showed a size increase after 1 hour of incubation with FBS. At this time point, the measured particle size was 356.94 ± 53 nm and the PDI value was 0.60 ± 0.240, suggesting fast protein adsorption and some aggregation. However, the observed size increase was lower compared to the not PEGylated formulation, showing the beneficial shielding effect of PEG. In the following hours SLNs decorated with 10% PEG presented sizes over 500 nm and high polydispersity.

Unlike the SLNs with 0 and 10 percent, surface decoration with 30 % DSPE-PEG$_{2kDa}$, showed very high colloidal stability in the presence of FBS for 24 hours and negligible size alteration was detected. Indeed, the starting particle size of SLNs decorated with 30 % DSPE-PEG$_{2kDa}$ was 146.16 ± 3.3 nm and PDI value was 0.218 ± 0.013 and after 24 hours the size was 159.76 ± 1.0 and PDI value was 0.135 ± 0.019.

7.6. Morphological investigation

In order to elucidate if the EXEN-loaded particles possess a spherical shape and solid lipid matrix core like the EXEN-free particles discussed in section 7.3.1, a morphologic analysis was undertaken by Transmission Electron Microscopy (TEM).

The TEM images of the EXEN-loaded SLNs obtained processing 10% (w/w) EXEN/total lipid feed ratio and 12:1 DOTAP/EXEN molar ratio and their PEGylated version decorated with DSPE-PEG_{2kDa} at weight ratios of 10 and 30 percent are shown in Figure 7.30.

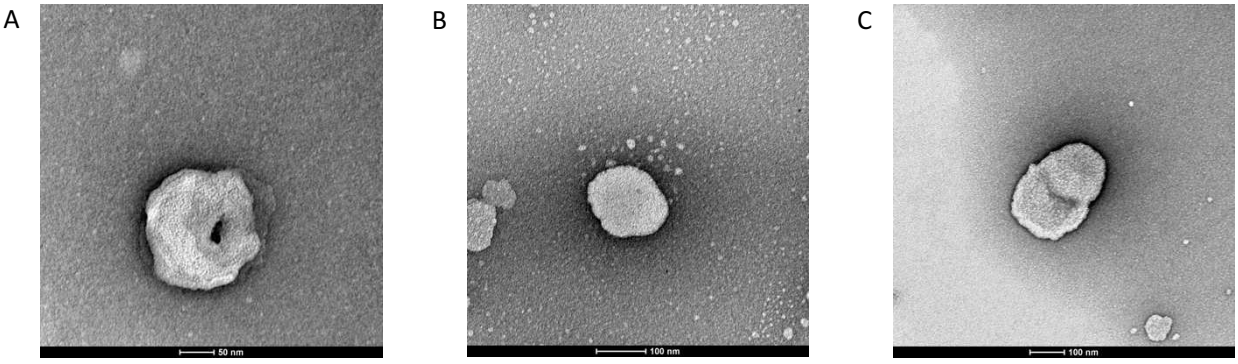

Figure 7.30. *Transmission electron microscopic images of EXEN loaded SLN without PEG coating (A), decorated with 10% (w/w) DSPE-PEG_{2kDa} (B) and with 30% (w/w) DSPE-PEG_{2kDa} (C). Scale bars for each image is 100 nm.*

The TEM images showed that solid core lipid particles were likely obtained. Indeed, liposomes imaged by TEM tend to collapse since the analysis is performed under vacuum conditions, which remove water inducing the liposomes to appear as 'ring-like' disks[385]. No effect was observed in terms of particle morphology after PEGylation. The sizes observed with the TEM analyses were in agreement with the sizes obtained by DLS analyses.

7.7. Mucin diffusion by FRAP analysis

Investigation of the diffusivity of the SLN in mucin is crucial to anticipate their potential for intestinal absorption and the need for improvement. As mucus acts as a selective barrier to the drugs or to drug delivery systems that are administered by oral route, it is very important to study their diffusion through mucin for drug delivery system development[386]. Indeed, the diffusion of drug delivery systems through mucin matrix has been studied by different groups[387-389]. Coating of the nanoparticle with the inert polymer PEG has been suggested as a strategy to improve the mobility of the nanoparticles in the mesh created by mucin[390]. Therefore, SLNs generated in this project were decorated with DSPE-PEG_{2kDa} as explained in section 6.2.3.5. to shield the cationic charges and form a dynamic hydration layer on the surface of the nanoparticles, thus decreasing the association to mucin and promote the

approach of the SLN to the intestinal epitelium[391]. FRAP analysis was performed to study the diffusivity of the EXEN-loaded SLNs through mucin and representative images and fluorescence recovery profiles are reported in *Figure 7.32.*

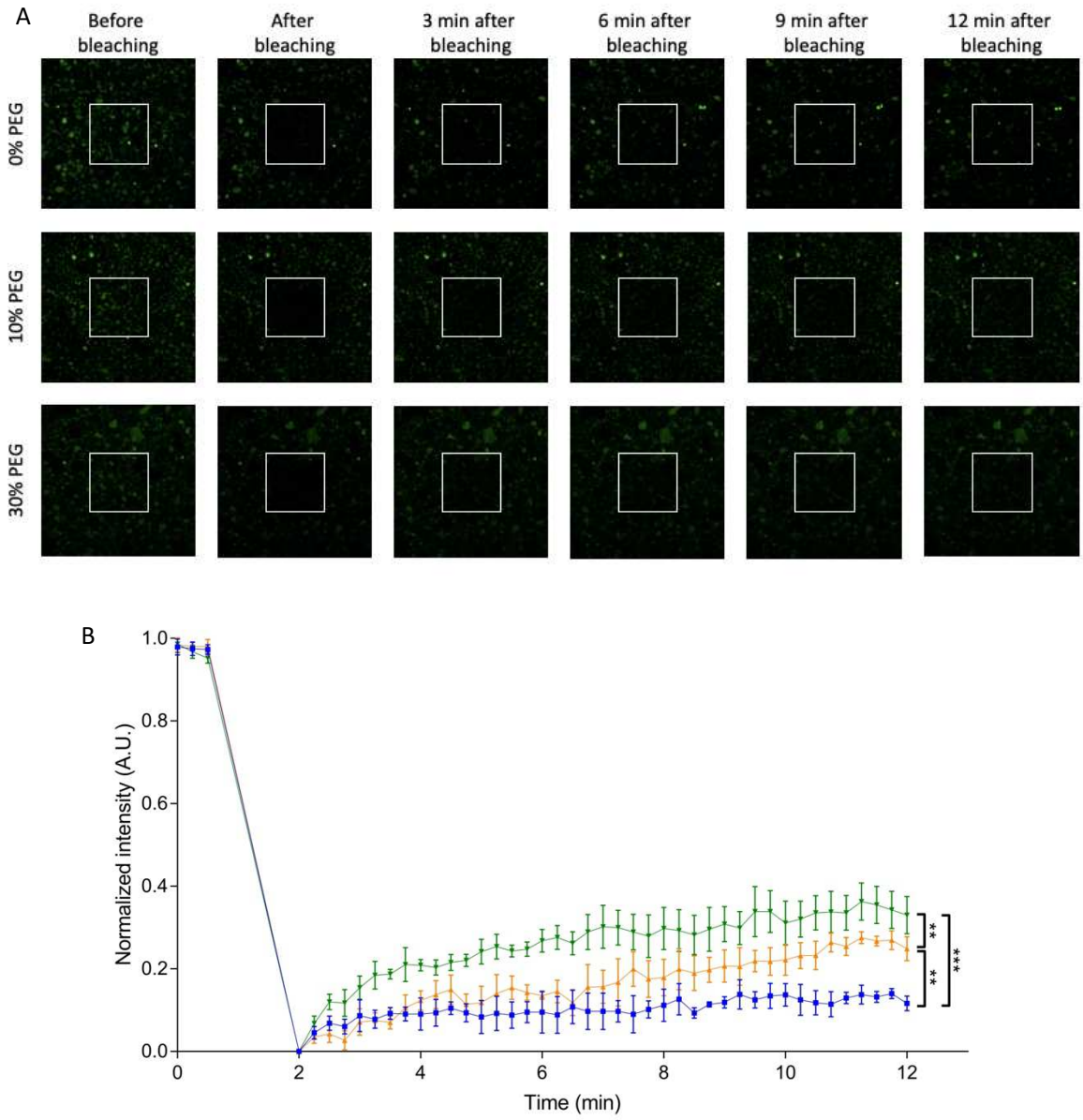

Figure 7.32. *Fluorescence recovery after photobleaching of fluorescein-labelled SLNs decorated with 0, 10 and 30 % (w/w) DSPE-PEG$_{2kDa}$ in 2% (w/w) mucin gel. Representative images before and after bleaching of mucin solution mixed with SLNs with 0% PEG (top raw), 10% PEG (middle raw), 30% PEG (bottom raw) (A) and representative normalized fluorescence recovery profiles obtained from the mucin solutions containing SLNs with 0% PEG (—), 10% PEG (—), 30% PEG (—). Statistical analysis: **p < 0.01, ***p < 0.001.*

Our results of FRAP analysis demonstrated that SLNs without PEG coating, strongly interact with the negatively charged mucin solution, which can be attributed to the highly positive zeta potential of the particles (+53 mV). Indeed, 12 minutes after the photobleaching process, the fluorescence recovery percentage was about 11%. As expected, the PEGylation of the SLNs increased the fluorescence

recovery of the bleached area. The percentage of the recovery was about 25% for the mucin solutions mixed with the 10 w/w% PEGylated SLNs. As the PEG ratio used for the SLNs decoration was increased to 30 w/w%, the fluorescence recovery ratio rose to 33% compared to that of the SLNs decorated with 10 w/w% PEG. PEGylation shields the SLN surface which lowers the mucoadhesion by reducing both electrostatic and hydrophobic interactions[392].

7.8. Stability of exenatide

7.8.1. Conformational stability

Circular dichroism (CD) is a spectroscopic method used to evaluate the conformation of peptides and proteins. In this thesis project, the CD was performed to evaluate the conformation of exenatide processed by microfluidics, released from SLNs after formulation, and also released from SLNs after lyophilization. During SLNs assembly, exenatide is exposed to 25% of ethanol (FRR = 3:1), shear stress at 12 mL/min in the microfluidic chamber, and dialysis to remove the organic solvent and non-loaded EXEN. EXEN released from SLNs has been additionally exposed to contact with DOTAP and the other lipids. Furthermore, EXEN released by SLN lyophilization is exposed to freezing and dehydration which can result in conformational stability change[393].

The results from CD spectroscopic analyses are shown in *Figure 7.32.*

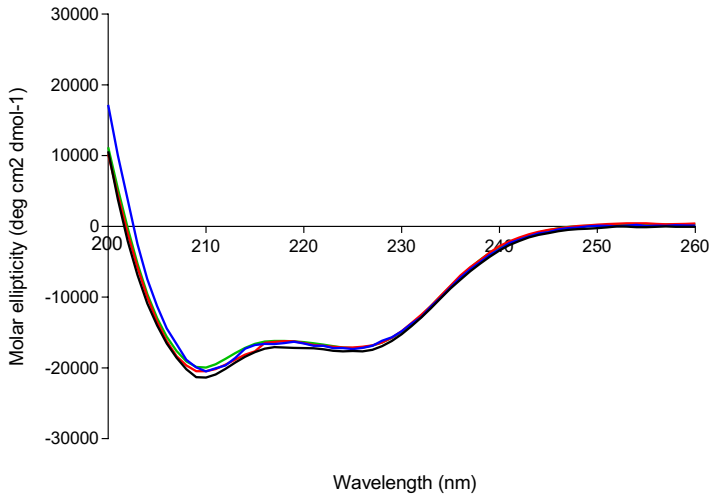

Figure 7.32. *Circular dichroism spectra of EXEN solutions: native peptide (—), microfluidic processed (—), released from freshly prepared SLNs (—) and released from freeze-dried SLNs (—) in Milli-Q water.*

The CD spectra of the EXEN exposed to the microfluidic process conditions, EXENreleased from the freshly prepared SLN, and from freeze-dried SLNs were similar to the spectra of the native non-treated EXEN, showing two minima, at about 208 nm and 222 nm, which is a fingerprint of the α-helical structure[394].

The secondary structure content of the exenatide was calculated with the software BeStSel software by elaborating the CD profiles as shown in Figure 7.33.

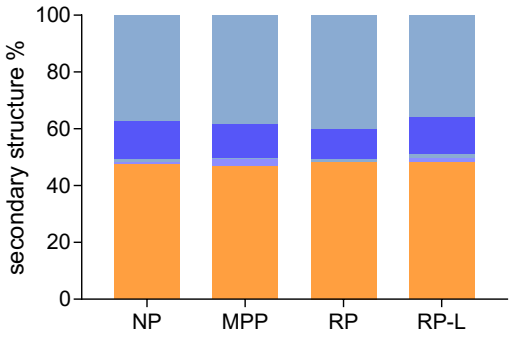

Figure 7.33. *Secondary structure content (%) of native peptide (NP), microfluidic processed peptide (MPP), peptide released from SLNs (RP) and peptide released from lyophilized SLNs (RP-L): α-helix (■), β-antiparallel (■), β-parallel (■), β-turn (■) and random coil (■).*

The α-helix content was predominant and corresponds to 47.5, 46.6, 48.3 and 48.2 % for native, microfluidic processed, EXEN released from freshly prepared SLNs and lyophilized SLNs, respectively. The conformation of peptides and proteins is crucial to ensure their therapeutic effect and can be easily altered under a variety of conditions such as high temperature, mechanical mixing and exposure to organic solvents. Results of the structural analysis of the EXEN processed in microfluidics and released from SLNs showed that alteration of the secondary structure and unfolding does not occur during exposure to the conditions required by the microfluidic nanoprecipitation technique and that reasonably the structure is also maintained within the core of the SLN. Furthermore, selected lyophilization conditions did not cause a change in the secondary structure content of the SLNs.

7.8.2. Chemical stability

Peptides and proteins can undergo a variety of chemical degradation fenomena. It has frequently been observed that peptides degrade at rates that are faster than those that can be inferred from the degradation rates of their individual amino acid residues.The most common degradation mechanism of peptides and proteins include hydrolysis, deamidation, and oxidation. These issues are caused by

process stress such as pH changes, heat, presence of organic solvents, light exposure and result in the biological activity loss[395].

We investigated the chemical stability of microfluidic processed EXEN, EXEN released from the freshly prepared SLNs and from freeze-dried SLNs were analyzed by electrospray ionization-time of flight mass spectrometry (ESI-TOF MS) and compared to the non-treated EXEN of Results from all four MS analyses are shown in the *Figure 7.34.*

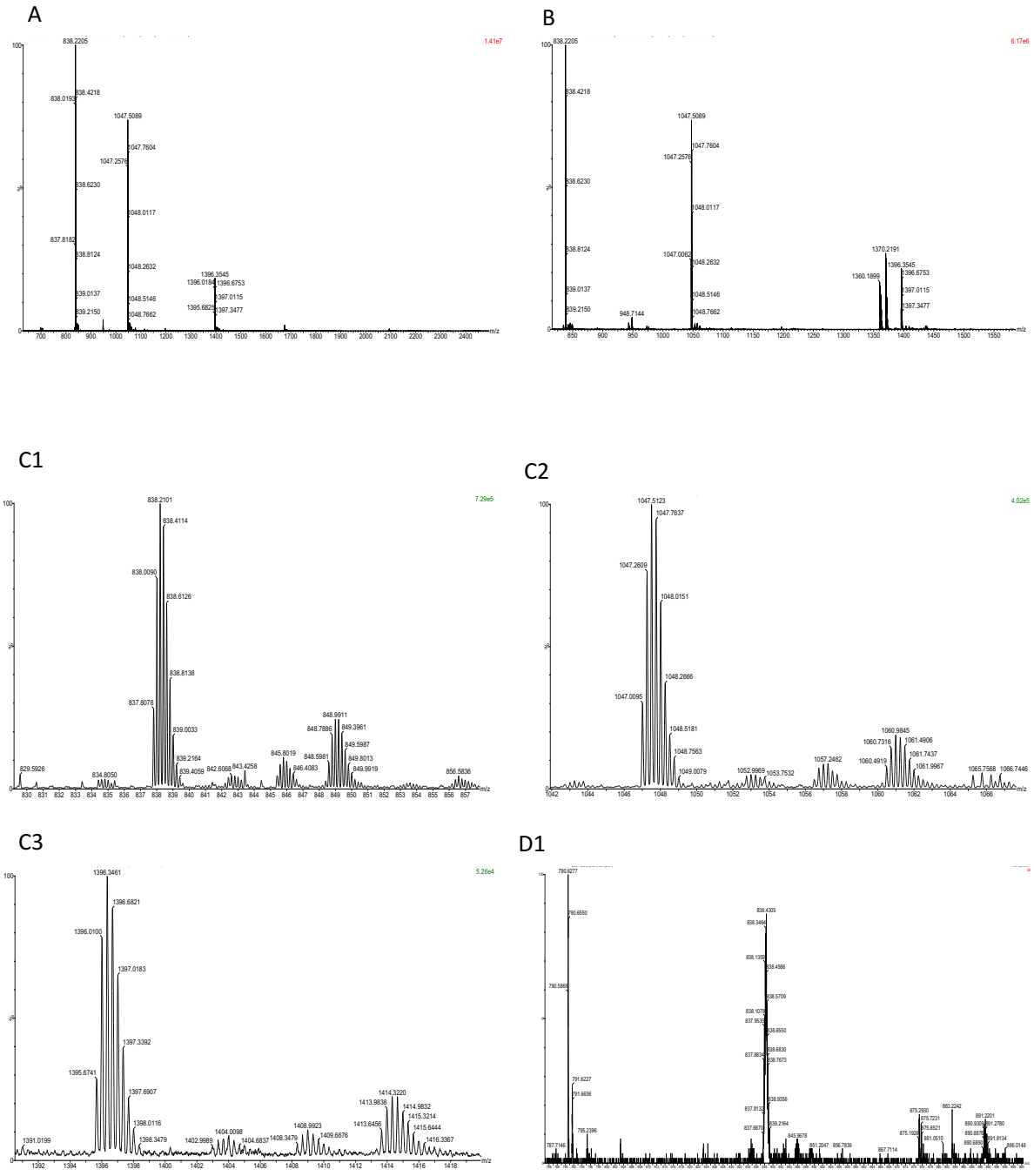

D2

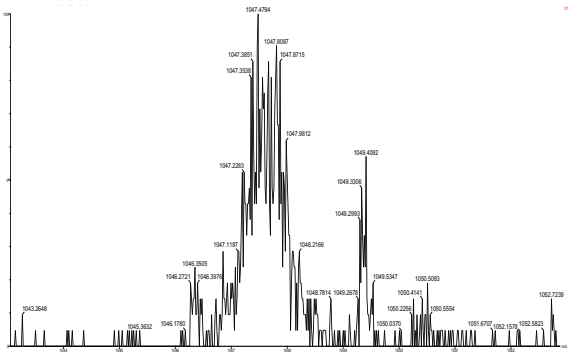

***Figure 7.34**. ESI-TOF mass spectra of native EXEN (A), microfluidic processed EXEN (B), EXEN released from SLNs (C1, C2, C3)) and EXEN released from lyophilized SLNs (D1 and D2).*

The positive electrospray ionization of native EXEN (4,186.7 Da) yielded the $[M+5H]^{5+}$ signal at *m/z* 838.21, $[M+4H]^{4+}$ at m/z 1047.50, and $[M+3H]^{3+}$ at m/z 1396.35 as most intense ions. The signals observed in Figure 7.32, Panel B, having m/z 838.22 ($[M+5H]^{5+}$), 1047.50 ($[M+4H]^{4+}$) and 1396.35 ($[M+3H]^{3+}$) confirmed the chemical integrity and no degradation of the exenatide upon exposure to the microfluidics process. Figure 7.32, Panels C1, C2, and C3 show m/z signals at 837.80, 1047.00, and 1396.01, which demonstrate the chemical integrity and no degradation of the exenatide released from the SLNs. Finally, mass spectroscopy analysis of the EXEN released from the freeze-dried SLNs showed signals at 838.22 ($[M+5H]^{5+}$) and 1047.50 ($[M+4H]^{4+}$) (Figure 7.34 Panels D1 and D2) showing that selected conditions for the freeze drying did not alter the chemical structure of the EXEN.

7.9. Enteric-coating of the capsules

This project aims at administering the SLNs by oral route. Therefore SLN and EXEN must be protected from the acidic environment of the stomach which was provided by encapsulating EXEN-loaded SLNs into hard gelatine capsules followed by enteric-coating. To this aim, the enteric coating of the No.4 hard gelatine capsules with Eudragit L100 was performed as described in *section 6.2.1.5.*

Preliminarily the capsules were loaded with Rhodamine/starch mixture to test the efficiency of the enteric coating in HCl pH 1.2 and SIF pH 7.4 by measuring the released rhodamine B by spectrofluorometric analysis. The release profile of rhodamine B from capsules is reported in *Figure 7.35*.

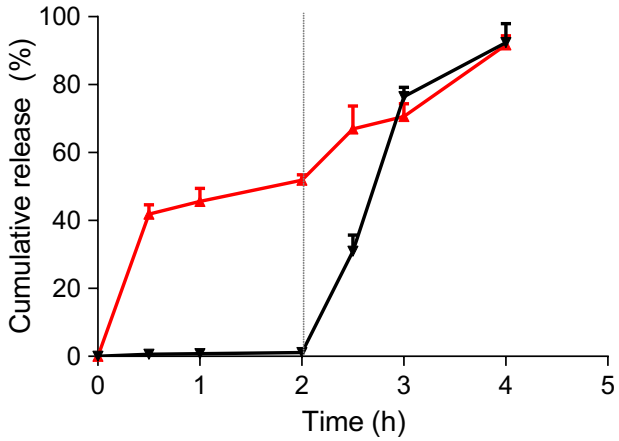

Figure 7.35. *The release profile of rhodamine B from non coated (—) and enteric-coated (—) hard gelatine capsules. The release was performed in HCl pH 1.2 for the first 2 hours, then the medium was replaced with SIF pH7.4.*

The coating thickness is an important factor in most enteric coating formulations, since it may drastically change the dissolving profile of the capsule. Our results showed that the enteric-coating of the capsules provides good enteric protection properties. As shown in *Figure 7.35*, no rhodamine B release in the acid environment was detected. Two hours of exposure time was selected in order to mimic the physiological gastric emptying[396]. When capsules were exposed to SIF, immediate rhodamine release was observed, indicating that the number of the coating step and the resulting thickness of the coating is sufficient for protecting the underlying capsule in an acidic environment while it also undergoes quick dissolution at pH 7.4 thus exposing the capsule to water and allowing for its dissolution and break. Furthermore, the low standard deviation along the release profile of the enteric-coated capsules was indicative of the homogeneous coating thickness of the capsules.

The release profile of Rhodamine B from non-coated hard gelatine capsules confirmed that the absence of coating induced the quick break of the capsules in the simulated gastric environment. Indeed, more than 40% of the encapsulated Rhodamine B was released in the first hour.

7.10. In-vitro cellular studies

7.10.1. Cytotoxicity studies

The MTT assay is a colorimetric test that measures cellular metabolic activity as an indicative parameter of the number of viable cells. Indeed, MTT is a yellow compound that is reduced by mitochondrial reductase present on live cells to a crystalline violet product (Figure 7.36). Crystals can

be dissolved using isopropanol or dimethyl sulfoxide (DMSO) and the resulting violet solution can be analyzed by spectrophotometry. The absorbance of the solution correlates with the number of living cells in the samples.

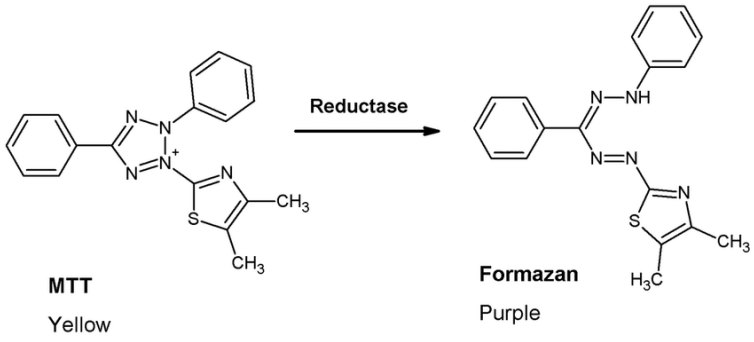

Figure 7.36. *Enzymatic reduction of MTT to formazan by the mitochondrial reductase of live cells.*

Cell viability studies were performed in order to test the possible cytotoxic effect of EXEN-loaded SLNs. Caco-2 cell line, a human intestinal epithelial cell line, was selected for the in-vitro studies, as it has been extensively used over the last twenty years as a model of the intestinal barrier. The SLN formulations prepared by processing 10% (w/w) EXEN/lipid feed ratio and 12:1 DOTAP/EXEN molar ratio and decorated with 0, 10, and 30 % w/w DSPE-PEG_{2kDa} were tested for cytotoxicity. Results of the cell viability are shown in *Figure 7.37.*

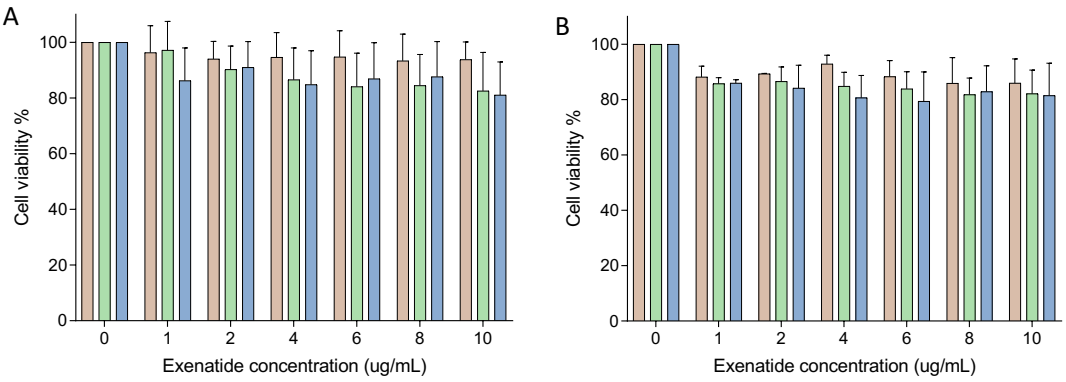

Figure 7.37.*The cell viability profile of the Caco-2 cells treated with EXEN-loaded SLNs (decorated with 0 (■), 10 (■) and 30 (■) % w/w DSPE-PEG_{2kDa} at increasing EXEN equivalent concentration before (A) and after (B) freeze-drying process and reconstitution at increasing EXEN concentration.*

Results of the cytotoxicity tests showed that PEG-free and PEG-coated EXEN loaded-SLNs composed of HSPC, cholesterol, and cationic lipid DOTAP are not significantly cytotoxic on Caco-2 cells after 4 hours of incubation. Indeed, at the increasing EXEN concentrations tested, cell viability was over 80

percent, which is considered as non-cytotoxic[397]. Even though cytotoxicity is a quite common feature of most of the cationic nanocarriers, having limited cytotoxicity can be explained by the fact that the DOTAP/[phospholipid and cholesterol] ratio is constrained in the SLNs.

The cytocompatibility of the PEG-free and PEG-coated EXEN loaded SLNs after the freeze-drying process with 2 % (w/v) 1:1 w/w trehalose/mannitol mixture and reconstitution in water was also investigated. Results of the cell viability is shown in *Figure 7.37, Panel B*. Similar to the freshly prepared SLNs, formulations after the lyophilization process have also shown a safe profile. Trehalose is a disaccharide found at high concentrations in a variety of organisms[398], and it is commonly used for the lyophilization process for its safe and efficient lyopreservation[399]. Besides that, mannitol has been widely used in pharmaceutical products over the past 60 years in virtue of its long-established safety profile[400]. Thereby, the selected concentration of lyoprotectans was safe within the dosage range tested.

7.10.2. Cellular association studies

Quantification of the cell association by flow cytometry analysis

The estimation of the cellular association of non-PEGylated and PEGylated SLNs was investigated by flow cytometric analysis using EXEN-loaded fluorescein-DHPE labeled SLNs. The mean fluorescence intensity (MFI) values and the number of positive cells were quantified and the results are shown in *Figure 7.38.*

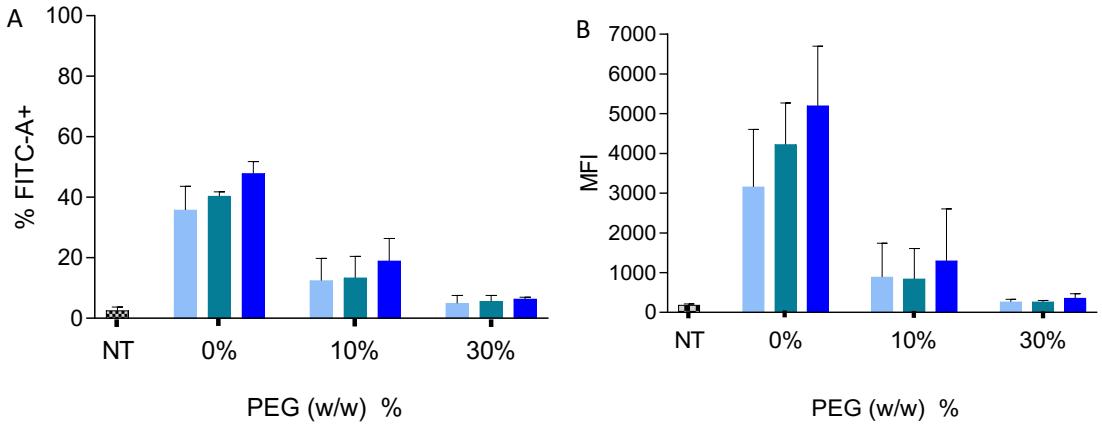

Figure 7.38. *Flow cytometric profile of Caco-2 cells before (not treated, NT (■)) and after 4 hours of incubation with SLNs decorated with 0, 10, and 30 % w/w DSPE-PEG$_{2kDa}$ at exenatide concentrations of 6 (■), 8 (■) and 10 (■) µg/mL. Results were expressed as a number of the positive cells % (A) and as Mean Fluorescence Intensity (MFI).*

Flow cytometric analysis showed up to 50% positive Caco-2 cells upon incubation with fluorescently labeled PEG-free EXEN-loaded SLNs at 10 µg/mL EXEN equivalent concentration. Indeed, the measured MFI value for this condition was 5198.5 ± 1500.3. Upon surface decoration with 10% w/w DSPE-PEG_{2kDa}, an expected decrease in the SLN association of cells was observed. The SLNs at 10 µg/mL exenatide equivalent concentration yielded only 18.95 ± 7.4 % of positive cells, and this value further decreased to 6.38 ± 0.58 % when cells were incubated with the SLNs decorated with 30% w/w DSPE-PEG_{2kDa}. These results were not surprising because PEG is a flexible hydrophilic polymer and effectively shields the nanoparticles' surface from the surrounding environment, thereby minimizing cellular association of the SLNs under in vitro conditions[401], which on the other hand, is mediated by the cationic charges on PEG-free SLN. Notably, the intestinal lumen transcytosis is mainly attributed to the M cells[402], which are located in the intestinal epithelium[403], which can be favored by the PEGylation of the positively charged nanoparticles that can prevent the stacking of particles in the mucus[377] .

It is widely acknowledged that the surface features of nanoparticles play a crucial role in absorption by intestinal epithelial cells. A balance between exposed surface cationic charges and shielding of those charges is thus crucial to compromise a good diffusion of particles across the mucus and a suitable approach of particles to epithelial cells for transcytosis.

Indeed, the selected formulations with a different degree of surface coating have been tested in vitro to better understand their behavior and will be further evaluated in ex-vivo and in vivo models.

Confocal imaging of Caco-2 cells

The cellular association of the SLNs was imaged by confocal microscopy on Caco-2 cells after 4 hours incubation with the EXEN-loaded fluorescein-DHPE labeled SLNs. The recorded images are shown in *Figure 7.39.*

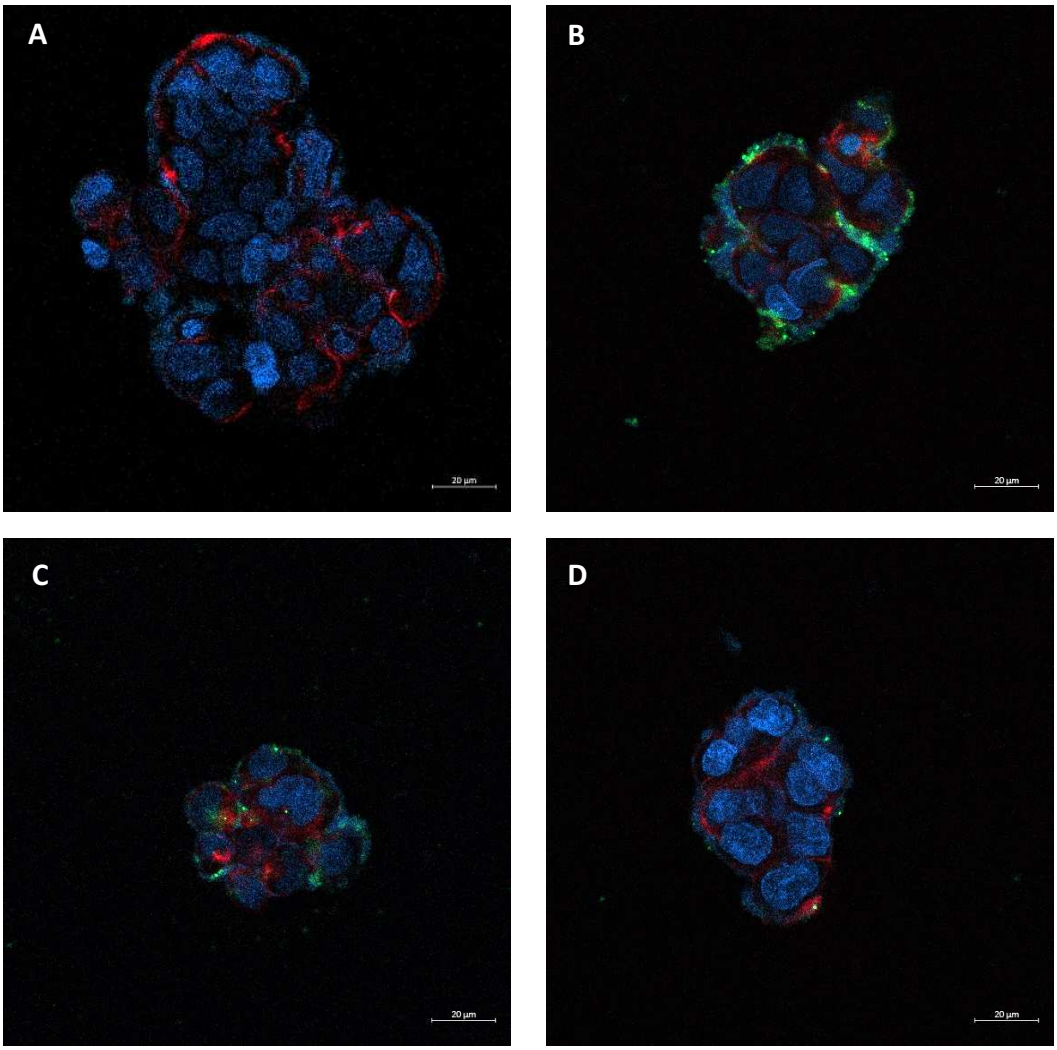

Figure 7.39. *Representative confocal images of untreated Caco-2 cells (A) and those after 4 hours of incubation with fluorescein-DHPE labeled SLNs decorated with 0 (B), 10 (C) and 30 (D) % (w/w) DSPE-PEG$_{2kDa}$ at EXEN equivalent concentration of 10 µg/mL. Cell nuclei were stained with DAPI (blue), cell membranes were stained with WGA-AF633 (red) and SLNs were labelled with Fluorescein-DHPE (green).*

The qualitative results obtained by confocal imaging were in agreement with the flow cytometric analysis performed to quantify the cellular association of the SLNs. Indeed, SLNs without surface decoration with PEG were highly associated to the Caco-2 cells (Figure 7.38., Panel B). On the other hand, the surface decoration of the SLNs with 10 and 30 w/w% of DSPE-PEG$_{2kDa}$ decreased their association to cells (Figure 7.39, Panels C and D, respectively) which was ascribed to the reduced electrostatic interaction of the cationic particles with anionic cell membrane.

8. CONCLUSIONS

This project was aimed at developing solid lipid nanoparticles by the microfluidics approach for the oral delivery of the antidiabetic agent, exenatide. The microfluidic processing conditions and SLN composition were systematically investigated in order to optimize the formulation. The selected SLN formulation presented a spherical shape, small size, low PDI, high colloidal stability, loading efficiency, and capacity, suggesting that the use of the hydrophobic ion paring technique and microfluidic is a suitable approach for the encapsulation of the exenatide to solid lipid nanoparticles.

The mucus layer present in the intestinal epithelium limits the oral delivery of the positively charged nanoparticles. Therefore the surface decoration of the SLNs with PEG was investigated to shield the cationic charge that results from the inclusion of DOTAP in the particle composition. Indeed, FRAP analysis showed that with the surface decoration of the SLNs with PEG, mobility of the SLNs in mucin is significantly increased.

The lyophilization process was investigated to obtain the SLNs in a solid state for hard gelatin capsule filling by including trehalose and the bulking agent mannitol as lyoprotectant at suitable concentration and ratio. The resulting lyophilized SLNs possess a uniform and elegant cake appearance, with no signs of collapse and cracking. Furthermore, selected conditions yield particles with size and homogeneity unaltered once redispersed in water with respect to those before lyophilization.

The circular dichroism and mass spectroscopic analyses were performed to evaluate the exenatide's conformational and chemical stability throughout the formulation process. The α-helix content and chemical stability were conserved during the processing steps to generate SLNs with the microfluidic techniques, and also through the freeze-drying process.

The enteric coating made with Eudragit L100 on hard gelatine capsules maintained the integrity of the capsules in a condition that simulates gastric fluid whereas in simulated intestinal fluid an immediate disintegration was observed, showing an effective coating.

In vitro cytotoxicity tests revealed that SLNs with and without PEG decoration did not cause toxicity to the Caco-2 cell line. The cytofluorimetric study and confocal imaging showed that particles associate with cells and that the extent of association inversely correlated with the PEG coating as a result of the shielding of the cationic charges on the SLN surface attributed to the cationic DOTAP in the lipid composition. Further in vitro and ex-vivo studies will allow us to select the formulation that most efficiently can undergo transcytosis providing suitable drug absorption.

In conclusion, the developed therapeutic system could offer a novel option for the oral administration of exenatide, providing a therapeutic option for the management of T2DM, as well as for different peptides to overcome the barriers related to the oral administration of biologics.

9. REFERENCES

1. Administration, U. F. a. D. What is Gene Therapy? https://www.fda.gov/vaccines-blood-biologics/cellular-gene-therapy-products/what-gene-therapy (accessed 16.12.2021).
2. Wirth, T.; Parker, N.; Ylä-Herttuala, S., History of gene therapy. *Gene* **2013,** *525* (2), 162-169.
3. Papanikolaou, E.; Bosio, A., The promise and the hope of gene therapy. *Frontiers in genome editing* **2021,** *3*, 618346.
4. Sung, Y.; Kim, S., Recent advances in the development of gene delivery systems. *Biomaterials research* **2019,** *23* (1), 1-7.
5. Manjila, S. B.; Baby, J. N.; Bijin, E. N.; Constantine, I.; Pramod, K.; Valsalakumari, J., Novel gene delivery systems. *International journal of pharmaceutical investigation* **2013,** *3* (1), 1.
6. Ginn, S. L.; Amaya, A. K.; Alexander, I. E.; Edelstein, M.; Abedi, M. R., Gene therapy clinical trials worldwide to 2017: An update. *The journal of gene medicine* **2018,** *20* (5), e3015.
7. Misra, A., *Challenges in delivery of therapeutic genomics and proteomics*. Elsevier: 2010.
8. Zhang, W.-W.; Li, L.; Li, D.; Liu, J.; Li, X. Z., 2018 #126}; Li, W.; Xu, X.; Zhang, M. J.; Chandler, L. A.; Lin, H., The first approved gene therapy product for cancer Ad-p53 (Gendicine): 12 years in the clinic. *Human gene therapy* **2018,** *29* (2), 160-179.
9. Darrow, J. J., Luxturna: FDA documents reveal the value of a costly gene therapy. *Drug Discovery Today* **2019,** *24* (4), 949-954.
10. Weng, Y.; Huang, Q.; Li, C.; Yang, Y.; Wang, X.; Yu, J.; Huang, Y.; Liang, X.-J., Improved nucleic acid therapy with advanced nanoscale biotechnology. *Molecular Therapy-Nucleic Acids* **2020,** *19*, 581-601.
11. Espeseth, A. S.; Cejas, P. J.; Citron, M. P.; Wang, D.; DiStefano, D. J.; Callahan, C.; Donnell, G. O.; Galli, J. D.; Swoyer, R.; Touch, S., Modified mRNA/lipid nanoparticle-based vaccines expressing respiratory syncytial virus F protein variants are immunogenic and protective in rodent models of RSV infection. *npj Vaccines* **2020,** *5* (1), 1-14.
12. Kumar, A.; Blum, J.; Le T, T.; Havelange, N.; Magini, D.; Yoon, I.-K., The mRNA vaccine development landscape for infectious diseases. *Nature reviews. Drug Discovery* **2022**.
13. Zamecnik, P. C.; Stephenson, M. L., Inhibition of Rous sarcoma virus replication and cell transformation by a specific oligodeoxynucleotide. *Proceedings of the National Academy of Sciences* **1978,** *75* (1), 280-284.
14. Reischl, D.; Zimmer, A., Drug delivery of siRNA therapeutics: potentials and limits of nanosystems. *Nanomedicine: Nanotechnology, Biology and Medicine* **2009,** *5* (1), 8-20.
15. Tokatlian, T.; Segura, T., siRNA applications in nanomedicine. *Wiley Interdisciplinary Reviews: Nanomedicine and Nanobiotechnology* **2010,** *2* (3), 305-315.
16. Fumoto, S.; Kawakami, S.; Hashida, M.; Nishida, K., Targeted gene delivery: importance of administration routes. *Novel Gene Therapy Approaches* **2013**, 3-31.
17. Villate-Beitia, I.; Puras, G.; Zarate, J.; Agirre, M.; Ojeda, E.; Pedraz, J. L., First insights into non-invasive administration routes for non-viral gene therapy. *Gene Therapy-Principles and Challenges* **2015**, 145-177.
18. Farris, E.; Heck, K.; Lampe, A. T.; Brown, D. M.; Ramer-Tait, A. E.; Pannier, A. K., Oral non-viral gene delivery for applications in DNA vaccination and gene therapy. *Current opinion in biomedical engineering* **2018,** *7*, 51-57.
19. Kriegel, C.; Amiji, M., Oral TNF-α gene silencing using a polymeric microsphere-based delivery system for the treatment of inflammatory bowel disease. *Journal of controlled release* **2011,** *150* (1), 77-86.
20. Cader, M. Z.; Kaser, A., Recent advances in inflammatory bowel disease: mucosal immune cells in intestinal inflammation. *Gut* **2013,** *62* (11), 1653-1664.

21. Du, L.; Yu, Z.; Pang, F.; Xu, X.; Mao, A.; Yuan, W.; He, K.; Li, B., Targeted delivery of GP5 antigen of PRRSV to M cells enhances the antigen-specific systemic and mucosal immune responses. *Frontiers in cellular and infection microbiology* **2018,** *8*, 7.
22. Kinsey, B. M.; Densmore, C. L.; Orson, F. M., Non-viral gene delivery to the lungs. *Current gene therapy* **2005,** *5* (2), 181-194.
23. Merkel, O. M.; Zheng, M.; Debus, H.; Kissel, T., Pulmonary gene delivery using polymeric nonviral vectors. *Bioconjugate chemistry* **2012,** *23* (1), 3-20.
24. Geiger, J.; Aneja, M. K.; Rudolph, C., Vectors for pulmonary gene therapy. *International journal of pharmaceutics* **2010,** *390* (1), 84-88.
25. Keil, T. W.; Feldmann, D. P.; Costabile, G.; Zhong, Q.; da Rocha, S.; Merkel, O. M., Characterization of spray dried powders with nucleic acid-containing PEI nanoparticles. *European Journal of Pharmaceutics and Biopharmaceutics* **2019,** *143*, 61-69.
26. Zhang, H.; Leal, J.; Soto, M. R.; Smyth, H. D.; Ghosh, D., Aerosolizable lipid nanoparticles for pulmonary delivery of mRNA through design of experiments. *Pharmaceutics* **2020,** *12* (11), 1042.
27. Hanson, L. R.; Frey, W. H., Intranasal delivery bypasses the blood-brain barrier to target therapeutic agents to the central nervous system and treat neurodegenerative disease. *BMC neuroscience* **2008,** *9* (3), 1-4.
28. Sava, V.; Fihurka, O.; Khvorova, A.; Sanchez-Ramos, J., Enriched chitosan nanoparticles loaded with siRNA are effective in lowering Huntington's disease gene expression following intranasal administration. *Nanomedicine: Nanotechnology, Biology and Medicine* **2020,** *24*, 102119.
29. Xu, D.; Khan, M. A.; Klufas, M. A.; Ho, A. C., Administration of Ocular Gene Therapy. *International ophthalmology clinics* **2021,** *61* (3), 131-149.
30. Garba, A. O.; Mousa, S. A., Bevasiranib for the treatment of wet, age-related macular degeneration. *Ophthalmology and Eye Diseases* **2010,** *2*, OED. S4878.
31. Rittenhouse, K. D.; Johnson, T. R.; Vicini, P.; Hirakawa, B.; Kalabat, D.; Yang, A. H.; Huang, W.; Basile, A. S., RTP801 gene expression is differentially upregulated in retinopathy and is silenced by PF-04523655, a 19-Mer siRNA directed against RTP801. *Investigative ophthalmology & visual science* **2014,** *55* (3), 1232-1240.
32. Moreno-Montañés, J.; Sádaba, B.; Ruz, V.; Gómez-Guiu, A.; Zarranz, J.; González, M. V.; Pañeda, C.; Jimenez, A. I., Phase I clinical trial of SYL040012, a small interfering RNA targeting β-adrenergic receptor 2, for lowering intraocular pressure. *Molecular Therapy* **2014,** *22* (1), 226-232.
33. Titze-de-Almeida, R.; David, C.; Titze-de-Almeida, S. S., The race of 10 synthetic RNAi-based drugs to the pharmaceutical market. *Pharmaceutical research* **2017,** *34* (7), 1339-1363.
34. Moreno-Montañés, J.; Bleau, A.-M.; Jimenez, A. I., Tivanisiran, a novel siRNA for the treatment of dry eye disease. *Expert Opinion on Investigational Drugs* **2018,** *27* (4), 421-426.
35. Ruz, V.; Gonzalez, V.; Bleau, A.-M.; Vargas, B.; Jimenez, A. I., Clinical Results of tivanisiran, a siRNA for the treatment of dry eye disease. *Investigative Ophthalmology & Visual Science* **2019,** *60* (9), 6738-6738.
36. Pouton, C. W.; Seymour, L. W., Key issues in non-viral gene delivery. *Advanced drug delivery reviews* **2001,** *46* (1-3), 187-203.
37. Jinturkar, K. A.; Misra, A., Challenges and Opportunities in Gene Delivery. In *Challenges in Delivery of Therapeutic Genomics and Proteomics*, Elsevier: 2011; pp 45-82.
38. Yin, H.; Kanasty, R. L.; Eltoukhy, A. A.; Vegas, A. J.; Dorkin, J. R.; Anderson, D. G., Non-viral vectors for gene-based therapy. *Nature Reviews Genetics* **2014,** *15* (8), 541-555.
39. Mahato, R. I.; Kawabata, K.; Takakura, Y.; Hashida, M., In vivo disposition characteristics of plasmid DNA complexed with cationic liposomes. *Journal of drug targeting* **1995,** *3* (2), 149-157.
40. Xiao, Y.; Shi, K.; Qu, Y.; Chu, B.; Qian, Z., Engineering nanoparticles for targeted delivery of nucleic acid therapeutics in tumor. *Molecular Therapy-Methods & Clinical Development* **2019,** *12*, 1-18.
41. Alexis, F.; Pridgen, E.; Molnar, L. K.; Farokhzad, O. C., Factors affecting the clearance and biodistribution of polymeric nanoparticles. *Molecular pharmaceutics* **2008,** *5* (4), 505-515.

42. Owens III, D. E.; Peppas, N. A., Opsonization, biodistribution, and pharmacokinetics of polymeric nanoparticles. *International journal of pharmaceutics* **2006,** *307* (1), 93-102.
43. Eliyahu, H.; Servel, N.; Domb, A.; Barenholz, Y., Lipoplex-induced hemagglutination: potential involvement in intravenous gene delivery. *Gene therapy* **2002,** *9* (13), 850-858.
44. Juliano, R.; Alam, M. R.; Dixit, V.; Kang, H., Mechanisms and strategies for effective delivery of antisense and siRNA oligonucleotides. *Nucleic acids research* **2008,** *36* (12), 4158-4171.
45. Kher, G.; Trehan, S.; Misra, A., Antisense oligonucleotides and RNA interference. *Challenges in Delivery of Therapeutic Genomics and Proteomics* **2011**, 325-386.
46. Chen, W.; Li, H.; Liu, Z.; Yuan, W., Lipopolyplex for therapeutic gene delivery and its application for the treatment of Parkinson's disease. *Frontiers in Aging Neuroscience* **2016,** *8*, 68.
47. Matsumura, Y.; Maeda, H., A new concept for macromolecular therapeutics in cancer chemotherapy: mechanism of tumoritropic accumulation of proteins and the antitumor agent smancs. *Cancer research* **1986,** *46* (12 Part 1), 6387-6392.
48. Rosenblum, D.; Joshi, N.; Tao, W.; Karp, J. M.; Peer, D., Progress and challenges towards targeted delivery of cancer therapeutics. *Nature communications* **2018,** *9* (1), 1-12.
49. Saha, R. N.; Vasanthakumar, S.; Bende, G.; Snehalatha, M., Nanoparticulate drug delivery systems for cancer chemotherapy. *Molecular membrane biology* **2010,** *27* (7), 215-231.
50. Wang, T.; Upponi, J. R.; Torchilin, V. P., Design of multifunctional non-viral gene vectors to overcome physiological barriers: dilemmas and strategies. *International journal of pharmaceutics* **2012,** *427* (1), 3-20.
51. Pei, D.; Buyanova, M., Overcoming endosomal entrapment in drug delivery. *Bioconjugate chemistry* **2018,** *30* (2), 273-283.
52. Mundra, V.; Mahato, R. I., Design of nanocarriers for efficient cellular uptake and endosomal release of small molecule and nucleic acid drugs: learning from virus. *Frontiers of Chemical Science and Engineering* **2014,** *8* (4), 387-404.
53. Earp, L.; Delos, S.; Park, H.; White, J., The many mechanisms of viral membrane fusion proteins. *Membrane trafficking in viral replication* **2004**, 25-66.
54. Oliveira, M. S.; Goulart, G. C. A.; Ferreira, L. A. M.; Carneiro, G., Hydrophobic ion pairing as a strategy to improve drug encapsulation into lipid nanocarriers for the cancer treatment. *Expert opinion on drug delivery* **2017,** *14* (8), 983-995.
55. Lozada, C.; Barlow, T.; Gonzalez, S.; Lubin-Germain, N.; Ballet, S., Identification and Characteristics of Fusion Peptides Derived From Enveloped Viruses. *Frontiers in Chemistry* **2021**, 688.
56. Semple, S. C.; Akinc, A.; Chen, J.; Sandhu, A. P.; Mui, B. L.; Cho, C. K.; Sah, D. W.; Stebbing, D.; Crosley, E. J.; Yaworski, E., Rational design of cationic lipids for siRNA delivery. *Nature biotechnology* **2010,** *28* (2), 172-176.
57. Koltover, I.; Salditt, T.; Rädler, J. O.; Safinya, C. R., An inverted hexagonal phase of cationic liposome-DNA complexes related to DNA release and delivery. *Science* **1998,** *281* (5373), 78-81.
58. Simões, S.; Moreira, J. N.; Fonseca, C.; Düzgüneş, N.; De Lima, M. C. P., On the formulation of pH-sensitive liposomes with long circulation times. *Advanced drug delivery reviews* **2004,** *56* (7), 947-965.
59. Liang, W.; Lam, J. K., Endosomal escape pathways for non-viral nucleic acid delivery systems. *Molecular regulation of endocytosis* **2012**, 429-456.
60. Smith, S. A.; Selby, L. I.; Johnston, A. P.; Such, G. K., The endosomal escape of nanoparticles: toward more efficient cellular delivery. *Bioconjugate chemistry* **2018,** *30* (2), 263-272.
61. Miyata, K.; Oba, M.; Nakanishi, M.; Fukushima, S.; Yamasaki, Y.; Koyama, H.; Nishiyama, N.; Kataoka, K., Polyplexes from poly (aspartamide) bearing 1, 2-diaminoethane side chains induce pH-selective, endosomal membrane destabilization with amplified transfection and negligible cytotoxicity. *Journal of the American Chemical Society* **2008,** *130* (48), 16287-16294.
62. Selby, L. I.; Cortez-Jugo, C. M.; Such, G. K.; Johnston, A. P., Nanoescapology: progress toward understanding the endosomal escape of polymeric nanoparticles. *Wiley Interdisciplinary Reviews: Nanomedicine and Nanobiotechnology* **2017,** *9* (5), e1452.

63. Lechardeur, D.; Lukacs, G. L., Intracellular barriers to non-viral gene transfer. *Current gene therapy* **2002,** *2* (2), 183-194.
64. Capecchi, M. R., High efficiency transformation by direct microinjection of DNA into cultured mammalian cells. *Cell* **1980,** *22* (2), 479-488.
65. Shi, B.; Zheng, M.; Tao, W.; Chung, R.; Jin, D.; Ghaffari, D.; Farokhzad, O. C., Challenges in DNA delivery and recent advances in multifunctional polymeric DNA delivery systems. *Biomacromolecules* **2017,** *18* (8), 2231-2246.
66. Almeida, R.; Allshire, R. C., RNA silencing and genome regulation. *Trends in cell biology* **2005,** *15* (5), 251-258.
67. Setten, R. L.; Rossi, J. J.; Han, S.-p., The current state and future directions of RNAi-based therapeutics. *Nature Reviews Drug Discovery* **2019,** *18* (6), 421-446.
68. Dana, H.; Chalbatani, G. M.; Mahmoodzadeh, H.; Karimloo, R.; Rezaiean, O.; Moradzadeh, A.; Mehmandoost, N.; Moazzen, F.; Mazraeh, A.; Marmari, V., Molecular mechanisms and biological functions of siRNA. *International journal of biomedical science: IJBS* **2017,** *13* (2), 48.
69. Kim, D. H.; Rossi, J. J., RNAi mechanisms and applications. *Biotechniques* **2008,** *44* (5), 613-616.
70. Alshaer, W.; Zureigat, H.; Al Karaki, A.; Al-Kadash, A.; Gharaibeh, L.; Ma'mon, M. H.; Aljabali, A. A.; Awidi, A., siRNA: Mechanism of action, challenges, and therapeutic approaches. *European Journal of Pharmacology* **2021,** *905*, 174178.
71. Wittrup, A.; Lieberman, J., Knocking down disease: a progress report on siRNA therapeutics. *Nature Reviews Genetics* **2015,** *16* (9), 543-552.
72. Singh, D.; Chaudhary, S.; Kumar, R.; Sirohi, P.; Mehla, K.; Sirohi, A.; Kumar, S.; Chand, P.; Singh, P. K., RNA interference technology—applications and limitations. In *RNA Interference*, IntechOpen: 2016.
73. Elbashir, S. M.; Harborth, J.; Lendeckel, W.; Yalcin, A.; Weber, K.; Tuschl, T., Duplexes of 21-nucleotide RNAs mediate RNA interference in cultured mammalian cells. *nature* **2001,** *411* (6836), 494-498.
74. Bumcrot, D.; Manoharan, M.; Koteliansky, V.; Sah, D. W., RNAi therapeutics: a potential new class of pharmaceutical drugs. *Nature chemical biology* **2006,** *2* (12), 711-719.
75. Saw, P. E.; Song, E.-W., siRNA therapeutics: a clinical reality. *Science China Life Sciences* **2020,** *63* (4), 485-500.
76. Urits, I.; Swanson, D.; Swett, M. C.; Patel, A.; Berardino, K.; Amgalan, A.; Berger, A. A.; Kassem, H.; Kaye, A. D.; Viswanath, O., A review of patisiran (ONPATTRO®) for the treatment of polyneuropathy in people with hereditary transthyretin amyloidosis. *Neurology and therapy* **2020,** *9* (2), 301-315.
77. Debacker, A. J.; Voutila, J.; Catley, M.; Blakey, D.; Habib, N., Delivery of oligonucleotides to the liver with GalNAc: from research to registered therapeutic drug. *Molecular Therapy* **2020,** *28* (8), 1759-1771.
78. Rossi, J. J.; Rossi, D. J., siRNA drugs: here to stay. *Molecular Therapy* **2021,** *29* (2), 431.
79. Chalbatani, G. M.; Dana, H.; Gharagouzloo, E.; Grijalvo, S.; Eritja, R.; Logsdon, C. D.; Memari, F.; Miri, S. R.; Rad, M. R.; Marmari, V., Small interfering RNAs (siRNAs) in cancer therapy: a nano-based approach. *International journal of nanomedicine* **2019,** *14*, 3111.
80. Gao, X.; Kim, K.-S.; Liu, D., Nonviral gene delivery: what we know and what is next. *The AAPS journal* **2007,** *9* (1), E92-E104.
81. Gonçalves, G. A. R.; Paiva, R. d. M. A., Gene therapy: advances, challenges and perspectives. *Einstein (Sao Paulo)* **2017,** *15*, 369-375.
82. Meacham, J. M.; Durvasula, K.; Degertekin, F. L.; Fedorov, A. G., Physical methods for intracellular delivery: practical aspects from laboratory use to industrial-scale processing. *Journal of laboratory automation* **2014,** *19* (1), 1-18.
83. Villemejane, J.; Mir, L. M., Physical methods of nucleic acid transfer: general concepts and applications. *British journal of pharmacology* **2009,** *157* (2), 207-219.

84. Kaladharan, K.; Kumar, A.; Gupta, P.; Illath, K.; Santra, T. S.; Tseng, F.-G., Microfluidic Based Physical Approaches towards Single-Cell Intracellular Delivery and Analysis. *Micromachines* **2021,** *12* (6), 631.
85. Wang, Q.; Jiang, W.; Chen, Y.; Liu, P.; Sheng, C.; Chen, S.; Zhang, H.; Pan, C.; Gao, S.; Huang, W., In vivo electroporation of minicircle DNA as a novel method of vaccine delivery to enhance HIV-1-specific immune responses. *Journal of virology* **2014,** *88* (4), 1924-1934.
86. Sundaram, J.; Mellein, B. R.; Mitragotri, S., An experimental and theoretical analysis of ultrasound-induced permeabilization of cell membranes. *Biophysical journal* **2003,** *84* (5), 3087-3101.
87. Kida, H.; Nishimura, K.; Ogawa, K.; Watanabe, A.; Feril, L. B.; Irie, Y.; Endo, H.; Kawakami, S.; Tachibana, K., Nanobubble mediated gene delivery in conjunction with a hand-held ultrasound scanner. *Frontiers in pharmacology* **2020,** *11*, 363.
88. Fraire, J. C.; Shaabani, E.; Sharifiaghdam, M.; Rombaut, M.; Hinnekens, C.; Hua, D.; Ramon, J.; Raes, L.; Bolea-Fernandez, E.; Brans, T., Light triggered nanoscale biolistics for efficient intracellular delivery of functional macromolecules in mammalian cells. *Nature Communications* **2022,** *13* (1), 1-16.
89. Robbins, P. D.; Ghivizzani, S. C., Viral vectors for gene therapy. *Pharmacology & therapeutics* **1998,** *80* (1), 35-47.
90. Lundstrom, K.; Boulikas, T., Viral and non-viral vectors in gene therapy: technology development and clinical trials. *Technology in cancer research & treatment* **2003,** *2* (5), 471-485.
91. Bulcha, J. T.; Wang, Y.; Ma, H.; Tai, P. W.; Gao, G., Viral vector platforms within the gene therapy landscape. *Signal transduction and targeted therapy* **2021,** *6* (1), 1-24.
92. Ylä-Herttuala, S., Endgame: glybera finally recommended for approval as the first gene therapy drug in the European union. *Molecular Therapy* **2012,** *20* (10), 1831-1832.
93. Wang, W.; Li, W.; Ma, N.; Steinhoff, G., Non-viral gene delivery methods. *Current pharmaceutical biotechnology* **2013,** *14* (1), 46-60.
94. Al-Dosari, M. S.; Gao, X., Nonviral gene delivery: principle, limitations, and recent progress. *The AAPS journal* **2009,** *11* (4), 671-681.
95. Patil, S.; Gao, Y.-G.; Lin, X.; Li, Y.; Dang, K.; Tian, Y.; Zhang, W.-J.; Jiang, S.-F.; Qadir, A.; Qian, A.-R., The development of functional non-viral vectors for gene delivery. *International journal of molecular sciences* **2019,** *20* (21), 5491.
96. Gantenbein, B.; Tang, S.; Guerrero, J.; Higuita-Castro, N.; Salazar-Puerta, A. I.; Croft, A. S.; Gazdhar, A.; Purmessur, D., Non-viral gene delivery methods for bone and joints. *Frontiers in Bioengineering and Biotechnology* **2020**, 1320.
97. Luten, J.; van Nostrum, C. F.; De Smedt, S. C.; Hennink, W. E., Biodegradable polymers as non-viral carriers for plasmid DNA delivery. *Journal of Controlled Release* **2008,** *126* (2), 97-110.
98. Hattori, Y., Progress in the development of lipoplex and polyplex modified with anionic polymer for efficient gene delivery. *Journal of Genetic Medicine and Gene Therapy* **2017,** *1* (1), 003-018.
99. Chen, C.-J.; Zhao, Z.-X.; Wang, J.-C.; Zhao, E.-Y.; Gao, L.-Y.; Zhou, S.-F.; Liu, X.-Y.; Lu, W.-L.; Zhang, Q., A comparative study of three ternary complexes prepared in different mixing orders of siRNA/redox-responsive hyperbranched poly (amido amine)/hyaluronic acid. *International Journal of Nanomedicine* **2012,** *7*, 3837.
100. Gu, J.; Chen, X.; Ren, X.; Zhang, X.; Fang, X.; Sha, X., CD44-targeted hyaluronic acid-coated redox-responsive hyperbranched poly (amido amine)/plasmid DNA ternary nanoassemblies for efficient gene delivery. *Bioconjugate chemistry* **2016,** *27* (7), 1723-1736.
101. Han, S.-E.; Kang, H.; Shim, G. Y.; Kim, S. J.; Choi, H.-G.; Kim, J.; Hahn, S. K.; Oh, Y.-K., Cationic derivatives of biocompatible hyaluronic acids for delivery of siRNA and antisense oligonucleotides. *Journal of drug targeting* **2009,** *17* (2), 123-132.
102. Mukherjee, A.; Waters, A. K.; Kalyan, P.; Achrol, A. S.; Kesari, S.; Yenugonda, V. M., Lipid–polymer hybrid nanoparticles as a next-generation drug delivery platform: state of the art, emerging technologies, and perspectives. *International journal of nanomedicine* **2019,** *14*, 1937.

103. Yang, X.-Z.; Dou, S.; Wang, Y.-C.; Long, H.-Y.; Xiong, M.-H.; Mao, C.-Q.; Yao, Y.-D.; Wang, J., Single-step assembly of cationic lipid–polymer hybrid nanoparticles for systemic delivery of siRNA. *Acs Nano* **2012,** *6* (6), 4955-4965.
104. Shi, J.; Xu, Y.; Xu, X.; Zhu, X.; Pridgen, E.; Wu, J.; Votruba, A. R.; Swami, A.; Zetter, B. R.; Farokhzad, O. C., Hybrid lipid–polymer nanoparticles for sustained siRNA delivery and gene silencing. *Nanomedicine: Nanotechnology, Biology and Medicine* **2014,** *10* (5), e897-e900.
105. Gao, L.-Y.; Liu, X.-Y.; Chen, C.-J.; Wang, J.-C.; Feng, Q.; Yu, M.-Z.; Ma, X.-F.; Pei, X.-W.; Niu, Y.-J.; Qiu, C., Core-shell type lipid/rPAA-Chol polymer hybrid nanoparticles for in vivo siRNA delivery. *Biomaterials* **2014,** *35* (6), 2066-2078.
106. Zu, H.; Gao, D., Non-viral vectors in gene therapy: Recent development, challenges, and prospects. *The AAPS Journal* **2021,** *23* (4), 1-12.
107. del Pozo-Rodríguez, A.; Delgado, D.; Solinís, M.; Gascón, A.; Pedraz, J., Solid lipid nanoparticles: formulation factors affecting cell transfection capacity. *International journal of pharmaceutics* **2007,** *339* (1-2), 261-268.
108. Gascón, A. R.; del Pozo-Rodríguez, A.; Solinís, M. Á., Non-viral delivery systems in gene therapy. In *Gene Therapy-Tools and Potential Applications*, IntechOpen: 2013.
109. Akinc, A.; Maier, M. A.; Manoharan, M.; Fitzgerald, K.; Jayaraman, M.; Barros, S.; Ansell, S.; Du, X.; Hope, M. J.; Madden, T. D., The Onpattro story and the clinical translation of nanomedicines containing nucleic acid-based drugs. *Nature nanotechnology* **2019,** *14* (12), 1084-1087.
110. Oner, E.; Kotmakci, M.; Baird, A.-M.; Gray, S. G.; Debelec Butuner, B.; Bozkurt, E.; Kantarci, A. G.; Finn, S. P., Development of EphA2 siRNA-loaded lipid nanoparticles and combination with a small-molecule histone demethylase inhibitor in prostate cancer cells and tumor spheroids. *Journal of nanobiotechnology* **2021,** *19* (1), 1-20.
111. Moss, K. H.; Popova, P.; Hadrup, S. R.; Astakhova, K.; Taskova, M., Lipid nanoparticles for delivery of therapeutic RNA oligonucleotides. *Molecular pharmaceutics* **2019,** *16* (6), 2265-2277.
112. Carvalho, B. G.; Ceccato, B. T.; Michelon, M.; Han, S. W.; de la Torre, L. G., Advanced microfluidic technologies for lipid nano-microsystems from synthesis to biological application. *Pharmaceutics* **2022,** *14* (1), 141.
113. Baden, L. R.; El Sahly, H. M.; Essink, B.; Kotloff, K.; Frey, S.; Novak, R.; Diemert, D.; Spector, S. A.; Rouphael, N.; Creech, C. B., Efficacy and safety of the mRNA-1273 SARS-CoV-2 vaccine. *New England journal of medicine* **2020**.
114. Anderson, E. J.; Rouphael, N. G.; Widge, A. T.; Jackson, L. A.; Roberts, P. C.; Makhene, M.; Chappell, J. D.; Denison, M. R.; Stevens, L. J.; Pruijssers, A. J., Safety and immunogenicity of SARS-CoV-2 mRNA-1273 vaccine in older adults. *New England Journal of Medicine* **2020,** *383* (25), 2427-2438.
115. Azambuja, J.; Schuh, R.; Michels, L.; Gelsleichter, N.; Beckenkamp, L.; Iser, I.; Lenz, G.; De Oliveira, F.; Venturin, G.; Greggio, S., Nasal administration of cationic nanoemulsions as CD73-siRNA delivery system for glioblastoma treatment: a new therapeutical approach. *Molecular neurobiology* **2020,** *57* (2), 635-649.
116. Juszkiewicz, K.; Sikorski, A. F.; Czogalla, A., Building blocks to design liposomal delivery systems. *International Journal of Molecular Sciences* **2020,** *21* (24), 9559.
117. Shim, G.; Kim, M.-G.; Park, J. Y.; Oh, Y.-K., Application of cationic liposomes for delivery of nucleic acids. *Asian journal of pharmaceutical sciences* **2013,** *8* (2), 72-80.
118. Michel, T.; Luft, D.; Abraham, M.-K.; Reinhardt, S.; Medina, M. L. S.; Kurz, J.; Schaller, M.; Avci-Adali, M.; Schlensak, C.; Peter, K., Cationic nanoliposomes meet mRNA: Efficient delivery of modified mRNA using hemocompatible and stable vectors for therapeutic applications. *Molecular Therapy-Nucleic Acids* **2017,** *8*, 459-468.
119. Lechanteur, A.; Sanna, V.; Duchemin, A.; Evrard, B.; Mottet, D.; Piel, G., Cationic liposomes carrying siRNA: impact of lipid composition on physicochemical properties, cytotoxicity and endosomal escape. *Nanomaterials* **2018,** *8* (5), 270.

120. Elsana, H.; Olusanya, T. O.; Carr-Wilkinson, J.; Darby, S.; Faheem, A.; Elkordy, A. A., Evaluation of novel cationic gene based liposomes with cyclodextrin prepared by thin film hydration and microfluidic systems. *Scientific reports* **2019,** *9* (1), 1-17.
121. Hattori, Y.; Nakamura, M.; Takeuchi, N.; Tamaki, K.; Ozaki, K. I.; Onishi, H., Effect of cationic lipid type in PEGylated liposomes on siRNA delivery following the intravenous injection of siRNA lipoplexes. *World Academy of Sciences Journal* **2019,** *1* (2), 74-85.
122. Kim, S. I.; Shin, D.; Choi, T. H.; Lee, J. C.; Cheon, G.-J.; Kim, K.-Y.; Park, M.; Kim, M., Systemic and specific delivery of small interfering RNAs to the liver mediated by apolipoprotein AI. *Molecular Therapy* **2007,** *15* (6), 1145-1152.
123. Khatri, N.; Baradia, D.; Vhora, I.; Rathi, M.; Misra, A., Development and characterization of siRNA lipoplexes: effect of different lipids, in vitro evaluation in cancerous cell lines and in vivo toxicity study. *AAPS PharmSciTech* **2014,** *15* (6), 1630-1643.
124. Buyens, K.; Lucas, B.; Raemdonck, K.; Braeckmans, K.; Vercammen, J.; Hendrix, J.; Engelborghs, Y.; De Smedt, S. C.; Sanders, N. N., A fast and sensitive method for measuring the integrity of siRNA-carrier complexes in full human serum. *Journal of controlled release* **2008,** *126* (1), 67-76.
125. Tagami, T.; Nakamura, K.; Shimizu, T.; Ishida, T.; Kiwada, H., Effect of siRNA in PEG-coated siRNA-lipoplex on anti-PEG IgM production. *Journal of Controlled Release* **2009,** *137* (3), 234-240.
126. Swart, L.; Koekman, C.; Seinen, C.; Issa, H.; Rasouli, M.; Schiffelers, R.; Heidenreich, O., A Robust Post-Insertion Method for the Preparation of Targeted siRNA LNPs. *International Journal of Pharmaceutics* **2022**, 121741.
127. Chono, S.; Li, S.-D.; Conwell, C. C.; Huang, L., An efficient and low immunostimulatory nanoparticle formulation for systemic siRNA delivery to the tumor. *Journal of Controlled Release* **2008,** *131* (1), 64-69.
128. Peer, D.; Park, E. J.; Morishita, Y.; Carman, C. V.; Shimaoka, M., Systemic leukocyte-directed siRNA delivery revealing cyclin D1 as an anti-inflammatory target. *Science* **2008,** *319* (5863), 627-630.
129. Zhang, H., Thin-film hydration followed by extrusion method for liposome preparation. In *Liposomes*, Springer: 2017; pp 17-22.
130. Barba, A. A.; Bochicchio, S.; Dalmoro, A.; Lamberti, G., Lipid delivery systems for nucleic-acid-based-drugs: From production to clinical applications. *Pharmaceutics* **2019,** *11* (8), 360.
131. Buyens, K.; De Smedt, S. C.; Braeckmans, K.; Demeester, J.; Peeters, L.; van Grunsven, L. A.; du Jeu, X. d. M.; Sawant, R.; Torchilin, V.; Farkasova, K., Liposome based systems for systemic siRNA delivery: stability in blood sets the requirements for optimal carrier design. *Journal of controlled release* **2012,** *158* (3), 362-370.
132. Jbara-Agbaria, D.; Blondzik, S.; Burger-Kentischer, A.; Agbaria, M.; Nordling-David, M. M.; Giterman, A.; Aizik, G.; Rupp, S.; Golomb, G., Liposomal siRNA Formulations for the Treatment of Herpes Simplex Virus-1: In Vitro Characterization of Physicochemical Properties and Activity, and In Vivo Biodistribution and Toxicity Studies. *Pharmaceutics* **2022,** *14* (3), 633.
133. Stuart, M. C.; Boekema, E. J., Two distinct mechanisms of vesicle-to-micelle and micelle-to-vesicle transition are mediated by the packing parameter of phospholipid–detergent systems. *Biochimica et Biophysica Acta (BBA)-Biomembranes* **2007,** *1768* (11), 2681-2689.
134. Van Hoogevest, P.; Wendel, A., The use of natural and synthetic phospholipids as pharmaceutical excipients. *European journal of lipid science and technology* **2014,** *116* (9), 1088-1107.
135. Rawicz, W.; Olbrich, K. C.; McIntosh, T.; Needham, D.; Evans, E., Effect of chain length and unsaturation on elasticity of lipid bilayers. *Biophysical journal* **2000,** *79* (1), 328-339.
136. Demel, R. A.; De Kruyff, B., The function of sterols in membranes. *Biochimica et Biophysica Acta (BBA)-Reviews on Biomembranes* **1976,** *457* (2), 109-132.
137. Liu, D.-Z.; Chen, W.-Y.; Tasi, L.-M.; Yang, S.-P., Microcalorimetric and shear studies on the effects of cholesterol on the physical stability of lipid vesicles. *Colloids and Surfaces A: Physicochemical and Engineering Aspects* **2000,** *172* (1-3), 57-67.

138. Anderson, M.; Omri, A., The effect of different lipid components on the in vitro stability and release kinetics of liposome formulations. *Drug delivery* **2004,** *11* (1), 33-39.
139. Gabizon, A.; Catane, R.; Uziely, B.; Kaufman, B.; Safra, T.; Cohen, R.; Martin, F.; Huang, A.; Barenholz, Y., Prolonged circulation time and enhanced accumulation in malignant exudates of doxorubicin encapsulated in polyethylene-glycol coated liposomes. *Cancer research* **1994,** *54* (4), 987-992.
140. Chao, T.-C.; Wang, W.-S.; Yen, C.-C.; Chiou, T.-J.; Liu, J.-H.; Chen, P.-M., A dose-escalating pilot study of sterically stabilized, pegylated liposomal doxorubicin (Lipo-Dox®) in patients with metastatic breast cancer. *Cancer investigation* **2003,** *21* (6), 837-847.
141. Swenson, C.; Perkins, W.; Roberts, P.; Janoff, A., Liposome technology and the development of Myocet™(liposomal doxorubicin citrate). *The Breast* **2001,** *10*, 1-7.
142. Briuglia, M.-L.; Rotella, C.; McFarlane, A.; Lamprou, D. A., Influence of cholesterol on liposome stability and on in vitro drug release. *Drug delivery and translational research* **2015,** *5* (3), 231-242.
143. Pozzi, D.; Marchini, C.; Cardarelli, F.; Amenitsch, H.; Garulli, C.; Bifone, A.; Caracciolo, G., Transfection efficiency boost of cholesterol-containing lipoplexes. *Biochimica et Biophysica Acta (BBA)-Biomembranes* **2012,** *1818* (9), 2335-2343.
144. Sawant, R. R.; Torchilin, V. P., Liposomes as 'smart'pharmaceutical nanocarriers. *Soft Matter* **2010,** *6* (17), 4026-4044.
145. Wang, H.-J.; Liu, Y.-H.; Zhang, J.; Zhang, Y.; Xia, Y.; Yu, X.-Q., Cyclen-based cationic lipids with double hydrophobic tails for efficient gene delivery. *Biomaterials science* **2014,** *2* (10), 1460-1470.
146. Xie, J.; Bi, Y.; Zhang, H.; Dong, S.; Teng, L.; Lee, R. J.; Yang, Z., Cell-penetrating peptides in diagnosis and treatment of human diseases: From preclinical research to clinical application. *Frontiers in Pharmacology* **2020,** *11*.
147. Derakhshankhah, H.; Jafari, S., Cell penetrating peptides: A concise review with emphasis on biomedical applications. *Biomedicine & Pharmacotherapy* **2018,** *108*, 1090-1096.
148. Koren, E.; Apte, A.; Sawant, R. R.; Grunwald, J.; Torchilin, V. P., Cell-penetrating TAT peptide in drug delivery systems: proteolytic stability requirements. *Drug delivery* **2011,** *18* (5), 377-384.
149. Aroui, S.; Kenani, A., Cell-Penetrating Peptides: A Challenge for Drug Delivery. *Cheminform. Its Appl* **2020**.
150. Keum, T.; Noh, G.; Seo, J.-E.; Bashyal, S.; Lee, S., In Vitro and Ex Vivo Evaluation of Penetratin as a Non-invasive Permeation Enhancer in the Penetration of Salmon Calcitonin through TR146 Buccal Cells and Porcine Buccal Tissues. *Pharmaceuticals* **2020,** *13* (11), 408.
151. Yoon, J.-S.; Jung, Y.-T.; Hong, S.-K.; Kim, S.-H.; Shin, M.-C.; Lee, D.-G.; Shin, W.-S.; Min, W.-S.; Paik, S.-Y., Characteristics of HIV-Tat protein transduction domain. *Journal of Microbiology* **2004,** *42* (4), 328-335.
152. Lindgren, M.; Hällbrink, M.; Prochiantz, A.; Langel, Ü., Cell-penetrating peptides. *Trends in pharmacological sciences* **2000,** *21* (3), 99-103.
153. Ruseska, I.; Zimmer, A., Internalization mechanisms of cell-penetrating peptides. *Beilstein journal of nanotechnology* **2020,** *11* (1), 101-123.
154. Oh, N.; Park, J.-H., Endocytosis and exocytosis of nanoparticles in mammalian cells. *International journal of nanomedicine* **2014,** *9* (Suppl 1), 51.
155. Uribe-Querol, E.; Rosales, C., Phagocytosis: our current understanding of a universal biological process. *Frontiers in immunology* **2020,** *11*, 1066.
156. Cuda, C. M.; Pope, R. M.; Perlman, H., The inflammatory role of phagocyte apoptotic pathways in rheumatic diseases. *Nature Reviews Rheumatology* **2016,** *12* (9), 543-558.
157. Vives, E.; Brodin, P.; Lebleu, B., A truncated HIV-1 Tat protein basic domain rapidly translocates through the plasma membrane and accumulates in the cell nucleus. *Journal of Biological Chemistry* **1997,** *272* (25), 16010-16017.

158. Suzuki, T.; Futaki, S.; Niwa, M.; Tanaka, S.; Ueda, K.; Sugiura, Y., Possible existence of common internalization mechanisms among arginine-rich peptides. *Journal of Biological Chemistry* **2002,** *277* (4), 2437-2443.
159. Richard, J. P.; Melikov, K.; Vives, E.; Ramos, C.; Verbeure, B.; Gait, M. J.; Chernomordik, L. V.; Lebleu, B., Cell-penetrating peptides: a reevaluation of the mechanism of cellular uptake. *Journal of Biological Chemistry* **2003,** *278* (1), 585-590.
160. Nakase, I.; Tadokoro, A.; Kawabata, N.; Takeuchi, T.; Katoh, H.; Hiramoto, K.; Negishi, M.; Nomizu, M.; Sugiura, Y.; Futaki, S., Interaction of arginine-rich peptides with membrane-associated proteoglycans is crucial for induction of actin organization and macropinocytosis. *Biochemistry* **2007,** *46* (2), 492-501.
161. Noguchi, K.; Obuki, M.; Sumi, H.; Klußmann, M.; Morimoto, K.; Nakai, S.; Hashimoto, T.; Fujiwara, D.; Fujii, I.; Yuba, E., Macropinocytosis-Inducible Extracellular Vesicles Modified with Antimicrobial Protein CAP18-Derived Cell-Penetrating Peptides for Efficient Intracellular Delivery. *Molecular Pharmaceutics* **2021,** *18* (9), 3290-3301.
162. Säälik, P.; Elmquist, A.; Hansen, M.; Padari, K.; Saar, K.; Viht, K.; Langel, Ü.; Pooga, M., Protein cargo delivery properties of cell-penetrating peptides. A comparative study. *Bioconjugate chemistry* **2004,** *15* (6), 1246-1253.
163. Kawaguchi, Y.; Takeuchi, T.; Kuwata, K.; Chiba, J.; Hatanaka, Y.; Nakase, I.; Futaki, S., Syndecan-4 is a receptor for clathrin-mediated endocytosis of arginine-rich cell-penetrating peptides. *Bioconjugate chemistry* **2016,** *27* (4), 1119-1130.
164. Fittipaldi, A.; Ferrari, A.; Zoppé, M.; Arcangeli, C.; Pellegrini, V.; Beltram, F.; Giacca, M., Cell membrane lipid rafts mediate caveolar endocytosis of HIV-1 Tat fusion proteins. *Journal of Biological Chemistry* **2003,** *278* (36), 34141-34149.
165. Veiman, K.-L.; Mäger, I.; Ezzat, K.; Margus, H.; Lehto, T. n.; Langel, K.; Kurrikoff, K.; Arukuusk, P.; Suhorutšenko, J.; Padari, K. r., PepFect14 peptide vector for efficient gene delivery in cell cultures. *Molecular pharmaceutics* **2013,** *10* (1), 199-210.
166. Ye, J.; Pei, X.; Cui, H.; Yu, Z.; Lee, H.; Wang, J.; Wang, X.; Sun, L.; He, H.; Yang, V. C., Cellular uptake mechanism and comparative in vitro cytotoxicity studies of monomeric LMWP-siRNA conjugate. *Journal of industrial and engineering chemistry* **2018,** *63*, 103-111.
167. Fernández-Carneado, J.; Van Gool, M.; Martos, V.; Castel, S.; Prados, P.; de Mendoza, J.; Giralt, E., Highly efficient, nonpeptidic oligoguanidinium vectors that selectively internalize into mitochondria. *Journal of the American Chemical Society* **2005,** *127* (3), 869-874.
168. Palm, C.; Jayamanne, M.; Kjellander, M.; Hällbrink, M., Peptide degradation is a critical determinant for cell-penetrating peptide uptake. *Biochimica et Biophysica Acta (BBA)-Biomembranes* **2007,** *1768* (7), 1769-1776.
169. Wexselblatt, E.; Esko, J. D.; Tor, Y., On guanidinium and cellular uptake. *The Journal of organic chemistry* **2014,** *79* (15), 6766-6774.
170. Meloni, B. P.; Mastaglia, F. L.; Knuckey, N. W., Cationic arginine-rich peptides (CARPs): a novel class of neuroprotective agents with a multimodal mechanism of action. *Frontiers in neurology* **2020,** *11*, 108.
171. Bonduelle, C. V.; Gillies, E. R., Dendritic guanidines as efficient analogues of cell penetrating peptides. *Pharmaceuticals* **2010,** *3* (3), 636-666.
172. Al-Azzawi, S.; Masheta, D.; Guildford, A.; Phillips, G.; Santin, M., Designing and characterization of a novel delivery system for improved cellular uptake by brain using dendronised Apo-E-derived peptide. *Frontiers in bioengineering and biotechnology* **2019,** *7*, 49.
173. Nazemi, A.; Gillies, E. R., Dendritic surface functionalization of nanomaterials: controlling properties and functions for biomedical applications. *Brazilian Journal of Pharmaceutical Sciences* **2013,** *49*, 15-32.
174. Lindhorst, T. K.; Elsner, K., Postsynthetic functionalization of glycodendrons at the focal point. *Beilstein journal of organic chemistry* **2014,** *10* (1), 1482-1487.

175. Kim, T.-i.; Baek, J.-u.; Bai, C. Z.; Park, J.-s., Arginine-conjugated polypropylenimine dendrimer as a non-toxic and efficient gene delivery carrier. *Biomaterials* **2007,** *28* (11), 2061-2067.
176. Tziveleka, L.-A.; Psarra, A.-M. G.; Tsiourvas, D.; Paleos, C. M., Synthesis and characterization of guanidinylated poly (propylene imine) dendrimers as gene transfection agents. *Journal of controlled release* **2007,** *117* (1), 137-146.
177. Chung, H. H.; Harms, G.; Min Seong, C.; Choi, B. H.; Min, C.; Taulane, J. P.; Goodman, M., Dendritic oligoguanidines as intracellular translocators. *Peptide Science: Original Research on Biomolecules* **2004,** *76* (1), 83-96.
178. Barattin, M.; Mattarei, A.; Balasso, A.; Paradisi, C.; Cantù, L.; Del Favero, E.; Viitala, T.; Mastrotto, F.; Caliceti, P.; Salmaso, S., pH-controlled liposomes for enhanced cell penetration in tumor environment. *ACS applied materials & interfaces* **2018,** *10* (21), 17646-17661.
179. Verbeke, R.; Lentacker, I.; Wayteck, L.; Breckpot, K.; Van Bockstal, M.; Descamps, B.; Vanhove, C.; De Smedt, S. C.; Dewitte, H., Co-delivery of nucleoside-modified mRNA and TLR agonists for cancer immunotherapy: Restoring the immunogenicity of immunosilent mRNA. *Journal of Controlled Release* **2017,** *266*, 287-300.
180. Bogaert, B.; Sauvage, F.; Guagliardo, R.; Muntean, C.; Nguyen, V. P.; Pottie, E.; Wels, M.; Minnaert, A.-K.; De Rycke, R.; Yang, Q., A lipid nanoparticle platform for mRNA delivery through repurposing of cationic amphiphilic drugs. *Journal of Controlled Release* **2022,** *350*, 256-270.
181. Gary, D. J.; Min, J.; Kim, Y.; Park, K.; Won, Y. Y., The Effect of N/P Ratio on the In Vitro and In Vivo Interaction Properties of PEG ylated Poly [2-(dimethylamino) ethyl methacrylate]-B ased si RNA Complexes. *Macromolecular bioscience* **2013,** *13* (8), 1059-1071.
182. Caliceti, P.; Salmaso, S.; Semenzato, A.; Carofiglio, T.; Fornasier, R.; Fermeglia, M.; Ferrone, M.; Pricl, S., Synthesis and physicochemical characterization of folate− cyclodextrin bioconjugate for active drug delivery. *Bioconjugate chemistry* **2003,** *14* (5), 899-908.
183. Torchilin, V. P., Recent advances with liposomes as pharmaceutical carriers. *Nature reviews Drug discovery* **2005,** *4* (2), 145-160.
184. Mohammed, A.; Weston, N.; Coombes, A.; Fitzgerald, M.; Perrie, Y., Liposome formulation of poorly water soluble drugs: optimisation of drug loading and ESEM analysis of stability. *International journal of pharmaceutics* **2004,** *285* (1-2), 23-34.
185. Nogueira, E.; Gomes, A. C.; Preto, A.; Cavaco-Paulo, A., Design of liposomal formulations for cell targeting. *Colloids and surfaces B: Biointerfaces* **2015,** *136*, 514-526.
186. Gleue, L.; Schupp, J.; Zimmer, N.; Becker, E.; Frey, H.; Tuettenberg, A.; Helm, M., Stability of Alkyl Chain-Mediated Lipid Anchoring in Liposomal Membranes. *Cells* **2020,** *9* (10), 2213.
187. Heim, M.; Römer, L.; Scheibel, T., Hierarchical structures made of proteins. The complex architecture of spider webs and their constituent silk proteins. *Chemical Society Reviews* **2010,** *39* (1), 156-164.
188. Sheldon, K.; Liu, D.; Ferguson, J.; Gariepy, J., Loligomers: design of de novo peptide-based intracellular vehicles. *Proceedings of the National Academy of Sciences* **1995,** *92* (6), 2056-2060.
189. Sung, M.; Poon, G. M.; Gariépy, J., The importance of valency in enhancing the import and cell routing potential of protein transduction domain-containing molecules. *Biochimica et Biophysica Acta (BBA)-Biomembranes* **2006,** *1758* (3), 355-363.
190. Kalafatovic, D.; Giralt, E., Cell-penetrating peptides: Design strategies beyond primary structure and amphipathicity. *Molecules* **2017,** *22* (11), 1929.
191. Xu, L.; Wang, X.; Liu, Y.; Yang, G.; Falconer, R. J.; Zhao, C.-X., Lipid nanoparticles for drug delivery. *Advanced NanoBiomed Research* **2022,** *2* (2), 2100109.
192. Arisawa, K.; Mitsudome, H.; Yoshida, K.; Sugimoto, S.; Ishikawa, T.; Fujiwara, Y.; Ichi, I., Saturated fatty acid in the phospholipid monolayer contributes to the formation of large lipid droplets. *Biochemical and biophysical research communications* **2016,** *480* (4), 641-647.
193. Lairon, D., Digestion and absorption of lipids. In *Designing functional foods*, Elsevier: 2009; pp 68-93.

194. Drabik, D.; Chodaczek, G.; Kraszewski, S.; Langner, M., Mechanical properties determination of DMPC, DPPC, DSPC, and HSPC solid-ordered bilayers. *Langmuir* **2020,** *36* (14), 3826-3835.
195. Papahadjopoulos, D.; Jacobson, K.; Nir, S.; Isac, I., Phase transitions in phospholipid vesicles fluorescence polarization and permeability measurements concerning the effect of temperature and cholesterol. *Biochimica et Biophysica Acta (BBA)-Biomembranes* **1973,** *311* (3), 330-348.
196. Schaefer, J. J.; Ma, C.; Harris, J. M., Confocal Raman microscopy probing of temperature-controlled release from individual, optically-trapped phospholipid vesicles. *Analytical chemistry* **2012,** *84* (21), 9505-9512.
197. Aydin, O.; Kanarya, D.; Yilmaz, U.; Tunc, C. Ü., Determination of Optimum Ratio of Cationic Polymers and Small Interfering RNA with Agarose Gel Retardation Assay. In *Antisense RNA Design, Delivery, and Analysis*, Humana, New York, NY: 2022; pp 117-128.
198. Engelberg, H.; Dudley, A., Plasma heparin levels in normal man. *Circulation* **1961,** *23* (4), 578-581.
199. Nakhaei, P.; Margiana, R.; Bokov, D. O.; Abdelbasset, W. K.; Jadidi Kouhbanani, M. A.; Varma, R. S.; Marofi, F.; Jarahian, M.; Beheshtkhoo, N., Liposomes: structure, biomedical applications, and stability parameters with emphasis on cholesterol. *Frontiers in Bioengineering and Biotechnology* **2021**, 748.
200. Perutková, Š.; Daniel, M.; Dolinar, G.; Rappolt, M.; Kralj-Iglič, V.; Iglič, A., Stability of the inverted hexagonal phase. *Advances in planar lipid bilayers and liposomes* **2009,** *9*, 237-278.
201. Lombardo, D.; Kiselev, M. A., Methods of Liposomes Preparation: Formation and Control Factors of Versatile Nanocarriers for Biomedical and Nanomedicine Application. *Pharmaceutics* **2022,** *14* (3), 543.
202. Dobrovolskaia, M. A.; Clogston, J. D.; Neun, B. W.; Hall, J. B.; Patri, A. K.; McNeil, S. E., Method for analysis of nanoparticle hemolytic properties in vitro. *Nano letters* **2008,** *8* (8), 2180-2187.
203. Siddon, A. J.; Tormey, C. A., The chemical and laboratory investigation of hemolysis. *Advances in Clinical Chemistry* **2019,** *89*, 215-258.
204. Das, B.; Tripathy, S.; Adhikary, J.; Chattopadhyay, S.; Mandal, D.; Dash, S. K.; Das, S.; Dey, A.; Dey, S. K.; Das, D., Surface modification minimizes the toxicity of silver nanoparticles: An in vitro and in vivo study. *JBIC Journal of Biological Inorganic Chemistry* **2017,** *22* (6), 893-918.
205. de la Harpe, K. M.; Kondiah, P. P.; Choonara, Y. E.; Marimuthu, T.; du Toit, L. C.; Pillay, V., The hemocompatibility of nanoparticles: a review of cell–nanoparticle interactions and hemostasis. *Cells* **2019,** *8* (10), 1209.
206. Rahimi, M.; Safa, K. D.; Alizadeh, E.; Salehi, R., Dendritic chitosan as a magnetic and biocompatible nanocarrier for the simultaneous delivery of doxorubicin and methotrexate to MCF-7 cell line. *New Journal of Chemistry* **2017,** *41* (8), 3177-3189.
207. Lv, H.; Zhang, S.; Wang, B.; Cui, S.; Yan, J., Toxicity of cationic lipids and cationic polymers in gene delivery. *Journal of controlled release* **2006,** *114* (1), 100-109.
208. López-García, J.; Lehocký, M.; Humpolíček, P.; Sáha, P., HaCaT keratinocytes response on antimicrobial atelocollagen substrates: extent of cytotoxicity, cell viability and proliferation. *Journal of functional biomaterials* **2014,** *5* (2), 43-57.
209. Abumanhal-Masarweh, H.; da Silva, D.; Poley, M.; Zinger, A.; Goldman, E.; Krinsky, N.; Kleiner, R.; Shenbach, G.; Schroeder, J. E.; Shklover, J., Tailoring the lipid composition of nanoparticles modulates their cellular uptake and affects the viability of triple negative breast cancer cells. *Journal of controlled release* **2019,** *307*, 331-341.
210. Merkel, O. M.; Beyerle, A.; Beckmann, B. M.; Zheng, M.; Hartmann, R. K.; Stöger, T.; Kissel, T. H., Polymer-related off-target effects in non-viral siRNA delivery. *Biomaterials* **2011,** *32* (9), 2388-2398.
211. Kim, B.-K.; Hwang, G.-B.; Seu, Y.-B.; Choi, J.-S.; Jin, K. S.; Doh, K.-O., DOTAP/DOPE ratio and cell type determine transfection efficiency with DOTAP-liposomes. *Biochimica Et Biophysica Acta (BBA)-Biomembranes* **2015,** *1848* (10), 1996-2001.

212. Tresset, G., The multiple faces of self-assembled lipidic systems. *PMC biophysics* **2009,** *2* (1), 1-25.
213. Mochizuki, S.; Kanegae, N.; Nishina, K.; Kamikawa, Y.; Koiwai, K.; Masunaga, H.; Sakurai, K., The role of the helper lipid dioleoylphosphatidylethanolamine (DOPE) for DNA transfection cooperating with a cationic lipid bearing ethylenediamine. *Biochimica et Biophysica Acta (BBA)-Biomembranes* **2013,** *1828* (2), 412-418.
214. Varkouhi, A. K.; Scholte, M.; Storm, G.; Haisma, H. J., Endosomal escape pathways for delivery of biologicals. *Journal of Controlled Release* **2011,** *151* (3), 220-228.
215. Goyal, R.; Jialal, I., Diabetes mellitus type 2. **2018**.
216. Prasad-Reddy, L.; Isaacs, D., A clinical review of GLP-1 receptor agonists: efficacy and safety in diabetes and beyond. *Drugs in context* **2015,** *4*.
217. Sharma, D.; Verma, S.; Vaidya, S.; Kalia, K.; Tiwari, V., Recent updates on GLP-1 agonists: Current advancements & challenges. *Biomedicine & Pharmacotherapy* **2018,** *108*, 952-962.
218. Shi, Y.; Sun, X.; Zhang, L.; Sun, K.; Li, K.; Li, Y.; Zhang, Q., Fc-modified exenatide-loaded nanoparticles for oral delivery to improve hypoglycemic effects in mice. *Scientific reports* **2018,** *8* (1), 1-9.
219. Salama, N. N.; Eddington, N. D.; Fasano, A., Tight junction modulation and its relationship to drug delivery. *Advanced drug delivery reviews* **2006,** *58* (1), 15-28.
220. Ismail, R.; Phan, T. N. Q.; Laffleur, F.; Csóka, I.; Bernkop-Schnürch, A., Hydrophobic ion pairing of a GLP-1 analogue for incorporating into lipid nanocarriers designed for oral delivery. *European Journal of Pharmaceutics and Biopharmaceutics* **2020,** *152*, 10-17.
221. Bruno, B. J.; Miller, G. D.; Lim, C. S., Basics and recent advances in peptide and protein drug delivery. *Therapeutic delivery* **2013,** *4* (11), 1443-1467.
222. Leader, B.; Baca, Q. J.; Golan, D. E., Protein therapeutics: a summary and pharmacological classification. *Nature reviews Drug discovery* **2008,** *7* (1), 21-39.
223. Bodanszky, M., Peptide chemistry. *A Practical Textbook* **1988**.
224. Upadhyay, A., Structure of proteins: evolution with unsolved mysteries. *Progress in biophysics and molecular biology* **2019,** *149*, 160-172.
225. Daudert, D. G., Exploring the Impact of Pretrained Bidirectional Language Models on Protein Secondary Structure Prediction. **2018**.
226. Yin, L.; Yuvienco, C.; Montclare, J. K., Protein based therapeutic delivery agents: contemporary developments and challenges. *Biomaterials* **2017,** *134*, 91-116.
227. Zapadka, K. L.; Becher, F. J.; Gomes dos Santos, A.; Jackson, S. E., Factors affecting the physical stability (aggregation) of peptide therapeutics. *Interface focus* **2017,** *7* (6), 20170030.
228. Banerjee, A.; Onyuksel, H., Peptide delivery using phospholipid micelles. *Wiley Interdisciplinary Reviews: Nanomedicine and Nanobiotechnology* **2012,** *4* (5), 562-574.
229. Dingermann, T., Recombinant therapeutic proteins: production platforms and challenges. *Biotechnology Journal: Healthcare Nutrition Technology* **2008,** *3* (1), 90-97.
230. Rafferty, J.; Nagaraj, H.; P McCloskey, A.; Huwaitat, R.; Porter, S.; Albadr, A.; Laverty, G., Peptide therapeutics and the pharmaceutical industry: barriers encountered translating from the laboratory to patients. *Current Medicinal Chemistry* **2016,** *23* (37), 4231-4259.
231. Zega, A., Azapeptides as pharmacological agents. *Current medicinal chemistry* **2005,** *12* (5), 589-597.
232. Tzefos, M.; Harris, K.; Brackett, A., Clinical efficacy and safety of once-weekly glucagon-like peptide-1 agonists in development for treatment of type 2 diabetes mellitus in adults. *Annals of Pharmacotherapy* **2012,** *46* (1), 68-78.
233. Lagassé, H. D.; Alexaki, A.; Simhadri, V. L.; Katagiri, N. H.; Jankowski, W.; Sauna, Z. E.; Kimchi-Sarfaty, C., Recent advances in (therapeutic protein) drug development. *F1000Research* **2017,** *6*.
234. Swierczewska, M.; Lee, K. C.; Lee, S., What is the future of PEGylated therapies? *Expert opinion on emerging drugs* **2015,** *20* (4), 531-536.

235. Lundstrom, K., *Nanocarriers for the delivery of peptides and proteins*. John Wiley & Sons, Ltd., Chichister, UK: 2009.
236. Zhang, Y.; Zhang, H.; Ghosh, D.; Williams III, R. O., Just how prevalent are peptide therapeutic products? A critical review. *International Journal of Pharmaceutics* **2020,** *587*, 119491.
237. Cvetković, R. S.; Plosker, G. L., Exenatide. *Drugs* **2007,** *67* (6), 935-954.
238. Ginter, E.; Simko, V., Type 2 diabetes mellitus, pandemic in 21st century. *Diabetes* **2013**, 42-50.
239. Wells, B. G.; DiPiro, J. T.; Schwinghammer, T. L.; DiPiro, C. V.; Education, M.-H., *Pharmacotherapy handbook*. Appleton & Lange: 2000.
240. Luna, B.; Feinglos, M. N., Oral agents in the management of type 2 diabetes mellitus. *American family physician* **2001,** *63* (9), 1747.
241. Nguyen, H.-N.; Wey, S.-P.; Juang, J.-H.; Sonaje, K.; Ho, Y.-C.; Chuang, E.-Y.; Hsu, C.-W.; Yen, T.-C.; Lin, K.-J.; Sung, H.-W., The glucose-lowering potential of exendin-4 orally delivered via a pH-sensitive nanoparticle vehicle and effects on subsequent insulin secretion in vivo. *Biomaterials* **2011,** *32* (10), 2673-2682.
242. Muskiet, M. H.; Tonneijck, L.; Smits, M. M.; Van Baar, M. J.; Kramer, M. H.; Hoorn, E. J.; Joles, J. A.; Van Raalte, D. H., GLP-1 and the kidney: from physiology to pharmacology and outcomes in diabetes. *Nature Reviews Nephrology* **2017,** *13* (10), 605-628.
243. Drucker, D. J., Mechanisms of action and therapeutic application of glucagon-like peptide-1. *Cell metabolism* **2018,** *27* (4), 740-756.
244. Dods, R. L.; Donnelly, D., The peptide agonist-binding site of the glucagon-like peptide-1 (GLP-1) receptor based on site-directed mutagenesis and knowledge-based modelling. *Bioscience reports* **2016,** *36* (1).
245. Bond, A. In *Exenatide (Byetta) as a novel treatment option for type 2 diabetes mellitus*, Baylor University Medical Center Proceedings, Taylor & Francis: 2006; pp 281-284.
246. Kolterman, O. G.; Kim, D. D.; Shen, L.; Ruggles, J. A.; Nielsen, L. L.; Fineman, M. S.; Baron, A. D., Pharmacokinetics, pharmacodynamics, and safety of exenatide in patients with type 2 diabetes mellitus. *American Journal of Health-System Pharmacy* **2005,** *62* (2), 173-181.
247. Chia, C. W.; Egan, J. M., Role and development of GLP-1 receptor agonists in the management of diabetes. *Diabetes, metabolic syndrome and obesity: targets and therapy* **2009,** *2*, 37.
248. Tong, F., Preparation of exenatide-loaded linear poly (ethylene glycol)-brush poly (l-lysine) block copolymer: potential implications on diabetic nephropathy. *International journal of nanomedicine* **2017,** *12*, 4663.
249. Phan, T. N. Q.; Ismail, R.; Le-Vinh, B.; Zaichik, S.; Laffleur, F.; Bernkop-Schnürch, A., The effect of counterions in hydrophobic ion pairs on oral bioavailability of exenatide. *ACS Biomaterials Science & Engineering* **2020,** *6* (9), 5032-5039.
250. Antosova, Z.; Mackova, M.; Kral, V.; Macek, T., Therapeutic application of peptides and proteins: parenteral forever? *Trends in biotechnology* **2009,** *27* (11), 628-635.
251. Walsh, G., *Biopharmaceuticals: biochemistry and biotechnology*. John Wiley & Sons: 2013.
252. Ugwoke, M. I.; Verbeke, N.; Kinget, R., The biopharmaceutical aspects of nasal mucoadhesive drug delivery. *Journal of pharmacy and pharmacology* **2001,** *53* (1), 3-22.
253. Ward, D.; Melbourn, I.; Way, S., Intranasal Delivery of Biologic Therapeutics and Vaccines. ONdrugDelivery: 2020.
254. Samaridou, E.; Alonso, M. J., Nose-to-brain peptide delivery–The potential of nanotechnology. *Bioorganic & medicinal chemistry* **2018,** *26* (10), 2888-2905.
255. Chesnut III, C. H.; Silverman, S.; Andriano, K.; Genant, H.; Gimona, A.; Harris, S.; Kiel, D.; LeBoff, M.; Maricic, M.; Miller, P., A randomized trial of nasal spray salmon calcitonin in postmenopausal women with established osteoporosis: the prevent recurrence of osteoporotic fractures study. *The American journal of medicine* **2000,** *109* (4), 267-276.

256. Andersson, K.-E.; Longstreth, J.; Brucker, B. M.; Campeau, L.; Cheng, L.; Francis, L.; Fein, S., Pharmacokinetic and pharmacodynamic properties of a micro-dose nasal spray formulation of desmopressin (AV002) in healthy water-loaded subjects. *Pharmaceutical Research* **2019,** *36* (6), 1-8.
257. Koon, A.; Perciavalle, K.; Oleis, J.; Arnall, J., Providing medication alternatives during intranasal desmopressin recall. *Journal of Oncology Pharmacy Practice* **2022,** *28* (1), 190-193.
258. Jadhav, K. R.; Gambhire, M. N.; Shaikh, I. M.; Kadam, V. J.; Pisal, S. S., Nasal drug delivery system-factors affecting and applications. *Current drug therapy* **2007,** *2* (1), 27-38.
259. Liu, J.; Gong, T.; Fu, H.; Wang, C.; Wang, X.; Chen, Q.; Zhang, Q.; He, Q.; Zhang, Z., Solid lipid nanoparticles for pulmonary delivery of insulin. *International journal of pharmaceutics* **2008,** *356* (1-2), 333-344.
260. Niven, R. W., Delivery of biotherapeutics by inhalation aerosol. *Critical Reviews™ in Therapeutic Drug Carrier Systems* **1995,** *12* (2-3).
261. Sayani, A. P.; Chien, Y. W., Systemic delivery of peptides and proteins across absorptive mucosae. *Critical reviews in therapeutic drug carrier systems* **1996,** *13* (1-2), 85-184.
262. Uchenna Agu, R.; Ikechukwu Ugwoke, M.; Armand, M.; Kinget, R.; Verbeke, N., The lung as a route for systemic delivery of therapeutic proteins and peptides. *Respiratory research* **2001,** *2* (4), 1-12.
263. Lip Kwok, P.; Chan, H., Chapter 2–Pulmonary Delivery of Peptides and Proteins. Academic Press Boston: 2011; pp 23-46.
264. Alqahtani, M. S.; Kazi, M.; Alsenaidy, M. A.; Ahmad, M. Z., Advances in oral drug delivery. *Frontiers in Pharmacology* **2021**, 62.
265. Zhang, B.; He, D.; Fan, Y.; Liu, N.; Chen, Y., Oral delivery of exenatide via microspheres prepared by cross-linking of alginate and hyaluronate. *PloS one* **2014,** *9* (1), e86064.
266. Yun, Y.; Cho, Y. W.; Park, K., Nanoparticles for oral delivery: targeted nanoparticles with peptidic ligands for oral protein delivery. *Advanced drug delivery reviews* **2013,** *65* (6), 822-832.
267. Li, R.; Laurent, F.; Taverner, A.; Mackay, J.; De Bank, P. A.; Mrsny, R. J., Intestinal transcytosis of a protein cargo and nanoparticles mediated by a non-toxic form of Pseudomonas aeruginosa exotoxin A. *Pharmaceutics* **2021,** *13* (8), 1171.
268. des Rieux, A.; Fievez, V.; Garinot, M.; Schneider, Y.-J.; Préat, V., Nanoparticles as potential oral delivery systems of proteins and vaccines: a mechanistic approach. *Journal of controlled release* **2006,** *116* (1), 1-27.
269. Banerjee, A.; Qi, J.; Gogoi, R.; Wong, J.; Mitragotri, S., Role of nanoparticle size, shape and surface chemistry in oral drug delivery. *Journal of Controlled Release* **2016,** *238*, 176-185.
270. Wang, Y.; Pi, C.; Feng, X.; Hou, Y.; Zhao, L.; Wei, Y., The influence of nanoparticle properties on oral bioavailability of drugs. *International journal of nanomedicine* **2020,** *15*, 6295.
271. Tong, T.; Wang, L.; You, X.; Wu, J., Nano and microscale delivery platforms for enhanced oral peptide/protein bioavailability. *Biomaterials Science* **2020,** *8* (21), 5804-5823.
272. Cao, S.-j.; Xu, S.; Wang, H.-m.; Ling, Y.; Dong, J.; Xia, R.-d.; Sun, X.-h., Nanoparticles: oral delivery for protein and peptide drugs. *AAPS PharmSciTech* **2019,** *20* (5), 1-11.
273. Del Rio, A. R.; Keppler, J. K.; Boom, R. M.; Janssen, A. E., Protein acidification and hydrolysis by pepsin ensure efficient trypsin-catalyzed hydrolysis. *Food & Function* **2021,** *12* (10), 4570-4581.
274. Langguth, P.; Bohner, V.; Heizmann, J.; Merkle, H.; Wolffram, S.; Amidon, G.; Yamashita, S., The challenge of proteolytic enzymes in intestinal peptide delivery. *Journal of controlled release* **1997,** *46* (1-2), 39-57.
275. Hochman, J.; Artursson, P., Mechanisms of absorption enhancement and tight junction regulation. *Journal of controlled release* **1994,** *29* (3), 253-267.
276. Hamman, J. H.; Enslin, G. M.; Kotzé, A. F., Oral delivery of peptide drugs. *BioDrugs* **2005,** *19* (3), 165-177.
277. Schipper, N. G.; Vårum, K. M.; Stenberg, P.; Ocklind, G.; Lennernäs, H.; Artursson, P., Chitosans as absorption enhancers of poorly absorbable drugs: 3: Influence of mucus on absorption enhancement. *European journal of pharmaceutical sciences* **1999,** *8* (4), 335-343.

278. Dicks, L. M.; Dreyer, L.; Smith, C.; Van Staden, A. D., A review: the fate of bacteriocins in the human gastro-intestinal tract: do they cross the gut–blood barrier? *Frontiers in Microbiology* **2018**, 2297.
279. Pacheco, D. P.; Butnarasu, C. S.; Vangosa, F. B.; Pastorino, L.; Visai, L.; Visentin, S.; Petrini, P., Disassembling the complexity of mucus barriers to develop a fast screening tool for early drug discovery. *Journal of Materials Chemistry B* **2019,** *7* (32), 4940-4952.
280. Boegh, M.; García-Díaz, M.; Müllertz, A.; Nielsen, H. M., Steric and interactive barrier properties of intestinal mucus elucidated by particle diffusion and peptide permeation. *European Journal of Pharmaceutics and Biopharmaceutics* **2015,** *95*, 136-143.
281. Nguyen, T.-T.-L.; Duong, V.-A.; Maeng, H.-J., Pharmaceutical formulations with P-glycoprotein inhibitory effect as promising approaches for enhancing oral drug absorption and bioavailability. *Pharmaceutics* **2021,** *13* (7), 1103.
282. Buckley, S. T.; Hubálek, F.; Rahbek, U. L., Chemically modified peptides and proteins-critical considerations for oral delivery. *Tissue Barriers* **2016,** *4* (2), e1156805.
283. Veronese, F. M.; Mero, A., The impact of PEGylation on biological therapies. *BioDrugs* **2008,** *22* (5), 315-329.
284. Soltero, R.; Ekwuribe, N., The oral delivery of protein and peptide drugs. *Innovations in Pharmaceutical Technology* **2001,** *1*, 106-110.
285. Zizzari, A. T.; Pliatsika, D.; Gall, F. M.; Fischer, T.; Riedl, R., New perspectives in oral peptide delivery. *Drug discovery today* **2021,** *26* (4), 1097-1105.
286. Shen, W.-C.; Wang, J.; Shen, D. In *Reversible lipidization for the delivery of peptide and protein drugs*, ALFRED BENZON SYMPOSIUM, MUNKSGAARD BOGHANDEL: 1998; pp 397-408.
287. Wang, J.; Chow, D.; Heiati, H.; Shen, W.-C., Reversible lipidization for the oral delivery of salmon calcitonin. *Journal of controlled release* **2003,** *88* (3), 369-380.
288. Pauletti, G. M.; Gangwar, S.; Siahaan, T. J.; Aubé, J.; Borchardt, R. T., Improvement of oral peptide bioavailability: Peptidomimetics and prodrug strategies. *Advanced drug delivery reviews* **1997,** *27* (2-3), 235-256.
289. Petrus, A. K.; Fairchild, T. J.; Doyle, R. P., Traveling the vitamin B12 pathway: oral delivery of protein and peptide drugs. *Angewandte Chemie International Edition* **2009,** *48* (6), 1022-1028.
290. Leone-Bay, A.; Santiago, N.; Achan, D.; Chaudhary, K.; DeMorin, F.; Falzarano, L.; Haas, S.; Kalbag, S.; Kaplan, D., N-acylated. Alpha.-amino acids as novel oral delivery agents for proteins. *Journal of medicinal chemistry* **1995,** *38* (21), 4263-4269.
291. Kahns, A. H.; Buur, A.; Bundgaard, H., Prodrugs of peptides. 18. Synthesis and evaluation of various esters of desmopressin (dDAVP). *Pharmaceutical research* **1993,** *10* (1), 68-74.
292. Li, C.; Wang, J.; Wang, Y.; Gao, H.; Wei, G.; Huang, Y.; Yu, H.; Gan, Y.; Wang, Y.; Mei, L., Recent progress in drug delivery. *Acta Pharmaceutica Sinica B* **2019,** *9* (6), 1145-1162.
293. Rezaie, H. R.; Esnaashary, M.; Öchsner, A., Classification of Drug Delivery Systems. In *A Review of Biomaterials and Their Applications in Drug Delivery*, Springer: 2018; pp 9-25.
294. Bhatia, S., Nanoparticles types, classification, characterization, fabrication methods and drug delivery applications. In *Natural polymer drug delivery systems*, Springer: 2016; pp 33-93.
295. Deng, Y.; Zhang, X.; Shen, H.; He, Q.; Wu, Z.; Liao, W.; Yuan, M., Application of the Nano-Drug Delivery System in Treatment of Cardiovascular Diseases. *Frontiers in Bioengineering and Biotechnology* **2019,** *7*.
296. Khalid, M.; El-Sawy, H. S., Polymeric nanoparticles: promising platform for drug delivery. *International journal of pharmaceutics* **2017,** *528* (1-2), 675-691.
297. Jhaveri, A. M.; Torchilin, V. P., Multifunctional polymeric micelles for delivery of drugs and siRNA. *Frontiers in pharmacology* **2014,** *5*, 77.
298. Liu, M.; Fréchet, J. M., Designing dendrimers for drug delivery. *Pharmaceutical science & technology today* **1999,** *2* (10), 393-401.
299. Ghosh, P.; Han, G.; De, M.; Kim, C. K.; Rotello, V. M., Gold nanoparticles in delivery applications. *Advanced drug delivery reviews* **2008,** *60* (11), 1307-1315.

300. Chertok, B.; Moffat, B. A.; David, A. E.; Yu, F.; Bergemann, C.; Ross, B. D.; Yang, V. C., Iron oxide nanoparticles as a drug delivery vehicle for MRI monitored magnetic targeting of brain tumors. *Biomaterials* **2008,** *29* (4), 487-496.
301. Carbone, C.; Leonardi, A.; Cupri, S.; Puglisi, G.; Pignatello, R., Pharmaceutical and biomedical applications of lipid-based nanocarriers. *Pharmaceutical patent analyst* **2014,** *3* (2), 199-215.
302. Wissing, S.; Kayser, O.; Müller, R., Solid lipid nanoparticles for parenteral drug delivery. *Advanced drug delivery reviews* **2004,** *56* (9), 1257-1272.
303. Martins, S.; Sarmento, B.; Ferreira, D. C.; Souto, E. B., Lipid-based colloidal carriers for peptide and protein delivery–liposomes versus lipid nanoparticles. *International journal of nanomedicine* **2007,** *2* (4), 595.
304. Hippalgaonkar, K.; Adelli, G. R.; Hippalgaonkar, K.; Repka, M. A.; Majumdar, S., Indomethacin-loaded solid lipid nanoparticles for ocular delivery: development, characterization, and in vitro evaluation. *Journal of ocular pharmacology and therapeutics* **2013,** *29* (2), 216-228.
305. Mei, Z.; Chen, H.; Weng, T.; Yang, Y.; Yang, X., Solid lipid nanoparticle and microemulsion for topical delivery of triptolide. *European journal of pharmaceutics and biopharmaceutics* **2003,** *56* (2), 189-196.
306. Koshkina, N. V.; Waldrep, J. C.; Roberts, L. E.; Golunski, E.; Melton, S.; Knight, V., Paclitaxel liposome aerosol treatment induces inhibition of pulmonary metastases in murine renal carcinoma model. *Clinical cancer research* **2001,** *7* (10), 3258-3262.
307. Wong, C. Y.; Al-Salami, H.; Dass, C. R., Recent advancements in oral administration of insulin-loaded liposomal drug delivery systems for diabetes mellitus. *International journal of pharmaceutics* **2018,** *549* (1-2), 201-217.
308. Hua, S., Orally administered liposomal formulations for colon targeted drug delivery. *Frontiers in pharmacology* **2014,** *5*, 138.
309. Balamurugan, K.; Chintamani, P., Lipid nano particulate drug delivery: An overview of the emerging trend. *Pharma Innov. J* **2018,** *7*, 779-789.
310. Beltrán-Gracia, E.; López-Camacho, A.; Higuera-Ciapara, I.; Velázquez-Fernández, J. B.; Vallejo-Cardona, A. A., Nanomedicine review: clinical developments in liposomal applications. *Cancer Nanotechnology* **2019,** *10* (1), 11.
311. Zangabad, P. S.; Mirkiani, S.; Shahsavari, S.; Masoudi, B.; Masroor, M.; Hamed, H.; Jafari, Z.; Taghipour, Y. D.; Hashemi, H.; Karimi, M., Stimulus-responsive liposomes as smart nanoplatforms for drug delivery applications. *Nanotechnology reviews* **2018,** *7* (1), 95-122.
312. Jash, A.; Ubeyitogullari, A.; Rizvi, S. S., Liposomes for oral delivery of protein and peptide-based therapeutics: challenges, formulation strategies, and advances. *Journal of Materials Chemistry B* **2021,** *9* (24), 4773-4792.
313. Paliwal, R.; Paliwal, S. R.; Kenwat, R.; Kurmi, B. D.; Sahu, M. K., Solid lipid nanoparticles: A review on recent perspectives and patents. *Expert opinion on therapeutic patents* **2020,** *30* (3), 179-194.
314. Scioli Montoto, S.; Muraca, G.; Ruiz, M. E., Solid lipid nanoparticles for drug delivery: Pharmacological and biopharmaceutical aspects. *Frontiers in Molecular Biosciences* **2020**, 319.
315. Singhal, G.; Patel, R.; Prajapati, B., Solid lipid nanoparticles: a review. Scientific reviews and chemical communications. *International Research Journal of Pharmacy* **2011,** *2* (2), 40-52.
316. Mandawgade, S. D.; Patravale, V. B., Development of SLNs from natural lipids: application to topical delivery of tretinoin. *International journal of pharmaceutics* **2008,** *363* (1-2), 132-138.
317. Lingayat, V. J.; Zarekar, N. S.; Shendge, R. S., Solid lipid nanoparticles: a review. *Nanoscience and Nanotechnology Research* **2017,** *2*, 67-72.
318. Geszke-Moritz, M.; Moritz, M., Solid lipid nanoparticles as attractive drug vehicles: Composition, properties and therapeutic strategies. *Materials Science and Engineering: C* **2016,** *68*, 982-994.

319. Yu, Y. H.; Kim, E.; Park, D. E.; Shim, G.; Lee, S.; Kim, Y. B.; Kim, C.-W.; Oh, Y.-K., Cationic solid lipid nanoparticles for co-delivery of paclitaxel and siRNA. *European Journal of Pharmaceutics and Biopharmaceutics* **2012,** *80* (2), 268-273.
320. Lobovkina, T.; Jacobson, G. B.; Gonzalez-Gonzalez, E.; Hickerson, R. P.; Leake, D.; Kaspar, R. L.; Contag, C. H.; Zare, R. N., In vivo sustained release of siRNA from solid lipid nanoparticles. *ACS nano* **2011,** *5* (12), 9977-9983.
321. Dumont, C.; Beloqui, A.; Miolane, C.; Bourgeois, S.; Préat, V.; Fessi, H.; Jannin, V., Solid lipid nanocarriers diffuse effectively through mucus and enter intestinal cells–But where is my peptide? *International journal of pharmaceutics* **2020,** *586*, 119581.
322. Ventola, C. L., Progress in nanomedicine: approved and investigational nanodrugs. *Pharmacy and Therapeutics* **2017,** *42* (12), 742.
323. Bandi, S. P.; Kumbhar, Y. S.; Venuganti, V. V. K., Effect of particle size and surface charge of nanoparticles in penetration through intestinal mucus barrier. *Journal of Nanoparticle Research* **2020,** *22* (3), 1-11.
324. Du, X.-J.; Wang, J.-L.; Iqbal, S.; Li, H.-J.; Cao, Z.-T.; Wang, Y.-C.; Du, J.-Z.; Wang, J., The effect of surface charge on oral absorption of polymeric nanoparticles. *Biomaterials science* **2018,** *6* (3), 642-650.
325. Crater, J. S.; Carrier, R. L., Barrier properties of gastrointestinal mucus to nanoparticle transport. *Macromolecular bioscience* **2010,** *10* (12), 1473-1483.
326. Mirchandani, Y.; Patravale, V. B.; Brijesh, S., Solid lipid nanoparticles for hydrophilic drugs. *Journal of Controlled Release* **2021,** *335*, 457-464.
327. Mehnert, W.; Mäder, K., Solid lipid nanoparticles: production, characterization and applications. *Advanced drug delivery reviews* **2012,** *64*, 83-101.
328. Boonyaratanakornkit, B. B.; Park, C. B.; Clark, D. S., Pressure effects on intra-and intermolecular interactions within proteins. *Biochimica et Biophysica Acta (BBA)-Protein Structure and Molecular Enzymology* **2002,** *1595* (1-2), 235-249.
329. Bezemer, J.; Radersma, R.; Grijpma, D.; Dijkstra, P.; Van Blitterswijk, C.; Feijen, J., Microspheres for protein delivery prepared from amphiphilic multiblock copolymers: 1. Influence of preparation techniques on particle characteristics and protein delivery. *Journal of controlled release* **2000,** *67* (2-3), 233-248.
330. Woo, B. H.; Kostanski, J. W.; Gebrekidan, S.; Dani, B. A.; Thanoo, B.; DeLuca, P. P., Preparation, characterization and in vivo evaluation of 120-day poly (D, L-lactide) leuprolide microspheres. *Journal of Controlled Release* **2001,** *75* (3), 307-315.
331. Cleland, J. L.; Mac, A.; Boyd, B.; Yang, J.; Duenas, E. T.; Yeung, D.; Brooks, D.; Hsu, C.; Chu, H.; Mukku, V., The stability of recombinant human growth hormone in poly (lactic-co-glycolic acid)(PLGA) microspheres. *Pharmaceutical research* **1997,** *14* (4), 420-425.
332. Igartua, M.; Hernandez, R.; Esquisabel, A.; Gascon, A.; Calvo, M.; Pedraz, J., Influence of formulation variables on the in-vitro release of albumin from biodegradable microparticulate systems. *Journal of microencapsulation* **1997,** *14* (3), 349-356.
333. Iqbal, M.; Zafar, N.; Fessi, H.; Elaissari, A., Double emulsion solvent evaporation techniques used for drug encapsulation. *International journal of pharmaceutics* **2015,** *496* (2), 173-190.
334. Anderluzzi, G.; Perrie, Y., Microfluidic manufacture of solid lipid nanoparticles: A case study on tristearin-based systems. *Drug Delivery Letters* **2020,** *10* (3), 197-208.
335. Arduino, I.; Liu, Z.; Rahikkala, A.; Figueiredo, P.; Correia, A.; Cutrignelli, A.; Denora, N.; Santos, H. A., Preparation of cetyl palmitate-based PEGylated solid lipid nanoparticles by microfluidic technique. *Acta Biomaterialia* **2021,** *121*, 566-578.
336. Shepherd, S. J.; Issadore, D.; Mitchell, M. J., Microfluidic formulation of nanoparticles for biomedical applications. *Biomaterials* **2021,** *274*, 120826.
337. Tomeh, M. A.; Zhao, X., Recent advances in microfluidics for the preparation of drug and gene delivery systems. *Molecular Pharmaceutics* **2020,** *17* (12), 4421-4434.
338. Chang, C.-C.; Fu, L.-M.; Yang, R.-J., Flow Field.

339. Brown, A.; Thomas, A.; Ordobadi, M.; Ip, S.; Heuck, G.; Ramsay, E., Liposomes.
340. Roces, C. B.; Lou, G.; Jain, N.; Abraham, S.; Thomas, A.; Halbert, G. W.; Perrie, Y., Manufacturing considerations for the development of lipid nanoparticles using microfluidics. *Pharmaceutics* **2020,** *12* (11), 1095.
341. Chen, D.; Love, K. T.; Chen, Y.; Eltoukhy, A. A.; Kastrup, C.; Sahay, G.; Jeon, A.; Dong, Y.; Whitehead, K. A.; Anderson, D. G., Rapid discovery of potent siRNA-containing lipid nanoparticles enabled by controlled microfluidic formulation. *Journal of the American Chemical Society* **2012,** *134* (16), 6948-6951.
342. Cullis, P. R.; Hope, M. J., Lipid nanoparticle systems for enabling gene therapies. *Molecular Therapy* **2017,** *25* (7), 1467-1475.
343. Ball, R. L.; Bajaj, P.; Whitehead, K. A., Achieving long-term stability of lipid nanoparticles: examining the effect of pH, temperature, and lyophilization. *International journal of nanomedicine* **2017,** *12*, 305.
344. Mohammady, M.; Yousefi, G., Freeze-drying of pharmaceutical and nutraceutical nanoparticles: the effects of formulation and technique parameters on nanoparticles characteristics. *Journal of Pharmaceutical Sciences* **2020,** *109* (11), 3235-3247.
345. Li, R. H.; Seo, S.-Y.; Eun, J.-S.; Lee, M.-K., Preparation and evaluation of freeze-dried solid lipid nanoparticles with various cryoprotectants. *Journal of Pharmaceutical Investigation* **2010,** *40* (1), 39-43.
346. Chen, C.; Han, D.; Cai, C.; Tang, X., An overview of liposome lyophilization and its future potential. *Journal of controlled release* **2010,** *142* (3), 299-311.
347. Niu, L., Formulation and delivery of polymeric nanoparticle-assisted vaccine against melanoma. **2015**.
348. López-Dıez, E.; Bone, S., The interaction of trypsin with trehalose: an investigation of protein preservation mechanisms. *Biochimica et Biophysica Acta (BBA)-General Subjects* **2004,** *1673* (3), 139-148.
349. Simperler, A.; Kornherr, A.; Chopra, R.; Bonnet, P. A.; Jones, W.; Motherwell, W. S.; Zifferer, G., Glass transition temperature of glucose, sucrose, and trehalose: an experimental and in silico study. *The Journal of Physical Chemistry B* **2006,** *110* (39), 19678-19684.
350. Soares, S.; Fonte, P.; Costa, A.; Andrade, J.; Seabra, V.; Ferreira, D.; Reis, S.; Sarmento, B., Effect of freeze-drying, cryoprotectants and storage conditions on the stability of secondary structure of insulin-loaded solid lipid nanoparticles. *International journal of pharmaceutics* **2013,** *456* (2), 370-381.
351. Schwarz, C.; Mehnert, W., Freeze-drying of drug-free and drug-loaded solid lipid nanoparticles (SLN). *International journal of pharmaceutics* **1997,** *157* (2), 171-179.
352. Maderuelo, C.; Lanao, J. M.; Zarzuelo, A., Enteric coating of oral solid dosage forms as a tool to improve drug bioavailability. *European Journal of Pharmaceutical Sciences* **2019,** *138*, 105019.
353. Khutoryanskiy, V. V., Longer and safer gastric residence. *Nature Materials* **2015,** *14* (10), 963-964.
354. Gupta, P.; Kumar, M.; Sachan, N., An overview on polymethacrylate polymers in gastroretentive dosage forms. *Open Pharmaceutical Sciences Journal* **2015,** *2* (1).
355. Thakral, S.; Thakral, N. K.; Majumdar, D. K., Eudragit®: a technology evaluation. *Expert opinion on drug delivery* **2013,** *10* (1), 131-149.
356. Basit, A. W., Advances in colonic drug delivery. *Drugs* **2005,** *65* (14), 1991-2007.
357. Stewart, J. C. M., Colorimetric determination of phospholipids with ammonium ferrothiocyanate. *Analytical biochemistry* **1980,** *104* (1), 10-14.
358. Thwala, L. N.; Santander-Ortega, M. J.; Lozano, M. V.; Csaba, N. S., Functionalized polymeric nanostructures for mucosal drug delivery. In *Biomedical applications of functionalized nanomaterials*, Elsevier: 2018; pp 449-487.

359. Zhang, J.; Lv, Y.; Wang, B.; Zhao, S.; Tan, M.; Lv, G.; Ma, X., Influence of microemulsion–mucin interaction on the fate of microemulsions diffusing through pig gastric mucin solutions. *Molecular pharmaceutics* **2015,** *12* (3), 695-705.
360. Murgia, X.; Pawelzyk, P.; Schaefer, U. F.; Wagner, C.; Willenbacher, N.; Lehr, C.-M., Size-limited penetration of nanoparticles into porcine respiratory mucus after aerosol deposition. *Biomacromolecules* **2016,** *17* (4), 1536-1542.
361. Manning, M. C.; Chou, D. K.; Murphy, B. M.; Payne, R. W.; Katayama, D. S., Stability of protein pharmaceuticals: an update. *Pharmaceutical research* **2010,** *27* (4), 544-575.
362. Bischoff, R.; Lepage, P.; Jaquinod, M.; Cauet, G.; Acker-Klein, M.; Clesse, D.; Laporte, M.; Bayol, A.; Van Dorsselaer, A.; Roitsch, C., Sequence-specific deamidation: isolation and biochemical characterization of succinimide intermediates of recombinant hirudin. *Biochemistry* **1993,** *32* (2), 725-734.
363. Arpaç, B.; Gökberk, B. D.; Küçüktürkmen, B.; Gündüz, I. Ö.; Palabıyık, İ. M.; Bozkır, A., Design and in vitro/in vivo evaluation of polyelectrolyte complex nanoparticles filled in enteric-coated capsules for oral delivery of insulin. *Journal of Pharmaceutical Sciences* **2022**.
364. Xu, Y.; Van Hul, M.; Suriano, F.; Préat, V.; Cani, P. D.; Beloqui, A., Novel strategy for oral peptide delivery in incretin-based diabetes treatment. *Gut* **2020,** *69* (5), 911-919.
365. Yang, J.-M.; Wu, L.-J.; Lin, M.-T.; Lu, Y.-Y.; Wang, T.-T.; Han, M.; Zhang, B.; Xu, D.-H., Construction and Evaluation of Chitosan-Based Nanoparticles for Oral Administration of Exenatide in Type 2 Diabetic Rats. *Polymers* **2022,** *14* (11), 2181.
366. Mastropietro, G.; Tiscornia, I.; Perelmuter, K.; Astrada, S.; Bollati-Fogolín, M., HT-29 and Caco-2 reporter cell lines for functional studies of nuclear factor kappa B activation. *Mediators of inflammation* **2015,** *2015*.
367. Batista, L. R.; Antoniosi Filho, N. R., Ethanol Content Determination in Medicine Syrups Using Headspace and Multidimensional Heart-Cut Gas Chromatography Coupled to Mass Spectrometry. *Journal of the Brazilian Chemical Society* **2020,** *31*, 394-401.
368. Indyk, L.; Fisher, H. F., [17] Theoretical aspects of isothermal titration calorimetry. In *Methods in enzymology*, Elsevier: 1998; Vol. 295, pp 350-364.
369. Srivastava, V. K.; Yadav, R., Isothermal titration calorimetry. In *Data processing handbook for complex biological data sources*, Elsevier: 2019; pp 125-137.
370. van Ballegooie, C.; Man, A.; Andreu, I.; Gates, B. D.; Yapp, D., Using a microfluidics system to reproducibly synthesize protein nanoparticles: Factors contributing to size, homogeneity, and stability. *Processes* **2019,** *7* (5), 290.
371. Belliveau, N. M.; Huft, J.; Lin, P. J.; Chen, S.; Leung, A. K.; Leaver, T. J.; Wild, A. W.; Lee, J. B.; Taylor, R. J.; Tam, Y. K., Microfluidic synthesis of highly potent limit-size lipid nanoparticles for in vivo delivery of siRNA. *Molecular Therapy-Nucleic Acids* **2012,** *1*, e37.
372. Lou, G.; Anderluzzi, G.; Schmidt, S. T.; Woods, S.; Gallorini, S.; Brazzoli, M.; Giusti, F.; Ferlenghi, I.; Johnson, R. N.; Roberts, C. W., Delivery of self-amplifying mRNA vaccines by cationic lipid nanoparticles: The impact of cationic lipid selection. *Journal of Controlled Release* **2020,** *325*, 370-379.
373. Jyotsana, N.; Sharma, A.; Chaturvedi, A.; Budida, R.; Scherr, M.; Kuchenbauer, F.; Lindner, R.; Noyan, F.; Sühs, K.-W.; Stangel, M., Lipid nanoparticle-mediated siRNA delivery for safe targeting of human CML in vivo. *Annals of hematology* **2019,** *98* (8), 1905-1918.
374. Chatzikleanthous, D.; Schmidt, S. T.; Buffi, G.; Paciello, I.; Cunliffe, R.; Carboni, F.; Romano, M. R.; O'Hagan, D. T.; D'Oro, U.; Woods, S., Design of a novel vaccine nanotechnology-based delivery system comprising CpGODN-protein conjugate anchored to liposomes. *Journal of Controlled Release* **2020,** *323*, 125-137.
375. Roces, C. B.; Port, E. C.; Daskalakis, N. N.; Watts, J. A.; Aylott, J. W.; Halbert, G. W.; Perrie, Y., Rapid scale-up and production of active-loaded PEGylated liposomes. *International Journal of Pharmaceutics* **2020,** *586*, 119566.
376. Lim, S. W.; Wong, Y. S.; Czarny, B.; Venkatraman, S., Microfluidic-directed self-assembly of liposomes: Role of interdigitation. *Journal of colloid and interface science* **2020,** *578*, 47-57.

377. Huckaby, J. T.; Lai, S. K., PEGylation for enhancing nanoparticle diffusion in mucus. *Advanced drug delivery reviews* **2018,** *124*, 125-139.
378. Pack, D. W.; Hoffman, A. S.; Pun, S.; Stayton, P. S., Design and development of polymers for gene delivery. *Nature reviews Drug discovery* **2005,** *4* (7), 581-593.
379. Clogston, J. D.; Patri, A. K., Zeta potential measurement. In *Characterization of nanoparticles intended for drug delivery*, Springer: 2011; pp 63-70.
380. Osanlóo, D. T.; Fransson, J.; Bergenståhl, B.; Millqvist-Fureby, A., Effects of drying methods on physical properties and morphology of trehalose/mannitol mixtures. *Drying Technology* **2022**, 1-20.
381. Kumar, K. N.; Mallik, S.; Sarkar, K., Role of freeze-drying in the presence of mannitol on the echogenicity of echogenic liposomes. *The Journal of the Acoustical Society of America* **2017,** *142* (6), 3670-3676.
382. van Winden, E. C., Freeze-drying of liposomes: theory and practice. *Methods in enzymology* **2003,** *367*, 99-110.
383. Gao, S.; McClements, D. J., Formation and stability of solid lipid nanoparticles fabricated using phase inversion temperature method. *Colloids and surfaces A: physicochemical and engineering aspects* **2016,** *499*, 79-87.
384. Cagliani, R.; Gatto, F.; Bardi, G., Protein adsorption: a feasible method for nanoparticle functionalization? *Materials* **2019,** *12* (12), 1991.
385. Bersani, S.; Vila-Caballer, M.; Brazzale, C.; Barattin, M.; Salmaso, S., pH-sensitive stearoyl-PEG-poly (methacryloyl sulfadimethoxine) decorated liposomes for the delivery of gemcitabine to cancer cells. *European Journal of Pharmaceutics and Biopharmaceutics* **2014,** *88* (3), 670-682.
386. Runnsjö, A.; Dabkowska, A. P.; Sparr, E.; Kocherbitov, V.; Arnebrant, T.; Engblom, J., Diffusion through pig gastric mucin: effect of relative humidity. *PloS one* **2016,** *11* (6), e0157596.
387. Rusu, L.; Lumma, D.; Rädler, J. O., Charge and size dependence of liposome diffusion in semidilute biopolymer solutions. *Macromolecular bioscience* **2010,** *10* (12), 1465-1472.
388. Lai, S. K.; O'Hanlon, D. E.; Harrold, S.; Man, S. T.; Wang, Y.-Y.; Cone, R.; Hanes, J., Rapid transport of large polymeric nanoparticles in fresh undiluted human mucus. *Proceedings of the National Academy of Sciences* **2007,** *104* (5), 1482-1487.
389. Larhed, A. W.; Artursson, P.; Gråsjö, J.; Björk, E., Diffusion of drugs in native and purified gastrointestinal mucus. *Journal of pharmaceutical sciences* **1997,** *86* (6), 660-665.
390. Lieleg, O.; Vladescu, I.; Ribbeck, K., Characterization of particle translocation through mucin hydrogels. *Biophysical journal* **2010,** *98* (9), 1782-1789.
391. Yamazoe, E.; Fang, J.-Y.; Tahara, K., Oral mucus-penetrating PEGylated liposomes to improve drug absorption: Differences in the interaction mechanisms of a mucoadhesive liposome. *International Journal of Pharmaceutics* **2021,** *593*, 120148.
392. Wang, Y. Y.; Lai, S. K.; Suk, J. S.; Pace, A.; Cone, R.; Hanes, J., Addressing the PEG mucoadhesivity paradox to engineer nanoparticles that “slip” through the human mucus barrier. *Angewandte Chemie International Edition* **2008,** *47* (50), 9726-9729.
393. Song, J. G.; Lee, S. H.; Han, H.-K., Biophysical evaluation of aminoclay as an effective protectant for protein stabilization during freeze-drying and storage. *International Journal of Nanomedicine* **2016,** *11*, 6609.
394. Li, X.; Zhao, Z.; Li, L.; Zhou, T.; Lu, W., Pharmacokinetics, in vitro and in vivo correlation, and efficacy of exenatide microspheres in diabetic rats. *Drug delivery* **2015,** *22* (1), 86-93.
395. Powell, M. F., Peptide stability in aqueous parenteral formulations: Prediction of chemical stability based on primary sequence. ACS Publications: 1994.
396. Weinman, J.; Gritter, K., Gastric emptying: normal values for a simple solid meal. Soc Nuclear Med: 2006.
397. López-García, R.; Ganem-Rondero, A., Solid lipid nanoparticles (SLN) and nanostructured lipid carriers (NLC): occlusive effect and penetration enhancement ability. *Journal of Cosmetics, Dermatological Sciences and Applications* **2015,** *5* (02), 62.

398. Ntai, A.; La Spada, A.; De Blasio, P.; Biunno, I., Trehalose to cryopreserve human pluripotent stem cells. *Stem Cell Research* **2018,** *31*, 102-112.
399. Wen, Y.-Z.; Su, B.-X.; Lyu, S.-S.; Hide, G.; Lun, Z.-R.; Lai, D.-H., Trehalose, an easy, safe and efficient cryoprotectant for the parasitic protozoan Trypanosoma brucei. *Acta Tropica* **2016,** *164*, 297-302.
400. André, P.; Villain, F., Free radical scavenging properties of mannitol and its role as a constituent of hyaluronic acid fillers: a literature review. *International Journal of Cosmetic Science* **2017,** *39* (4), 355-360.
401. Soenen, S. J.; Manshian, B. B.; Abdelmonem, A. M.; Montenegro, J. M.; Tan, S.; Balcaen, L.; Vanhaecke, F.; Brisson, A. R.; Parak, W. J.; De Smedt, S. C., The cellular interactions of PEGylated gold nanoparticles: effect of PEGylation on cellular uptake and cytotoxicity. *Particle & Particle Systems Characterization* **2014,** *31* (7), 794-800.
402. Kucharzik, T.; Lügering, N.; Rautenberg, K.; Lügering, A.; Schmidt, M.; Stoll, R.; Domschke, W., Role of M cells in intestinal barrier function. *Annals of the New York Academy of Sciences* **2000,** *915* (1), 171-183.
403. Kong, S.; Zhang, Y. H.; Zhang, W., Regulation of intestinal epithelial cells properties and functions by amino acids. *BioMed research international* **2018,** *2018*.